UNIVERSITÀ DI PARMA

UNIVERSITÀ DEGLI STUDI DI PARMA

DOTTORATO DI RICERCA IN
INGEGNERIA INDUSTRIALE

CICLO XXXVII

VIRTUALIZATION APPROACHES FOR THE DESIGN, CHARACTERIZATION, AND CONTROL OF FOOD INDUSTRY PLANTS

Coordinatore: Chiar.mo Prof. Gianni Royer Carfagni

Tutore: Chiar.mo Ing. Federico Solari

Co-Tutore: Chiar.mo Prof. Ing. Roberto Montanari

Dottoranda: Natalya Lysova

Anni Accademici 2021/2022 - 2023/2024

Contents

Chapter 1

Introduction

Contents

1.1 Aims of the research project

This Doctoral thesis presents the activities and results obtained over three years of research, that focused on developing virtualization approaches for industrial plant control and design.

The activities were carried out in Parma, heart of the food valley, so the main focus of the projects included in this document is the food industry sector. Several the applications and analyses, however, could be easily extended to other sectors as well, generalising even more the obtained results.

The activities of the Doctoral project were conducted in collaboration with researchers and professors of the University of Parma, and the consulting and R&D firm FMB Eng.In.E. During these three years, on both sides of my role, I had the great opportunity to work with different companies and industrial stakeholders, learning about their needs and the crucial aspects that must be investigated in order to make industrial production more efficient, sustainable and to achieve high levels of quality.

As stated in the project title, the focus of the research project is to assess how, where, and when the digital technologies can support industrial progress. The context of the present work, therefore, is Industry 4.0 and smart manufacturing, as well as some of the Industry 4.0 abilitating technologies that are allowing the industrial context to become increasingly more efficient, integrated and connected.

The main tool used to carry out the presented activities is simulation. In a sector, such as the food one, where the applications are characterized by a high degree of complexity (geometries, products, technologies, conditions, etc.), numerical simulation is an invaluable tool that allows for deep characterization of the processes, derivation of detailed and specific insights, as well as for efficient testing of alternative conditions on a validated model. The latter in particular is a key aspect of how simulation can support sustainability: minimizing the physical testing required, it is possible to save a lot of resources, materials, time, and money. Furthermore, since the need of products for the tests is significantly reduced, the waste of food is reduced as well.

One of the main simulation techniques applied in the projects included in this thesis is Computational Fluid Dynamics (CFD) simulation, as it allows to precisely model phenomena involving flow and heat and mass transfer. This numerical technique allows to overcome the limitation of analytical models, and evaluate the complex applications characterizing food industry. In the following chapters, CFD has been used to characterize both convention and innovative food processes, thus strongly contributing to their

development and to the scientific literature on the subject.

One of the main drawbacks of CFD simulation, however, are the need of extensive know-how required to effectively and efficiently set-up the simulations, the cost of licensing if commercial software are employed, computational resources, but above all time.

Indeed, the time required to obtain CFD results is the main aspect that affects the usability of the results for industrial applications. Nowadays, simulation results are mostly used to carry out exploratory campaigns to design, characterize and optimize devices and processes, while their application in monitoring and control activities is extremely limited.

The results that can be obtained, however are extremely valuable: the variables of interest, indeed, can be several, and they are calculated in potentially every point of the domain (based on the spatial discretisation), thus generating an actual Big Data.

As always in the field of Big Data, however, it is fundamental to know what values are required, and how to analyse them.

This is one of the main ideas explored in this thesis. The developed simulation models indeed, once appropriately validated, are meant to be used for parametric experimental campaigns, to characterize the system across all the possible operating conditions. By appropriately defining a set of input and output parameters, for which a deep understanding of the process and the objectives is required, it is possible to obtain data sets that can be easily analysed and modelled with statistical and mathematical techniques. This allows to obtain reduced order models of the analysed process or device, that can be indeed applied for real-time operations.

One of the main possibilities explored focuses on developing digital models based on simulation results, possibly integrated with experimental and historical data, to be implemented in Digital Twin contexts.

Digital Twins are integrated, data-driven representations of dynamic entities - such as, but not limited to, industrial plants and devices - that consist of three main components: (*i*) a physical entity defined as "physical twin", (*ii*) its virtual representation by means of digital models, referred to as "digital shadow", and (*iii*) a continuous real-time communication between the two. Digital Twins can be applied for several purposes. Some of the main applications of interest investigated in this document include monitoring, control, and predictive maintenance of industrial plants.

Another application investigated, that will be developed and validated in future research activities concerns the development and deployment of "virtual sensors" based on simulation data. The main idea is to exploit the Big Data generated with the simulations to characterize in-depth the system, and obtain models providing insights about points

of interests where real sensors are not available, or even impossible to install.

Remaining in the field of "virtual sensors", one approach currently under investigation is based the use of machine and computer vision techniques. A bibliometric analysis of the literature, aiming at identifying applications and fields currently investigated is presented in one of the chapters. Nowadays, in the food industry, these techniques are used mainly for spot-on quality checks, and applications concerning sorting, grading, and defect identification. Generally, the result of these evaluations is the classification of different product categories, or the removal of non suitable product units and contaminants.

Based on the industrial collaborations carried out over the third year of the Doctoral project, involving the application of vision techniques in food processing lines, one research questions that emerged was: Is it possible to go beyond the current application of vision-based techniques, integrating them in plant monitoring and control applications? This topic is further discussed in the dedicated chapter.

Another field of application of simulation treated in this thesis concerns inventory management, applied to the field of perishable products, thus remaining in the food industry field. In this context, to achieve the usual cost-minimization and profit-maximization objectives of inventory system optimization, several additional factors must be considered.

The first one is obviously related to the perishability of the products: items can not be stored for potentially infinite time, but can be handled only over a brief period of shelf life, at the end of which they must be disposed of as they can not be sold anymore.

Other aspects concern the demand: managing inventory systems of perishables in business to business (B2B) contexts is extremely different from managing business to consumer ones. In the first scenario, as the seller/reseller a decision maker could choose the product lots to sell, obviously opting for a first-expired-first-out (FEFO) appproach (that in this context generally coincides with first-in-first-out FIFO) that would minimize wastes.

In B2C scenarios, however the choice is a prerogative of the consumer, whose demand of perishable products is generally strongly age-dependent. The baseline product picking approach, therefore, would be last-expired-first-out (LEFO), thus choosing the freshest products with the longest residual shelf life over the older products. This inevitably results in an extensive amount of food waste, as certified in several reports on the subject.

The chapter dedicated to the inventory management of perishable products explores modelling approaches and assumptions related to the subjects, and integrates the evaluations performed with insights deriving from a survey exploring the impact of discounting policies on the purchase of food products near expiration.

From these premises, it is clear that digital technologies can strongly support the industrial sector. Food industry in particular, that is often perceived as one of the industrial sectors less interested in innovative approaches, can strongly benefit from their implementation and is well-aware of that. This is confirmed also by the fact that several projects included in the next chapters were carried out, and are currently investigated in collaboration with industrial stakeholders.

In a context characterized by world population continuously increasing, and the rapid global development, resulting in ever-growing consumer demand of food products with increasingly more strict quality and safety requisites, precise control of food industry processes and plants is essential, together with the optimization of the existing processing technologies and the development of new ones.

This thesis aims to contribute to this research field by presenting a collection of case studies about conventional and innovative processing technologies, different modelling approaches, and advanced automation and control frameworks based on the integration of different technologies and data. Moreover, based on the results achieved and building on the carried out activities, future research activities are proposed.

1.2 Structure of the thesis

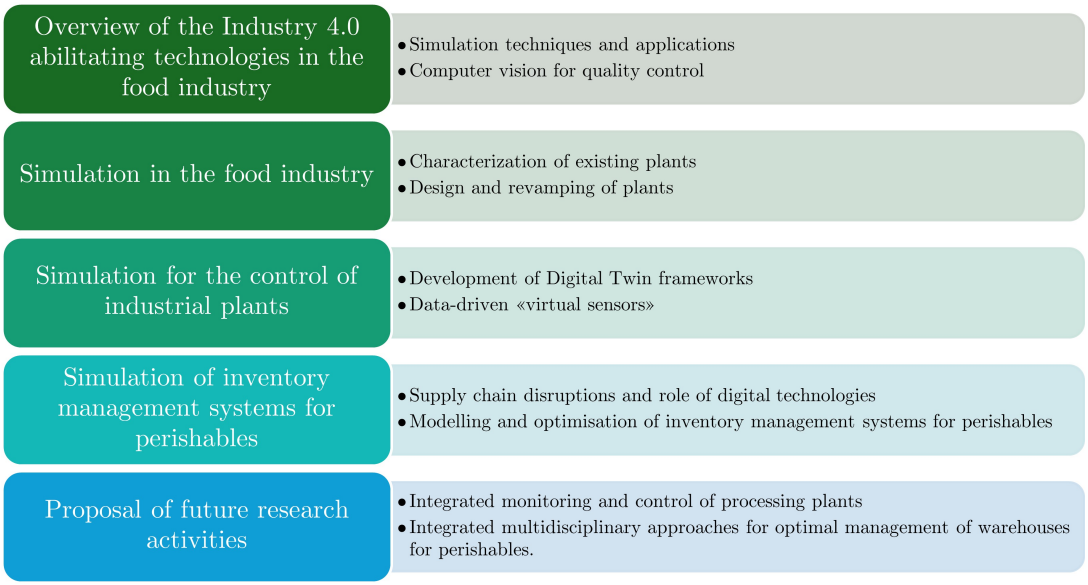

Figure 1.1: Overview and structure of the thesis contents.

The thesis is structured as shown in Figure 1.1, and is organized as a collection of papers, most of which have already been published in peer-reviewed journals and conference papers.

Although the papers selected for this thesis were written in collaboration with doctoral advisors and other researchers, they all include significant contributions from myself in terms of methodology, writing, analysis of results, and drawing of conclusions.

Moreover, the selected articles are based on projects that are still active and ongoing. Several of these involve collaborations with industrial stakeholders, who are referenced and acknowledged on the first page of each relevant section.

The structure of the thesis follows a logical progression: beginning with the characterization of existing food industry plants and the design of new ones, as well as the assessment of different processing technologies, the discussion then moves to monitoring and control applications, concluding with inventory management of perishable products.

Each thematic chapter starts with a brief introduction, aiming to provide a concise overview of the topic and an introduction to its relevance in industrial settings. Since the included papers deal with a variety of industrial applications, a review of the relevant literature was maintained for each paper.

Throughout the chapters of this thesis, emerging technologies and innovative methods for monitoring and control are analyzed and discussed, all linked by the *fil rouge* of the simulation approach used to enhance efficiency in the food industry.

To enhance readability and accessibility, each chapter begins with a table of contents, and each section starts with a word cloud to provide an at-a-glance overview of the main topics.

The list of figures is presented in Appendix A, while the tables are listed in Appendix B. The complete list of articles published over the course of the Doctoral program is reported in Appendix C.

Chapter 2

Innovative digital technologies in the food sector

Contents

2.1 Use of simulation techniques in the food industry

Among the different Industry 4.0 abilitating technologies, simulation techniques can be extremely beneficial to the food industry. Indeed, they can be applied to different steps of industrial processes, starting from the design of a device or a plant, to the management of inventory systems of food products [1, 2].

With regard to the design and characterization phases, simulation allows to perform preliminary tests and implement changes to the system geometry and configurations acting on the digital model of the device or of the plant, thus limiting the necessity of physical testing and the consequent waste of time and resources. This is a great advantage, from the points of view of both economics and sustainability. In these applications, the aim of simulation can be to assess whether the objectives of a particular treatment can be reached with a given configuration, optimize the product quality, the system and process performance, and pursue energy efficiency.

In the food industry, products are often fluid, with a single or multiple phases based on the product. Moreover, food fluids generally present a complex behaviour, that is not a linear function of the applied forces, but that varies based on the structure and composition of the given product, shear rate applied, and the fluid temperature [3]. The peculiar characteristic of food fluids, therefore, should not be neglected when defining a digital model of a plant, because it would lead to an extensive decrease in the model's accuracy. In addition, the geometries of the devices can become quite complex, aiming to optimize the efficiency of the food industry treatments.

Considering both the complexities in the device structures and the processed products, it is often impossible to characterize food industry devices and plants with analytical models, at least without making several simplifying assumptions. These assumptions, however, can be sometimes too strong, and lead to non-optimal design of plants and process conditions [4]. Numerical simulation techniques, in particular Computational Fluid Dynamics (CFD), become essential in these cases to correctly characterize and design food industry systems, allowing to simulate complex fluids, phenomena, and geometries under several conditions and configurations. This approach is essential in processes where fluid flow, heat transfer, and mass transfer are critical, such as, among others, thermal processing of foods, non-thermal alternative methods, mixing and blending and drying processes [5–7].

Another simulation technique that is becoming increasingly more adopted in the food industry is the Discrete Element Method (DEM), which applies to processes involving granular materials, such as powders, grains, and particulates. The advantage of this technique is that it allows to deeply understand how the discrete particles interact with each other and with the surfaces of the simulated domain, becoming essential in applications such as grinding, mixing, drying and conveying of granular products. In

particular, applications like pneumatic conveying and drying processes can extensively benefit from the coupling of DEM and CFD simulation techniques, reproducing the interaction between solid particles and fluid flows, such as air or liquids and thus more accurately predicting flow behavior, as well as heat and mass transfer.

For logistics and supply chain management applications, other simulation techniques are generally adopted. One of the most widespread ones is Discrete Event Simulation (DES), that simulates the operation of a system as a sequence of discrete events over time. Each event represents a change in the system's state, such as the start or end of a process. In particular, with regard to the food industry, DES is commonly applied to model production lines, distribution processes, equipment utilization, and inventory management. A - simpler - alternative to DES is Discrete-Time Simulation (DTS), where the characterization and the update of the system progresses in time steps of fixed duration. Thanks to the digital models developed, it is possible to identify possible bottlenecks and operations with non-optimal configurations, making it possible for the decision makers to intervene on the identified issues and increase the overall efficiency of the system.

The modelling and simulation techniques available nowadays are a great number, with several of them that could greatly benefit quality, safety and efficiency in the food industry. In this thesis, the main techniques adopted are CFD, in the context of food processing, and DTS in the context of inventory management. These two techniques are described more in detail in the following sections, with details about their working principles, advantages and limitations, as well as applications in the domain of the food industry.

2.2 Computer vision techniques for quality control in the food industry

The research in this chapter has been included in the peer-reviewed conference paper [8] *Lysova, N., Solari, F., and Montanari, R. (2024). Investigating Research Trends in Computer Vision for Food Quality Control: A Bibliometric Approach. Proceedings of the 6th International Conference on Industry 4.0 and Smart Manufacturing (ISM 2024).*

Abstract

The production throughputs of the food industry grow continuously due to the ever-increasing customer demand. At the same time, food safety measures become increasingly strict. To this end, efficient quality control is essential to ensure quality and safety for consumers, and to guarantee efficient and valuable production for industrial stakeholders. Computer vision is often applied to this end, usually integrated with other Industry 4.0 technologies and process automation. Computer vision applications in quality control, indeed, can greatly enhance supply chain management in the food industry by maintaining consistent product quality and minimizing waste.

In [8] a keyword-based analysis is carried out to assess the main research trends and topics in the field of computer vision for quality control in the food industry. The bibliometric analysis aims to assess the main applications of the technology in terms of processes and products and the main issues targeted by the analyses. Finally, the results of the bibliometric investigation allow to identify and highlight topics that present potential for future investigations in the field.

Introduction

Quality control is a critical aspect of the food industry, essential to ensure that the products meet safety, aesthetic, and nutritional standards. These practices, indeed, are essential to satisfy strict regulatory requirements, guarantee public health and safety, as well as to preserve the loyalty of the customers and the reputation of the brands [9]. Quality control is not limited to a single step or check of the final product, but includes several controls throughout the production cycle, starting from the inspection of the raw materials, whose suitability represents the foundation for the acceptability of the final products. These controls, depending on the methodology adopted, can be destructive, when a sample or the whole product is collected and disposed of after the test, or non-destructive, when the control does not affect the product and can also be carried out in real-time on line.

Traditionally, quality controls in the food industry are carried out by the operators, thus relying on manual inspection, visual control, and, more in general, sensorial evaluation. These activities, however, are intrinsically subject to human error, are time-consuming, and sometimes labor-intensive. With production rates getting increasingly higher due to ever-growing customer demand, the quality requirements becoming more stringent, and the evaluation procedures more sophisticated and thorough, it is becoming more difficult to guarantee high quality and safety standards relying only on human control. To this end, thanks to the technological advancement in the computer science, artificial intelligence, and automation fields, quality controls based on computer vision now represent a promising, and increasingly more adopted alternative [10].

Computer vision techniques include the extraction, analysis, and interpretation of visual information from the physical world by means of rapid, accurate, and non-destructive analyses [11, 12]. By leveraging image processing techniques, advanced algorithms, and artificial intelligence, computer vision can partially replicate human perceptions and detect even subtle defects [13]. Some of the main advantages of such systems, indeed, are the precision, the short processing times, and the replicability. Automated quality control can be implemented at several stages of the production process, with the most common being inspection of raw materials [14], sorting and grading [15], process monitoring [16, 17], and packaging inspection [18]. Besides the already mentioned benefits, thanks to its characteristics, computer vision can significantly enhance supply chain management in the food industry, by ensuring consistent product quality and reducing waste through early, rapid, and precise detection of defects [19]. By minimizing the occurrence of defects and thus consumer complaints and eventual product recalls, this technology can help to strongly reduce operational costs and avoid potential disruptions.

Currently, excluding the books on the subject, the reviews available in the literature generally focus on a single product/product category, specific processes, or the adopted

technique, without providing a comprehensive overview of the application of computer vision in the food industry [20–27]. Moreover, very few studies use a bibliometric approach in this context to analyze the trends in the use of keywords and identify research trends and gaps [28–30].

This research aimed to investigate the trends and the main applications of computer vision for quality control in the food industry. To this end, after a descriptive analysis of the retrieved literature, a bibliometric analysis was performed on 742 records retrieved from Scopus. The analysis of the keywords allowed to determine the most relevant themes in the field and their evolution over time. Moreover, the classification of the keywords according to their frequency and persistence of use allowed to identify topics that present high potential for future investigations. Finally, a thematic analysis was carried out to assess the main practical applications in terms of products and monitored issues. In this way, by means of quantitative analyses, this paper aimed to provide a summary of the research trends in the use of computer vision for quality control in the food industry, identifying possible research gaps. Indeed, while the food industry has been generally characterized by a lower digital maturity compared with other industrial sectors, it is now rapidly growing and evolving, leveraging digital technologies that have been usually applied in contexts where the products have higher added value and/or impact on the following processing steps or the functioning of a system, e.g., the automotive industry. In particular, this paper aimed to identify applications in food processing contexts where computer vision could be used not as a classification or grading tool, or a method to distinguish "acceptable" products from "bad" ones, but rather as a "sensor" to be implemented in a framework of real-time plant monitoring and control.

Literature review

As stated in the Introduction, literature reviews in the field of computer vision for quality control in the food industry generally focus on a specific topic, that could be a product, a process, or a technique.

Several papers review the scientific literature focusing on specific products or product categories. In [20], the authors have reviewed the most significant sensing technologies used in the olive oil industry to supervise and control the virgin olive oil production process, monitoring parameters such as acidity, peroxide indexes, ripening indexes, organoleptic properties, and minor components. In [21], the authors have investigated the use of computer vision systems for the quality control of beer. The authors have pointed out how the adoption of this technology allows to ensure the reliability and reproducibility of the obtained results related to several beer quality characteristics such as color, bubble size and distribution, foam stability, etc. In [22], the applications of machine vision for quality controls of different meats are evaluated, to objectively quantify

parameters related to meat color, texture, marbling, pH, tenderness, freshness, etc., while in [23] applications of the artificial senses in fish freshness determination are discussed. In [24], the detection of quality deterioration of fresh foods is addressed. In particular, the paper presents an overview of the main technologies and equipment usually adopted for these evaluations.

In other cases, the reviews have focused on a specific process, as in the case of [25], that targets the process of food drying. After presenting different computer vision systems, the authors have presented two novel AI-driven solutions to monitor the visual attributes of food during fluidized bed drying. Other literature reviews target specific computer vision technologies, such as hyperspectral imaging for food quality and safety [26], or near-infrared imaging for the assessment of food quality [27].

The number of bibliometric studies on the topic of computer vision for quality control in the food industry appears to be very limited to date. In [28] machine vision applications in fruit sorting and grading have been analyzed in order to highlight the major challenges of the technology and identify trends and possible research gaps by means of keyword-based analyses. In this way, it was possible to identify the main techniques used for this task, and the parameters usually quantified. In [29], the visualization of relationships between the most published sources and countries, visualization of networks of terms occurrence, and the thematic map of keywords of literature with "mushroom" and "storage" as keywords have been presented in the context of preservation and quality evaluation of postharvest edible mushrooms. Finally, [30] has targeted farm animal welfare in China, to present the state of the research and determine possible gaps in the field that deserve further investigation.

Through a bibliometric analysis of computer vision applications for quality control, this paper aims to identify possible applications of vision-based techniques in the food industry, that could be the subject of future investigations. The analysis targets computer vision applications, so as not to neglect techniques such as object detection, segmentation, or classification. The goal is to identify areas where computer vision could be integrated into Industry 4.0 monitoring and control of food processing lines. In particular, it aims to define contexts that could benefit from "vision-based sensors" as discussed in [31] for the dairy industry, where the concept of Dairy 4.0 architecture has been introduced, consisting of four layers (physical, acquisition/machine vision, digital twin, and zero defect manufacturing layers), with the final goal of achieving zero defect manufacturing.

Methodology

In order to perform the bibliometric analysis, the papers were retrieved from the Scopus database. In particular, the search was performed by first defining the query. As the investigated topic was related to the implementation of computer vision techniques for

quality control in the food sector, the query was defined as follows:

TITLE-ABS-KEY ("computer vision" AND food AND quality).

Then, a filter was applied to the papers resulting from the query (929), to select only those written in English (900). The metadata of the papers was exported in .csv format for further analysis. Finally, the last filter was applied to remove papers without author keywords, resulting in a final sample of 742 papers.

A first descriptive analysis was carried out to characterize the sample in terms of, among others, papers published every year, the most active authors in the field, and the most represented countries. The whole sample of 900 papers written in English was considered at this stage. Then, an analysis of the author keywords was performed with MS Excel™ to identify the main research themes, after removing those that did not present the field of author keywords. The following steps were followed to pre-process the data:

- Extraction of the complete list of author keywords;
- Normalization of the keywords, by removing variations, typos, and plurals, as well as terms with the same meaning but written in different ways. A total of 1953 keywords resulted from this stage;
- Evaluation of the number of occurrences of each keyword in the evaluated years using pivot tables.

The data obtained was used to evaluate the trend in the use of the most relevant keywords. Moreover, the data was used to classify the research topics according to their frequency (f_i) and persistency (p_i) of use over time, according to the procedure presented in [32]. To this end, two indexes were calculated: Average Frequency Count (AFC) and Average Persistency Count (APC). AFC is equal to the average frequency of occurrence of a keyword, calculated as the sum of the occurrences of all keywords, divided by the number of keywords. APC, on the other hand, is evaluated by averaging the persistence of all the keywords, i.e., number of years since the first appearance, calculated as 2024 - year of first appearance + 1. By comparing the values of frequency and persistence of use of every keyword with the average value, four distinct classes of keywords can be identified:

- $f_i \geq AFC$ and $p_i \geq APC$: the keyword has been consistently used over a significant period, thus likely being a key topic in the discipline, and it is classified as *"well-established"*.

- $f_i \geq AFC$ and $p_i < APC$: the keyword has been used frequently over a relatively brief period, and it is classified as *"trendy"*. These keywords often represent rapidly growing topics, that could potentially be further investigated in future research activities.

- $f_i < AFC$ and $p_i \geq APC$: the keyword has been present in the literature for a long period, but its use has not been significant, and possibly, not constant; these keywords are classified as *"intermittent"*.

- $f_i < AFC$ and $p_i < APC$: the keyword has been used rarely over a brief period and is defined *"emerging"*. These topics appear to be new, but they attract less attention compared to the *"trendy"* ones.

Based on these categories, it is possible to classify the research themes and identify the most promising and relevant ones. For instance, it is very likely that trendy topics will draw significant attention, whereas this may not be the case for intermittent themes.

Finally, a thematic analysis was performed by screening the keywords to identify the products investigated in the analyses and the issues addressed; these terms were then clustered to identify the main applications of computer vision for quality control in the food industry.

Results and Discussion

Descriptive statistics

As stated, 900 records, including articles, conference papers, reviews, books, and book chapters were retrieved from the Scopus database after applying the filter to the document language (English). The first records in this sample are two conference papers dating back to 1984, with one of them already investigating a computer vision approach as an alternative to the manual sorting of fresh tomatoes [33].

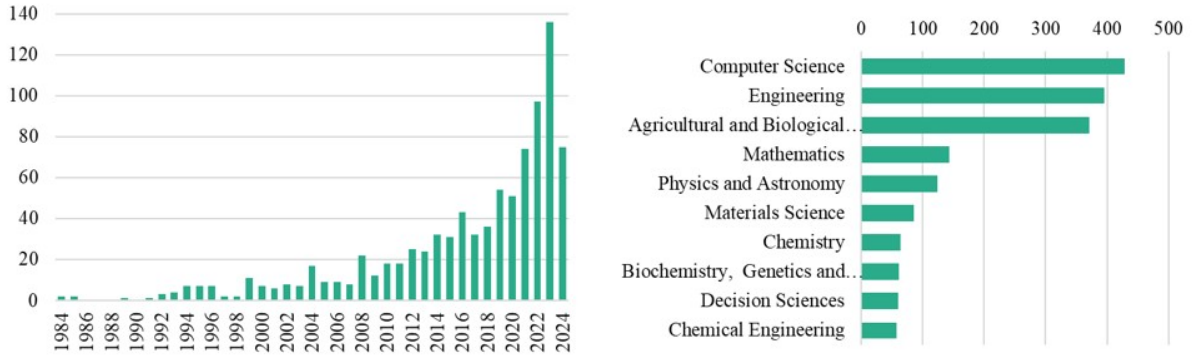

(a) Papers published over the years.

(b) Classification of the papers by subject area (Scopus).

Figure 2.1: Descriptive statics of the publishing trends over the years and subject areas.

(a) Authors with the highest number of papers.

(b) Countries with the highest number of papers in the analyzed sample.

Figure 2.2: Descriptive statics of the most prolific authors and most represented countries.

The publication of literature in the field of computer vision applied to quality control in the food industry has steadily grown in the following decades, as shown in Figure 2.1a. The number of records for the year 2024 is related to the time of writing (July 2024).

According to the Scopus classification, these records can be classified into several subject areas, which can definitely be expected due to the broad range of possible applications of computer science and the many different issues that may be encountered in the food industry (Figure 2.1b). The subjects with the highest number of papers are Computer Science, Engineering, and Agricultural and Biological Sciences. It must be noted that a given paper can be indexed with more than one subject.

The author who has contributed the most is Dr. Sun D.W., with a total of 42 contributions among articles, reviews, conference papers, books, and book chapters (Figure 2.2a): as can be seen, the number of his contributions is higher than the sum of the following four researchers. With reference to the countries publishing the most on the subject, India appears to be leading the ranking, followed by China and the United States (Figure 2.2b). India and China, indeed, are rapidly growing and highly populated coun-

tries, with large agricultural sectors but also prominent universities and research centers. Thanks to the economic growth they have been experiencing in the last decades, government support and investments in technology and infrastructure have increased, allowing to achieve significant technological advancements in technologies able to improve food quality and safety and satisfy the significant consumer demand.

Keyword analysis

The keyword analysis was performed on 742 records, identified after removing those without author keywords from the original sample. After the normalization, and the removal of the query keywords not to influence the results (computer vision, food, quality), a total of 1953 keywords remained, related to articles published in the period 1996-2024. The most relevant terms, with a minimum occurrence of 10 times, are reported in Table 2.1.

Table 2.1: The most frequently used keywords in the identified papers.

Keyword	**Occurrences**	**Keyword**	**Occurrences**
Deep Learning	105	Food safety	15
Machine vision	101	Artificial Neural Network (ANN)	15
Machine learning (ML)	87	Automation	15
Image processing	86	Spectroscopy	13
Convolutional Neural Network (CNN)	63	Precision agriculture	13
Image analysis	52	Internet of Things (IoT)	13
Artificial Intelligence (AI)	46	Food industry	13
Food Quality	35	Apples	13
Classification	34	YOLOv5	12
Support vector machine (SVM)	28	Sensors	12
Hyperspectral imaging	28	Quality inspection	12
Color	27	Near infrared spectroscopy (NIR)	12
Computer vision system	25	Electronic Nose	12
Transfer learning	24	Chemometrics	12
Quality control	22	Segmentation	11
Neural networks	20	Object detection	11
Feature Extraction	20	Vegetables	10
Image segmentation	16	Quality evaluation	10
Fruit	16	Digital Image Processing	10
Agriculture	16		

The links between the keywords, as well as their use over time, can be observed in Figure 2.3, generated using the bibliometric software VOSviewerTM, with the keywords colored according to the average year of occurrence. Two main clusters, both in terms of themes and years, can be identified: one related to the foundations and standard techniques of computer vision and image processing, with terms including, among others, classification, segmentation, feature extraction, and color, whose average year of use dates back to up to 2014. On the other side of the image, a newer cluster can be identified, featuring artificial intelligence techniques, as well as innovative and relevant applications in the fields of agriculture and automation. These trends are confirmed by the graph in Figure 2.4: terms of the first cluster (machine vision, image processing, image analysis), in green, present a steady, however not very high, use over time. The terms of the second cluster, related to artificial intelligence, on the other hand (deep learning, machine learning, convolutional neural network), have been introduced recently, but their use has seen a very rapid escalation in this field like in several others. These technologies, indeed, allow to make quality control through computer vision much more thorough and powerful, but also increasingly more accessible to industrial shareholders.

After analyzing the general trends in the use of the keywords over time, a quantitative analysis based on the frequency and persistence of use was carried out on the 1953 keywords over the period 1996-2024. First, AFC and APC values were calculated, resulting in AFC=3.8 and APC=8.74; for the purpose of the analysis, these values were rounded to AFC=4 and APC=9.

Based on these thresholds, the keywords were classified as *"well-established"*, if they were characterized by frequent use over a long period, *"trendy"* if they were frequently used in the last years, *"intermittent"* if their use was rare, and distributed over several years, and *"emerging"* if they appeared few times over the last years. The results of the analysis are reported in Figure 2.5.

It can be seen that the most used keywords are related to artificial intelligence techniques and image analysis and image processing methods. In addition, some application areas emerge above others, represented by the keywords agriculture and plant diseases among the trendy topics, and fruit in the well-established, thus confirming that the prevalent applications of computer vision for quality control are currently in the agricultural sector. Moreover, among the trendy topics, non-destructive control appears to be a promising topic.

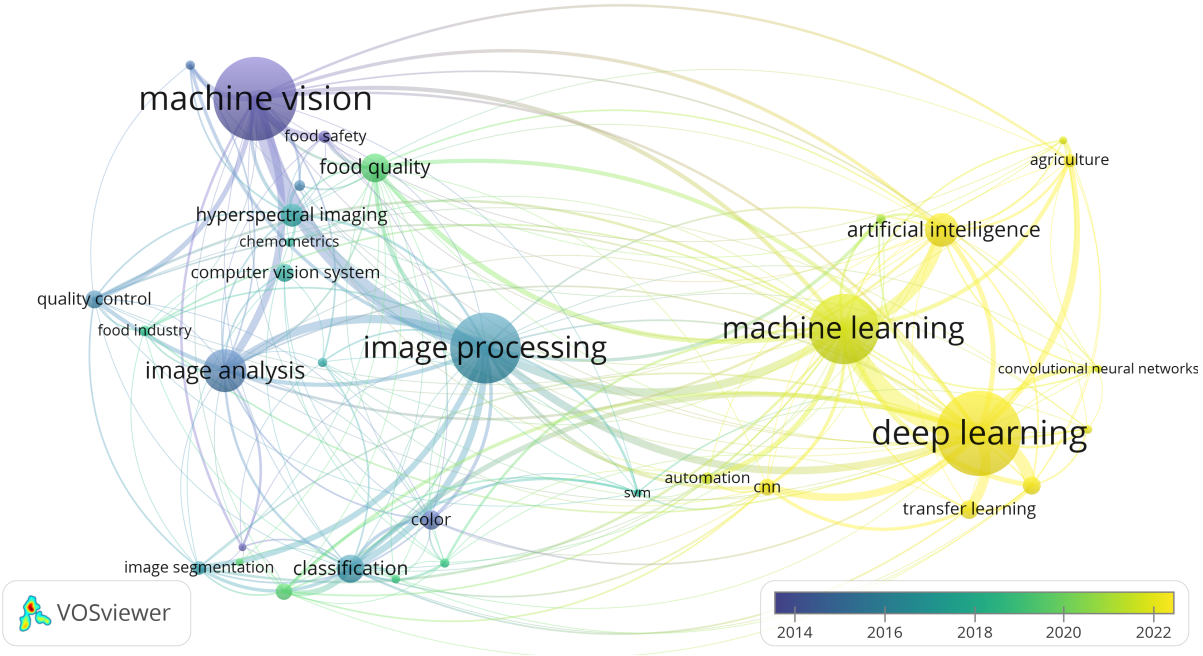

Figure 2.3: Overlay representation of the most relevant keywords, colored according to the average year of use.

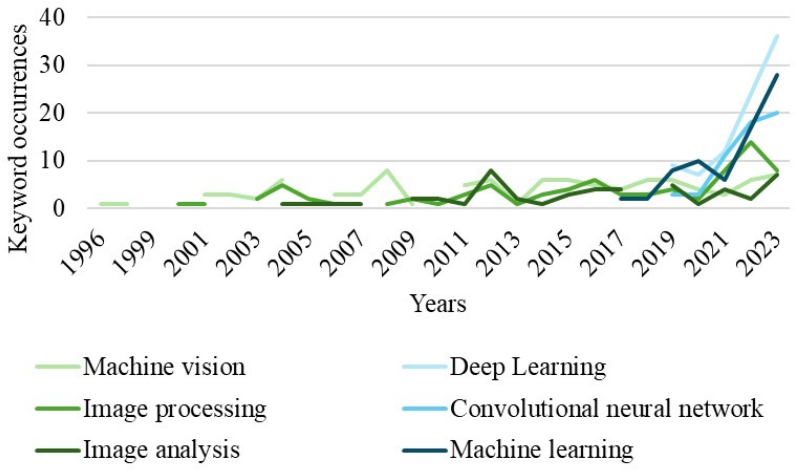

Figure 2.4: Trends in the use of some of the most relevant keywords over time.

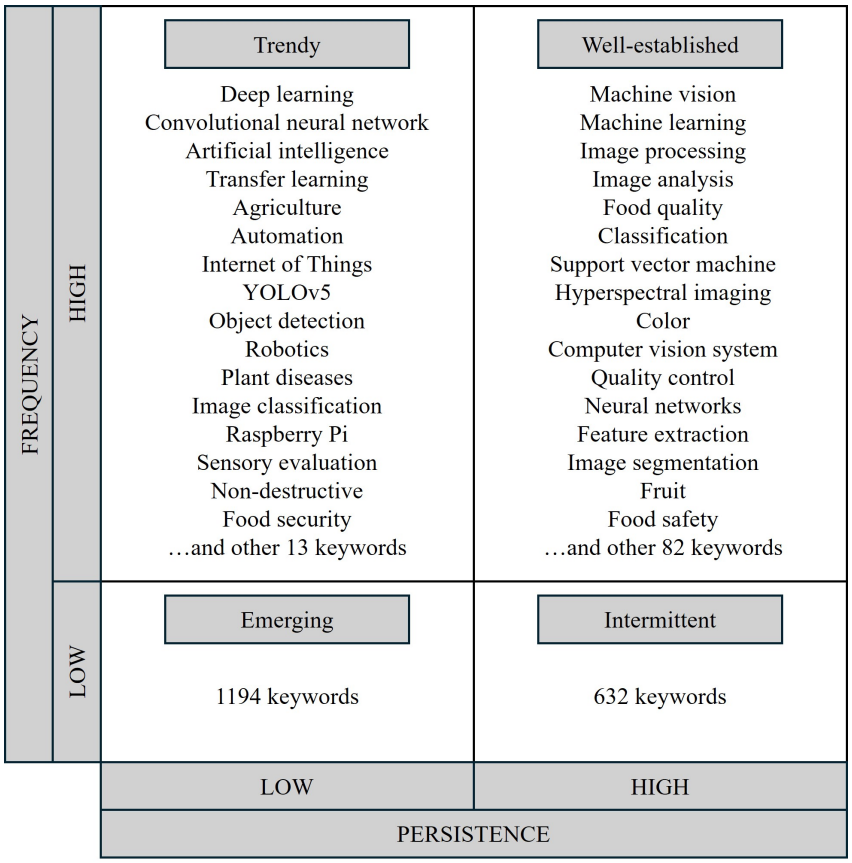

Figure 2.5: Results of the keyword classification based on the frequency and persistence of use.

Thematic analysis

The thematic analysis was conducted to identify the product categories and the main quality and safety issues currently investigated in the literature in terms of quality control based on computer vision. The keywords were then grouped by product category (Table 2.2) and defect category (Table 2.3). The main product categories identified included, as expected, fruits, vegetables, and grains. Interestingly, several applications were found for the meat and fish sectors. Other relevant applications refer to the food processing industry, with the occurrences of bakery products, frozen products, pizza, and cheese.

With regard to the quality control of fruits, the identified keywords can be divided into two categories: general applications (fruit, fruit quality, fruit classification, fruit grading, fruit ripeness, fruit rot, fruit maturity, etc.) and applications to specific fruits. The fruits that appeared more frequently in the analysis resulted being apples (apples, organic apples, apple disease, apple classification, etc.), tomatoes (tomatoes, tomato grading, tomato maturity, tomato disease, tomato storage, tomato black mold disease, etc.), bananas (bananas, banana ripeness, etc.) and citrus fruits (oranges, lemons, citrus diseases, citrus quality, citrus decay, citrus sorting, citrus postharvest, citrus color index, etc.). A particular category of fruit and vegetable products that emerged from the analysis is that of sliced products (fresh-cut nectarines, mango slices, banana slices,

Table 2.2: Most discussed products and topics.

Topic/product	**Occurrences**	**Topic/product**	**Occurrences**
Meat	50	Beer	10
Fruits (specific)	49	Pizza	10
Fruits (general)	47	Cheese	10
Rice	31	Corn	9
Vegetables	26	Bakery products	8
Fish (specific)	23	Bread	8
Grains and legumes	23	Tea	7
Fish (general)	16	Chips	7
Wheat	13	Fresh-cut fruits and vegetables	6
Citrus	12	Spices	6
Nuts and dried fruits	12	Milk	5
Sweets	12	Frozen food	4
Animals (farming)	11	Oils	3
Eggs	11	Sauces	3

apple slices, fresh-cut apples, potato slices), highlighting the use and the importance of automated quality control with highly sensitive ready-to-eat products, characterized by a very brief shelf-life and high sensitivity to oxygen, for which thorough quality control is essential. To target the quality of agricultural products, issues such as fungi and diseases, the occurrence of browning and bruising, ripeness stage, and signs of general decay are generally observed. Moreover, in the category of agricultural products, a high occurrence of terms relative to wheat, rice, grains, and legumes can be observed. In the case of wheat, the monitored aspects include the characteristics of the kernels (size, weight, possible discoloration), as well as wheat diseases and wheat rust. Similar evaluations are carried out for rice, according to the occurrence of keywords such as rice category, rice grain quality, rice classification, rice weight estimation, rice disease, rice crops, rice leaf disease, and rice plant disease. Among the other grains and legumes, the monitored sorts include barley, cereals, chickpeas, and lentils among others.

With regard to the meat products, the keywords refer to three main categories: raw meat (e.g., pork, poultry, beef, loin), cooked meat, cured meat and charcuterie (e.g., pre-sliced pork ham, dry-cured ham, turkey ham, dry sausage, Iberian ham). General quality and safety control of meat products emerges as well, with the occurrence of terms such as meat safety, meat color change, meat adulteration, meat grading, etc. Among the keywords related to the evaluation of the quality of fish products, the most cited products include seafood and salmon, which are the fish products most processed on an industrial level and most widely consumed.

Among animal products, great attention is given to eggs, with the occurrence of keywords related to egg freshness, egg grading, egg storage, egg crack detection, and defective egg detection, among others. Other products evaluated through computer vision

Table 2.3: Examples of some of the main issues currently monitored in the food industry, divided by topic.

Topic	**Topic**	**Topic**
Fungi and diseases	Browning	Insects
Black mold	Browning	Insect detection
Fungus detection	Browning determinant	Insect identification
Incompletely closed glumes	Browning ratio	Insect monitoring
Stripe rust	Enzymatic browning	
Meat and animal products	Non-enzymatic browning	Other issues and defects
Blood spots	Bruising	Acrylamide
Bones detection	Bruising	Ripeness
Carcass defect	Bruise detection	Food adulteration and fraud
Intramuscular fat	Early bruises	Bacterial growth
Rigor mortis	Integrity	Impurity detection
Skin and fillet color	Seal inspection	Inclusions
Fruit decay	Seaming integrity	Stiffness
Post-harvest decay	Crack detection	Surface defect detection
Rotten fruit detection	Glass defects	Toxic substances
Stem end rot	Safety	Variety/impurity classification
Skin delamination	Intrusion detection	
	Motion detection	
	Skin detection	

appear to be milk and its derivatives, as demonstrated by the presence of terms related to milk adulteration, milk packing process, pasteurized milk, and whey solids, as well as several types of cheese.

Transversal analyses, independent of the type of product, target aspects that impact more specifically food safety, including the integrity of the packaging (seal inspection, seaming integrity, crack detection, glass defects), the safety of the environment in terms of intrusion and motion detection, skin detection to identify cases when the operators are not wearing gloves, as well as the detection of insects on site.

Besides the - mostly- raw materials discussed above, in this study, particular emphasis is given to applications in the field of processed food. Indeed, these categories could be those where vision-based techniques could be leveraged as "sensors" to be integrated within Industry 4.0 real-time monitoring and control frameworks, with the final aim of pursuing zero defect manufacturing. As an example, considering the automated quality controls of pizza, the analyses to be performed are particularly complex and diverse, because of the high variability of this type of product and the different processing stages vision-based controls could be applied to. The analyses carried out during the production of pizzas include, according to the keywords analyzed, those related to the pizza base, crust thickness, pizza sauce, pizza toppings, as well as the final stages of pizza packaging.

More in general, concerning the development and implementation of vision-based sensors in the food processing field, the main categories identified among the analyzed keywords, where some kind of vision control is already present, include bread products (e.g., bread, dough, breadcrumbs, bread baking, bread freshness), bakery products (e.g., biscuits, cookies, gluten-free products), pasta and noodles, chips (e.g., tortilla chips, potato crisps, potato chips, french fries, corn tortillas), dairy products, beer, and pizza.

Conclusions

In this paper, a bibliometric analysis of the applications of computer vision techniques for quality control in the food industry was carried out on 742 records retrieved from the Scopus database. The goal of the analysis was to identify the main research themes currently discussed in the literature, as well as to outline the most relevant food products and quality issues evaluated. Moreover, the aim was to identify applications to processed foods, where vision-based techniques could be leveraged as "sensors" for real-time monitoring and control of food industry processes.

Based on the keyword analysis, it can be seen that most papers on the topic, to date, deal with technologies, methods, and systems utilized to carry out quality evaluations. Well-established terms in the literature include standard methods of image analysis and image processing, as well as some artificial intelligence techniques. In the last years, thanks to rapid technological development, there was a strong increase in the use of terms related to more sophisticated artificial intelligence techniques, as well as other Industry 4.0 technologies such as Internet of Things and robotics. From the analysis of the most frequently used keywords, it can be also deduced that the food industry sector where computer vision for quality control is applied the most nowadays is the agricultural one. This is confirmed by the results of the thematic analysis, where the prevalent food categories identified are fruits, vegetables, and grains. Among these, an interesting category is represented by fresh sliced fruits, particularly prone to browning and decay. Another category of food products often evaluated with automated quality control techniques is that of animal products, with several papers dealing with meat and fish products, as well as the quality control of milk and eggs. Other relevant applications target processed foods, including particularly complex ones such as pizza with toppings.

The variety of possible applications, that obviously go well beyond those discussed in the literature, highlights the flexibility of computer vision techniques for quality control, and the potential application to several food industry processes. The increase in the use and development of these automated techniques could have an enormous impact on the food industry and supply chains: by substituting or complementing human controls, it is possible to increase production rates without compromising food quality, as machine controls are performed in extremely short times compatible with the industrial production. Moreover, by reducing the probability of the occurrence of unidentified defects, it is possible to reduce the number of customer complaints, safety risks, and product recalls.

As demonstrated by the keyword analysis, there is high potential for research in the field, with several trendy topics deserving of further investigation to advance the field of computer vision applied to food safety and quality control. Probably the most relevant, and wide, opportunity for future research activities, is related to the practical applications of these innovative tools and techniques to real case studies and industrially

processed food products. While the products addressed in the literature are indeed a lot, many processed foods appear sporadically and could benefit from the implementation of innovative control methods and techniques, in line with Industry 4.0 concepts.

Chapter 3

Simulation for the design and characterization of industrial plants

Contents

3.1 Introduction

This section of the thesis presents several case studies where simulation — particularly Computational Fluid Dynamics (CFD) — was crucial for investigating, characterizing, optimizing, and even designing industrial plants and devices.

The section is divided into two main parts:

- Simulation for the characterization of plants
- Simulation for the design and revamping of plants

These sections include a total of six case studies, most of which conducted in collaboration with industrial partners. The studies demonstrate the flexibility of CFD and numerical simulation in food industry applications, as well as the significant impact and benefits that these numerical techniques can bring.

3.2 Computational Fluid Dynamics

Computational Fluid Dynamics (CFD) is a branch of fluid mechanics that uses numerical methods and algorithms to simulate and analyse fluid flows. By iteratively solving the governing equations of fluid dynamics in an appropriately discretized domain, CFD allows to predict how fluids, both liquids and gases, will behave under various conditions.

CFD finds application across several industrial sectors, playing a particularly relevant role in those where fluid behaviour is essential for the process outcomes such as, for example, aerospace, automotive, and food industry.

A typical CFD simulation workflow consists, generally, of the following steps:

- Problem definition: before proceeding with the simulation settings, it is crucial to correctly identify the problem, the phenomena involved, the boundary conditions, and the parameters of interest to monitor. One of the most critical aspects is related to the selection of appropriate flow characteristics.

  A fundamental decision that must be made is that between steady or transient simulation. Steady-state simulations assume that flow properties do not change over time (e.g., in regime conditions), making them computationally less expensive. Transient simulations, on the other hand, capture time-dependent behaviour and are necessary for dynamic conditions, unsteady flows, and oscillatory phenomena. Another key consideration is whether the flow is compressible or incompressible. Compressible flows exhibit significant density variations due to pressure and temperature changes, while incompressible flows assume constant density, which is a valid approximation for most low-speed applications. In compressible flow simulations, a density-based solver is typically used, whereas for incompressible flows, a pressure-based solver is more appropriate

  Additionally, it is crucial to identify the relevant governing equations and physical models that will be used in the simulation. This includes determining whether to incorporate heat transfer, multi-phase flow, or chemical reactions.

  Moreover, for many practical applications, the modelling of turbulence plays a crucial role in accurately predicting flow behaviour. To this end, based on the value of Reynolds number, it is necessary to evaluate whether the flow is laminar, transitional, or turbulent. In case the flow is turbulent, or falls in the transition region, turbulence modelling is required, and selecting an appropriate approach such as for instance RANS (Reynolds-Averaged Navier-Stokes), LES (Large Eddy Simulation), or DNS (Direct Numerical Simulation) becomes important. The choice of turbulence model significantly impacts both accuracy and computational cost, making it a crucial consideration in the problem definition stage. In industrial

CFD applications, the most commonly used approach is RANS due to its computational efficiency, and ability to provide reasonably accurate results for a wide range of applications. In particular, RANS approach is typically used for steady-state simulations, while LES and DNS are more suitable for transient cases and applications requiring higher precision. In addition, hybrid models such as Detached Eddy Simulation (DES) and hybrid RANS-LES approaches are increasingly being adopted in cases where fully resolving turbulence is not feasible, as they combine the computational efficiency of RANS with the accuracy of LES.

By carefully assessing these factors at the beginning of the CFD workflow, the simulation can be set up in a way that balances accuracy, computational efficiency, and correspondence to real-world conditions.

- Generation of the geometry: it is necessary to model the domain to be used for the simulation, which consists of the domain where the fluid flow occurs. For example, to simulate flow inside a pipe, the geometry of the domain would consist of the inner 3D cylinder, neglecting, in most cases, the modelling of the solid wall. Non essential geometry details could be simplified at this stage to reduce the computational cost of the simulation. To this end, it is good practice to perform preliminary evaluations, to assess that indeed the removal of the details did not significantly impact the simulation results. Based on the obtained simulation results, it may be necessary to make some adjustments to the geometry with an iterative approach.

- Generation of the mesh: the numerical solution of the differential equations governing fluid motion requires an appropriate discretization of the domain. This process transforms the differential equations into a system of algebraic equations, which are solved at a finite number of discrete points in space and time, allowing for an approximate solution of the fluid behaviour.

  Meshes can generally be classified as "structured", with an organized connectivity pattern and efficient for simple geometries, or "unstructured", offering greater flexibility for complex geometries by using a mix of elements such as tetrahedrons, hexahedrons, prisms, or polyhedra. In many cases, hybrid meshes are used to balance computational efficiency and accuracy by combining structured and unstructured regions. Moreover, by combining or agglomerating tetrahedral elements, polyhedral meshes can be generated, effectively reducing the total element count while maintaining accuracy. These meshes, with multiple faces per element, can lead to improved numerical stability, better flow resolution, and faster convergence compared to tetrahedral meshes.

  Mesh quality plays a crucial role in the accuracy and stability of CFD simulations. Indeed, poor-quality elements can lead to numerical errors, slow convergence, and

unstable results. Common metrics for evaluating mesh quality include aspect ratio, skewness, and orthogonal quality. To ensure numerical accuracy, mesh sensitivity analyses should be performed, verifying that further mesh refinement does not significantly alter the solution (i.e., the solution is independent of the discretization). The number of elements and their type significantly affect computational cost and memory usage, making mesh optimization a critical aspect of CFD simulations.

- Definition of the materials: this stage involves the specification of the physical properties of the fluid or solid domains involved in the analysis. These properties typically include density, viscosity, thermal conductivity, specific heat, and other relevant parameters depending on the simulation type and the included models (e.g., compressible or incompressible flow, multiphase flow, or heat transfer analysis).

  Accurate material definition is essential to ensure realistic modelling of fluid behaviour, turbulence effects, and energy transport. In commercial CFD software, the properties of several materials can be found in built-in databases. These properties, however, can be modified by user, to reflect the requirements of specific applications and introduce possible dependencies on other variables, such as temperature. In the case of food engineering applications, this is particularly important, since most products present complex rheological behaviour and the properties are strongly dependent on the temperature [3].

- Definition of the initial and boundary conditions: this step is essential for accurately reproducing the application of interest through simulation. It involves the definition of key parameters such as flow inlets and outlets, thermal boundary conditions, and other relevant constraints. Common types of boundary conditions include velocity inlets, pressure outlets, wall conditions, and symmetry planes. Thermal boundary conditions, such as fixed temperature, heat flux, or convection, are essential to conduct heat transfer simulations. Additionally, initial conditions define the starting state of the simulation, including velocity, pressure, temperature, and turbulence parameters. These conditions are particularly important for transient simulations, where the solution evolves over time.

  Proper selection of boundary and initial conditions significantly impacts simulation stability, and convergence. Moreover, it is essential to guarantee adequate correspondence between the model and the real application.

- Iterative solution of the governing equations: after defining appropriate solver and numerical schemes, the CFD software iteratively solves the governing equations of fluid flow and of the other involved phenomena within each cell of the mesh until the solution converges, stabilizes, or -ideally- both.

With "solution convergence" it is meant that the normalized residuals (errors in numerical solution) reach values below a defined threshold. The correctness of the results for a giving problem, however, strongly depends on the problem definition. The correspondence between the simulation results and real-world applications should be always checked with appropriate tests, in order to validate the developed model.

- Post-processing of the results: this step includes the analysis of the results to draw meaningful conclusion about the system behaviour. Once the simulation is complete, this step is essential for interpreting the results to draw meaningful conclusions about the system's operation. This involves visualizing flow fields, extracting numerical data, and validating results against experimental or analytical benchmarks. Common visualization and analysis approaches include contour plots, streamlines, vector fields, and iso-surfaces. Numerical values can be used to generate plots, or exported for further analyses. Ensuring proper post-processing is particularly relevant, as it allows to identify significant trends, detect anomalies, and refine the model if necessary.

- Validation: this is a critical step in CFD (and generally in all simulation techniques) as it allows to confirm the accuracy and reliability of the simulation setup and results. It involves comparing numerical results with experimental data, analytical solutions, or benchmark cases to confirm that the chosen simulation approach, boundary conditions, and numerical methods are correctly implemented. In fact, proper validation ensures that the simulation outcomes can be effectively used for engineering decision-making.

The equations governing the behavior of a fluid consist of three fundamental equations, forming a system of partial differential equations known as the Navier-Stokes equations. These three equations describe the conservation of mass, momentum, and energy in fluid dynamics, forming the foundation of CFD and fluid mechanics analyses. According to the Theory guide of ANSYS Fluent [34], the commercial software used in most of the works included in the thesis, the equations are defined as follows.

$$\frac{\partial \rho}{\partial t} + \nabla \cdot (\rho \vec{v}) = 0 \tag{3.1}$$

$$\frac{\partial}{\partial t}(\rho \vec{v}) + \nabla \cdot (\rho \vec{v} \vec{v}) = -\nabla p + \nabla \cdot (\overline{\overline{\tau}}) + \rho \vec{g} + \vec{F} \tag{3.2}$$

$$\overline{\overline{\tau}} = \mu \left[\left(\nabla \vec{v} + \nabla \vec{v}^T \right) - \frac{2}{3} \nabla \cdot (\vec{v} I) \right] \tag{3.3}$$

$$\frac{\partial}{\partial t}(\rho E) + \nabla \cdot (\vec{v}(\rho E + p)) = \nabla \cdot (k \nabla T) - \nabla \cdot (\overline{\overline{\tau}} \vec{v}) + S_h \tag{3.4}$$

$$E = h - \frac{p}{\rho} + \frac{v^2}{2} \tag{3.5}$$

The continuity equation for mass conservation is presented in Equation 3.1, where t is time, ρ is the density of the fluid, and $\vec{v}$ is the overall velocity vector. Conservation of momentum is described by Equation 3.2, where p is the static pressure, $\rho\vec{g}$ is the gravitational body force, and $\vec{F}$ vector considers external body forces. The stress tensor $\overline{\overline{\tau}}$ is defined in Equation 3.3, where μ is the molecular viscosity and I is the unit tensor. Since the problem includes heat transfer, the energy equation is solved and defined as expressed in Equation 3.4, where the total energy E is defined as in Equation 3.5, k is the thermal conductivity of the material and h is the enthalpy. The source term S_h represents external heat sources, such as radiation, chemical reactions, or Joule heating. The energy equation is extremely relevant in cases involving heat transfer, compressible flows, or temperature-dependent material properties. On the other hand, in incompressible isothermal flows, where temperature variations have no significant impact, this equation can be omitted to reduce computational cost.

The governing equation of the additional phenomena present in the case studies, as well as the detailed explanation of the setting and approaches used, are presented and discussed in the dedicated sections.

The most commonly used numerical methods for solving fluid dynamics equations are Finite Difference Method (FDM), Finite Element Method (FEM), and Finite Volume Method (FVM).

The Finite Difference Method is a well-established numerical technique for approximating the solutions of differential equations by discretizing derivatives through finite difference approximations. This method involves dividing the computational domain into a structured grid, and replacing continuous derivatives with discrete differences between function values at neighbouring nodes. This technique is particularly advantageous for problems involving structured meshes, due to its computational efficiency and ease of implementation. By defining appropriate boundary conditions, the governing partial differential equations are reformulated into a system of algebraic equations, which can be conveniently solved numerically.

The Finite Element Method is another numerical technique for solving partial differential equations, often used in problems involving complex geometries and multi-physics interactions. It discretizes the computational domain into smaller subdomains called finite elements, using shape functions to approximate the solution over each element.

Finally, the Finite Volume Method is a numerical approach for solving partial differential equations by discretizing the computational domain into control volumes. Unlike FDM, which approximates derivatives at discrete points, and the FEM, which reformulates equations in a variational form, FVM directly applies the integral form of conservation equations to each control volume, ensuring local conservation of mass, momentum,

and energy. This, and the fact that FVM efficiently handles even complex geometries and unstructured grids, makes FVM particularly well-suited for CFD applications. In particular, FVM is used in leading CFD software, such as ANSYS Fluent, adopted for the studies contained in this thesis.

3.3 Simulation for the characterization of food industry plants

This first section includes simulation-based valuations of ohmic heating (a non-conventional thermal treatment), non-thermal methods based on UV-C radiation for decontaminating food fluids, characterization and residual useful life estimation of a cyclone-bag filter for milling applications, and simulations of sloshing within beverage cans after filling on rotary machines.

With just four case studies, it is evident how flexible CFD and numerical methods can be for characterizing food industry plants and gaining a deep understanding of their operations.

Each case presented in this section is an innovative study, either in terms of the specific process considered, the simulation and analysis approach adopted, or both. The contribution of each application is detailed in its respective section.

All four projects are currently ongoing, with additional evaluations and experimental campaigns underway to further support industrial development and contribute to the scientific literature in this field.

3.3.1 Characterization of a UV-C reactor for fruit juices

The research in this chapter has been included in the peer-reviewed article [35] *Solari, F., Lysova, N., Martelli, F., Volpi, A., Bottari, B., and Montanari, R. (2024). Performance assessment, through numerical simulation and experimental evaluation, of a thin-film ultraviolet reactor for the processing of fruit juices. International Journal of Food Engineering. https://doi.org/10.1515/ijfe-2023-0033*
and in the conference paper [36] *Montanari, R., Volpi, A., Solari, F., and Lysova, N. (2022). Performance assessment, through CFD simulation, of an ultraviolet reactor for the processing of fruit juices. Proceedings of the 8th International Food Operations and Processing Simulation Workshop (FoodOPS 2022). https://doi.org/10.46354/i3m.2022.foodops.010.*

The authors would like to express their gratitude to Paolo Manghi, Fabrizio Giovati, Francesco Stocchi and Pietro Pasini of the company Parmalat S.p.a. (Lactalis Group) for their crucial support in conducting the experimental tests.

Abstract

The study presents a numerical approach to investigate the performance of a thin-film ultraviolet reactor in treating three different fruit juices (apple, orange and pineapple) with UV-C radiation, under six flow rate conditions. Minimum, average and maximum doses were calculated for each configuration, by integrating, over time the irradiance over one thousand different streamlines. The presented approach allows for calculating the dose distribution achieved, thus assessing both the fulfilment of regulatory requirements and the uniformity of the treatment.

Experimental tests were finally performed on both apple and orange juice, with a flow rate of 80 L/h. For apple juice, more than 3 log_{10} CFU/mL reductions were obtained on *Escherichia coli* ATCC 11229, while, for orange juice, a negligible reduction (0.05 Log CFU/mL) was achieved. These results, according to biodosimetry data from other studies, correspond to UV-C dose distributions that confirm those calculated.

Introduction and state-of-the-art

Consumption of fruit juices, both as a finished product and as an ingredient for other recipes, has been constantly increasing worldwide in recent years. Fruit juices are a source of several nutrients that have important beneficial effects on human health (vitamins, antioxidants, minerals, etc.). On the other hand, they may also contain pathogenic and spoiling microorganisms, resulting from the normal microflora contaminating the raw material or the product at some point of the production process, which can affect the safety of juice or lead to its rapid deterioration [37]. Since most juices are classified as high-acid foods (pH<4.5), in which *Clostridium botulinum* spores are unable to germinate, a pasteurization treatment is sufficient to ensure the commercial sterility of the food. Despite this, foodborne outbreaks caused by the ingestion of contaminated fruit juices have occurred in recent years [38]. These phenomena are related to the development of more resistant or acid-adapted microbial strains that are able to survive normal heat treatments [39–41]. For this reason, regulatory organizations, such as the Food and Drugs Administration, have introduced new mandatory requirements for juice manufacturers to ensure consumer safety. Specifically, the FDA has mandated a minimum treatment resulting in at least a 5-log_{10} reduction of the "most resistant microorganism of public health significance that is likely to occur in the juice" [42]. Very intense heat treatments, however, can damage the nutritional content of fruit juices, which consist mainly of thermolabile compounds. In recent years, consumer demand has increasingly shifted toward products with organoleptic and sensory characteristics as similar as possible to those of fresh products. As a consequence, the interest in non-thermal treatments has grown more and more, as evidenced by the increasing number of scientific publications on the subject [43–48].

A comprehensive review of non-thermal pasteurization treatments that can be used on fruit juices without altering their nutritional and sensory characteristics was performed in [49]. The authors have cited high hydrostatic pressure, ultraviolet light, $UV - TiO_2$ photocatalytic oxidation, pulsed electric fields, pulsed light, ultrasound, ozone, cold plasma, ohmic heating, and high-pressure carbon dioxide methods.

Among the non-thermal pasteurization treatments, ultraviolet light has attracted considerable interest over the years because it achieves high levels of inactivation of microorganisms, preserving nutritional and sensory properties, and significantly reducing energy consumption compared with traditional treatments [50]. As a result of the many studies conducted, UV radiation treatment has been approved in the United States as an alternative treatment to thermal pasteurization for fresh juices. A minimum dose of 400 J/m^2 at the sterilizing wavelength (254 nm) must be achieved in all parts of the products to ensure the right level of reduction [51, 52]. In Europe, on the other hand, to date, there is still no specific regulation. This point highlights that further studies

are required to arrive at a deeper understanding of the technology and, consequently, at an increasingly conscious use of the same. The UV pasteurization process uses light radiation in the UV-C region, which has a wavelength range between 200 nm and 280 nm, to inactivate microorganisms. In industrial applications, 254 nm wavelength is generally adopted. At this wavelength the radiation penetrates the membranes of microorganisms and is absorbed by their DNA, causing their inactivation.

This radiation, while having an effective bactericidal effect, is characterized by a low penetration rate through almost all materials. The ability of a material to absorb a given light radiation is quantified by the absorption coefficient, which, through the Lambert-Beer law, correlates the amount of light absorbed by a material to the concentration and thickness of the material itself. In the specific case of UV radiation for non-thermal pasteurization treatments, the absorption coefficient at 254 nm is referred to [53]. For materials having low absorption coefficients, such as water with no or few suspended elements and filtered air, UV radiation manages to be effective even on fluid thicknesses of a few centimetres. In these contexts, the technology has been extensively studied and there are numerous industrial applications. Another context in which the technology is well known and has been used for several years is the treatment of surfaces and packaging materials. However, the application of UV is restricted for certain beverages due to the presence of coloured compounds and suspended solids which interfere with the penetration of UV light and reduce the antimicrobial capacity of this treatment. For these beverages, although numerous studies can be found in the literature, industrial applications are still very scarce. The main reasons behind this poor diffusion can be found in both the lack of specific regulations in some parts of the world and the high dependence of treatment performance on product characteristics, such as the type and concentration of solutes and suspended solids. This high sensitivity requires an in-depth study to be carried out for each application context. Indeed, the results presented in the scientific literature on the subject, tend to be very specific and dependent on the context studied and, consequently, difficult to generalise.

In [54], for example, the authors have focused their study on the application of the Dean Vortex technology on pineapple juice and have found that a dose of 13.75 mJ/cm^2 was necessary to achieve a 5-log_{10} reduction in *Salmonella typhimurium*. In [55] the authors have tested the same technology on naturally cloudy apple juice, identifying *Lactobacillus plantarum* BFE 5092 and *Escherichia coli* DH5α as target microorganisms. They have concluded that doses of 1.9 and 7.7 kJ/L are required to achieve 5-log_{10} and 6-log_{10} reductions, respectively.

A thin film reactor (CiderSure 3500-B device), equipped with eight low-pressure lamps and working with a juice thickness ranging between 0.21 mm and 0.48 mm, has been tested in [56]. The authors have obtained a reduction of 1.91-log_{10} and 1.4-log_{10} in the total plate count and the yeast and mould count, respectively, by applying a dose of

21.52 mJ/cm^2.

In [57] a simple reactor geometry, characterized by a single lamp inserted inside a corrugated spiral steel tube, was considered. The authors have treated guava-pineapple juice and orange juice, using a system consisting of 10 reactors in series. On guava-pineapple juice, they have provided a dose of 1377 J/L, which resulted in a reduction of 3.31-log_{10} in aerobic plate count and of 4.48-log_{10} in yeast and mould count. On orange juice, which is characterized by a higher absorption coefficient, they have provided a dose of 1607 J/L, which resulted in a reduction of 0.3-log_{10} in both aerobic plate count and yeast and mould count. In [58] the authors have obtained higher reductions when treating orange juice: 3-log_{10} reduction in aerobic plate count and 2.4-log_{10} reduction in yeast and mould count after a dose of 123 mJ/cm^2. Their experimental equipment consisted of a 50 mm diameter and 450 mm long glass tube, fixed vertically, equipped with a 6 W UV-C lamp enclosed in a quartz tube, on which a thin film of orange juice flows by gravity. The thickness of the thin film was in the range of 0.21 mm to 0.48 mm.

From the studies cited, it is clear that the process performance is highly dependent on several parameters, such as the type of juice, its physical-chemical properties, the target microorganism, and the characteristics of the experimental equipment. These parameters can be summarized as follows: process parameters (flow behaviour, UV light intensity), product characteristics (absorption coefficient, suspended solids), and interaction between process parameters and product characteristics [59]. Another aspect that clearly emerges from the studies in the literature is the inconsistency of the results due to the lack of a standardized procedure for evaluating the performance of a UV reactor. Furthermore, the cited studies, while providing indications on the average dose applied, often provide no insight into the treatment uniformity. Several authors [56, 60, 61] have pointed out that excessive exposure to UV radiation can cause undesirable alterations in foods, such as ascorbic acid losses, furan formation or decrease in carotenoids, phenolic acids and antioxidant capacity. In [62] the formation of furan in apple juice at radiation doses of 30000 J/m^2 was addressed. Thus, while it is important to provide to every point of the product the minimum dose required to obtain the desired logarithmic reductions in the target microorganism, it is also important to prevent the product from excessive exposure to radiation.

To this end, Computational Fluid Dynamics (CFD), by allowing the detailed resolution of both the flow and irradiance at each point of the domain, can be very useful in evaluating the performance of a reactor in terms of minimum, maximum and average dose provided. CFD has been widely used in recent years to evaluate the performance of UV treatments [63–65]. To date, however, there are still few studies concerning the UV treatment of opaque fluids [36, 66–68].

In this study, we use a simulation approach to investigate the performance of a stainless steel UV-C reactor in treating three fruit juices, i.e., apple, orange and pineap-

ple. A simulation campaign was carried out, considering six flow rates and evaluating the performances of the reactor in terms of dose distribution under different operating conditions. An experimental procedure was then conducted to validate the simulation results and evaluate the microbial reduction that can be achieved thanks to the UV-C treatment in the reactor considered.

The results obtained show how the performance of the simulated device, characterized by a simple structure without any hygienic criticalities and low construction costs, is strongly influenced by both the characteristics of the juice and the flow rate.

The proposed approach presents the following advantages:

1. it allows accurate prediction of the performance achievable under different operating conditions, allowing them to be adapted, a priori, to the juice and reactor characteristics, thus allowing more accurate control over the process itself;

2. it allows a comprehensive evaluation of the system performance in terms of dose distribution;

3. it allows for highlighting the main criticalities of the reactor, thus suggesting the geometrical and constructive aspects on which to intervene to optimize its performance.

Finally, our study demonstrates how CFD simulation allows for a deeper understanding of the process and, as a result, for greater control over the process itself.

Materials and methods

Physical characterization of the juices

To accurately reproduce the behaviour of the fruit juices within the reactor, proper rheological characterization of the products is necessary, as well as the quantification of the interaction between the juices and UV-C radiation at 254 nm. For this purpose, absorption coefficients were evaluated at the sterilizing wavelength (253.7 nm). The data reported in [53] was used for pineapple juice. Apple juice and orange juice, which were used for experimental validation, were characterized by means of spectrophotometry (Aquamate - Thermo Electron Corporation). Both juices were characterized at three different dilutions (1/1, 1/10 and 1/100 for apple juice, and 1/100, 1/500 and 1/1000 for orange juice) and the absorption coefficient was calculated as the average of the values obtained. Also viscosity was measured using a concentric cylinder geometry (Couette cell) mounted on an ARES rheometer (Ta Instruments, New Castle,DE, USA). For pineapple juice, which was not used in the validation test, the values reported in [69] for dynamic viscosity were considered. The data are summarized in Table 3.1.

Table 3.1: Dynamic viscosity and absorption coefficients for the three fruit juices

Fruit juice	**Dynamic viscosity [Pa s]**	**Absorption coefficient [cm^{-1}]**
Orange	0.04	48
Pineapple	0.053	73
Apple	0.002	26

Ultraviolet pasteurizer

The study focused on a type of reactor that meets the following requirements: (*i*) cost-effectiveness (from both investment and operating costs points of view), (*ii*) hygiene (ease of cleaning) and (*iii*) flexibility (possibility of being applied to different types of products and a wide range of flow rates).

Therefore, a solution characterized by a simple structure, free of critical constructional and hygienic issues, and modular, i.e., a solution that would allow the installation of multiple devices in series, was adopted. It is evident that in this type of configuration, laminar flow conditions occur inside the reactor, while the FDA requires that the dose should preferably be applied in a turbulent flow regime. With regard to that, it should be pointed out that in a standard industrial application, the flow rate of juice to be treated is much higher than what can be treated with the reactor considered. It is therefore necessary to install several reactors in series. In such a configuration in the transition from one reactor to another, the fluid is subjected to a sudden discontinuity in flow field conditions (180-degree change in flow direction) that induces a strong mixing of the fluid, which consequently increases the uniformity of the treatment.

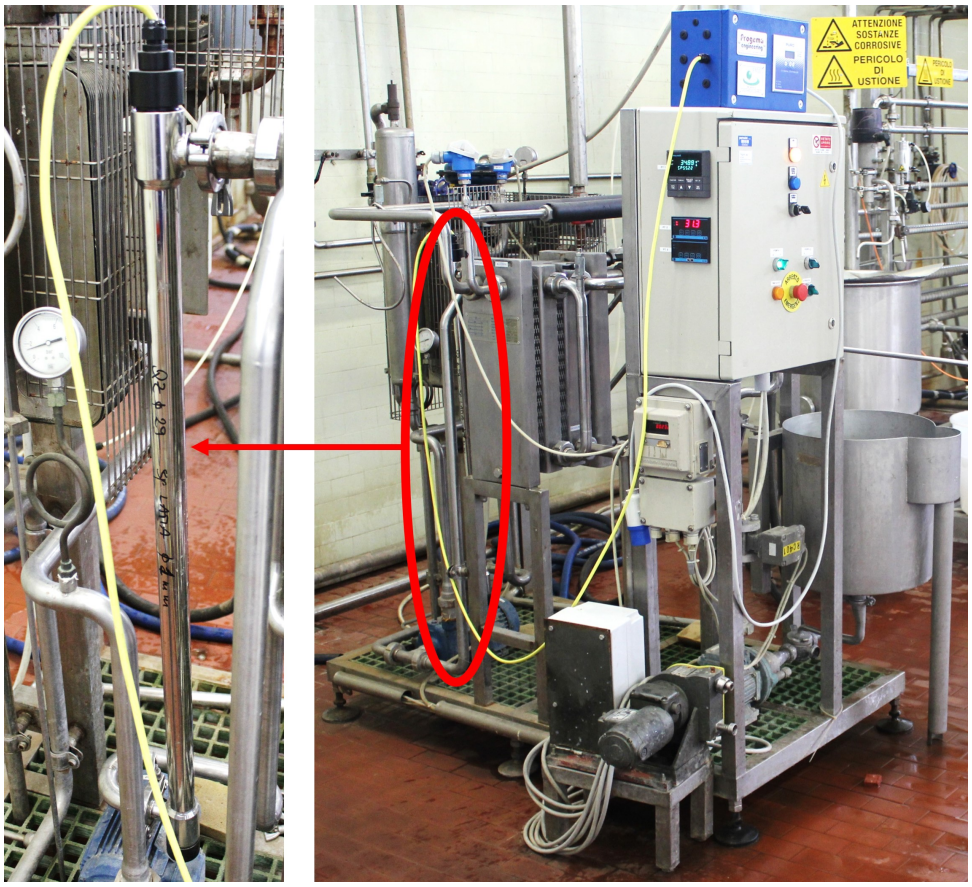

Figure 3.1: Experimental apparatus for microbiological tests.

Hence, even with the use of such a simple configuration, through proper plant sizing and configuration, it is possible to meet the FDA requirements.

A tubular, stainless steel single-lamp reactor was analyzed. The device consists of an amalgam UV-C lamp, having a total power of 110 W (35 W at 254 nm), enclosed by a quartz tube having an external diameter of 28 mm that prevents direct contact between the lamp and the fluid, and then mounted coaxially to the stainless steel reactor, having a length of 850 mm and an internal diameter of 31 mm. The thickness of the thin juice film irradiated, therefore, is 1.5 mm. The pilot plant and its 3D geometry modelled in Ansys SpaceClaim [70] are presented in Figure 3.1 and Figure 3.2, respectively.

Flow field and irradiance simulation

Ansys® Release 2022 R2 [34, 71] was used for the numerical modelling of the reactor. A tetrahedral mesh was used to discretize the domain. To accurately reproduce the process, the mesh size was determined starting from the estimation of the viscous sublayer thickness at the walls, as well as the light radiation gradient close to the quartz tube surface. The Reynolds number was calculated for all the configurations, resulting in values always lower than 2100, thus indicating laminar flow conditions. The viscous sublayer thickness, δ, was estimated at a dimensionless wall distance $y+ = 5$ (eq. 3.6).

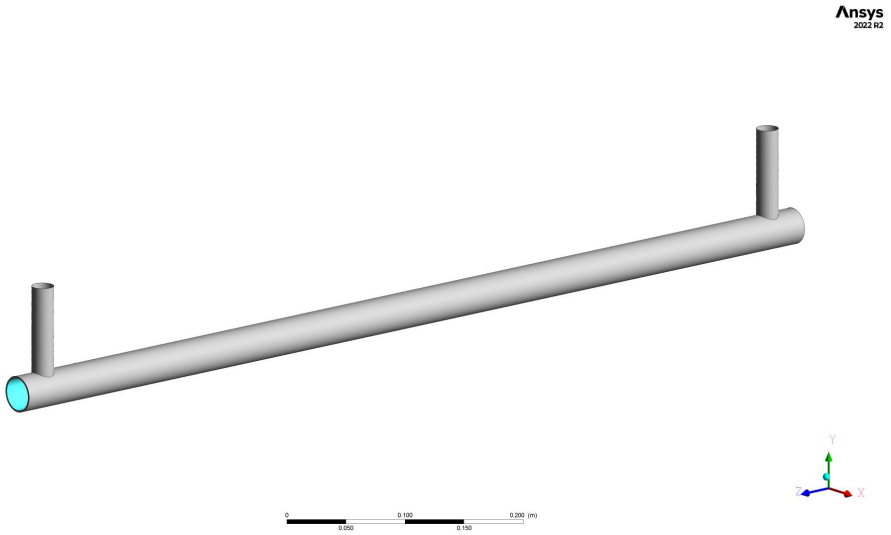

Figure 3.2: Geometry of the reactor.

$$\delta = \frac{5\mu}{\sqrt{\rho\tau}} \tag{3.6}$$

Where τ is the wall stress and can be estimated from the friction factor, C_f , which, in the case of laminar flow can be calculated with the Hagen-Poiseuille law (eq. 3.7 and 3.8):

$$\tau = \frac{1}{2} \cdot \rho \cdot v^2 \cdot C_f \tag{3.7}$$

$$C_f = \frac{16}{Re} \tag{3.8}$$

To be conservative, the calculation was performed at the highest flow rate and for the least viscous fluid (apple juice).

The UV irradiance was computed using the Discrete Ordinates (DO) radiation model which is based on the Beer-Lambert law [72]. This model is based on the discretization of the fluid domain into a finite number of discrete solid angles where the radiative transfer equation is solved. In this study, to achieve good accuracy, an angular discretization of 5 x 5 for the theta and phi divisions, and 3 x 3 for theta and phi pixels were set up. Theta and phi divisions define the number of control angles used to discretize each octant of the angular space, while the pixels, for both theta and phi, are used to control the pixelation that accounts for any control volume [72].

The mesh sizing was determined taking into account both the velocity gradient and the UV-irradiance gradient.The gradient of the UV irradiance was estimated by calculating the distance from the quartz sleeve at which the radiation was zero. Again, to be conservative, this was calculated for the juice with the highest absorption coefficient (i.e., pineapple juice). In this case, the UV irradiance was found to reach the value of 0 at a

distance from the quartz sleeve of about 0.7 mm. On the other hand, the viscous sublayer thickness resulted in 0.3 mm. The minimum mesh size at the wall was set considering that, to reconstruct in detail the viscous sublayer, at least 3 mesh elements must be within it. Moreover, to accurately calculate the radiation gradient, at least 10 mesh elements were included within the calculated distance of 0.7 mm. To this end, a boundary layer mesh, constituted by 10 layers, was generated, setting the height of the elements in contact with the quartz sleeve at 0.03 mm, with a growth factor of 25% for subsequent mesh layers. In order to ensure the accuracy of the results, the orthogonal quality of the mesh elements was evaluated. It is calculated using the vector normal to the face, for each face of the mesh element. To obtain acceptable results, the orthogonal quality must be, for all elements, greater than 0.15. In this study, the minimum orthogonal quality was above this threshold value, thus the mesh quality was considered acceptable. In Figure 3.3 a detail of the mesh on a longitudinal section plane is represented.

The inlet boundary condition was defined by setting the fluid velocity, calculated as the volume flow rate divided by the inlet area, while a relative pressure of 0 Pa was specified at the outlet section. The no-slip condition was set on all reactor surfaces. Radiation intensity per unit area (468.1 W/m^2), calculated as the ratio between the lamp power at the wavelength of 254 nm (35 W) and the surface area of the sleeve (0.075 m^2), was specified for the quartz surface.

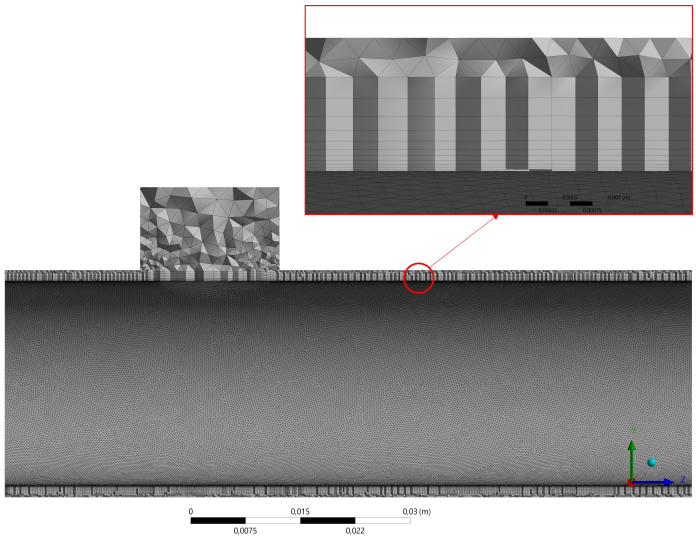

Figure 3.3: Discretization of the computational domain, with a detail showing the boundary layer mesh created to accurately calculate velocity and irradiance gradients close to the quartz sleeve.

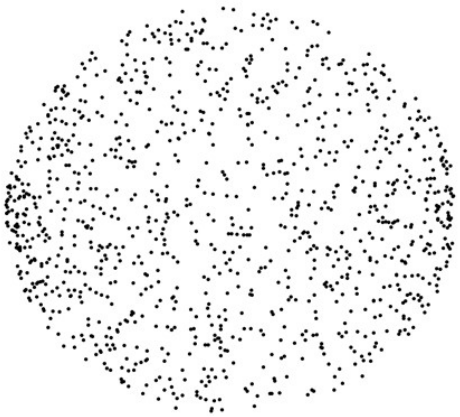

Figure 3.4: Particle distribution over the inlet section.

The trajectories of one thousand fluid particles, uniformly distributed over the inlet section (Figure 3.4), were calculated using the discrete phase model (DPM), based on a Lagrangian approach. Particles were considered to have the same density as the juice and, therefore, their size distribution becomes irrelevant and consequently has not been defined. Finally, the UV dose distribution was computed by integrating the light intensity along each trajectory over time. The advantage achievable from installing multiple reactors in series was also evaluated. Particle tracking results, in terms of particle coordinates on the outlet section from the first reactor, were used as particle coordinates at the inlet section of the second reactor, and so on.

Experimental campaign

To validate the simulation results, experimental tests were conducted on the UV-C reactor described in previous sections, with a flow rate of 80 L/h and without recirculation of the treated product. The experimental campaign comprised two days of tests, conducted with a one-week interval between them. The tests were performed by irradiating with UV-C two different fruit juices contaminated in a controlled manner, without supplying heat to the products. On each day of testing, 40 L of each juice were contaminated in a controlled manner. Before and between the tests on the two different juices, the plant was washed by recirculating for 15 minutes a disinfectant solution of hydrogen peroxide and peracetic acid at 50°C, and then it was rinsed with clean water. To ensure repeatability, treated and untreated juices were sampled in duplicate.

Apple and orange juices were selected as investigated substrates. The tests were performed starting from apple and orange juice concentrates at 70 and 65 Brix degrees, respectively. The concentrates were reconstituted through dilution with reverse osmosis water to achieve the standard concentration of pure undiluted juices, i.e., 11.2 Brix. The two juices were characterized by pH values of 3.73 (apple) and 3.53 (orange).

Before the experimental tests, *Escherichia coli* ATCC 11229, a non-pathogenic strain for humans, was revitalized twice in TSB (Tryptic Soy Broth) (Oxoid, Milan, Italy) (inoculum of 3% v/v) incubated for 16 h at 37 °C under aerobic conditions. It was then inoculated in fresh TSB (3% v/v) and incubated for 15 h at 37 °C, to obtain a bacterial concentration of 8.5 log_{10} CFU /ml. After centrifugation (10000 rpm for 10 minutes at 4 °C), the cells were collected, washed twice in Ringer solution (Oxoid) and suspended in sterile bidistilled water.

Apple and orange juice (40 L) were then inoculated individually with each bacterial suspension to obtain an estimated *E. coli* concentration of 6 log_{10} CFU/ mL in each sample. Samples of untreated juice, i.e., control samples, were collected to evaluate the initial microbial load. The contaminated product was then loaded into the plant by pouring it into the dedicated tank to start the irradiation procedure. Then after 10 minutes of treatment with UV-C, two treated samples were collected as summarized in Table 3.2. The samplings were carried out in proximity to a Bunsen burner to minimize the risk of contamination from the surrounding environment. The replicates of the samples were collected within a few minutes interval. Consequently, the distinct juice samples were subjected to identical treatment conditions, including the same flow rate and radiation dose.

Microbiological analyses

The absence of coliform bacteria in freshly prepared juices was verified by performing counting on Chromocult Coliform Agar (Merck, USA).Microbial concentration was

Table 3.2: Experimental and sampling procedure

Day	Juice	Time	Operation
1		11:43	Collection of 2 control samples
	Apple	11:50	Loading of the contaminated product
		12:01	1° sample of treated juice
		12:04	2° sample of treated juice
	-	12:10	Washing and rinsing of the plant
		12:57	Collection of 2 control samples
	Orange	13:02	Loading of the contaminated product
		13:13	1° sample of treated juice
		13:16	2° sample of treated juice
	-	13:20	Washing of the plant
2		11:30	Collection of 2 control samples
	Apple	11:32	Loading of the contaminated product
		11:43	1° sample of treated juice
		11:46	2° sample of treated juice
	-	11:50	Washing and rinsing of the plant
		12:49	Collection of 2 control samples
	Orange	12:51	Loading of the contaminated product
		13:02	1° sample of treated juice
		13:05	2° sample of treated juice
	-	13:10	Washing of the plant

evaluated just after the inoculum before any treatment (T0), and after UV pasteurization treatment (T1) by plating on Chromocult Coliform Agar serial dilutions of the samples for 24 h of incubation at 37 °C in aerobic condition. For each sampling, counts were performed in triplicate. Average values ± standard deviation were reported as log_{10} CFU/mL. Colonies were counted and the CFU/mL concentration was calculated by applying the following eq. 3.9.

$$C_x = \frac{\sum C}{(1 \cdot na + 0.1 \cdot nb + 0.01 \cdot nc) \cdot d} \tag{3.9}$$

where $\sum C$ is the summary of all the counted colonies, na is the number of plates of the first countable serial dilution, nb is the number of plates of the second countable serial dilution, nc is the number of plates of the third countable serial dilution, and d is the serial dilution factor of the first countable serial dilution. For the microbiological counts, the detection limit was 3 log_{10} CFU/mL.

Results and discussion

Flow field and irradiance simulation

As stated in the previous section, for each configuration both the flow field and the irradiance were computed. The velocity distribution on a longitudinal section plane, in the case of orange juice and a flow rate of 5 L/h, is presented in Figure 3.5.

Based on the fluid-dynamic results the trajectories of 1000 fluid particles were calculated. The resulting velocity streamlines, in the case of orange juice at a flow rate of 5 L/h, are presented in Figure 3.6.

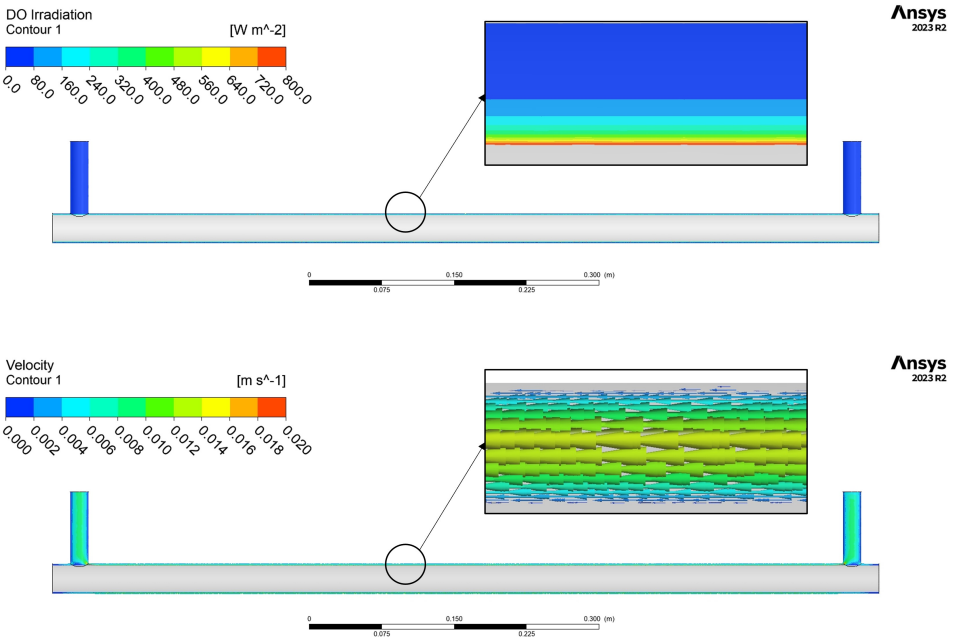

Figure 3.5: Reactor-internal velocity and irradiance field with a detail related to the distribution in the thin film

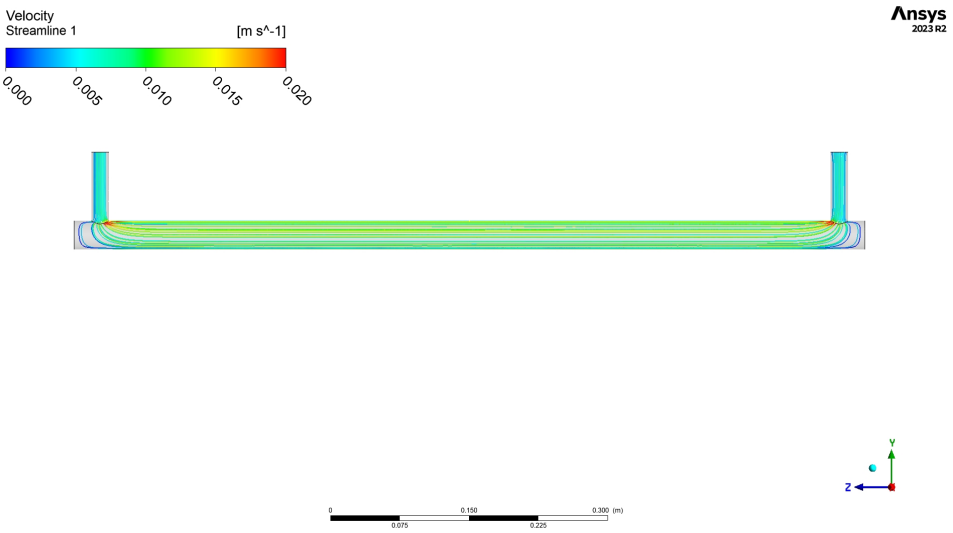

Figure 3.6: Streamlines along which the irradiance was integrated to calculate the dose distribution.

The irradiance was calculated for each juice, considering the corresponding absorption coefficients. In Figure 3.7 the irradiance as a function of the distance from the quartz sleeve surface is reported. It is evident that the irradiance strongly depends on the absorption coefficient. In particular, the "useful" thickness appears to be about 1 mm in

the case of apple juice, and less than 0.8 mm for the other juices. As a consequence, to enhance treatment performance, it would be appropriate to reduce the thickness of the fluid film. In the device considered, however, the thickness of the fluid was not reduced further to avoid very tight machining tolerances and, consequently, higher construction costs.

After computing both the trajectories and the irradiance, the UV dose absorbed along each streamline was calculated by integrating the light intensity along each path line over time. Figure 3.8 reports a comparison of the dose distribution obtained for apple juice at different flow rates, while Figure 3.9 shows the dose distribution calculated for the three fruit juices at the flow rate of 10 L/h.

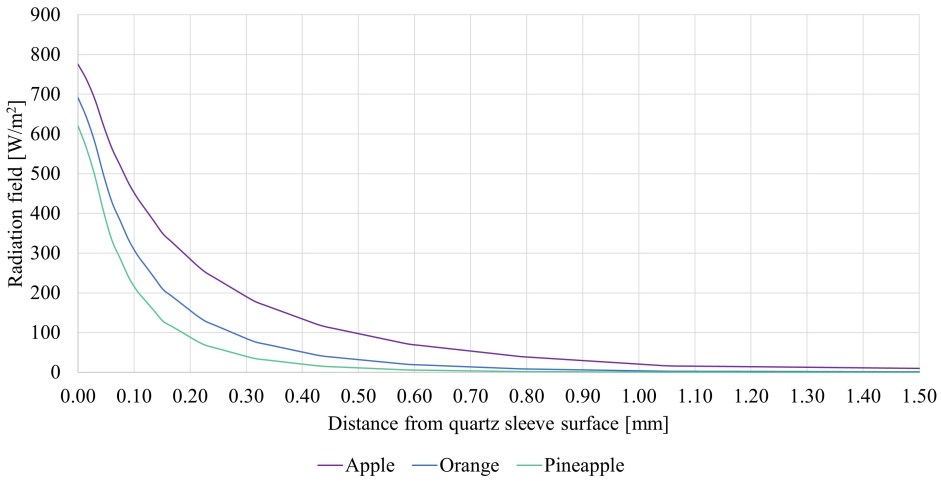

Figure 3.7: Irradiance pattern in the radial direction for the three juices considered.

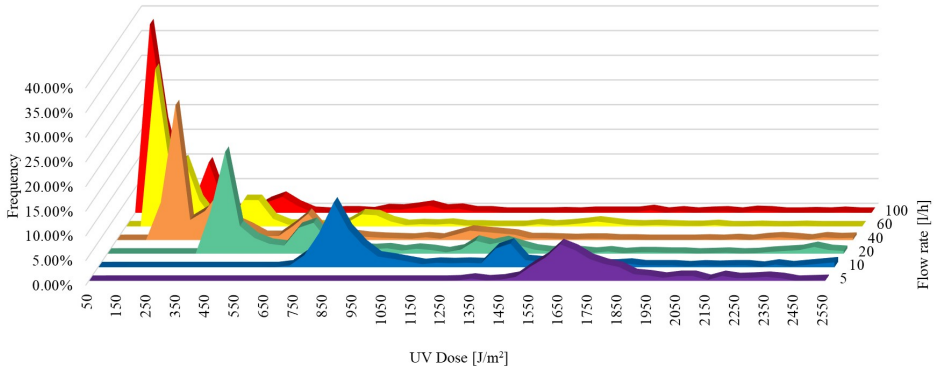

Figure 3.8: Variation of dose distribution as the flow rate changes in the case of apple juice.

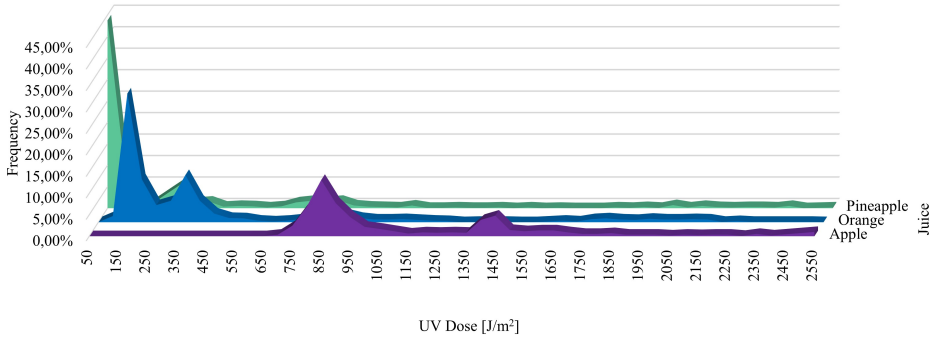

Figure 3.9: Variation of dose distribution as the fruit juice changes in the case of a flow rate of 10 L/h.

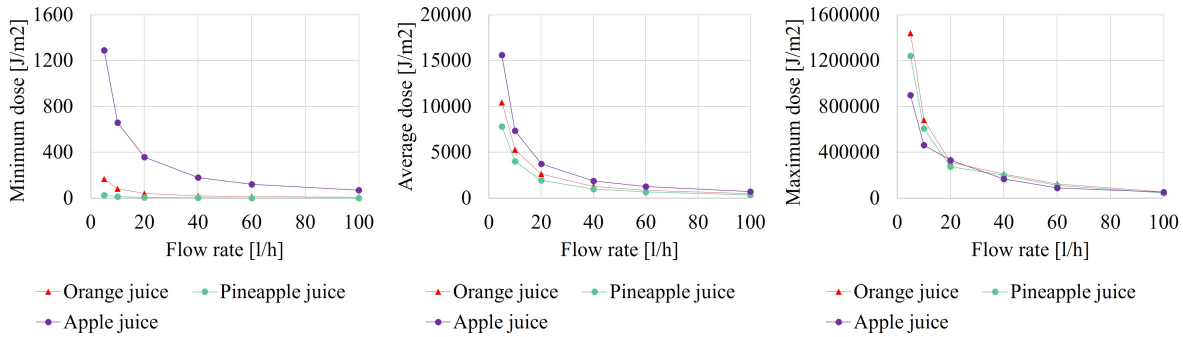

Figure 3.10: Trends in minimum dose, average dose, and maximum dose as the flow rate changes for the three juices considered.

Obviously, as the flow rate increases, the dose distribution shifts toward lower values, similar to what occurs as the absorption coefficient increases. The dose distributions in

the different configurations analyzed were summarized in terms of minimum, average, and maximum doses absorbed by the fruit juice (Figure 3.10).

It can be observed that in the case of apple juice, due to a lower absorption coefficient, more efficient treatments were obtained in terms of both minimum dose and average dose. In addition, due to lower viscosity values, the treatments turned out to be more uniform. In the case of apple juice, up to a flow rate of 10 L/h, the minimum dosage imposed by the USFDA is achieved with only one reactor. For a higher flow rate, as well as for orange juice and pineapple juice the installation of several reactors in series would be required. To better investigate the impact that the installation of multiple reactors in series would have, we proceeded as described in the dedicated section. Figure 3.11 represents the evolution of particle positions at the inlet of each reactor. It can be seen that, starting from a perfectly uniform distribution, they tend to concentrate in the central area of the section.

Figure 3.12 represents the trend of minimum dose as the number of reactors increases, in the case of orange juice and considering a flow rate of 80 L/h. It increases more than proportionally with respect to the number of reactors: 5 reactors in series would be sufficient to achieve a dose above 195 J/m^2, which, according to [66], should be sufficient to achieve a 5-log_{10} abatement on *Escherichia coli* K12.

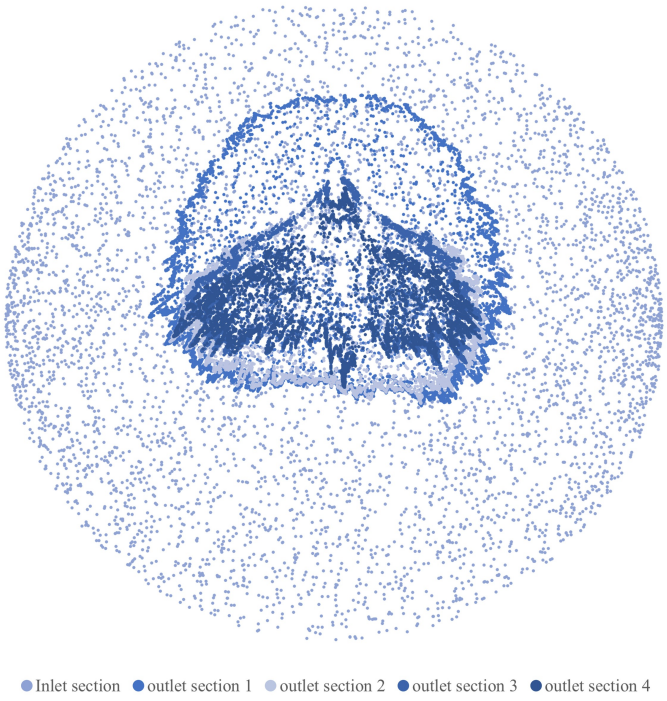

Figure 3.11: Evolution of particle positions at the inlet of each reactor, when multiple reactors are installed in series.

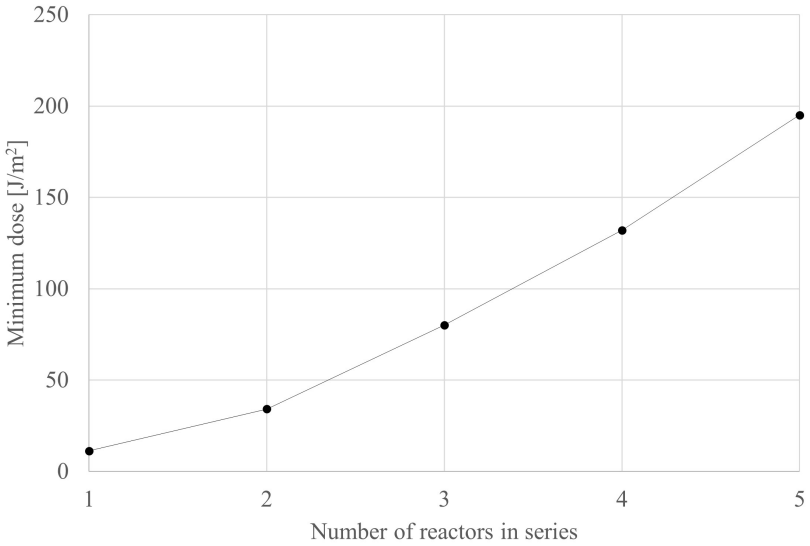

Figure 3.12: Minimum dose as the number of reactors in series varies (orange juice, 80 L/h)

Results of the experimental campaign

The microbial count results, comprehensive of the two days of testing are reported in Table 3.3. For the microbiological counts performed, the detection limit was 3 log_{10} CFU/mL.

The results obtained in UV pasteurization highlight the inefficacy of the treatment of orange juice. Considering all the replicates, an average reduction of 0.05 log_{10} CFU/mL of

the target microorganism was observed. These results can be explained by the turbidity of orange juice [53]. Is also important to underline that a great variability in UV resistance among *E. coli* strains was found. For example, in [73] the authors have found high disparities among several strains of *E. coli*. Opposite results were found for the UV-C-treated apple juice. A strong efficacy in the reduction of *Escherichia coli* was found. A reduction of more than 3 log_{10} CFU/mL was detected. This result confirms the efficacy of this non-thermal treatment on apple juice and other clear juices as already underlined by other studies [74, 75].

Table 3.3: Average microbial count and reduction achieved with the UV-C treatment

Matrix	**Sample**	**Description**	**Average concentration of *E. coli* ATCC 11229**
Apple	T0	Untreated control sample	5.91 ± 0.05 [Log CFU/mL]
Apple	T1	UV average	< 3 [Log CFU/mL]
Apple	Δ	Δ microbial reduction	> 3 [Log CFU/mL]
Orange	T0	Untreated control sample	5.78 ± 0.14 [Log CFU/mL]
Orange	T1	UV average	5.73 ± 0.15 [Log CFU/mL]
Orange	Δ	Δ microbial reduction	0.05 [Log CFU/mL]

Validation

As the fluid flow inside the device is straightforward, the experimental campaign aimed at validating the simulation results of the irradiance. The validation therefore was performed in terms of the supplied dose, and it was based on the inactivation achieved and measured through microbial counts.

As stated previously, there is an important issue of inconsistency in the doses and corresponding inactivation levels in fruit juices reported in the literature, mainly due to a lack of standardized methods. In [66] the experimental UV dose range required for a 5-log_{10} reduction in *E. coli* K12 in apple cider was reported as 188-788 J/m^2. The minimum dose necessary to achieve 1-log_{10} reduction (D90) was determined by dividing the minimum experimental dose by 5, obtaining a value of D90 = 37.6 J/m^2. In [76], an inactivation of approximately 5.9 log_{10} CFU/mL was obtained when supplying a dose of 140 J/m^2 to Rome apple variety cider with a CiderSure 3500 thin film reactor.

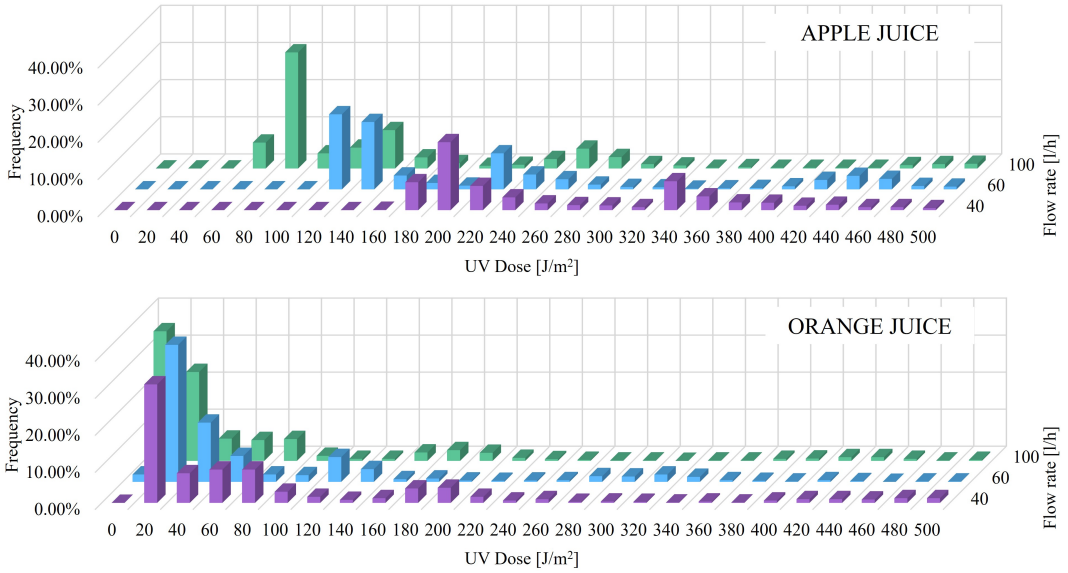

Figure 3.13: Dose distribution for apple juice (a) and orange juice (b) and flow rates between 40 L/h and 100 L/h.

This study in particular is relevant because the Rome cider had characteristics comparable to the apple juice considered in this study (11.8 Brix, pH 3.76). In this case, D90 was calculated as 23.73 J/m^2. These values are consistent, on average, with those reported in Appendix A "UV Rate Constants for Bacteria" [77] for the inactivation of *E. coli* in water media. During the experimental campaign, an inactivation of more than 3 log_{10} CFU/mL was detected, so a minimum dose of at least 80-100 J/m^2 approximately was expected.

The simulated conditions consisted of flow rates from 5 to 100 L/h, so the experimentally reproduced flow rate of 80 L/h was within the evaluated operating range. In these conditions the residence time inside the UV reactor is 5 seconds. The distribution of doses supplied to the 1000 injected particles, for both apple and orange juice, is reported in Figure 3.13 for the flow rates of 40, 60 and 100 L/h, limited to a relevant range. It can be observed that, in the case of apple juice, at 100 L/h, 70% of the particles were subjected to a dose between 60 and 260 J/m^2, with the remaining particles subjected to higher doses. At a flow rate of 60 L/h, 70% of the particles received a dose between 120 and 460 J/m^2, while at 40 L/h 70% of the particles received a dose between 180 and 700 J/m^2. In the case of a flow rate of 80 L/h, therefore, it is expected to have a radiation dose ranging from 100 to 400 J/m^2 approximately for 70% of the particles, with the remaining being subjected to higher doses. The results of the simulation, in the case of apple juice, therefore, are coherent with the reduction achieved and the doses reported in the literature.

With regard to the orange juice, which is much more opaque than apple juice (Table 3.1), the doses supplied resulted much lower, with most of the particles being subjected

to an estimated dose of less than 20 J/m^2, not sufficient to effectively abate the microbial load. This is confirmed by the results of the microbiological analyses, where no reduction was detected after the UV-C treatment.

Conclusions

In this study, the application of CFD simulation for the evaluation of the performance of a UV reactor for fruit juices was investigated. Results highlighted that for a complete characterization of the process, it is not enough to focus only on the average dose, but it is essential to carefully consider the whole dose distribution. This is the aspect that most differentiates the present work from existing literature. Indeed, in terms of average dose, it could be concluded that the analyzed reactor is able to supply the doses required by the U.S. Food and Drug Administration for all three juices. Considering the minimum doses, however, it is evident that the requirements were met only for apple juice. In particular, it was observed that the analyzed reactor at the operating conditions considered is unable to achieve the minimum dose of 400 J/m^2 on orange juice and pineapple juice, while, when treating a flow rate of up to 10 L/h of apple juice, it meets USFDA requirements in terms of the minimum provided dose. The experimental tests conducted, however, have shown that referring only to the minimum dose is too conservative. In fact, treating a flow rate of 80 L/h of apple juice, for which the simulation predicts a minimum dose of about 90 J/m^2, more than 3-log_{10} abatement on Escherichia coli were obtained. To get a more precise indication, it is good to refer to the dose distribution, identifying the dose range that most of the fluid (e.g., 70-80%) undergoes, thus obtaining, as a result, an expected range of logarithmic reductions.

For higher flow rates, as well as for the treatment of other juices characterized by higher absorption coefficients, such as orange juice and pineapple juice, it would be necessary to increase the exposure times by installing more reactors in series. It has been proved that system performance increases more than linearly as the number of consecutive reactors increases. To further increase the performance of the system, both in terms of minimum and average dose and in terms of uniformity, geometric modifications that would allow for increasing the mixing degree could be considered (such as the insertion of baffle elements or the use of spirally corrugated tubes). On the other hand, these modifications have a non-negligible degree of complexity in machines characterized by very tight construction tolerances, and they must be carefully evaluated from both hygienic and economic points of view. In this study, as mentioned in the Introduction, the objective was to evaluate the performance of a system characterized by high simplicity and flexibility, so none of these modifications was evaluated. This, however, may be an interesting topic for future investigations. The study demonstrates that the method proposed has several advantages over a standard experimental approach:

1. It allows for predicting how the performance of the reactor may vary, according to the physical characteristics of the fluid treated;

2. It allows for evaluating the system performance in terms of dose distribution and not only in terms of minimum and/or mean dose;

3. It allows for evaluating the uniformity of the treatment, and assessing if there are fluid regions subjected to excessively low or high radiation doses;

4. It allows for the assessment of any critical issues in the plant and helps to devise construction changes that could improve its performance.

Future research activities will focus on conducting further experimental tests on the simulated machine, to measure its actual performance with different types of juices. In the experimental phase, it will also be interesting to evaluate whether, when the desired reductions are achieved, the formation of undesirable by-products may occur.

3.3.2 Simulation of a continuous ohmic reactor for protein-rich foods

The research in this chapter has been included in the peer-reviewed conference paper [78] *Lysova N., Solari F., Aprili G. and Montanari R. Advancing Ohmic Treatment of Egg Products: Insights from Numerical Simulation. Proceedings of the 6th International Conference on Industry 4.0 and Smart Manufacturing (ISM 2024).*

The authors would like to express their gratitude to the company Emmepiemme Srl for the crucial support in conducting the analysis and in preparing the present article.

Abstract

In recent years, the market has been increasingly shifting towards more natural products, and non-conventional technologies are gaining increasing attention, as they allow to better preserve the organoleptic and nutritional properties of foods. Ohmic treatment is based on the Joule effect, with the heat produced by generating an electric current passing through the product. It offers several advantages in terms of heating uniformity, reduced fouling of the devices, and increased energy efficiency for products difficult to efficiently heat with traditional treatments. These characteristics make it an optimal choice for protein-rich products, like eggs and dairy products, which are often heterogeneous and particularly sensitive to high temperatures causing protein denaturation. In these applications, it is therefore essential to correctly design and dimension the ohmic heater to prevent the formation of hot spots that would irremediably affect the quality of the product. In this study, CFD simulation was used to evaluate the process performance during the continuous ohmic treatment of liquid whole eggs. The results obtained highlighted a strong relationship between the fluid dynamics inside the reactor and the temperature field. The insights obtained will be of great support to industrial stakeholders in the design phase and in implementing the ohmic treatment.

Introduction

It is well known that in recent years, with the increase in the population and significant economic development worldwide, the demand for industrial food products has considerably increased. Moreover, this demand is increasingly shifting towards high-quality, minimally processed foods that retain, as much as possible, their natural organoleptic characteristics and nutritional content.

Thermal treatments based on the exchange of heat between the food product and a heating medium, often divided by a metallic wall, represent the golden standard in the food industry, as they allow – if the system is correctly designed – to effectively reach the temperatures necessary for microbial inactivation. These treatments, however, have a significant impact on the organoleptic and nutritional characteristics of food products, mainly due to the non-uniformity in the temperature distribution and the overheating of the products near the walls. This is particularly the case of products with high protein and/or sugar content [79], such as egg products, i.e., egg whites, egg yolk, and whole eggs [80, 81]. These products, indeed, are particularly prone to fouling and thermal damage, which leads to the denaturation of the proteins and consequent food spoilage.

The specific application evaluated in this study refers to liquid egg products. The use of these products instead of whole shell eggs has increased over the years in the food industry, due to easier handling and lower microbiological risks. Egg products, indeed, present a high risk of contamination by *Salmonella enteridis* and *Listeria monocytogenes*, and need to be pasteurized to inactivate the vegetative microbial load and guarantee food safety. In the USA, it is recommended to achieve at least 5 Log reductions of *Salmonella* in egg yolk and whole eggs, by means of thermal treatments characterized by time-temperature combinations of approximately 3.5 min at 60-61.1 °C. In Europe, the required treatment is stronger, with traditional treatments characterized by a 5-6 min holding time at 65°C or higher [82]. The thermal treatment of egg products, however, presents important criticalities, as the proteins tend to denature at high temperatures, leading to rheological changes in the product and, eventually, solidification and unacceptable commercial quality.

Alternative technologies have been evaluated over the years for the treatment of liquid egg products [83]. One of the techniques that has seen a higher interest and industrial application is ohmic heating [84, 85]. Ohmic treatment is an electro-heating technique based on the flow of an electrical current through processed food, a medium characterized by a certain electrical resistance. Its working principle, based on Ohm's law and the Joule effect, grants the instantaneous generation of heat in the food, whose magnitude is correlated to the applied voltage and the electrical conductivity of the medium. The advantages of ohmic heating are nowadays well known: while the treatment is indeed thermal, the generation of heat from within, instead of the traditional

heating from the pipe walls, offers significant improvements in terms of temperature uniformity and reduced thermal damage, thus resulting in higher product quality (in terms, among others, of nutritional properties, aroma, and color), reduced fouling and cleaning of the plant, and overall higher treatment efficiency. Moreover, it allows to guarantee shorter processing times, thus lowering the temperatures necessary to achieve microbiological stability [86–88]. Ohmic heaters themselves are usually characterized by simple geometries, therefore allowing for easier cleaning processes and installation. Another big advantage of ohmic heating is related to the treatment of products with pieces and particles: when the phases have comparable electrical conductivities, it is possible to heat the product uniformly, strongly decreasing the temperature differences between solids and fluids compared to traditional treatments. Moreover, the implementation of ohmic treatment, which exploits electrical energy, is becoming nowadays more interesting and convenient for enterprises due to the increase in the availability of self-produced electricity from renewable sources. The products treated with this methodology on an industrial level are generally vegetable-based, such as products and sauces derived from vegetables and fruits. Other applications may include dairy products and creams, egg and meat products, but also products of the pharmaceutical and chemical industries. Multiple studies have highlighted the potential of ohmic heating and the reduced damage it causes to the nutritional and technological properties of egg products [89–91]. Ohmic heating, indeed, is a very fast method for heating liquid whole egg products: it is reported that the product temperature can be increased up to 60°C from 10°C in 105 s by applying a voltage gradient of 20 V/cm [89].

To gain an in-depth understanding of the treatment and evaluate its effects at every point of the device, numerical techniques such as Computational Fluid Dynamics (CFD) simulation can be adopted [1, 92]. This modeling technique has been applied in [93] to analyze the thermal processing of liquid eggs during high-frequency ohmic heating in a static chamber, highlighting the occurrence of potential non-uniformities in the temperature distribution. In [94], CFD simulation was used to characterize the ohmic treatment of mango pulp inside a continuous industrial device and Response Surface Methodology (RSM) was applied to investigate the impact of the voltage and product velocity on the outlet temperature, showing that low product flow rates may lead to a higher probability of thermal damage, while higher flow rates require careful evaluation and proportion of the applied voltage.

In this study, the ohmic treatment of whole eggs inside a continuous industrial ohmic heater is evaluated by means of CFD simulation. After reproducing the industrial geometry, the results are analyzed to identify the impact of the flow field on the uniformity and efficacy of the ohmic treatment. The study is carried out in collaboration with an Italian plant manufacturer, Emmepiemme Srl, which specializes, among others, in the development and production of industrial ohmic heaters. Nowadays the design process

of an ohmic heater is conducted as follows: preliminary collection of data from the client and choice of the generic device geometry followed by the selection of the power and appropriate modules. In case of non-conventional requests or new designs, a comparison with previous works is carried out, followed by the definition of the appropriate modules and measures. After the design and construction phases, preliminary test sessions are carried out on-site, followed by tests in the final industrial environment. Possible criticalities are highlighted, analyzed, and addressed; if these are not solved, the process starts again until a solution is found. In particular, the temperature distribution inside the ohmic cell is a critical point for the process. The use of CFD simulation in the design phases of ohmic plants may lighten these steps, allowing to highlight possible issues and criticalities early in the process. This would allow to reduce the time required for the design phase and the need for prototypes, thus strongly decreasing the production costs.

The paper is organized as follows. In Section 2, the methodology of the study is presented, consisting of an overview of the ohmic treatment, the description of the pilot plant evaluated, as well as the simulation settings and the characteristics of the simulated product. Section 3 contains the results of the simulation and their discussion. Finally, Section 4 concludes the study by summarizing the main findings and proposing possible future research activities.

Literature review

While the benefits of ohmic heating are well-known, its application to egg products has only recently become more diffuse in the food industry. Also in the literature, the topic has not been extensively explored: at the time of writing (July 2024) the search for the query "ohmic AND heat* AND egg" in the title, abstract and keywords on the Scopus database resulted in 31 records with publication dates ranging between 1996 and 2024 (Figure 3.14a). Moreover, the publications present an intermittent trend, without significant increases in recent years despite the promising results in the papers published to date and the technological advances worldwide. As can be seen in Figure 3.14b, presenting the co-occurrence of keywords used at least twice in the papers colored based on the average year of use, the main topics addressed to date appear to be related to the technological properties and characteristics of the product after the treatment [89–91]: this can be seen by the strong and well-established connection between the keywords "ohmic heating" and "rheology", as well as by the presence of the terms "pasteurization" and "protein denaturation".

In [89], the rheological properties of liquid whole eggs during ohmic heating were investigated, highlighting how the change in the protein structure at high temperatures results in changes in the rheological behavior and, consequently, in the fluid dynamics. In [90] the authors have evaluated the effects of ohmic heating on the technological

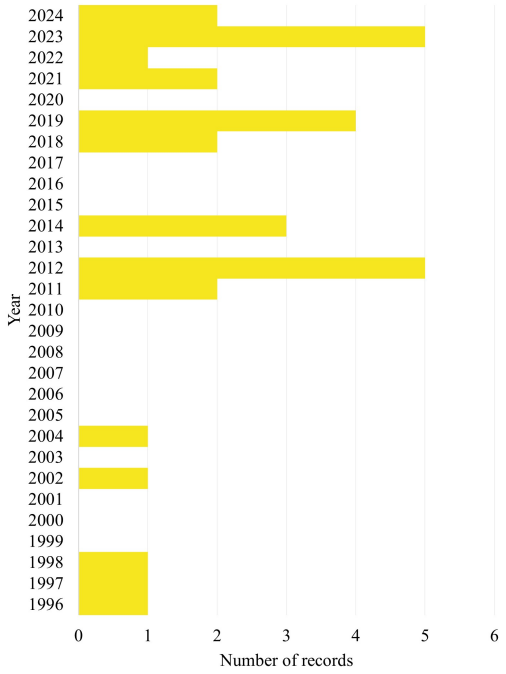

(a) Trend in the publication of papers dealing with ohmic heating of eggs.

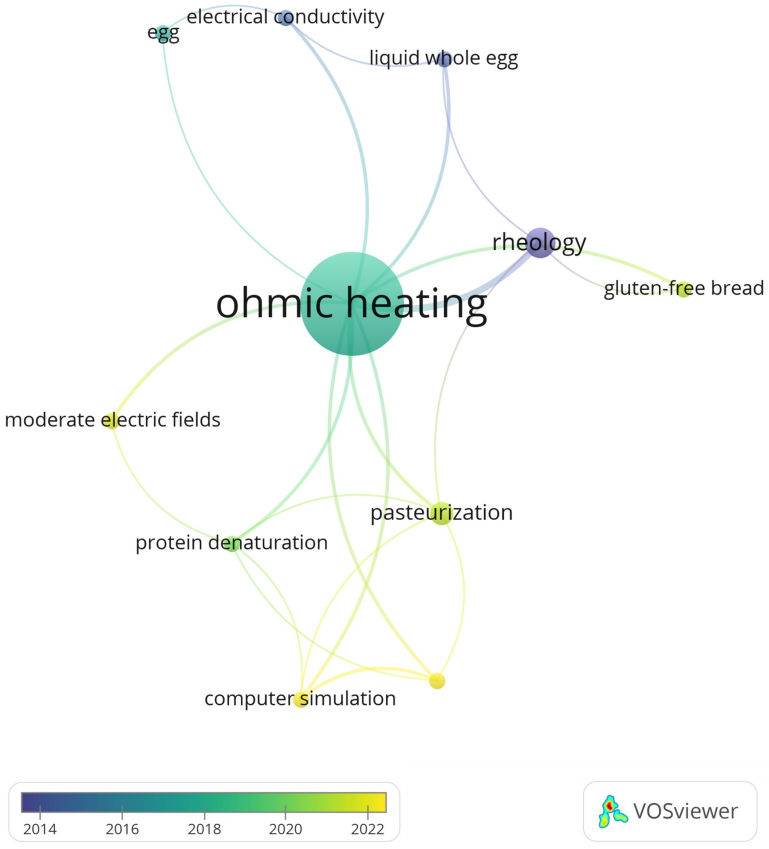

(b) Co-occurrence of keywords in the papers dealing with ohmic heating of eggs.

Figure 3.14: Bibliometric analysis of the literature on the ohmic heating of egg products.

properties of whole eggs, demonstrating that this alternative technology can preserve and even improve them. Indeed, gelling performances were found to be similar to the raw and conventionally treated whole egg samples, while foaming capacity was improved. Moreover, while color changes are expected with any thermal treatment, ohmic-heated samples showed the lowest differences from the raw product. In [91], the effects of different combinations of temperature and voltage on liquid whole egg ohmic processing were evaluated. The results demonstrated that different effects can obviously be expected under different processing conditions. In particular, while higher temperatures resulted in overall stronger impacts on color, product rheology and generation of volatile compounds, an interaction effect between temperature and voltage was highlighted for the coagulation capacity and bioactive compounds.

A recent research topic can be observed, related to the keyword "computer simulation". Like in several industrial fields, particularly in the food industry where the products usually present complex behavior, the field of ohmic heating of liquid eggs can benefit from the detailed insights that can be obtained from numeric simulations. This topic, indeed, is represented by two recent papers by a Japanese research group [93, 95], dealing with the pasteurization of eggs by ohmic heating inside a static polystyrene chamber, reproduced using computer simulation carried out with COMSOL Multiphysics software. In particular, in [93], the pasteurization degree, as well as hot and cold spots were identified using a 3D simulation. The results showed that, for the simulated treatment chamber, the product in the near-wall regions reached generally lower temperatures, so adding external heating allowed to achieve better heating uniformity. In [95], computer simulation was used to assess the temperature and velocity fields and their effects on the treatment inside an agitated ohmic system, quantifying the pasteurization value and the degree of protein denaturation. Two rotational speeds were evaluated, highlighting their effect on the observed characteristics. In both cases, computer simulation allowed to investigate treatment effectiveness and efficiency in a way that would not have been otherwise possible with physical sensors, thus obtaining results of great importance for practical applications. The field of numeric simulation applied to ohmic heating of liquid egg products, therefore, appears to be a promising research direction, that could greatly contribute to the advancement of the technology. However, ohmic treatment of eggs performed with continuous processing plants, generally adopted in industrial applications, appears to date unexplored. This paper, and the future research activities that will follow, aim to bridge this research gap.

Methodology

Industrial ohmic heater

The ohmic heater evaluated in this study was obtained starting from an industrial device

adopted for the treatment of whole eggs, composed of two linear modules joined by a 180° bend (Figure 3.15a). In the application considered, the product, with a flow rate of 14'000 l/h, is heated from 60°C to 66.5°C while being recirculated several times to reach the desired temperature, and it is then kept at the target temperature for a brief thermal holding time. The recirculation, usually with multiple passages, is one of the peculiarities that characterizes the analyzed device, as it is not usually implemented in traditional ohmic heaters. The aim of this approach is to increase temperature uniformity and overcome the strong difficulties encountered when heating egg products, resulting in better overall quality. In the present case, the flow rate of the new product entering the heater is assumed to be 1/7 of the total processed flow rate, thus resulting in seven recirculations for each unit of mass, on average.

Each module includes three electrodes, consisting of specially shaped discs of ferroelectric material, and two sections of tube made of borosilicate glass installed between them. Metal spacers equipped with insulation blocks are mounted on the external part of the electrodes to ensure insulation. In this way, the passage of high-frequency alternated electrical current takes place exclusively inside the glass tubes. In the specific application, the diameter of the upstream and downstream pipes is lower than that of the glass sections, thus conical restrictions and enlargements are present to connect the section with different dimensions. The actual industrial device presents cooling systems to prevent overheating. These cooling systems are not considered in this study, which aims to analyze the efficiency and the effect of the treatment on its own (Figure 3.15b).

Table 3.4: Physical characteristics of liquid whole egg retrieved in the literature.

Term	**Symbol**	**Value**	**Units**
Density	ρ	1019.5	kg/m^3
Specific heat capacity	c_p	3425	J/kg K
Thermal conductivity	λ	0.518	W/kg K
Electrical conductivity	σ	0.0113*T-2.8351	S/m
Consistency index	**K**	0.02	Pa s^n
Flow behavior index	**n**	0.8874	-

Product characteristics

The product considered for the simulations consists of liquid whole eggs; its properties were retrieved from the literature and are reported in Table 3.4. In particular, the density and non-Newtonian power law coefficients (consistency and flow behavior indexes) were retrieved in [89], specific heat capacity and thermal conductivity from [96], while the electrical conductivity from [93]. In particular, the electrical conductivity, which is a critical parameter in ohmic heating applications, was modeled as temperature-dependent.

Simulation settings

(a) Continuous industrial ohmic heater used with liquid egg products.

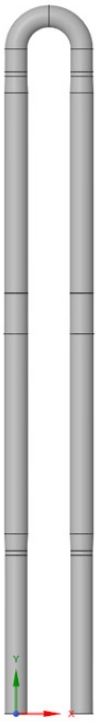

(b) 3D geometry of the ohmic heater used for the simulations.

Figure 3.15: Device for continuous ohmic heating of egg products.

To perform the simulations, first, the geometry of the fluid domain was defined. Then, a mesh was generated to discretize the domain for the following iterative solution with ANSYS Fluent 2022R2 of the governing equations for the conservation of mass, momentum and energy, based on the boundary conditions defined (Figure 3.16). In the figure, the steel pipes are represented in grey, the glass sections in light blue, and the electrodes in orange. The inlet and outlet pipes, as well as the bend, have a diameter of 49 mm, while the glass pipe section diameter is 52 mm.

The computational domain was discretized with a polyhedral mesh including an inflation layer near the walls to accurately capture the fluid dynamics and thermodynamics gradients. To ensure that discretization does not negatively affect the results obtained, all elements must meet specific shape criteria. According to the ANSYS Fluent Theory Guide [34], the mesh quality was assessed in terms of minimum orthogonal quality and maximum skewness. Regarding the former, values greater than 0.15 could be considered acceptable, while the latter could be considered acceptable when values do not exceed 0.85. After performing a mesh sensitivity analysis by varying the element size, a dedicated evaluation was carried out to analyze the effect of the discretization of the boundary layer, by carrying out the simulation with different inflation settings in the wall region as reported in Table 3.5. The final mesh used for the evaluations, with 3mm element size and 9-layer inflation near the walls with a first layer thickness of 5e-5mm and a 1.2

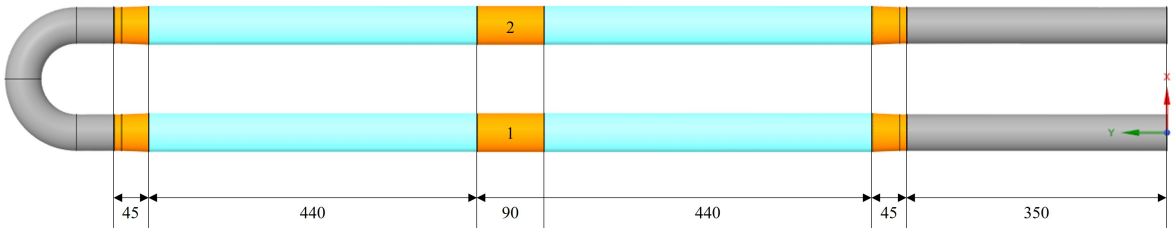

Figure 3.16: Geometry (rotated) and dimensions of the ohmic heater in millimeters.

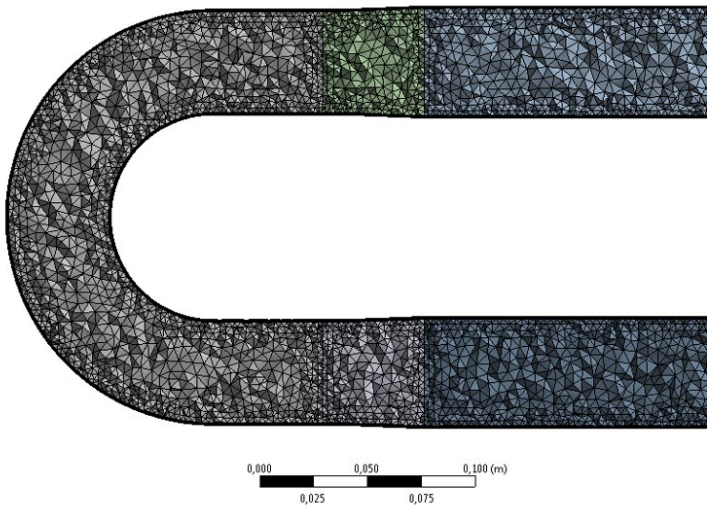

Figure 3.17: Mesh used to discretize the fluid domain for the simulations.

growth factor, is presented in Figures 3.17 and 3.18, with minimum orthogonal quality of 0.21 and maximum skewness of 0.79.

After defining the computational domain to reproduce the industrial scale ohmic heater, its performance was evaluated both in terms of the temperature increase, passing from the inlet to the outlet section, and in terms of treatment uniformity, assessed based on temperature distribution across the whole fluid domain. A special focus was given to fluid regions with excessively high temperatures that can cause protein degradation and undesirable changes in the organoleptic characteristics of the product.

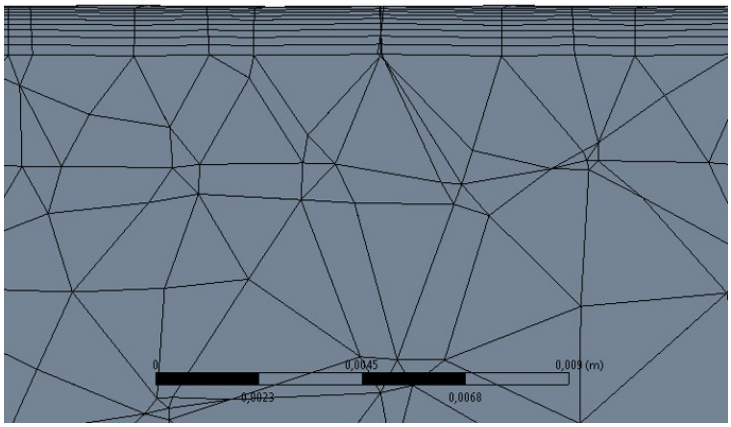

Figure 3.18: Detail of the inflation in the wall region.

Table 3.5: Number of elements in the evaluated mesh configurations.

Treatment of the near-wall region	**Element size 2mm**	**Element size 3mm**	**Element size 4mm**
First layer thickness of 5e-5mm, 9 layers, 1.2 growth factor	5'324'446	2'241'859	1'279'992
First layer thickness of 1e-4mm, 9 layers, 1.2 growth factor	-	2'110'637	-
Smooth layer thickness (first layer thickness 1.9e-4mm ca.), 0.272 transition ratio	-	1'993'383	-

The boundary conditions were set both in terms of fluid dynamics and electrical points of view (Table 3.6). A velocity of 2.06 m/s, calculated based on the recirculating flow rate, was imposed at the inlet section, a relative pressure of 0 Pa with respect to the reference atmospheric pressure was imposed at the outlet section, and the $SSTk-\omega$ turbulence model was set.

Moreover, the dedicated potential model, with Joule heating, was enabled and a potential difference was defined between the electrodes installed as schematized in Figure 3.16 according to the data reported in Table 3.6. In this way, ANSYS Fluent would solve the electric potential equation (eq. 3.10), where σ is the electrical conductivity, E is the electric potential and S is the source term. The Joule heating source term S_h generated inside the medium due to the flow of the electric current is computed with eq. 3.11. When solving the potential equation (eq. 3.10), Joule heating can be added to the energy equation solved by the software.

$$\nabla \cdot (\sigma \nabla E) + S = 0 \tag{3.10}$$

Table 3.6: Boundary conditions considered for the CFD simulations.

Term	Value	Units
Flow rate	14'000	l/h
Inlet velocity	2.06	m/s
Inlet temperature	60	°C
Voltage of the central electrode 1	1'275	V
Voltage of the central electrode 2	1'110	V
Voltage of the top and bottom electrodes	0	V

$$S_h = \frac{1}{\sigma}|\nabla E|^2 \tag{3.11}$$

The simulations were performed under steady-state conditions, setting a fixed voltage that would deliver the same power as the real process that uses alternating high-frequency current. The results were then obtained by iteratively solving the governing equations: continuity, energy, the two equations of the turbulence model, and the potential equation. The SIMPLE scheme was used for pressure-velocity coupling; with reference to spatial discretization, second-order discretization was used for pressure, while second-order upwind was used for momentum, energy, and turbulent kinetic energy and specific dissipation rate of the $SSTk-\omega$ turbulence model.

Results and Discussion

The results of the simulations are reported in the following Figures 3.19-3.21, with contours and vectors of the variables of interest plotted on an XY plane passing through the center of the pipes. Figure 3.19a presents the electric potential across the domain, Figure 3.19b represents the contours of velocity limited between 0 and 2.8 m/s, while Figure 3.19c shows the trend in the temperature increase. Figures 3.20 and 3.21 present detailed views that allow for a greater understanding of the treatment inside the device. As anticipated, these results were obtained with a mesh characterized by 3mm element size and 9-layer inflation near the walls with a first layer thickness of 5e-5mm, selected after carrying out a mesh sensitivity analysis. From the evaluation, it was possible to observe that the passage from 3mm to 2mm element size did not significantly impact the results obtained, while it strongly increased the number of elements and thus the computational cost of the simulations. With regard to inflation, on the other hand, it was noted that a high level of discretization is necessary to capture the local phenomena in the near-wall region.

Ohmic heating is based on the passing of an electric current through the product, causing its temperature to increase due to the dissipation of electrical energy. While the heat generation itself is uniform, product heating can still be affected by flow patterns

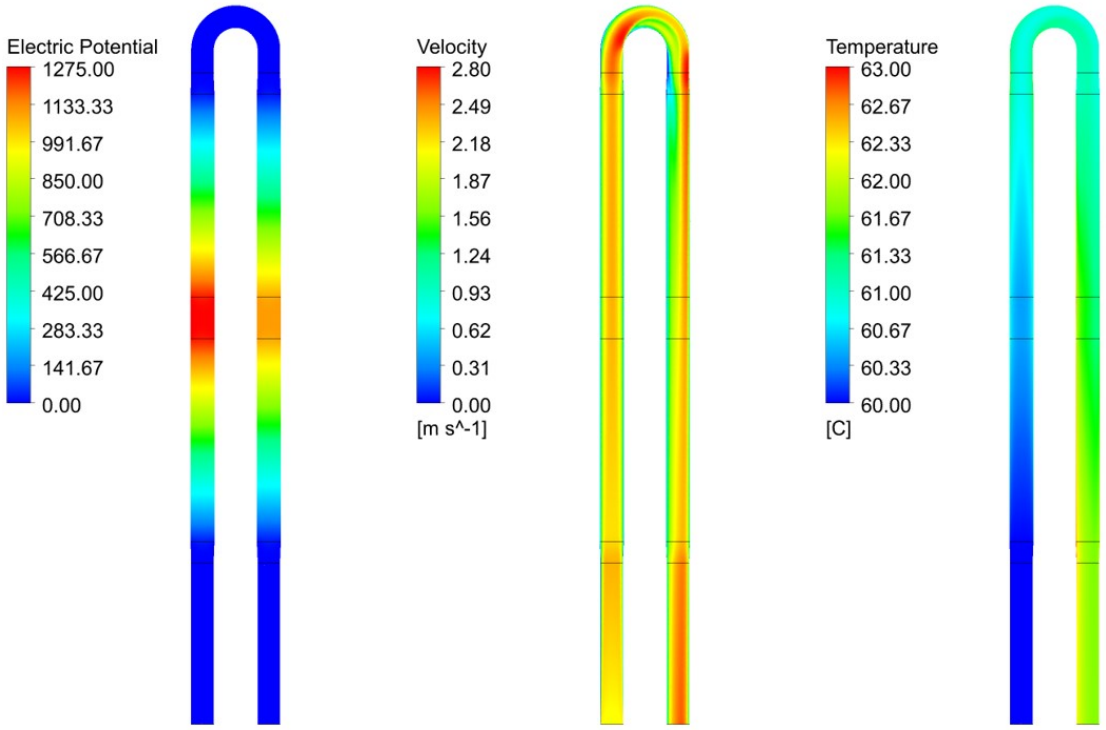

(a) Contour of electric potential across the ohmic heater.

(b) Contour of the velocity module.

(c) Contour of temperature.

Figure 3.19: Contours of the variables of interest on a XY section plane.

and electrical field variations. From Figure 3.19 and Figure 3.20, it can be easily observed that there is a strong correlation between the fluid dynamics and the distribution of temperatures inside the device. In particular, the flow inside pipes is generally characterized by no-slip conditions at the wall and higher velocities towards the center of the pipe. Obviously, portions of fluid that travel at different velocities are subject to different treatment times. In the near-wall region, where the velocities are the lowest, the product is subject to the longest heating time. These insights support the previously mentioned need to carefully discretize the near-wall region, as neglecting to do so could preclude the identification of potential treatment criticalities and localized hot spots.

As temperature uniformity has been proven to be strongly influenced by the flow field, it follows that components that disrupt fluid flow can also influence product heating: this is for example the case of curves, elbows, and similar components. Moreover, this behavior is not limited to the region after the bend but, due to the limited dimensions of the reactor, influences the treatment in the whole second section. In Figure 3.21a, the velocity gradient is higher on the right side of the pipe compared to the left one, indicating an asymmetric velocity profile due to the pipe bend. This asymmetry significantly affects the treatment, creating non-uniform temperature distributions within the pipe (Figure 3.21b). This behavior is once again motivated by the fact that the temperature reached inside the device is a function of the residence time which, as stated, increases at lower

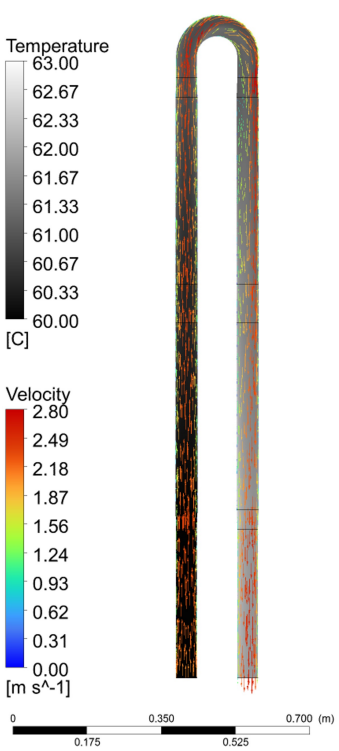

(a) Overlay of velocity vectors on a temperature contour.

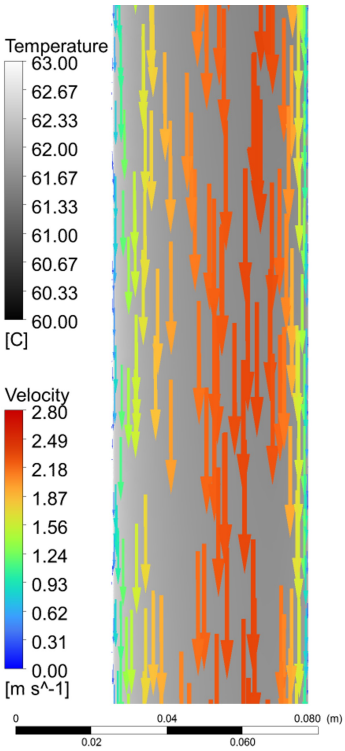

(b) Detail of the section with the highest temperature non-uniformity linked to the asymmetry in the velocity field.

Figure 3.20: Relation between the temperature and velocity fields.

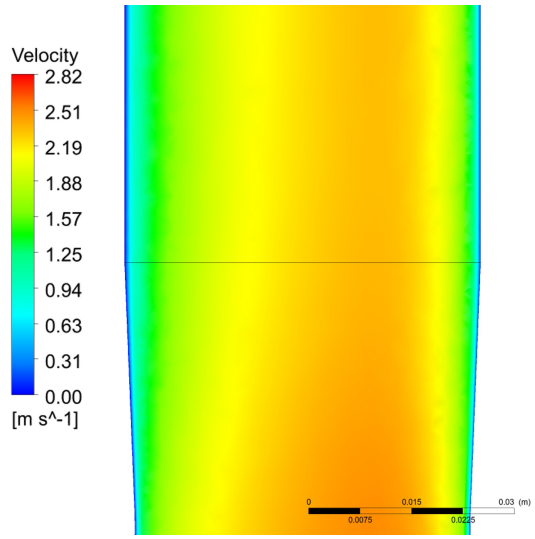

(a) Details of the velocity field.

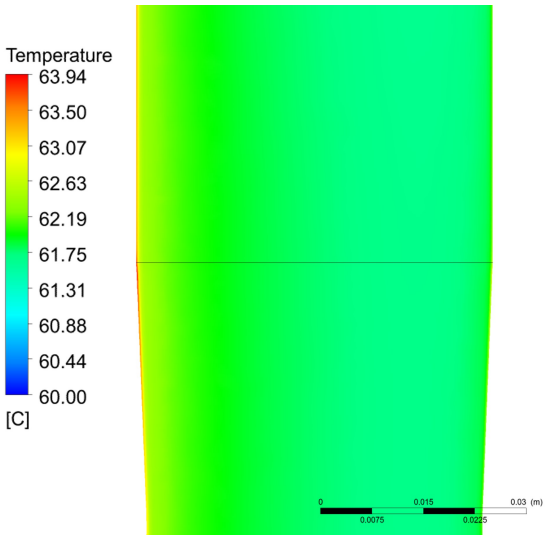

(b) Details of the temperature field.

Figure 3.21: Detail of the locations where hot spots could possibly generate.

velocities, giving the fluid more time to absorb heat.

On the left side of the pipe in Figure 3.21b, indeed, the temperature locally assumes higher values, resulting in hot points that can affect the product quality due to the high sensitivity of protein-rich liquid whole egg to temperature, and the proximity of the temperature range at which the protein denaturation starts to occur, i.e., above 65°C. The obtained insights can be leveraged in the design phase, to optimize the device geometries, aiming to reduce the asymmetries in the velocity field, thus enhancing the uniformity of the thermal treatment.

Moreover, it has been reported that the ratio between the flow rates of new and recirculated product inside the device plays a huge role in determining the treatment performance: a lower percentage of new (colder) product leads to higher temperature uniformity, while when the two flow rates coincide, i.e, the product is treated in just one pass like in the case of traditional ohmic heaters, the temperature disuniformities are the highest. This phenomenon should be further investigated by means of computer simulation, in combination with detailed insights about the flow field, in order to maximize treatment efficiency while guaranteeing the highest possible product quality.

Conclusions

In the present study, the ohmic heating of liquid whole eggs inside a continuous industrial device was reproduced by means of CFD simulation. For the analysis, the boundary conditions were set both in terms of fluid dynamics and electrical points of view, aiming at an accurate numerical reproduction of the treatment. A first evaluation was carried out to determine the level of domain discretization necessary to effectively capture the behavior in the system. From this analysis emerged the need for detailed discretization of the near-wall region, that would allow to capture possible localized phenomena and hot points. The results of the simulations highlighted the strong dependence of the temperature reached by the product on the fluid dynamics inside the device. In particular, asymmetries in the velocity field due to pipe bends and flow disturbances lead to non-uniformities in the temperature distribution, which could result in over-heating of some portions of the product and protein denaturation in the case of products such as liquid eggs and milk derivates. In these cases, if the treatment uniformity cannot be improved, the presence of dedicated cooling systems becomes crucial.

The insights derived can greatly support industrial manufacturers during the design phase of ohmic heaters. Indeed, besides gaining a deeper understanding of the treatment dynamics, the simulations carried out in parallel to the design phase could allow to estimate the impact of modifications on the heating efficacy and uniformity, reducing the need for prototypes and thus decreasing the production costs. Furthermore, simulation results could support the designers in the selection, sizing, and positioning of cooling

systems to achieve the maximum beneficial effect.

More importantly, exploiting the particular configuration of continuous ohmic heater with product recirculation analyzed, it should be investigated how different ratios of untreated to recirculated product impact the heating uniformity, in order to determine the optimal ratio and operating conditions. Future research activities will focus on further developing the simulation model, in order to more faithfully replicate the real process conditions. Moreover, it will be crucial to validate the simulation model with experimental tests on a real pilot plant. Afterwards, it will be possible to extend the analysis to other heater geometries and products.

3.3.3 Simulation of a cyclone-bag filter under different clogging conditions and estimation of the remaining useful life

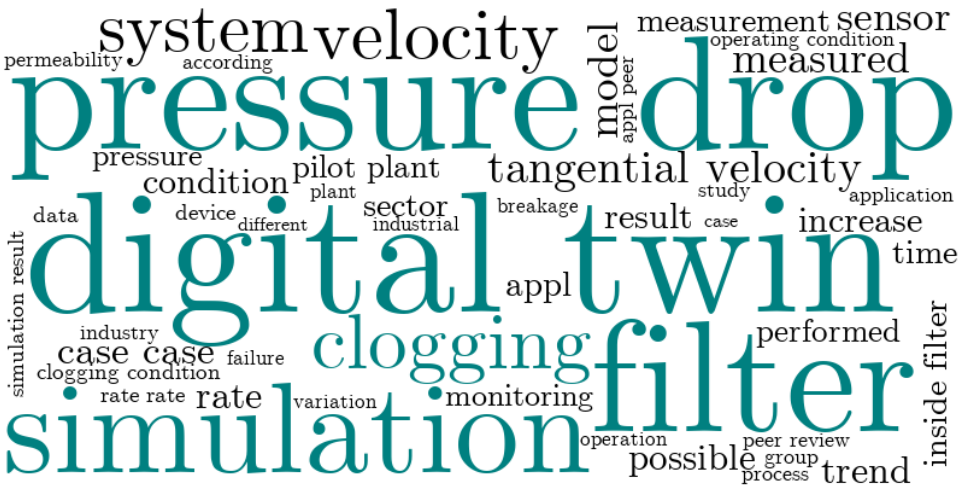

The research in this chapter has been included in the peer-reviewed article [97] *Solari, F., Lysova, N., and Montanari, R. (2023). Digital Twin Based on Historical Data and Simulation Results: Fault Detection and Estimation of the Remaining Useful Life of a Cyclone Bag Filter. Applied Sciences, 13(14), 8297. https://doi.org/10.3390/app13148297.*

The authors would like to express their gratitude to the company OCRIM S.p.a. for the crucial support in conducting the analysis and in preparing the present article.

Abstract

This study deals with the development of a digital twin for monitoring the operating conditions of a cyclone bag filter installed on the suction system of a wheat mill. The model aims to be used for fault identification and real-time prediction of the remaining useful life (RUL). Computational fluid dynamics simulations were performed to characterize in detail the fluid-dynamic behavior of the airflow inside the system under different conditions of filter sleeve clogging. Furthermore, the simulation results were used to identify a location for the installation of a new velocity sensor that would allow, together with the pressure drop measured at the ends of the filter, monitoring of the systems' conditions. A model able to assess the filter's operating state, identify failure events or operating anomalies, and make a prediction of the RUL was then developed. A possible implementation of the developed model, based on the simulation results that aimed to optimize the management of the sleeve cleaning cycles was also proposed. The developed digital model was then tested on a working cycle lasting one year, in which a sleeve failure was simulated. It was shown how the simultaneous monitoring of the two identified quantities allows for the correct identification of the failure and the accurate prediction of the RUL

Introduction

Grain milling plants process raw wheat to produce flour. The operations performed include, among others, the cleaning, sorting, separating and grinding stages. During these operations, the materials are usually moved with pneumatic systems that use compressed air. At the end of the process, before the air can be released back into the atmosphere, it must be purified from the suspended flour particles to comply with the current regulations [98]. To this end, filters and cyclone separators are commonly adopted to purify the discharged air stream [99–101]. To enhance the separating performance, and filter even the finest particles that cyclones alone fail to separate, cyclone and bag filters can be combined, to simultaneously exploit both the cyclonic and the filtering effects [102]. The filtering elements, often bags made of fabric or synthetic materials, tend to entrap flour particles which decreases the separation efficiency over time [103]. Periodic pulse jets of compressed air are commonly adopted to remove the entrapped particulate [104, 105]. The clogging of the filter bags, however, still tends to increase during the normal functioning of the device due to the deep deposition and retention of particles [106]. Other common malfunctions of cyclone bag filters include the wear and the tear of fabric sleeves. Generally, according to the manufacturers and end-users of these devices, the maintenance is limited to the substitution of the worn-out clogged sleeves at fixed time intervals of about a year, when the system pressure drop reaches a critical set-point value. Indeed, this operation is time-consuming and requires stopping and then restarting the entire processing line. Unplanned maintenance operations are sometimes required in the case of sleeve ruptures that can be detected only when the damage is severe and the plant needs to be stopped for timely intervention. Indeed, without being able to monitor what is happening inside the filter, these failures are detected when the discharged air stream appears white due to the massive presence of unfiltered flour. The ability to monitor the plant and detect the onset of failures could certainly generate a competitive advantage for companies. Indeed, by detecting the failures earlier, the operators could schedule predictive maintenance interventions at a convenient moment, instead of having to abruptly stop the plant and perform reactive maintenance.

This kind of optimization is crucial in the current industrial environment, which is characterized by scarcity of resources, frequent reductions in customer demand due to global crises, and ever-increasing competition among industrial players. In this scenario, to successfully stay in business, the companies need to define and leverage appropriate strategies that can generate competitive advantages.

The shift to Industry 4.0, which has been unfolding globally in recent years, involves a transition towards a highly digitized and interconnected business environment built upon several innovative technologies that have been evolving over the last decades [107]. The implementation of Industry 4.0 enabling technologies is undeniably a highly bene-

ficial approach, able to dramatically optimize the company's performance. Indeed, the deployment of novel cutting-edge technologies, often combined with lean organization approaches, generally results in streamlined processes and operations, as well as increased efficiency and productivity levels [108]. No less important is the reduced environmental impact, that can be obtained by efficiently using the resources and optimizing the operating and maintenance processes [109].

Digital twins are key components of Industry 4.0. First introduced in [110], digital twins can be defined as virtual replicas of technical assets, integrating knowledge and data resulting from modeling and simulation activities, with historical and real-time data captured by sensors during the real operation [14]. The digital twin functioning is based on Industry 4.0 technologies, such as simulation, Internet of Things, artificial intelligence and machine learning, cloud computing and blockchain technology [111]. The digital models developed can replicate multiscale physical systems, from single components and de-vices to entire plants and even cities. Furthermore, digital twins can be leveraged in human-robot systems for a plethora of different applications [112]. By creating digital twins of their systems, the companies can gain several benefits, including data collection and analysis, constant monitoring of the system functioning, identification of trends and patterns, problem detection and optimization of maintenance activities, as well as process enhancement and minimization of human decision making [113]. An important application of industrial digital twins, indeed, is in the maintenance sector [114–118]. In particular, the application of the digital twin to preventive maintenance has received much interest in recent years. Predictive maintenance has been applied in various sectors, such as intelligent manufacturing, the power industry, construction industry, aerospace industry, and ship-building industry. The manufacturing sector is where the largest number of applications of the digital twins oriented to preventive maintenance can be found; in particular, the digital twins have been implemented in several areas, such as process equipment, automobile manufacturing, cyber-physical systems, product life cycle management and fault diagnosis [117].

In general, most of the applications of predictive maintenance based on digital twin technology are developed from a physics-based model representation type; a few works can still be found in the literature in which the digital twins were developed based on a hybrid-approach model representation type, integrating real data with the results obtained from numerical simulations [115]. Indeed, digital twins can be developed based on historical data measured by sensors, simulation results, or as an integration of both [119–124]. The available data can be analyzed by means of non-deep learning methods, such as regression models, or deep-learning methods, such as deep neural networks. Among these latter, mass customization system and Social Internet of Things emerged as a valid application of interconnecting deep learning technology and digital twin technology to keep the system in good working condition [125].

With reference to industrial equipment, the simulations are often performed with Computational Fluid Dynamics (CFD) techniques, that allow the characterization of the system and its functioning in-depth under different operating conditions. The simulations can be performed to test what-if scenarios and alternative configurations without having to carry out experimental tests, thus minimizing the use and the waste of resources. In addition, the simulations allow monitoring of the values of the parameters of interest at each point of the device, resulting in a series of "virtual sensors" [126, 127]. This allows monitoring of the system operation, even at locations where physical sensors could not be installed. An example of a simulation applied to milling operations is presented in [128] where a multiscale DEM-PBM approach was used to model the breakage behavior in a co-milling process. The use of discrete element modeling for the interactions and the collisions between the particles, combined with population balance modeling, utilized to describe the breakage events and the evolution of the particle size distribution, allowed the authors to gain insights into the mechanism of kernel breakage and thus optimize its performance. CFD simulation has been extensively applied to all kinds of industrial plants and devices in the last decades [129,130], including food industry applications [1, 7, 131–133]. With reference to filtering devices, CFD simulation was used to optimize the functioning of cyclone separators [134–137], fabric filters [105, 138], as well as cyclone separators combined with cartridge or fabric filters [102, 139, 140]. Both [139] and [102] highlight how combining cyclones with filtering inserts can be beneficial; the separation efficiency is higher in the combined system compared to standard cyclones, while the average cleaning intervals are longer compared to cartridge filters. Furthermore, in addition to higher efficiency, cyclone-bag filters decrease the floor space demand, as they allow the combination of two otherwise separate operations.

In this study, CFD simulation was used to characterize in detail the functioning of a cyclone bag separator for industrial grain milling plants. The analysis started from a validated model [140] and was extended to evaluate the device functioning at increasing clogging levels. The simulations allowed for the characterization of the fluid flow inside the domain and the definition of a location for a new sensor, that would enable the detection of clogging and failure conditions. Moreover, they would be able to know, for a given operating condition, the flow distribution inside the filter, allowing accurate control of the sleeve cleaning system, and increasing the cleaning frequency on those sleeves most affected by the airflow. The simulation results were validated with experimental tests by reproducing in the real pilot plant, the simulated conditions. The data collected during both the simulation and the experimental campaigns were integrated to generate a digital model of the plant, that was connected to its physical counterpart by means of a LabView Data Acquisition module. The generated digital twin collects and analyses the data at different time scales, allowing it to detect abnormal values, identify variations and trends in the functioning, as well as estimate the remaining useful life (RUL) of the

device. In this way, it is possible to enhance the system performance by continuously monitoring the plant and its conditions, thus being able to react to functioning variations in a timely manner and optimize the maintenance operations. The contribution of this article to the existing literature can be summarized in four points. (*i*) development of a simulative model capable of locally reproducing filter behavior as the degree of sleeve clogging changes; (*ii*) conceptualization of a digital twin-based predictive maintenance model developed based on a hybrid-approach model representation type, on the basis of simulative results and experimental data; (*iii*) development of a control model, based on a non-deep learning method, for routine sleeve cleaning operations, depending on specific operating conditions, to ensure better operating conditions and increase RUL; (*iv*) application of digital twin technology in a context, such as wheat and cereal milling, for which no specific study is yet present in the literature.

Materials and Methods

Pilot plant

The study was conducted on an industrial-scale pilot plant reproducing the suction system commonly used in the milling industry to draw the finer particles of bran and flour out of machines and keep the working environment clean (see Figure 3.22). The system consists of a bag filter, a fan, piping, connections, flow control valves, and sensors. A schematic representation of the pilot plant is reported in Figure 3.23.

The main element under study is the cyclone bag filter, which consists of a cylindrical steel body with a conical bottom, that contains 31 fabric sleeves. The airflow enters tangentially inside the separator, so that a percentage of the bran and flour dust, particularly the coarser ones, are initially separated by a cyclonic effect and do not impact against the sleeves. The percentage of dust that is separated by the cyclonic effect is collected in the conical bottom and can be extracted, and recovered, thanks to a rotary valve; the remaining particles remain trapped in the fabric of the sleeves, gradually decreasing their permeability. This results in rapid clogging of the sleeves, causing the need for their rapid replacement. Indeed, a compressed air cleaning system is installed on the filter, which, at regular time intervals, flows compressed air counter currently through the sleeves to remove the dust trapped in them. This flow, however, can clean the sleeves only partially, as the dust that has penetrated deeper into the porous matrix is not removed. Moreover, since to date, it is not possible to know the actual state of each sleeve, the sequence of sleeve cleaning is decided a priori and remains unchanged throughout the entire life cycle.

Once the permeability of the sleeves is no longer sufficient to ensure proper airflow, the sleeves must be replaced. Usually, sleeve replacement is performed when a differential pressure sensor, installed upstream and downstream of the sleeves, measures a pressure drop higher than a threshold value (generally set at about 15 mbar). The intervention of

Figure 3.22: Cyclonic bag filter pilot plant used for experimental testing

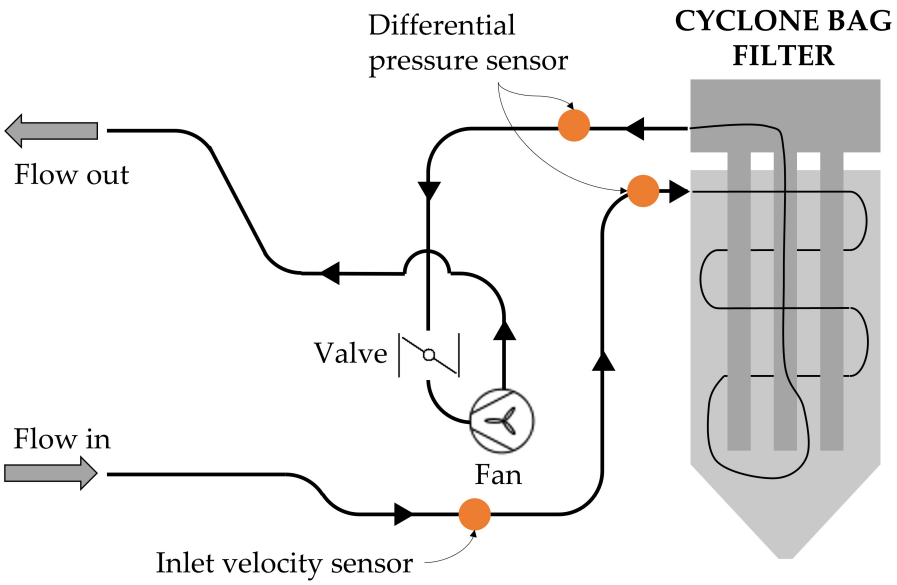

Figure 3.23: Schematic representation of the pilot plant.

sleeve replacement is very time-expensive and requires stopping the production process for the time needed to complete the substitution. Therefore, all sleeves are usually replaced together to minimize the number of interventions. To maximize the up-time of the filter and its performance, it is therefore highly desirable that the clogging of different sleeves occurs as uniformly as possible. On the one hand, it is therefore preferable to maximize the percentage of dust separated by the cyclonic effect and, at the same time, it is important to foresee the occurrence of abnormalities in filter operation so that timely action can be taken to restore proper operating conditions. Finally, it would be beneficial to know the actual working conditions of each sleeve, since it would allow the optimization of the cleaning operations by increasing the frequency of the air jets on the sleeves most affected by airflow and decreasing the frequency on the others.

Numerical simulation

The operation of the cyclone bag filter was investigated through CFD simulation at optimal operating conditions, i.e., with clean sleeves, and at increasing clogging levels. The aim of these simulations was to evaluate the impact of the clogging on the system's operation. The first quantity evaluated was the pressure drop. However, this information by itself is not exhaustive, as a variation in the pressure drop could be caused by several issues that could not be related to clogging, such as a variation in flow rate, the presence of broken sleeves, or a combination of both aspects. To this end, the simulations performed were exploited to determine if, and how, the gradual increase in the clogging level of the filtering sleeves would impact other physical quantities that could be measured by installing additional sensors on the device. Firstly, to perform the simulations, a 3D model of the cyclone bag filter was developed with Ansys SpaceClaim [70]. The real dimensions of the filter were reproduced, and all 31 sleeves were modeled inside the device. The thickness of the sleeve walls was not directly reproduced as a separate volume in the geometry, as it would result in a dramatic increase in the computational weight of the simulation. Instead, the physical presence of the filtering medium was accounted for in the simulation settings. The geometrical features of the system are reported in Table 3.7. According to the manufacturers and the end-users of these filters, as well as the results of previously performed simulations validated in [140], the clogging tends not to be uniform along the sleeve length. To this end, a division into three sectors was introduced, resulting in top, middle, and bottom sectors being defined for each of the 31 sleeves. The geometry generated is presented in Figure 3.24.

Table 3.7: Main dimensions of the system.

Dimension	Value	Units
Separator height	5308	mm
Separator diameter	1300	mm
Conical bottom height	1550	mm
Sleeves length	3000	mm
Sleeves diameter	123	mm

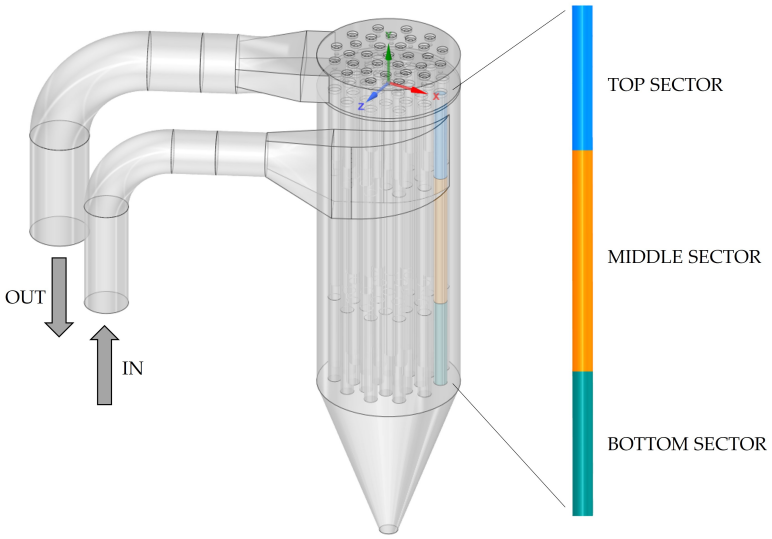

Figure 3.24: Three-dimensional reproduction of the filter for fluid dynamic simulation. On the right is the detail of the division of the sleeves into three vertical sectors.

The domain was then discretized in a finite number of volumes with Ansys Meshing [141], generating a tetrahedral mesh, appropriately refined to accurately reproduce the airflow even in the narrowest gaps between the sleeves. To decrease the number of volumes, and thus the computational time, the conversion of the tetrahedral mesh volumes to polyhedra was performed. This operation resulted also in an increase in both the mesh quality and the convergence properties [142, 143]. Finally, Ansys Fluent [34, 71] was used to simulate the functioning of the filter by solving the flow field and turbulence equations at each volume node. The fabric filtering sleeves were reproduced with the "porous jump" model, a 1D simplification that allows for the calculation of the pressure drop introduced by a porous medium without having to directly model the momentum field inside it. To this end, the thickness of the sleeves and their permeability had to be specified. A number of iterations sufficient to guarantee the convergence and the stability of the solutions were performed for each simulation. The settings and the boundary conditions considered are summarized in Table 3.8.

Apart from the division into sectors along the sleeve length, a non-uniformity in clogging among sleeves of the same sector was also hypothesized. To confirm these as-

Table 3.8: Main settings used for CFD simulations.

Type of analysis	steady-state	
Solver	pressure-based	
Turbulence	$SSTk-\omega$ model [144]	
Boundary conditions	velocity inlet	15; 17.5; 20 and 22.5 m/s
	pressure outlet	0 gauge pressure
	sleeve walls	porous jump model with known permeability and thickness of the medium
Pressure–velocity coupling	Coupled	
Spatial discretization	Gradient	Least squares cell based
	Pressure	PRESTO! [34, 71]
	Momentum	Second order upwind
	Turbulent Kinetic Energy	Second order upwind
	Specific Dissipation rate	Second order upwind

sumptions, a first simulation with completely clean sleeves was carried out. The flow rates of the air processed by each sleeve, as well as the velocity streamlines inside the domain, were evaluated, confirming both hypotheses. A division of the sleeves into four groups was then performed, clustering the sleeves that processed comparable flow rates into the same group. This division allowed the definition of a "clogging sequence" based on the position of the sleeves with reference to the inlet of the particulate-laden airflow and the magnitude of the flow rate passing through the filtering medium. A simulation campaign was carried out by gradually increasing the levels of clogging, reproduced in the simulation by decreasing the permeability value of the sleeves. In particular, the obstruction conditions of each case were based on the distribution of the flow rates calculated in the previous one, e.g., the conditions of the second simulation were defined according to the results of the first one, and so on. To model the different clogging conditions, the permeability of the filtering medium was gradually decreased, proportionally to the obstruction percentage, according to Equation 3.12.

$$a_c = a \cdot (1 - c_{\%}) \tag{3.12}$$

where α_c is the sleeve permeability for the case under study, α is the permeability of the clean sleeve and $c_{\%}$ is the obstruction percentage of the sleeve. The conditions simulated are presented in Table 3.9, with the indication of the percentage of clogging of each group of sleeves divided into three longitudinal sectors.

The results of the simulations and the flow field inside the device were finally analyzed to assess the impact of the filter obstruction, with the aim of identifying some locations for additional sensors that would allow monitoring and evaluating the clogging conditions during the real-time functioning of the filter. To this end, the evaluation of

Table 3.9: Clogging conditions considered for the CFD simulation.

Sleeves		**Clogging Case (% of obstruction)**							
Sector	**Group**	**1**	**2**	**3**	**4**	**5**	**6**	**7**	**8**
1 (top)	1	0	20	40	55	70	80	95	95
	2	0	20	40	55	70	85	95	95
	3	0	15	30	45	60	75	90	95
	4	0	15	30	45	60	75	90	95
2 (middle)	1	0	0	5	10	20	30	50	70
	2	0	5	10	15	25	35	50	70
	3	0	5	10	15	25	30	40	55
	4	0	5	10	15	25	30	40	55
3 (bottom)	1	0	0	0	5	10	15	20	20
	2	0	0	0	5	10	15	15	15
	3	0	0	0	5	10	15	15	15
	4	0	0	0	5	10	10	10	15

the tangential velocity values in the near wall region was performed on four longitudinal lines, displaced at 90° from the other (Figure 3.25).

The results of the simulations were also used to quantify the air flow rate passing through each sleeve under different clogging conditions. We referred specifically to the flow rate filtered by the top sector of each sleeve, which is the sector most impacted by the compressed air jet. The results were then used to modify both the sequence and the frequency of cleaning operations with compressed air according to the magnitude of the air flow rate. Since CFD simulations are time-expensive they were launched in advance, building a database containing all their results. This database can then be used for real-time control of the system.

Data measurement and collection

The system draws air from the outdoor environment through an intake duct, having an internal diameter of 400 mm, that leads directly to the inlet volute of the cyclonic bag filter. The flow rate of air is measured by a KIMO differential pressure device equipped with a Debimo air flow measuring blade. The operating principle of this device replicates that of the pitot tube, in which the velocity is calculated based on the difference between total pressure and static pressure; in this case, the measurement is not made at a single point, as in the case of a standard pitot tube, but is obtained by averaging the measurements taken at five different points uniformly distributed along the diameter of the pipe section. The conversion of the differential pressure value into velocity is made according to Equation 3.13.

$$v = C_M \sqrt{\frac{2\Delta p}{\rho}} \tag{3.13}$$

where C_M is a conversion coefficient, depending on the geometry of the device,

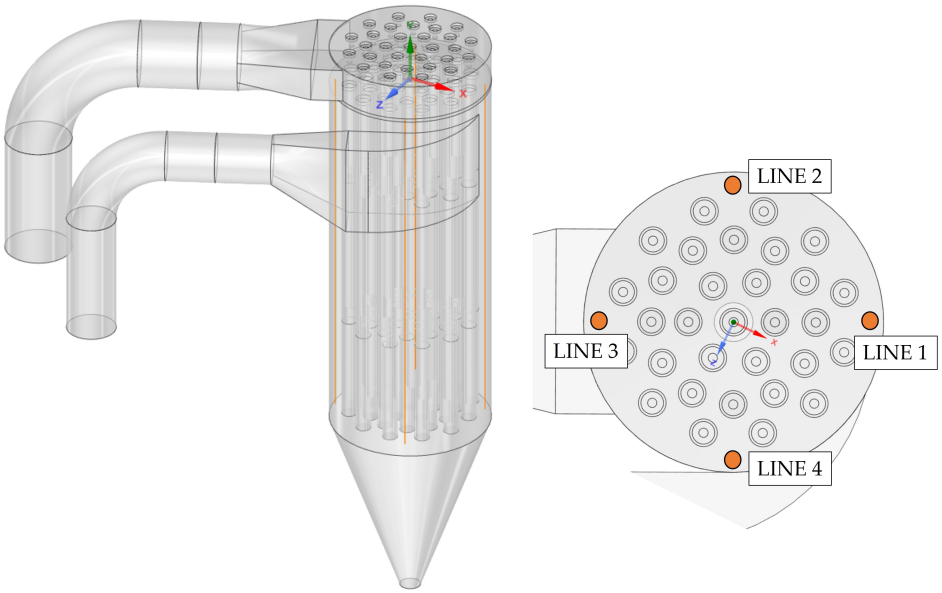

Figure 3.25: Detail of the lines on which the results were evaluated in terms of tangential velocities.

provided by the manufacturer. The technical specifications of the device are provided in Table 3.10.

Table 3.10: Technical specifications of KIMO differential pressure device equipped with a Debimo air flow measuring blade.

Pressure Range	**Velocity Range**	**Operating Temperature**	**Sensitivity**	**Precision**
±10,000 Pa	3–100 m/s	0 ÷ +70 °C	0.01 mbar	±0.5%

The outlet section of the filter, at the head of the cylindrical body, is connected to the suction section of the fan. The fan, located downstream of the filter, generates a vacuum in the same, and throughout the upstream section. A butterfly valve is installed in the pipeline connecting the filter to the fan. This valve, together with the control of the fan frequency by means of an inverter, allows the regulation of the flow rate processed by the system. The duct at the outlet of the fan returns the flow of purified air to the outdoor environment. At the ends of the filter, the pressure drop generated by the filter itself is monitored with an Endress Hauser Deltabar S PMD75, whose technical specifications are given in Table 3.11.

Table 3.11: Technical specifications of Endress Hauser Deltabar S PMD75.

Pressure Range	**Operating Temperature**	**Accuracy**
10 mbar – 40 bar	-40 – +70 °C	±0.035%

An EE650 hot-wire anemometer was selected to measure the velocities inside the filter, and it was installed in the location identified by the CFD simulations. To install the sensor, a hole was drilled in the cylindrical body wall. The anemometer was then inserted from the outside, and, using the graduated scale, it was placed at the desired acquisition point (taking into account the thickness of the wall). The technical specifications of the sensor are given in Table 3.12.

Table 3.12: Technical specifications of EE650 hot-wire anemometer.

Velocity Range	**Operating Temperature**	**Accuracy**
0 – 20 m/s	-25 – +50 °C	±(0.2 m/s + 3% of measured value)

Experimental method

Since the pilot plant is not installed in a mill and the air is drawn from the outdoor environment, the airflow is clean; therefore, the sleeve clogging conditions must be artificially reproduced. The reduction in sleeve permeability was experimentally reproduced by making portions of the sleeves impermeable to the flow, proportionally to the desired percentage of permeability reduction. To reduce the permeability as evenly as possible along the sleeves, completely free sections of filtering material and sections with zero permeability were alternated. The impermeability of the filter fabric was achieved by using food-grade film, which was wrapped over the defined portions of the sleeve according to the desired clogging condition. The choice was made for two reasons: (1) good adhesion of the film on itself, without the need to use adhesives that could damage the surface of the fabric sleeves; (2) flexibility and ease of shaping of the film that allows it to adhere properly to the sleeves, especially with the vacuum created during the system functioning, that tends to suck the film, making it adhere perfectly to the surface. The specific clogging conditions of Case 1, Case 6, and Case 8 were experimentally reproduced. Permeability values on the various sectors and the respective lengths of the sections to be coated with the plastic film are given in Table 3.13.

Table 3.13: Permeability and length of sections to be wrapped for each group and sector. C [%] is clogging percentage; P [m^2] is permeability ; L [mm] is the length of the bag to be wrapped with plastic film.

Sleeves		**Case 1**			**Case 6**			**Case 8**		
		C	**P**	**L**	**C**	**P**	**L**	**C**	**P**	**L**
1 (top)	Sector 1	0%	6.72×10^{-11}	0	80%	1.344×10^{-11}	680	95%	3.36×10^{-12}	808
	Sector 2	0%	6.72×10^{-11}	0	85%	1.008×10^{-11}	722.5	95%	3.36×10^{-12}	808
	Sector 3	0%	6.72×10^{-11}	0	75%	1.68×10^{-11}	637.5	95%	3.36×10^{-12}	808
	Sector 4	0%	6.72×10^{-11}	0	75%	1.68×10^{-11}	637.5	95%	3.36×10^{-12}	808
2 (middle)	Sector 1	0%	6.72×10^{-11}	0	20%	5.376×10^{-11}	170	50%	3.36×10^{-12}	425
	Sector 2	0%	6.72×10^{-11}	0	35%	4.368×10^{-11}	297.5	70%	2.016×10^{-11}	595
	Sector 3	0%	6.72×10^{-11}	0	30%	4.704×10^{-11}	255	55%	3.024×10^{-11}	468
	Sector 4	0%	6.72×10^{-11}	0	30%	4.704×10^{-11}	255	55%	3.024×10^{-11}	468
3 (bottom)	Sector 1	0%	6.72×10^{-11}	0	10%	6.048×10^{-11}	170	20%	5.38×10^{-11}	170
	Sector 2	0%	6.72×10^{-11}	0	5%	5.384×10^{-11}	42.5	15%	5.712×10^{-11}	128
	Sector 3	0%	6.72×10^{-11}	0	10%	6.048×10^{-11}	170	20%	5.376×10^{-11}	170
	Sector 4	0%	6.72×10^{-11}	0	10%	6.048×10^{-11}	85	15%	5.712×10^{-11}	128

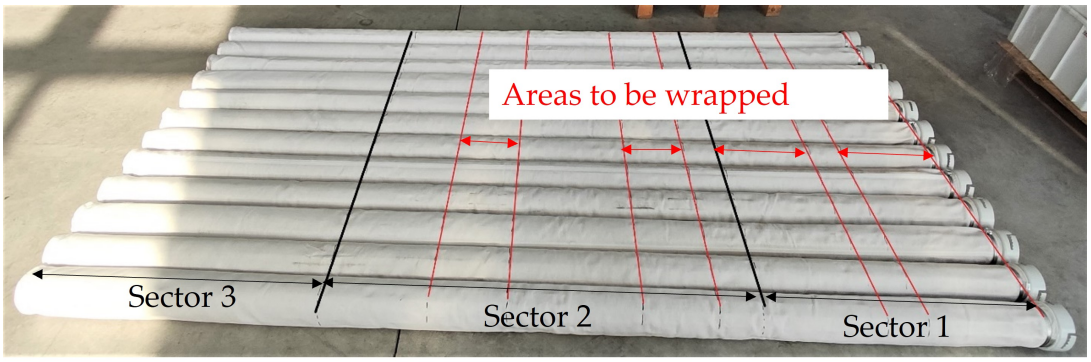

Figure 3.26: Detail of the pattern of alternation between areas covered with the film and free areas.

To have a more homogeneous permeability along each sector, it was decided to divide the area to be covered with film into two bands of equal size, interposing the clean zones in between them, as shown in Figure 3.26.

Digital Twin framework development

Based on the results of the simulations, a location for the installation of an additional velocity sensor was determined. Experimental tests were performed by varying the operating conditions, i.e., reproducing three different clogging levels and changing the inlet air flow rate.

For each clogging condition, the air flow rate was varied gradually between 1.89 m^3/s (corresponding to an inlet velocity at the filter of 15 m/s) and 2.83 m^3/s (corresponding to an inlet velocity at the filter of 22.5 m/s). Pressure drops at the ends of the filter and air velocity at the point were recorded by means of a data acquisition system developed in Lab-View which collected data from all the sensors every 2 s [145]. The duration of each test was approximately 1 h. Experimental results were then compared with simulation results for validation.

Based on the historical and simulation data collected, a virtual replica of the device was generated. Specifically, the historical data refer to the pressure drop at the ends of the filter and the tangential velocity measured inside the filter at the point identified through simulations. The results of the simulations used in the construction of the digital twin consist of the value of the flow rate passing through each sleeve under the different simulated clogging conditions. This digital model was then connected to the physical counterpart for the near real-time monitoring of the filter, with data logging performed at appropriate time intervals according to the standard operating time scales, as well as trend analysis of the system functioning. Indeed, the trend analysis performed as a moving average of a set number of time steps would allow for the early detection of the onset of malfunctions and the estimation of the remaining useful life. Additionally, simulation data allow real-time correction of the sequence and frequency of compressed air

jets, depending on the air flow absorbed by each sleeve, to preserve the correct operating conditions for as long as possible.

Generation of a model for predicting the service life of sleeves from the historical data

To develop the digital twin of the cyclone bag filter, first, the digital model was generated based on simulation results and historical experimental data measured by the sensors installed on the plant. Thanks to the data collected, it was possible to model the behavior of the filter at different flow rates, including the variations in the system pressure drop and tangential velocity as the clogging level increased. The connection between the digital and the physical twin was performed using the LabView software connected to a data acquisition (DAQ) module. The sensor data (pressure drop and tangential velocity) were recorded every 30 s, and then a moving average was performed every 60 time steps, in accordance with the typical time scales of these plants. Therefore, one measurement period i corresponds to 30 min.

As described above, currently, sleeve replacement is carried out when the pressure drop generated by the sleeves exceeds a certain threshold value. As a first step, therefore, it is possible to develop a Residual Useful Life (RUL) prediction model based on the trend of pressure drop monitored in real time. The method used to develop such a model is based on the calculation of the sleeve clogging rate per unit of time at time$t(C_{r,t})$ to estimate the residual remaining time to reach the maximum admissible clogging (expressed as maximum allowable pressure drop, Δp_{max} and equal to 15 mbar).

The sleeve clogging rate was estimated by measuring the pressure drop increase per measurement period. To have a prediction as stable as possible, since the air filtration process is susceptible to fluctuations in air flow rate values and consequently in pressure drops, and since the clogging rate is very low (usually sleeves are replaced every year or every year and a half approximately), it was decided to use the moving average method. The pressure drop value at the time t (Δp_t) was calculated as the average of the values of the previous n measurement periods, where n must be sufficiently high to smooth pressure drop fluctuations but not too large, to average between measurement periods in which sleeve permeability has not changed too much.

$$RUL_t = \frac{\Delta p_{\max} - \Delta p_t}{C_{r,t}} \tag{3.14}$$

$$\Delta p_t = \frac{\sum_{i=t-n}^{t} \Delta p_t}{n} \tag{3.15}$$

$$C_{r,t} = \frac{\Delta p_t}{\Delta t_{t-n,t}} \tag{3.16}$$

In addition, especially at the beginning of the sleeve life, since the clogging rate is very slow, there would be a very overestimated prediction of the RUL For this reason, the value of RUL calculated with the Equations 3.14 – 3.16 is always compared with the value of RUL calculated with reference to a planned replacement 1.5 years after the sleeve replacement. The lowest RUL value between the two is always considered.

The pressure value alone, however, can make an accurate prediction only when the operating conditions remain in the standard range. When, for example, the breakage of a sleeve occurs, due to the abrasive effect on it of flour and bran dust, or due to repeated impact with other sleeves, there would be a reduction in pressure drop at the ends of the filter. This reduction in pressure drops, according to Equations 3.14 – 3.16 would lead to the calculation of a higher RUL value, when in fact replacement should be planned as soon as possible. Therefore, additional monitoring needs to be combined with pressure drop monitoring for a more accurate assessment of RUL In this study, we focused on the measured tangential velocity value at the point identified through fluid dynamic simulations. Under standard operating conditions, there is an increasing velocity trend at this point. In the event of a sleeve rupture, a discontinuity in the velocity trend would be recorded at this point, which would then allow the anomaly to be identified.

The presence of simulation and historical data under different conditions lays the foundation for the continuous estimation of the filter clogging level based on the sensor measurements. Furthermore, it allows estimating an expected range of values for the measured data, making it possible to generate immediate alarms if the deviation from the estimates is higher than a limit value. Thanks to continuous data acquisition, it is possible to monitor the trends in the measured values, correlating them to the possible failures potentially affecting the plant [99, 146, 147]. In particular, the filter condition is estimated based on the difference in the values measured at consecutive measurement periods (see Table 3.14).

This deviation can be compared to defined reference values (δ_p, Δ_p, δ_v, δ_v) to detect fault conditions. In particular, δ_p and δ_v account for the sensor accuracy: the clogging rate, as well as possible minor malfunctions, can be monitored according to the variation between the pressure drop and velocity measurements of two consecutive time periods and their comparison with δ_p and δ_v, respectively. Δ_p and δ_v, on the other hand, represent maximum allowable variations in standard operating conditions, and a variation between consecutive measurements higher than these critical values is likely to indicate severe failures. In this way, it is possible to automatically schedule alarms, and eventually plant arrests, whenever a severe failure is detected. Furthermore, by performing an adequate moving averaging of the data, it is possible to perform a continuous estimation of the RUL (Figure 3.27). Thanks to the digital twin, the system monitoring and the detection of failures can be automatically and constantly performed, minimizing human decision-making and possible human errors (Figure 3.28).

Table 3.14: Logics of condition monitoring for real-time anomaly detection, based on the comparison of the values measured in consecutive time periods.

Estimated Failure Based on the Pressure Drop	**Trend in Pressure Drop**	**Trend in Tangential Velocity**	**Detected Plant State**
Clogging	dp(i) - dp(i-1) $> \delta_p$	v(i) - v(i-1) $> \delta_v$	CASE 1: Standard clogging.
	dp(i) -dp(i-1) $> \Delta_p$		CASE 2: Severe failures possibly involving other plant components, or strong and sudden clogging, caused by atypical particulate conditions.
	dp(i) - dp(i-1) $> \delta_p$	|v(i) - v(i-1)| $< \delta_v$	CASE 3: Atypical clogging, possibly affecting bottom sectors.
	dp(i) - dp(i-1) $> \delta_p$	v(i) - v(i-1) $< -\delta_v$	CASE 4: Atypical clogging or other malfunctions.
Other anomalies	|dp(i) - dp(i-1)| $< \delta_p$	v(i) - v(i-1) $> \delta_v$	CASE 5: Anomaly, possibly concurrent failures.
	|dp(i) - dp(i-1)| $< \delta_p$	|v(i) - v(i-1)| $< \delta_v$	CASE 6: Standard functioning with weak clogging.
	|dp(i) - dp(i-1)| $< \delta_p$	v(i) - v(i-1) $< -\delta_v$	CASE 7: Atypical, possibility of concurrent minor failures.
Breakage	dp(i) - dp(i-1) $< -\delta_p$	v(i) - v(i-1) $> \Delta_v$	CASE 8: Bag breakage occurring at the bottom sectors.
	dp(i) - dp(i-1) $< -\delta_p$	|v(i) - v(i-1)| $< \delta_v$	CASE 9: Possible coexistence of minor failures.
	dp(i) - dp(i-1) $< -\delta_p$	v(i) - v(i-1) $< -\Delta_v$	CASE 10: Bag breakage in the top sectors.

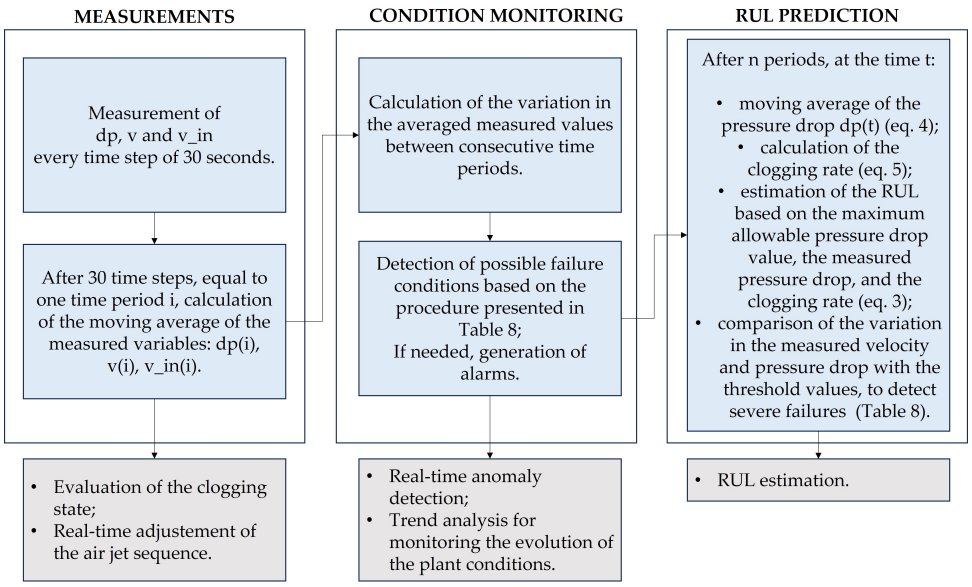

Figure 3.27: Schematic representation of the procedure adopted for the RUL estimation.

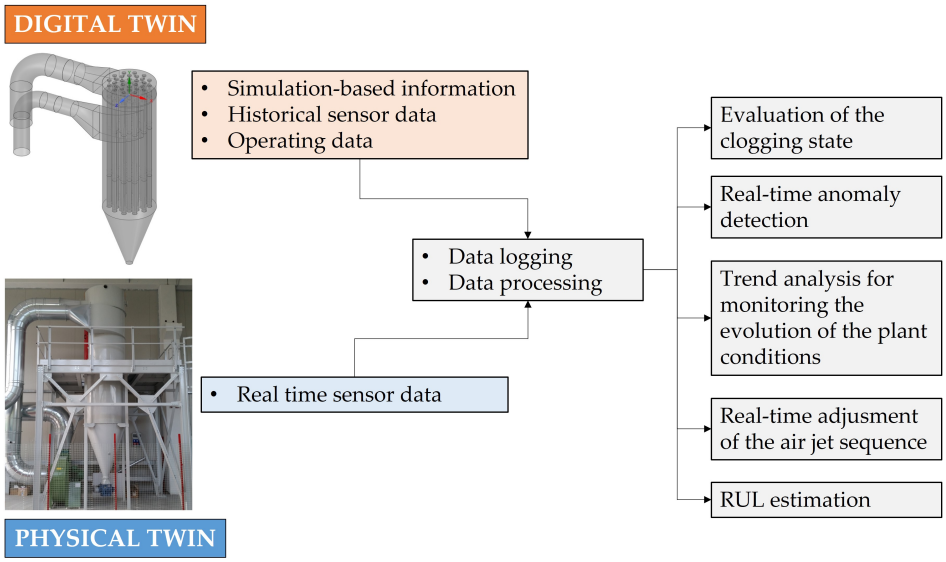

Figure 3.28: Schematic representation of the developed digital twin framework.

In particular, the method was used to report the occurrence of sleeve breakage and, consequently, generate an alarm and a request for a replacement intervention when the velocity variation between two consecutive time periods exceeded the value of δ_v and, at the same time, a pressure drop reduction greater than a threshold value δ_p was recorded. Obviously, the values of δ_v and δ_p must be defined and calibrated according to the filter geometry, sensors' characteristics, and operating conditions. In this study, they were set to 0.2 m/s and 0.1 mbar, respectively.

Generation of a model for the real-time adjustment of the sequence and frequency of compressed air jets

From the simulations conducted under different sleeve clogging conditions, the air flow

rate through each sleeve was derived. In particular, the focus was on the upper part of the sleeve (sector 1), as this is where the compressed air jet is most effective in removing the particles trapped in the fabric. The basic hypothesis, supported by experimental evidence reported by both the filter manufacturer and the end users, is that the greater the air flow through the sleeve, the greater the clogging rate. Based on this, it would therefore be recommended to associate the frequency with which compressed air is injected through the sleeve with the air flow rate through it.

Based on the framework described in the previous paragraph, the digital twin can detect whether the system is operating under standard clogging conditions or not. In the first case, the measured pressure drop value allows the identification of the actual clogging condition. From there, thanks to the simulation performed under those specific clogging conditions, the model is able to trace the air flow rate through each sleeve, and based on that, it can define the optimal sequence and frequency of cleaning operations.

Results

Simulation results

The results of the simulations at different operating conditions were analyzed to determine a trend in the pressure drop and the flow field inside the system as the clogging increased.

First, the flow pattern inside the device was monitored by plotting the velocity streamlines inside the domain. A clear swirling flow configuration emerged, as shown in Figure 3.29, representing the velocity streamlines observed from four positions rotated by 90° one to another.

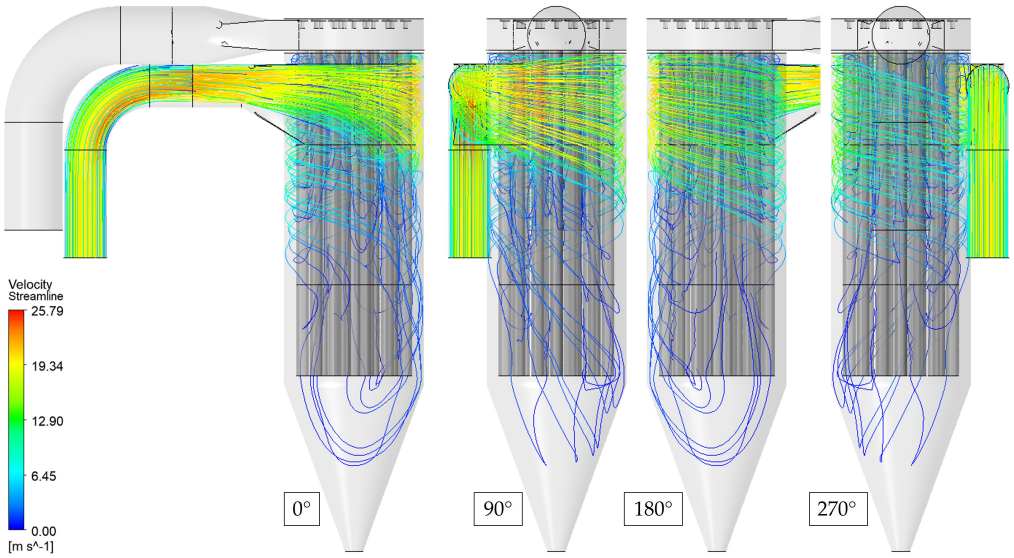

Figure 3.29: Air streamlines inside the filter.

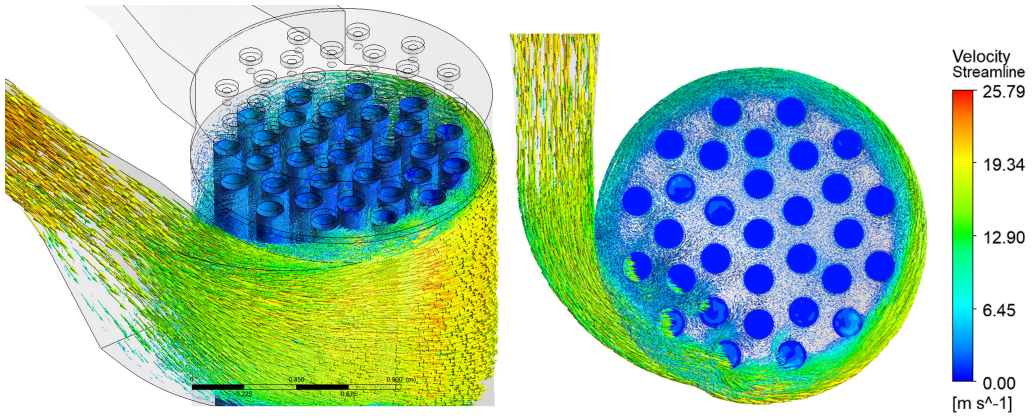

Figure 3.30: Velocity vectors in the filter inlet volute.

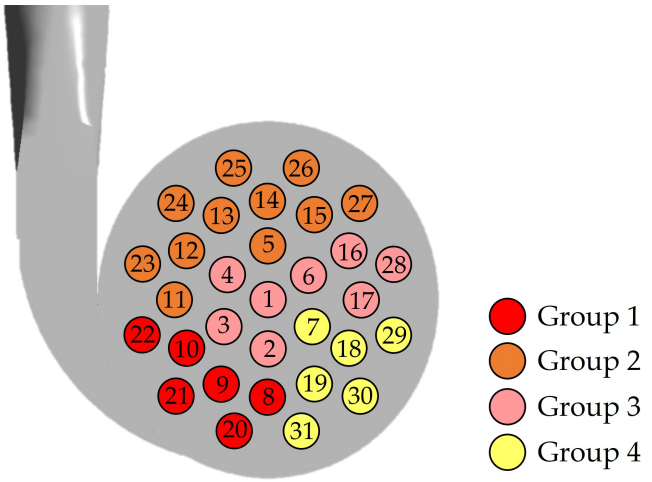

Figure 3.31: Classification of sleeves into four groups.

The first simulation with completely clean sleeves confirmed the assumption of non-uniformity in the flow rate distribution across the filtering sleeves, as can be seen in Figure 3.30. Four groups of sleeves were therefore defined, based on the flow rate elaborated, reflecting their tendency to obstruct. Even though the sleeves in groups 1 and 4 processed comparable flow rates, they were divided into two separate groups based on their position with reference to the air flow inlet: the sleeves in group 1, indeed, are exposed to a much more contaminated air flow. Figure 3.31 represents the four groups identified and the sleeves, numbered from 1 to 31, assigned to each of them.

To detect the variation in the flow field as the clogging increased, the velocity values were monitored for the eight cases simulated. Tangential velocity near the filter walls appeared to be the most appropriate value to monitor for the pilot plant simulated. Indeed, even though variations could be observed in the ascending and descending velocities at different operating conditions, tangential velocity appeared to be the best choice, both due to its magnitude and the ease of measurement (Figure 3.32).

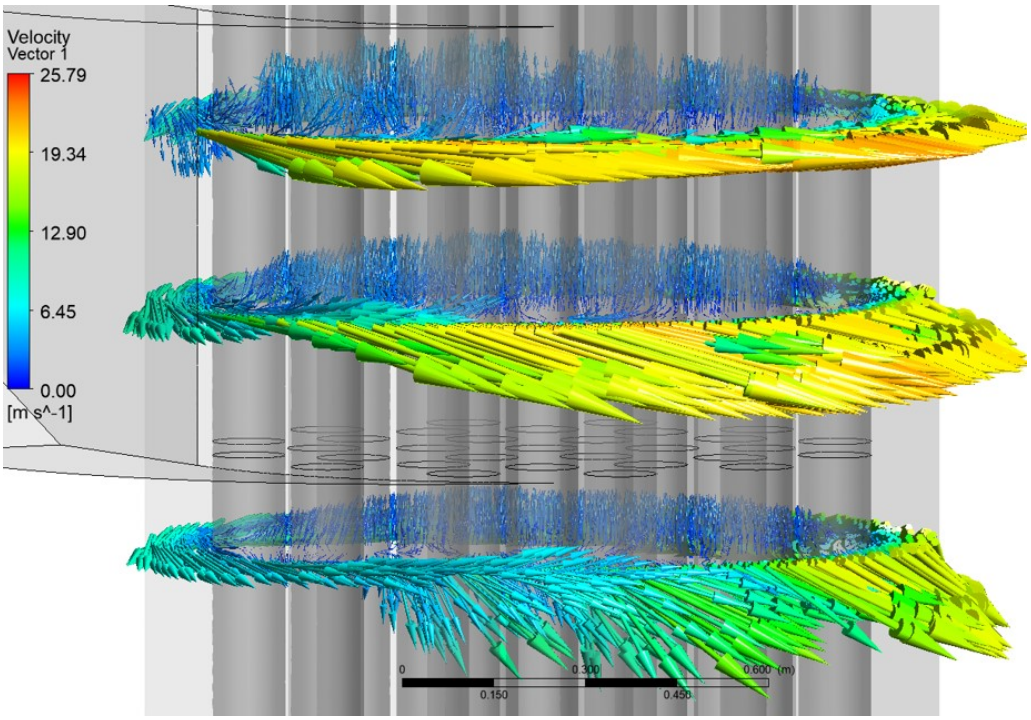

Figure 3.32: Velocity vectors on three transversal planes.

Tangential velocity was monitored for the different conditions simulated on the four longitudinal lines presented in Figure 3.25, at a distance of 5 cm from the filter wall. In the plots presented in Figure 3.33, the origin of the x-axis corresponds to the top of the sleeves. A clear trend in the calculated velocities, with the plotted lines sorted according to the clogging level, can be observed on several locations of lines 2 and 3. Due to the layout and the geometrical features of the pilot plant, the new sensor was installed on line 3, at a distance of 2400 mm from the top of the sleeves.

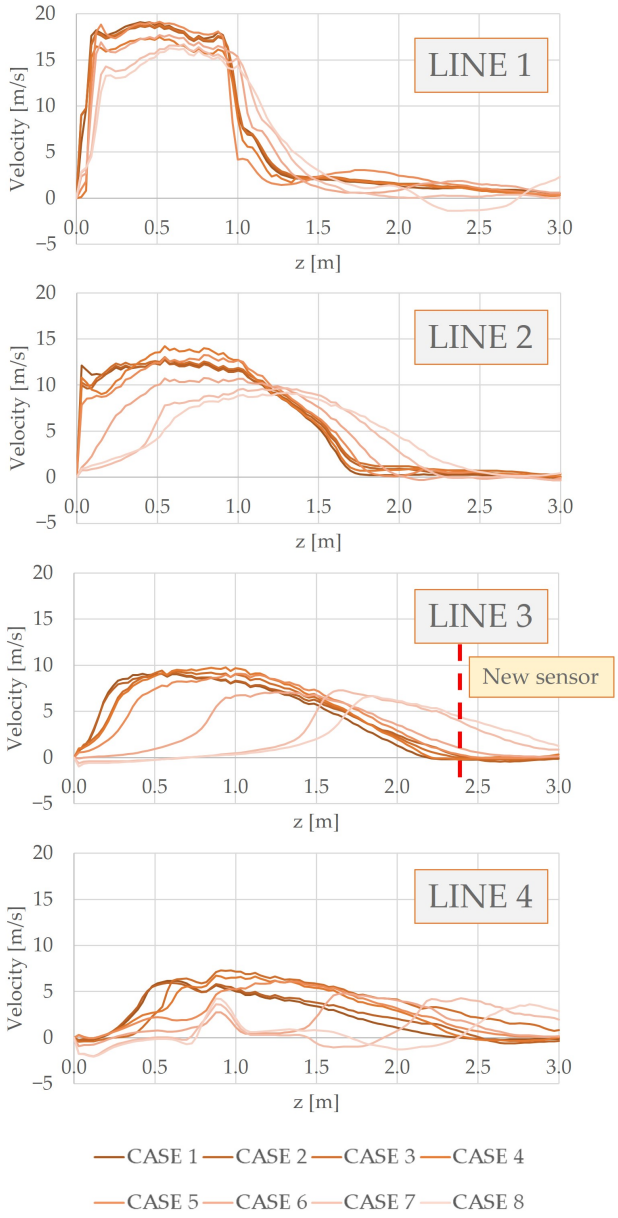

Figure 3.33: Tangential velocity trends on the four lines represented in Figure 4 for the eight different clogging conditions.

The results of the simulations, therefore, allowed the highlighting of trends in both the system pressure drop and the tangential velocity values at different clogging levels. These trends were validated with experimental tests on the pilot plant. The results for the air flow rates passing through sector 1 of each sleeve are shown in Table 3.15. The sleeves are sorted in descending order according to the air flow rate passing through them. Based on the results obtained, a possible cleaning sequence with the respective frequencies, expressed in terms of time between injections, is also shown in Table 3.15.

Table 3.15: Air flow rate flowing through sector 1 of each sleeve for the different clogging conditions considered. S is the sleeve number, while FR is the flow rate in m^3/h.

Time between Compressed Air Injection	**Case 1**		**Case 2**		**Case 3**		**Case 4**		**Case 5**		**Case 6**		**Case 7**		**Case 8**	
	S	**FR**	**S**	**FR**	**S**	**FR**	**S**	**FR**	**S**	**FR**	**S**	**FR**	**S**	**FR**	**S**	**FR**
30 s	25	300.78	25	285.38	25	250.43	25	220.23	25	186.08	16	174.75	16	118.39	14	83.43
	26	291.85	26	274.53	26	239.06	26	215.01	4	182.59	28	174.25	28	117.97	26	81.87
	10	277.25	10	261.24	14	224.42	14	201.21	26	181.91	3	170.38	3	116.51	15	80.35
	14	267.75	14	254.49	24	213.40	4	198.83	3	181.30	4	167.76	4	115.28	21	80.22
	13	256.22	21	245.76	13	211.85	16	195.30	16	178.90	6	166.30	6	114.94	13	79.52
	21	252.46	24	244.36	10	211.27	13	194.91	2	178.26	1	165.72	1	114.66	25	79.54
	24	250.37	13	243.13	16	202.94	3	194.69	1	177.89	17	165.44	17	114.12	10	79.25
	9	240.77	9	241.08	4	202.83	3	194.49	6	174.98	2	160.83	9	113.48	5	79.06
60 s	15	240.74	15	230.18	15	202.76	2	194.16	19	170.37	29	159.82	3	113.06	27	78.11
	22	240.60	12	228.63	3	201.62	6	191.29	15	159.65	18	153.88	12	113.74	12	77.37
	12	238.85	22	228.12	12	197.61	4	190.66	7	167.58	9	158.94	19	111.73	16	77.01
	11	234.78	11	223.80	9	197.19	12	187.81	7	156.00	19	153.30	7	109.63	7	76.19
	23	228.74	23	220.29	6	197.19	8	184.42	8	166.90	10	154.73	7	111.35	9	76.90
	27	228.54	27	216.86	21	195.25	13	184.40	10	152.37	31	109.50	10	76.28	10	76.28
	5	221.62	3	214.97	3	193.65	17	182.90	13	161.83	9	152.04	14	69.84	3	76.28
	3	217.34	16	214.38	5	192.44	18	181.88	24	151.88	24	152.18	3	87.18	2	84.35
90 s	16	216.63	4	212.96	27	187.76	12	181.24	31	158.14	31	149.42	15	67.13	18	75.56
	4	215.98	5	212.75	11	186.89	5	176.55	15	155.98	22	143.12	13	66.44	29	75.49
	8	212.23	6	204.45	2	186.39	28	175.35	29	155.41	26	139.65	25	66.21	11	75.42
	20	210.46	1	201.51	23	186.19	27	174.47	30	152.90	25	135.33	10	65.66	4	75.08
	6	205.15	20	198.86	22	184.95	23	171.23	27	150.90	20	134.82	5	65.57	17	74.94
	1	201.68	17	195.86	17	184.07	11	170.80	12	150.71	8	132.98	21	64.70	2	74.71
	17	196.12	2	195.17	7	179.41	10	169.29	5	149.81	14	130.22	9	63.75	19	74.70
	2	194.42	28	192.97	28	178.74	8	169.25	20	148.69	27	124.71	27	63.65	28	74.41
120 s	28	194.30	8	189.97	18	176.97	31	166.69	11	145.03	15	123.16	12	63.20	7	74.34
	7	186.35	7	188.12	19	173.03	9	165.46	23	142.70	13	122.03	11	61.69	8	74.22
	18	184.83	18	185.42	20	169.50	30	163.11	10	142.62	24	117.14	24	60.96	24	74.13
	19	177.85	19	181.98	8	168.37	29	162.45	8	142.52	5	116.12	8	60.95	22	72.24
	29	172.82	30	173.55	29	162.70	22	157.85	9	141.54	12	114.30	20	60.40	31	71.85
	30	172.31	29	173.11	31	156.91	20	157.04	22	137.64	11	113.85	22	59.77	30	71.53
	31	163.92	31	166.41	30	153.45	21	152.05	21	136.64	23	110.00	23	58.79	23	70.32

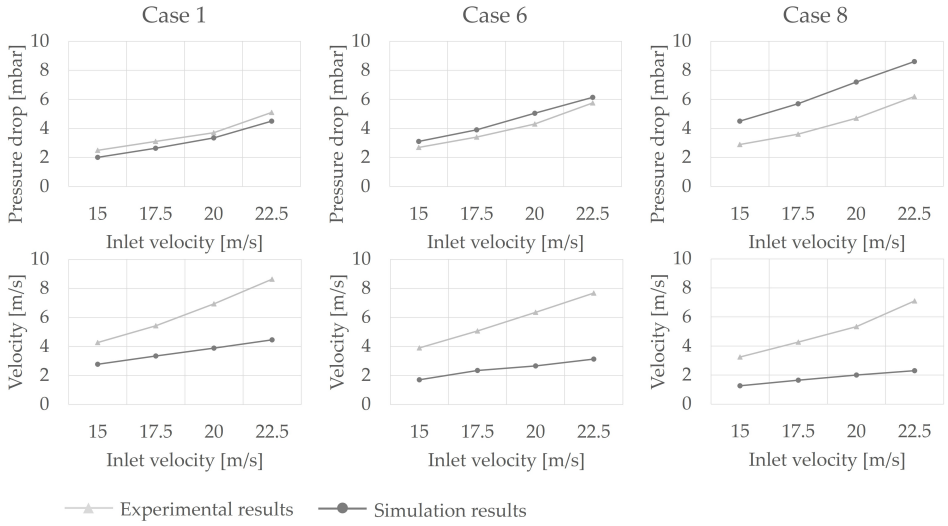

Figure 3.34: Comparison between experimental and simulation results for Case 1 (left), Case 6 (center) and Case 8 (right) both in terms of pressure drops (top) and tangential velocity at the point inside the filter (bottom).

Validation of simulation results

A comparison between experimental results and simulation results, both in terms of pressure drops and in terms of tangential velocity at the defined sensor location inside the filter, is reported in Figure 3.34.

Building of the Digital model

All the experimental results collected were processed in MATLAB, and the regression curves for both the pressure drop and the tangential velocity, in the function of the inlet velocity, were generated using the curve fitting tool. Results are reported in Figures 3.35 and 3.36. The graphs confirm all the statements given above.

Test of the Digital model for issue detection and RUL prediction

The digital twin developed was then tested on a real work cycle, during which both the pressure drop at the ends of the filter and the velocity at the identified point within the filter were continuously monitored. During the work cycle, at each time instant, the digital twin calculated the RUL As described in the methods section, the RUL was calculated based on the moving average carried out on the values of pressure drops measured in the n previous periods. To define the optimal value of n, a sensitivity analysis was conducted as$n$changed. The result is shown in Figure 3.37. A value of$n$equal to 196 h yields a very stable prediction.

After about 7200 h of work, a sleeve breakage was simulated. This can be appreciated from Figure 3.38, where a sharp drop in both pressures and velocities can be observed.

A comparison between the predicted RUL without combined monitoring of pressure drop and tangential velocity at the identified point, and thus without the possibility of

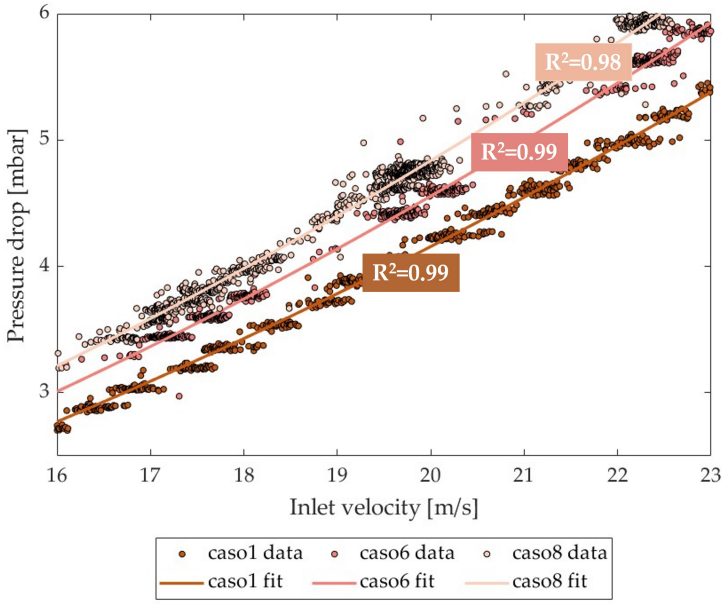

Figure 3.35: Experimental data and correlation curves between measured pressure drop and air flow rate for different tested conditions of sleeve clogging.

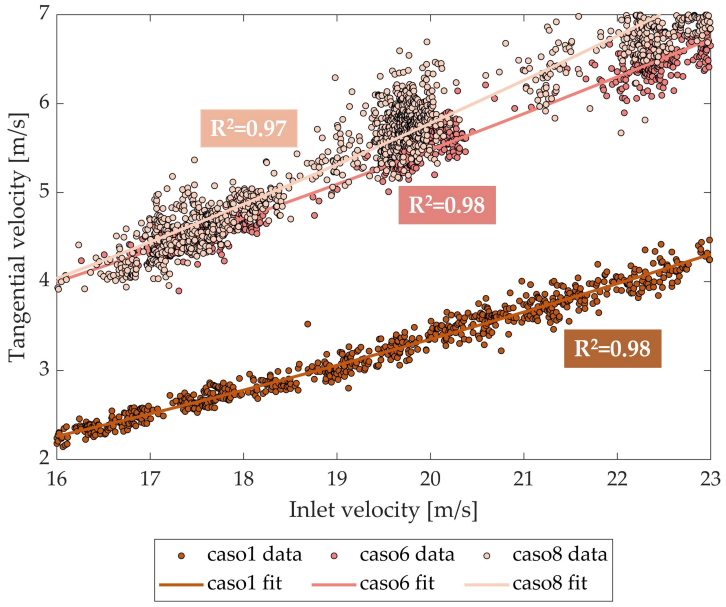

Figure 3.36: Experimental data and correlation curves between the measured tangential velocity at the point inside the filter and air flow rate for different tested conditions of sleeve clogging.

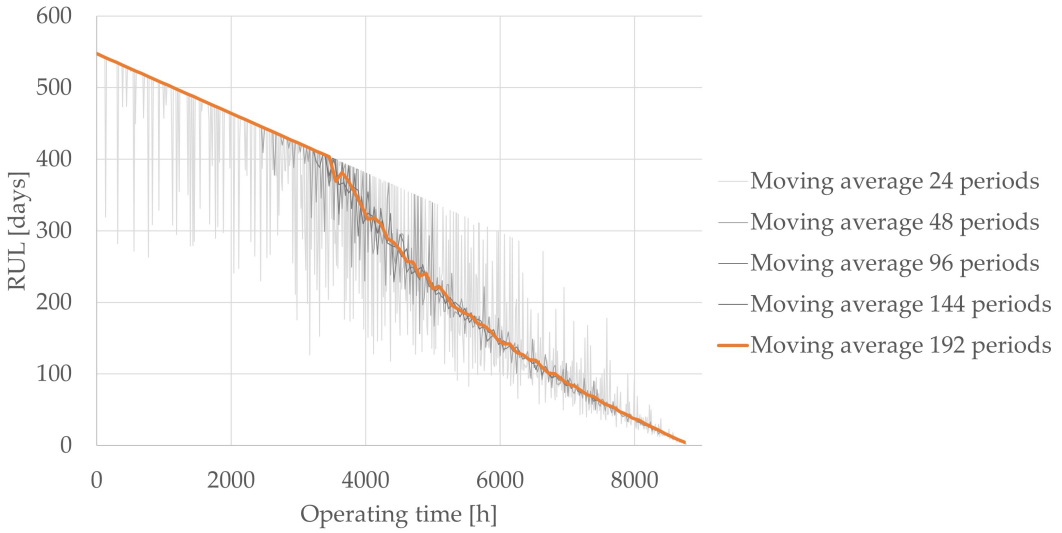

Figure 3.37: Experimental data and related correlation curves between the recorded tangential velocity at the point inside the filter and air flow rate for different tested conditions of sleeve clogging.

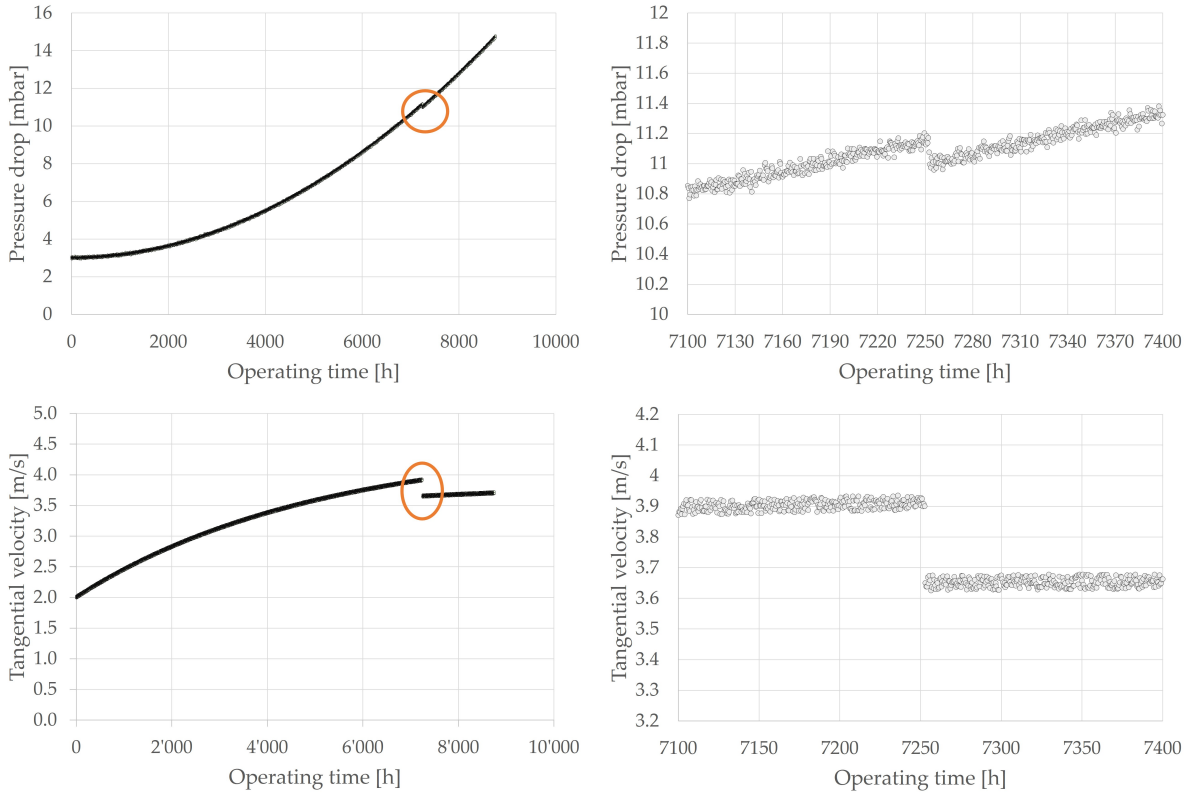

Figure 3.38: Discontinuities in pressure and tangential velocity trends as a result of a sleeve rupture.

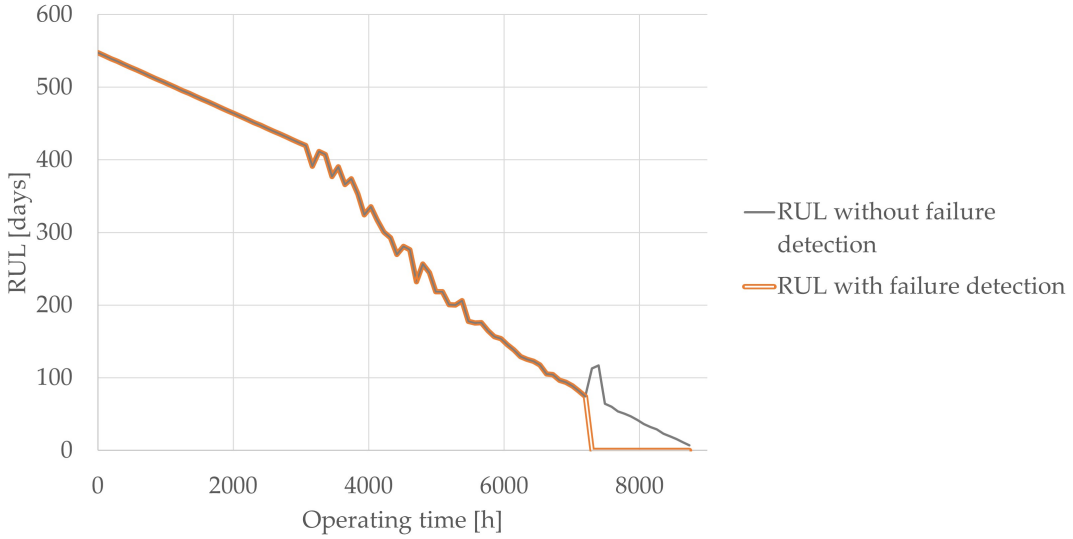

Figure 3.39: RUL forecasting with or without failure detection.

fault detection, and the predicted RUL with combined monitoring of the two variables is shown in Figure 3.39. It is evident that the digital twin was able to detect the rupture and, as a consequence, it forced the RUL to zero, whereas the RUL evaluated by observing only the pressure drop would even lead to increasing the prediction of the RUL at the time of breakage.

Discussion

The results show that the results of the simulations and experimental results are in good agreement. The trends of measured and simulated pressure drops as the air velocity at the filter inlet changes are parallel. The deviation between the curves could be related to the uncertainty in the air velocity measurement with the KIMO sensor, which, due to space constraints, was installed close to a curve. More significant deviations are observed for the pressure drops for case 8, which could be related to the fact that coating the sleeve with the food-grade film is not perfectly equivalent to clogging the sleeve evenly. Obviously, this difference increases as the level of fouling increases, and this is why the deviation is more pronounced for case 8 than for case 6.

The velocity trends at the measured point inside the filter are also in agreement. There are more significant deviations in this case, and this may be mainly related to three aspects, which may also explain why the deviations increase as the air flow rate at the filter inlet increases:

1. The data extracted from the simulation is exclusively related to the tangential component of the velocity vector, while the anemometer reading, although correctly positioned, without taking into account human error, is partially affected by the other velocity components, due to its construction characteristics.

2. The way the sleeves are constrained to the head of the filter allows them to oscillate, given even the 3 m length, is not constrained to the base or anywhere else. The oscillation can impact the flow field distribution, even significantly affecting the velocity value measured by the sensor.

3. The presence of areas completely obstructed by the film alternating with completely clean areas affects airflow differently than a sleeve that is uniformly obstructed.

Thus, it can be concluded that the experimental results confirm the correlations between pressure drops and air flow rate and between the measured velocity at the identified point inside the filter and air flow rate. They also confirm that pressure drops increase as sleeve clogging increases and that the air velocity at the identified point inside the filter increases if clogging proceeds in a standard manner.

In this study, it was not possible to validate the model for the real-time adjustment of the sequence and frequency of compressed air jets, whose results are reported in Table 3.15. In fact, by using food-grade film to artificially reproduce sleeve clogging, compressed air injections would have been ineffective. It will be necessary in future activities to test and validate this model in a real production setting in order to verify the effectiveness of the proposed method and to optimize both the sequence and the frequency based on experimental evidence.

The digital twin developed demonstrated that it can accurately predict the sleeves' RUL and identify failures. At present, it has been trained with data under normal clogging conditions. Future activities will have to focus on experimenting with many more operating conditions to increase its robustness to make it industrially viable. Moreover, simulation results can be used to expand the capabilities of the digital twin by providing data that are of great operational interest but would be physically difficult to acquire (e.g., the upward velocity within the sleeves, the impact velocity against the sleeves, the flow rate filtered by each sleeve, etc.).

Conclusions

In this study, the digital twin of a cyclonic bag filter designed for the suction system of a wheat mill was developed. The digital twin, by combined monitoring of the pressure drop at the ends of the filter and the tangential velocity measured at a point within the filter, appropriately identified through fluid dynamics simulations, proved to be able to estimate the condition of the system, detect failure events, and predict the sleeves' RUL Further activities could be conducted to improve the reliability of the digital twin: (i) Carry out experimental tests under different sleeve clogging conditions to increase the volume of historical data and deepen the understanding of the plant behavior; (ii) Identify any values of interest to be monitored on the simulated and validated digital model, which cannot be physically acquired, and which could increase the potential of the digital twin;

(*iii*) Implement the digital twin on an industrial plant and test its operation under real operating conditions.

3.3.4 Simulation of sloshing inside beverage container after filling on a rotary filler

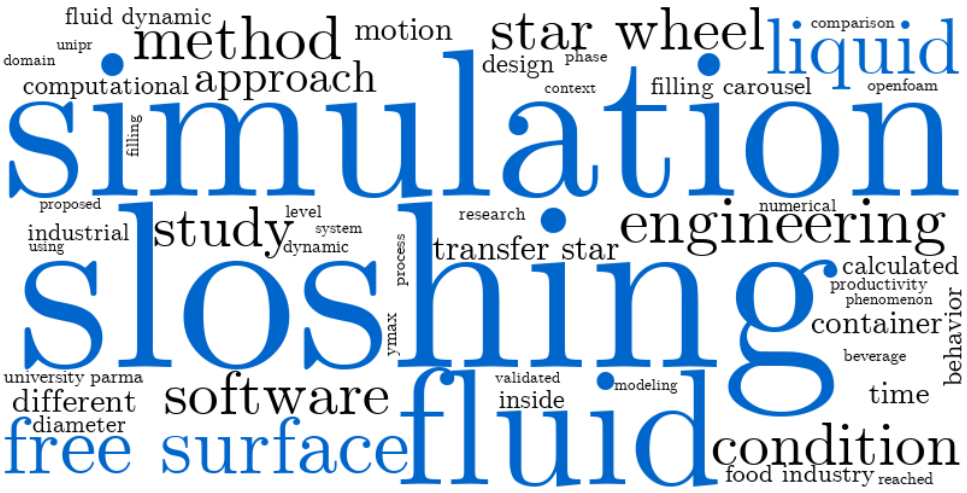

The research in this chapter has been included in the peer-reviewed conference paper [148] *Solari, F., Lysova, N., Montanari, R., Scano, F., Bedogni, E., and Copelli, G. (2024). Computational fluid dynamics simulation of sloshing inside beverage cans on a rotary filling machine. ECMS 2024 Proceedings Edited by Daniel Grzonka, Natalia Rylko, Grazyna Suchacka, Vladimir Mityushev, 394–400. https://doi.org/10.7148/2024-0394.*

The authors would like to express their gratitude to the company KOSME S.r.l. for the crucial support in conducting the analysis and in preparing the present research.

Abstract

Sloshing is a critical issue in many industrial contexts. In the food industry, it becomes particularly relevant during the filling of beverage cans and bottles with automatic rotary machines, when the uncapped filled containers move to the transfer star wheel, suddenly changing direction of motion and potentially causing the spilling of the product. Deep knowledge of the system behavior and the fluid dynamics in the domain is essential to guarantee the safety and quality of the final products and processing environment. In this study, Computational Fluid Dynamics (CFD) was used to simulate sloshing in beverage cans using two CFD software: commercial ANSYS Fluent and open-source OpenFOAM. Some modeling strategies are explored with the aim of making the simulation more efficient without impacting the results, and an approach for tracking the maximum fluid level in the can is proposed. The modeling methodology was validated by means of an analytical model and by comparing the results calculated by the two software. Finally, operational insights were derived based on the results of a sensitivity analysis carried out by varying the star wheel diameter and the system productivity.

Introduction

Sloshing, the transient movement of liquids within a confined container, poses significant challenges in various industries. In transportation and maritime contexts, it can lead to loss of control over the vehicle or compromise the stability of the ship due to the movement of large volumes of fluid.

The phenomenon of sloshing, however, also affects the processing activities of the food industry, mainly in the stages following the filling of containers, when they are transferred towards the sealing station. In this case, the undesirable effect is related to the spilling of fluids, which happens when the product overflows from the container due to the major stresses and acceleration experienced during the motion. Spilling leads to loss of product, contamination of the processing environment, and possible deposition of fluids on the outer walls of the container that could compromise the integrity of the product and the sealing process, undermining both the safety and the quality of the final product.

This phenomenon is particularly relevant during the filling of beverage cans, due to the very limited headspace and the high rotation speeds of the transfer star wheel that increase the probability of sloshing. In this case, the occurrence of sloshing and spilling mainly impacts the seaming of the cans.

A deep understanding of the dynamics of the fluid inside the cans as they travel between the filling and sealing stations, as well as a detailed knowledge about the behavior of the free surface, are crucial for correctly defining the productivity, thus the rotational velocity of the machines, reducing testing times, wastes, and quality issues. In this context, numerical simulation can be of significant support, providing the decision-makers with useful insights and data for detailed analyses, while considerably reducing experimental testing.

Over time, analytical models of sloshing have been developed and validated (Ibrahim 2005) regarding mostly simple geometries and standard boundary conditions. To increase the modeling precision and correspondence to the actual conditions, simulation can be a crucial tool [149]. For example, simulation can be used to predict the severity of sloshing in relevant applications [150]. As always when it comes to simulation results, validation is required, and it can be usually based on the comparison with theoretical or experimental results [149, 151]. To capture in detail the fluid dynamics involved with the sloshing phenomenon, Computational Fluid Dynamics (CFD) plays a key role, as it allows for modeling complex fluid-structure interactions under various conditions, considering realistic container geometries, custom transfer trajectories, as well as complex and even multiphase fluids usually processed in the food industry. CFD has been applied to simulate a huge variety of food industry processes in the last years [1, 152], also thanks to the increase in the computation resources and the presence of numerous simulation software.

To perform CFD simulation, indeed, several commercial and open-source software are available. While commercial CFD software offer benefits such as technical support, updates and enhanced usability, open-source tools provide flexibility and free access, albeit requiring more expertise.

Despite the relevance of sloshing in the beverage industry, to the best of the authors' knowledge, no studies in the literature have dealt with this particular issue to date. Indeed, most articles in the literature have focused on the sloshing of fluids in tanks [153] during transportation, sloshing occurrences and effects in the aerospace [154, 155] and naval applications, and the different methods that could be implemented to mitigate this phenomenon, e.g., introduction of different geometries and characteristics of baffles [156, 157]. In the context of sloshing in the field of automatic machines, [158] have presented a technique for analyzing sloshing in cylindrical containers performing rectilinear movements. [159] have proposed a discrete linear model of sloshing, implementable in real-time for the feedforward anti-sloshing control of container motion.

This article presents a simulation approach, implemented with both commercial ANSYS Fluent and open-source OpenFOAM CFD software, to predict sloshing during the transfer of beverage containers after filling. The calculated inclination angle of the free surface is validated with theoretical data. In addition, using two different tools allows to inter-validate the simulation models by comparing the respective results. Some modeling strategies are explored, aiming at making the simulations more rapid and efficient. Then, the results of the simulations are discussed, proposing an approach for tracking the level of the fluid during the transfer of the container and detecting the occurrence of sloshing. Finally, a sensitivity analysis is performed to assess the effect of different transfer star wheel diameters and productivity levels on the maximum level reached by the fluid.

Methods

Analyzed scenario

The fluid behavior inside a can during the transition from the filling carousel to the transfer star wheel, as depicted in Figure 3.40, was analyzed. For this purpose, the period from the end of the filling process to the exit from the transfer star wheel was simulated. In the simulated machine, the filling is completed about 40 degrees before the carousel change; it was assumed that, at that time, the free surface conformation within the can was already stabilized.

Since the filling carousel has a larger diameter than the transfer star wheel, and since the tangential velocity must be the same, the latter has a higher rotational speed. A real industrial context was considered, characterized by a productivity of 20'000 cans per hour (c/h). 0.5-litre can geometry, having an inner diameter of 0.033 m and height of 0.15 m, was modeled.

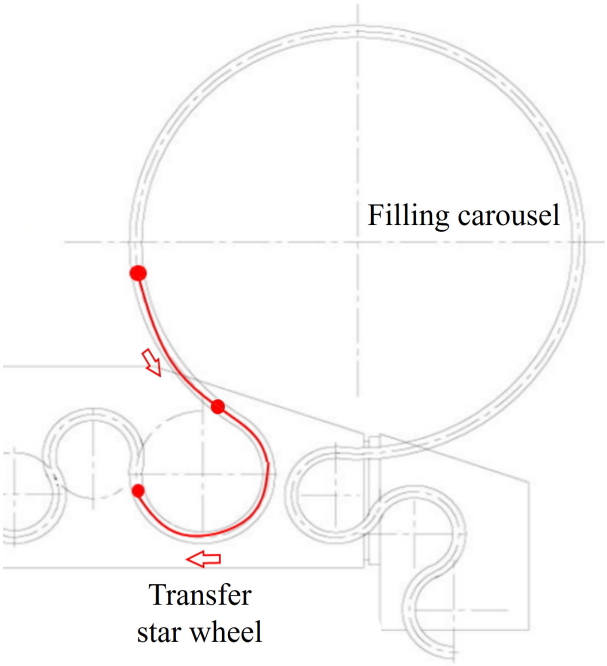

Figure 3.40: Scheme of the simulated filling line

Table 3.16 reports the geometric characteristics and the operating conditions assumed for the two carousels. Based on the data, the law of motion of the can, in terms of the evolution of angular velocity over time, and as a consequence, of centrifugal acceleration over time, can be derived.

In Figure 3.41, the angular velocity and the centrifugal acceleration characterizing the motion of the can are presented: at 0.5 s the can is assumed to transfer from the filler to the star wheel.

Numerical simulation

In this study, we explore the capabilities of CFD simulation for studying sloshing phenomena in industrial bottling processes.

Aiming to assess the reliability of the proposed approach, the results obtained with two different software, namely ANSYS Fluent and OpenFOAM, were compared.

The single reference frame (SRF) method was adopted to reproduce the behavior of the fluid inside the can as it moved within an absolute reference frame with a given

Table 3.16: Characteristics of the two carousels

	Diameter [mm]	**Number of heads**	**Rotational speed [rev min^{-1}]**
Filling carousel	1080	24	13.89
Transfer star wheel	720	16	20.83

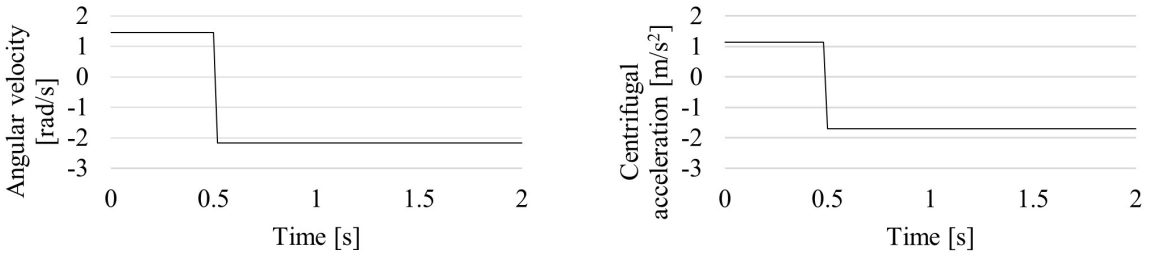

(a) Angular velocity.

(b) Centrifugal acceleration.

Figure 3.41: Velocity and centrifugal acceleration characterizing the motion of the can in the simulated system.

Table 3.17: Characteristics of the fluids

	Air	**Water**
Density [kg m^{-3}]	1.225	998.2
Dynamic viscosity [Pa s]	1.8e-5	1.0e-3
Surface tension [N m^{-1}]	0.072	

law of motion. This method consists of an alternative approach, less computationally demanding compared to the traditional moving mesh method, that can be adopted when simulations involve moving regions, allowing to study them in their respective reference frames.

A multiphase simulation was set up using the Volume-of-Fluid (VOF) method, which is appropriate for the simulation of immiscible fluids being separated by a well-defined interface surface (free surface) [160]. Air and water were considered as fluids, whose properties, although well known, are summarized in Table 3.17.

Under the conditions considered, a significant but not abrupt free surface perturbation was expected, not affecting the entire volume of fluid contained in the can, but only the upper part. For this reason, it was decided to include only the upper 3 cm of the can in the calculation, as the lower part of the cylinder contributed minimally to the sloshing dynamics. This assumption was validated by comparing the results obtained by simulating the whole can geometry with those obtained with the reduced domain. To ensure a high-resolution capture of the fluid behavior, a hexahedral mesh, with equilateral elements having a dimension of 3 mm, was defined (Figure 3.42). To better compare the results obtained, the same mesh was used with both solvers.

The law of motion was finally assigned to the mesh by imposing the acceleration field represented in Figure 3.41. Moreover, a gravitational field, with a downward acceleration of $9.81 m/s^2$, was applied.

Inclination of the free surface

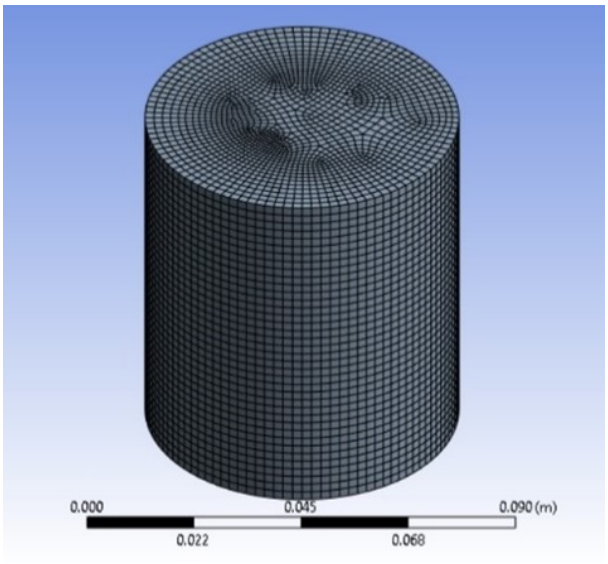

Figure 3.42: Hexahedral mesh of the computational domain

To identify the initial condition, i.e., the shape of the liquid-free surface inside the can at the end of the filling process, especially in terms of inclination angle (θ) with respect to the horizontal plane, an ad-hoc simulation was conducted. Starting from a resting condition ($\theta = 0°$), the revolution of the can on the filling carousel was simulated until a stationary condition was reached. The inclination of the free surface was then measured and compared with the angle calculated by solving the balance of forces acting on the fluid (eq. 3.17), as described also in [149]:

$$\theta = arctan(\frac{a_r}{g}) \tag{3.17}$$

Where a_r is the centrifugal acceleration in the radial direction and g is the gravitational acceleration, acting in the y direction.

This comprehensive procedure served as a robust foundation for determining the initial free surface angle in the first carousel and ensured accurate initialization for subsequent simulations. Furthermore, it allowed to validate the simulation approach with well-established theoretical notions.

After the initial inclination angle was obtained and validated as described, the simulation of the transition phase from the filling carousel to the transfer star wheel was performed. The simulation was run using both software packages, setting the angle determined as the initial condition. The simulation outcomes were then compared, to check whether the results obtained with both software, in terms of liquid sloshing inside the can, starting from an identical initial condition, were the same. This further step is intended as an inter-validation step of obtained results.

Maximum fluid level Y_{max}

To qualitatively assess sloshing, it is sufficient to observe the behavior of the free surface during the movement of the can. To make a more accurate and precise assessment, the maximum height reached by the free surface during the can motion, Y_{max}, was also calculated and traced over time. This parameter can be very useful in assessing the impact sloshing may have on the process quality and efficiency. When Y_{max} is lower than the total height of the can, even if sloshing is happening, the liquid doesn't leak out. In this scenario, therefore, sloshing does not represent an issue. On the other hand, when Y_{max} exceeds the maximum height of the can, the liquid may overflow from the can and negatively affect the filling process. The comparison of the results obtained with the two software was then performed in two ways:

- a comparison of the trend over time of the maximum height reached by the free surface.
- a frame-by-frame comparison between the shape of the free surface computed by the two software in specific time intervals.

Finally, the proposed method was used to evaluate the effect that some operational and design parameters have on liquid behavior. In particular, the impact of transfer star wheel diameter and line productivity was evaluated.

Results

The first phase of the study aimed to identify the computational domain. To have a trade-off between computational time and results accuracy, it was decided to compare the results achieved considering only the upper part of the can (30 mm), with the results obtained considering the whole can. The results are shown in Figure 3.43a.

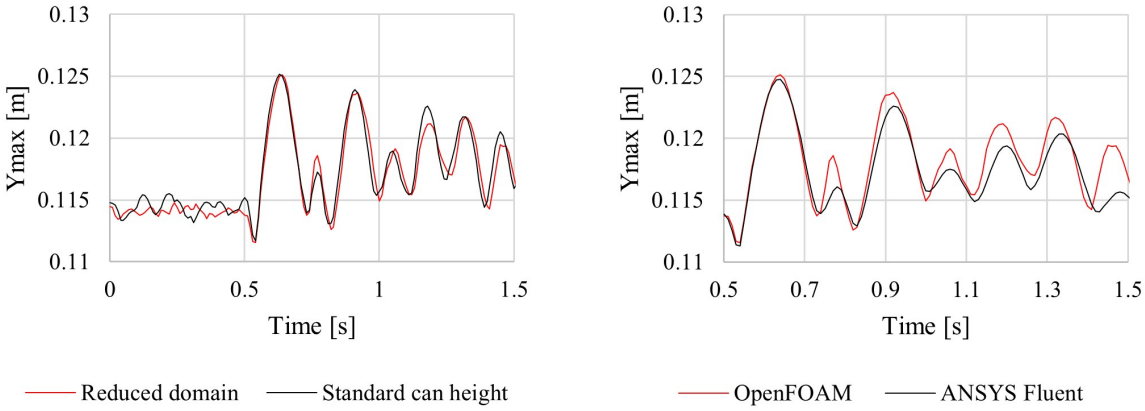

(a) Comparison of standard vs reduced domain

(b) Comparison of results calculated with OpenFOAM vs ANSYS Fluent.

Figure 3.43: Comparison of the results with different settings and software.

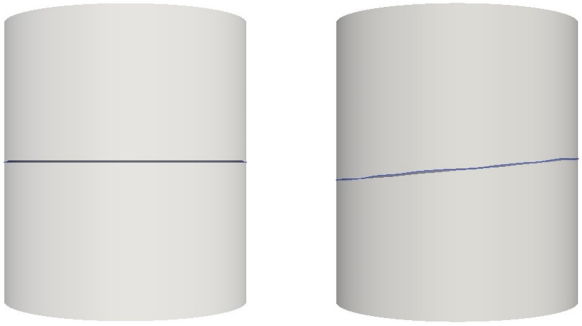

Figure 3.44: Initial and final states of the free surface.

Based on the graph, it can be observed that as the can moves from the filling carousel to the transfer star wheel (t = 0.5 s) sloshing occurs. A wave is generated that reaches its maximum peak 0.14 s after the transfer and then continues fluctuating throughout the period considered. The results of the two simulations are perfectly overlapping: the percentage deviation between the two curves is always less than 3.9%. It can therefore be concluded that the liquid in the bottom of the can does not significantly affect the dynamics of sloshing and can consequently be excluded from the computational domain.

The second phase of the study focused on identifying the liquid condition at the exit of the filling carousel. To validate this condition, the angle of inclination of the free surface under the effect of the centrifugal force generated by the rotation of the carousel was calculated in two different ways. The balance of forces acting on the free surface (eq. 1) leads to an angle value of 6.64 degrees. Below are the results of a simulation that, starting from a resting condition ($\theta = 0°$), simulates the revolution of the can on the filling carousel until the inclination angle of the free surface is stabilized (Figure 3.44).

Measuring the inclination angle that the free surface reaches under stationary conditions yields a theta value of 6.24 degrees which results in a deviation of 6% from the theoretical value, calculated with eq.1. This deviation can be considered acceptable because it is included within the range of accuracy that the mesh size allows for.

The following phase of the study focused on the sloshing occurring as the beverage can moved from the filling carousel to the transfer star wheel. A comparison between the results obtained with ANSYS Fluent and those obtained with OpenFOAM, is shown in Figure 3.43b for the value of Y_{max}, while a representation of the free surface, calculated with the two software, at several time steps is presented in Figure 3.45.

It can be concluded that the results of the two CFD software agree both in the prediction of the maximum fluid level reached inside the can and in the oscillation frequency of the wave itself. Even the shapes of the free surface calculated by the two software appear to be in good agreement.

Finally, the proposed simulation approach was used to evaluate the impact that some processing and geometric parameters have on liquid behavior (Figure 3.46). The evolution

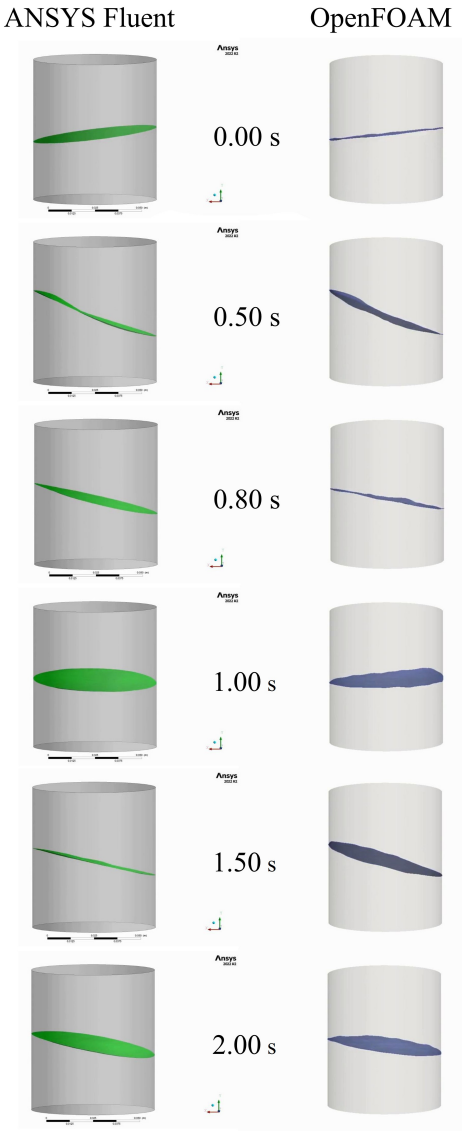

Figure 3.45: Free surface of the fluid inside the can at different time steps, calculated with ANSYS Fluent (left) and OpenFOAM (right)

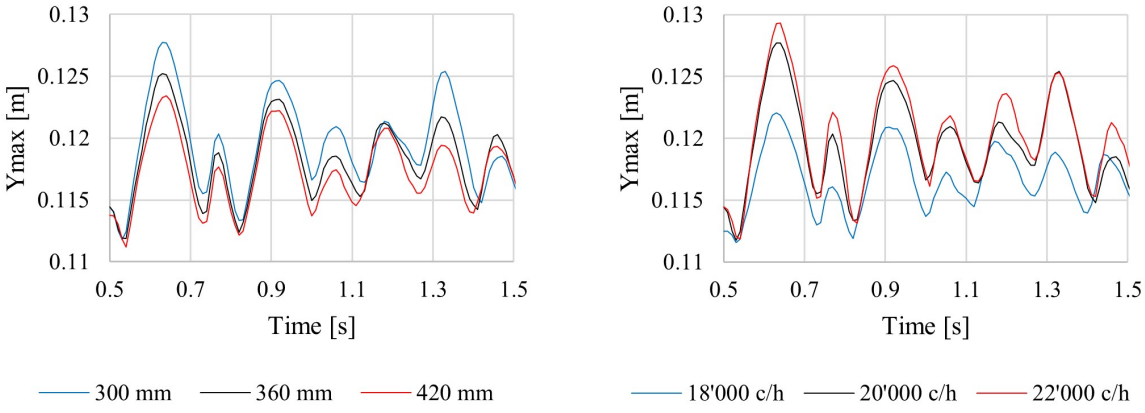

(a) Different star wheel diameters.

(b) Different productivity levels.

Figure 3.46: Sensitivity analysis of Y_{max}

of Y_{max} reached by the liquid inside the can for different diameters of the transfer star wheel is presented in Figure 3.46a, while the levels observed with different productivity values are shown in Figure 3.46b. It can be seen that the maximum height reached by the liquid decreases as the diameter of the transfer star increases.

This correlation appears to be linear. On the other hand, regarding the correlation between Ymax and productivity, it can be seen that between 18'000 and 20'000 cans per hour, there is a much greater difference than between 20'000 and 22'000 cans per hour. This indicates that this correlation is probably not linear in nature. This aspect needs to be investigated in more detail in future research studies.

Conclusions

In the present study, a method for predicting liquid sloshing occurring during container motion in transfer carousels during the filling process is presented.

In-depth knowledge of this phenomenon is a big advantage in both the design and management phases of automatic filling. A rigorous step-by-step approach was followed to identify the optimal simulation settings that would allow to obtain accurate results in times consistent with industrial needs. The reliability of the simulation approach was first validated by comparing the results with those obtained from an analytical model in a simple case study (i.e., can in uniform rotary motion around a fixed axis).

A subsequent inter-validation phase, conducted by comparing the results obtained with two different software (i.e., ANSYS Fluent and OpenFOAM) in a more complex case study, reproducing a real-world context in which the can passes from the filling carousel to the transfer star, confirmed the consistency of the results. The findings suggest that both tools can significantly support the optimization phase of the industrial processes by accurately modeling complex fluid dynamics, thereby reducing testing time and enhancing production efficiency.

The developed approach represents a novelty within the scientific literature because to date there is no study outlining fluid dynamic simulation models to simulate sloshing during filling processes. The presented approach allows to evaluate the behavior of the liquid inside the can between the end of the filling process and the seaming by allowing to assess the impact that some design and operational parameters have on the behavior of the liquid. In future activities, experimental tests will be performed to further validate the proposed approach.

3.4 Simulation for the design and revamping of industrial plants

This second section of the chapter, dedicated to the implementation of simulation techniques in the food industry, first presents a modelling approach to support the design of an innovative device for the UV-C surface decontamination of food and vegetable products.

This treatment, which acts only on the surface of the products due to its extremely poor penetration abilities, nonetheless allows for effective microbial decontamination (if the radiation dose is correctly dimensioned) and can induce stress-based self-defense effects (*hormesis*) that increase the product's shelf life and improve the retention of nutritional compounds. The developed model has been validated through experimental testing and will be further utilized in the next design stages of the industrial device.

Additionally, a case study is presented in which CFD simulation was used to evaluate the concentration treatment of tomato sauce. The plant's performance was assessed based on its current configuration to identify design errors and quantify their impacts. Specifically, the simulations accounted for the non-Newtonian behaviour of tomato sauce, a factor often overlooked in standard design and sizing procedures.

The insights gained from this study are expected to be highly beneficial for industrial practitioners, both for revamping existing plants to correct design flaws, and for designing new systems. Notably, it clearly illustrates the risks of relying on overly simplified assumptions in the design phase.

As with the studies presented in the first section of the chapter, these projects are ongoing and will be further developed to provide valuable insights for both industrial practitioners and engineering researchers.

In particular, for the tomato evaporator case, the digital model of the plant, once integrated with currently missing sections, is intended to be implemented within an integrated real-time control framework.

3.4.1 Characterization of the operation of an industrial evaporator for tomato products

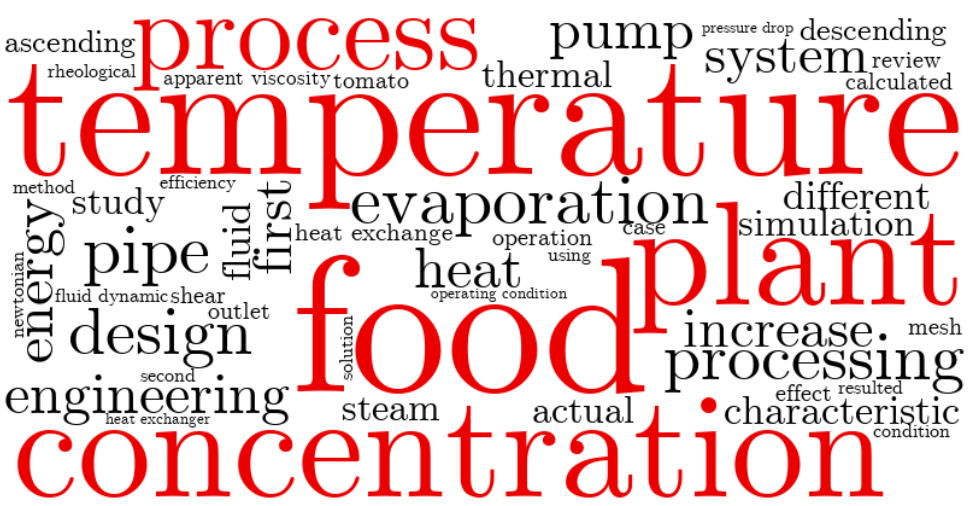

The research in this chapter has been included in the peer-reviewed conference paper [4] *Solari F., Lysova N., Dalla Fiora A., Volpi A., Rizzi A. and Montanari R. Mitigating Design Errors in Standardized Food Processing Plants: Insights from CFD Simulation of a Tomato Concentration Process. (2024). Proceedings of the 10th International Food Operations and Processing Simulation Workshop (FoodOPS 2024). https://doi.org/10.46354/i3m.2024.foodops.014.*

The authors would like to express their gratitude to the company Greci Industria Alimentare S.p.a. for the crucial support in conducting the analysis and in preparing the present research.

Abstract

Concentration is widely used in food processing to produce both semi-finished and finished products by removing a given amount of water from the product; to this end, the energy required can be provided in the form of heat. During this process, a product passes from an initial concentration, which, depending on the product, can be in the range of 2-10 Brix degrees, to concentrations of even more than 40 Brix, significantly varying its rheological characteristics. Such characteristics may vary significantly also depending on the type of product, its origin, and other processing conditions. The plant therefore should be ideally designed considering all these aspects.

Plant manufacturing companies, however, are moving toward increased standardization of their solutions, potentially leading to design errors and inefficiencies. In this study, a tomato concentration plant installed at a company located in Parma, northern Italy, is analyzed. Using Computational Fluid Dynamics simulation, the actual operating conditions are reproduced, considering the real rheological characteristics of the product. The analysis conducted allowed to identify and quantify the main weaknesses of the plant and analyze the benefits achievable by implementing possible corrective actions. The insights of this analysis can be generalized to improve the efficiency of industrial concentration processes.

Introduction

In many sectors of the food industry, the evaporation process is widely adopted to remove a certain amount of water from the product to increase its useful life or simply to reduce its volume [161]. In the case of solid products, we speak about the drying process; in the case of liquid products, i.e., vegetable and fruit juices, it is referred to as the concentration process [162].

Industrially, different methods could be adopted to achieve concentration, e.g., thermal concentration [163], membrane concentration [164, 165], freeze concentration [166, 167], and chemical concentration. In the food sector, still today, the most commonly adopted technique is the thermal concentration method which can be performed through single-effect or multi-effect evaporators [168]. This second solution represents an evolution of the first from an energy-saving point of view, as these devices use the steam from one effect to heat the next one [169].

In recent years, the energy efficiency of such plants has been further increased by introducing Mechanical Vapor Recompression (MVR) and Thermal Vapor Recompression (TVR) [170–172]. These solutions consist of regenerating the steam exiting the first stage by mechanical recompression (using an electric compressor) or by mixing it with high-enthalpy steam from the steam generator, respectively. In this way, the steam increases its heat-exchange potential and improves the thermal efficiency of the process. These solutions are much more compact than multi-stage evaporators as they operate with a single effect in which the steam produced during evaporation is continuously regenerated and used to feed the heat exchanger. This results in significant savings in terms of both space requirements and initial investment but can lead to some issues related to the quality of the finished product. In fact, during the process, the product substantially changes its physical and rheological properties, and the performance of the system will be consequently impacted [173].

Considerable effort is therefore required at the design phase to ensure that the system keeps a good efficiency even when the product characteristics change. Furthermore, food products are characterized by high variability, and their characteristics can vary from year to year and from harvest to harvest. Consequently, also the plant operator must continuously adjust the operation of the plant so as to comply with the variable characteristics of the product. In addition, many food fluids are characterized by complex rheology, which often presents a non-Newtonian behavior, which makes it very difficult to design and control the plant using traditional approaches based on analytical methods [3]. In this context, fluid dynamic simulation can serve as a pivotal instrument [92, 174–176].

In this study, the operation of an industrial MVR plant for tomato pulp concentration is analyzed. The plant analyzed has been operating for several years and revealed issues highlighting some design defects. The purpose of the study is to investigate these

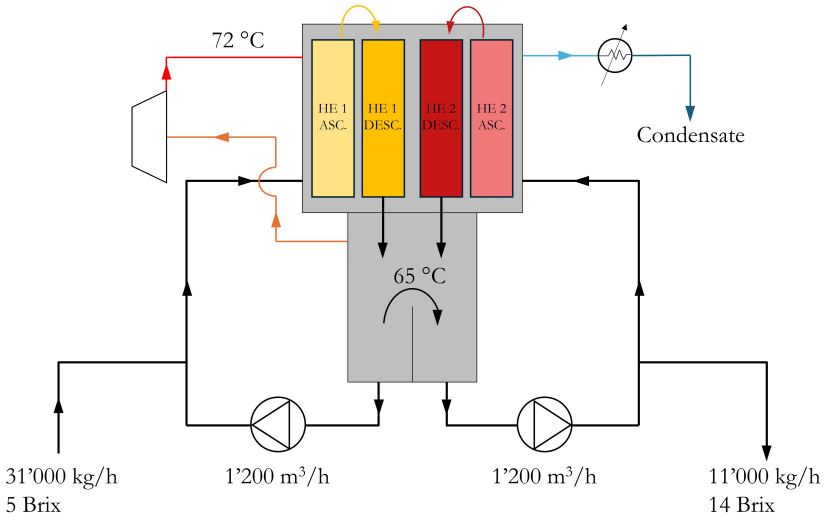

Figure 3.47: Schematic representation of the plant.

issues with a fluid-dynamic simulation approach to highlight the causes and propose improving solutions.

Materials and methods

Description of the plant

The plant is a tomato pulp concentration plant with MVR. It consists of four heat exchange sections, two ascending and two descending. The first ascending section consists of 369 pipes, having an internal diameter of 31.6 mm. It is fed by a 200 kW single-stage centrifugal pump having a total head of 26 meters at a flow rate of 1200 m^3/h, and feeds, in series, the descending section, consisting of 456 pipes, having an internal diameter of 31.6 mm, in which the fluid flows by gravity. All the pipes have a length of 12 m.

The pump draws the product to be recirculated from a tank which is continuously fed by the incoming product having a concentration of 5 Brix. The incoming product flow rate is 31'000 kg/h, while the product flow rate recirculated by the pump through the heat exchange sections is 1'236'000 kg/h. The product is then recirculated approximately 40 times.

The product exiting the descending heat exchange section, after releasing a certain percentage of water by flash evaporation, returns to the same tank. This tank is in communication, through a weir, with a second tank, where the exceeding product is collected. A second pump similar to the first one, but with a higher total head (35 meters), draws the product from this second tank and feeds the second ascending heat exchange section. This section consists of 369 pipes with an internal diameter of 31.6 mm and feeds, similarly to what was described previously, a descending heat exchange section consisting of 456 pipes with an internal diameter of 31.6 mm, where the fluid flows by

gravity. Like in the first descending section, at the outlet of the second one, the product releases all the heat absorbed in the heat exchange sections undergoing an evaporative flash, before returning to the second tank. From this second tank a flow rate of 11'100 kg/h of concentrated product, having a concentration of 14 Brix, is continuously drawn.

The water evaporated at the exit of the two descending heat exchange sections is sent to a compressor to be recompressed and is then returned to the jacket of the heat exchangers at a temperature of 72°C. The evaporation chamber is also connected to a condenser to keep the pressure below the atmospheric one to allow evaporation at low temperatures (65°C). The plant is schematized in Figure 3.47.

The present study focuses on the first ascending section for which the real pressure drops, considering the actual rheology of the product, were calculated and compared with the pump characteristic curve in order to identify the real operating point and the resulting heat exchanger performance.

Product characterization

The product considered in this study, i.e., rustic tomato paste, was characterized to determine the physical properties to include in the simulations. The density of the product was 1030 kg/m^3. With regard to viscosity, the product resulted non-Newtonian, so the apparent viscosity was evaluated at different shear rates and temperatures to derive the consistency (K) and the flow behavior (n) indexes of the power law model. Values of $n < 1$, like in the case of this product, indicate a shear-thinning behavior. To this end, rheological measurements were conducted at five different temperatures between 40°C and 85°C (40°C, 50°C, 65°C, 75°C, 85°C). A Haake RheoStress 600 concentric-cylinder rotational viscometer equipped with Z40 DIN measuring system was used (internal diameter = 39.7 mm, external diameter = 43.4 mm). A shear rate range between 0 to 200 s^{-1} was considered. In this way, it was possible to analyze the dependence of the apparent viscosity on both the shear rate and the temperature. Results are reported in Table 3.18 together with the apparent viscosity calculated at a shear rate of 100 s^{-1}. Knowing the values of K_0 and n_0 at a reference temperature T_0, and the activation energy E_a, the apparent viscosity (η) at a certain temperature can be calculated with eq. 3.18, where R is the thermodynamic constant, and T_0 is considered to be 65°C.

$$\eta = K_0 \cdot \dot{\gamma}^{n_0-1} \cdot \exp\left[\frac{E_a}{R} \cdot \left(\frac{1}{T} - \frac{1}{T_0}\right)\right] \tag{3.18}$$

Table 3.18: Rheological characterization.

T [°C]	**K [Pa s^n]**	**n**	**η_{100}**
40	11.341	0.271	0.391
50	9.665	0.281	0.348
65	**7.662**	**0.294**	**0.297**
75	6.750	0.300	0.268
85	5.896	0.308	0.244

Simulation campaign

The region between the inlet section of the first ascending heat exchanger and the outlet section of the 369 pipes was considered the simulated fluid domain. The pipes had a length of 12 m (Figure 3.48). The domain was discretized by adopting a multizone approach: tetrahedral mesh was used for the intake manifold, while the 369 pipes were discretized by means of a hexahedral mesh.

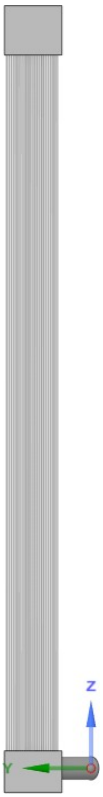

Figure 3.48: Ascending section of the first heat exchanging section.

On the wall of each pipe, where the heat exchange takes place, an inflated mesh layer was created, with a first layer thickness of 0.3 mm and consisting of 11 layers, each characterized by a growth factor of 20 percent with respect to the previous one. According to ANSYS Fluent Theory Guide [34], the mesh quality was assessed in terms

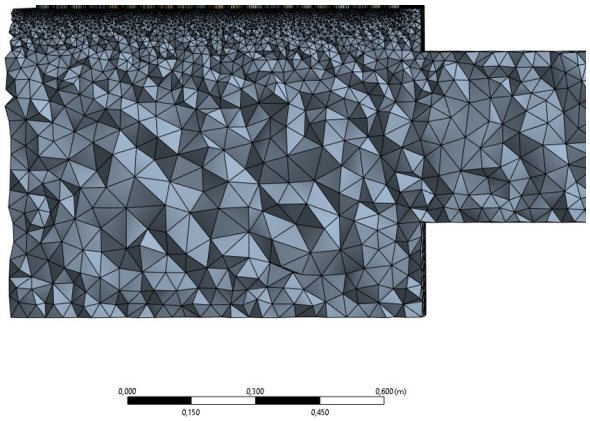

Figure 3.49: Detail of the tetrahedral mesh of the intake manifold.

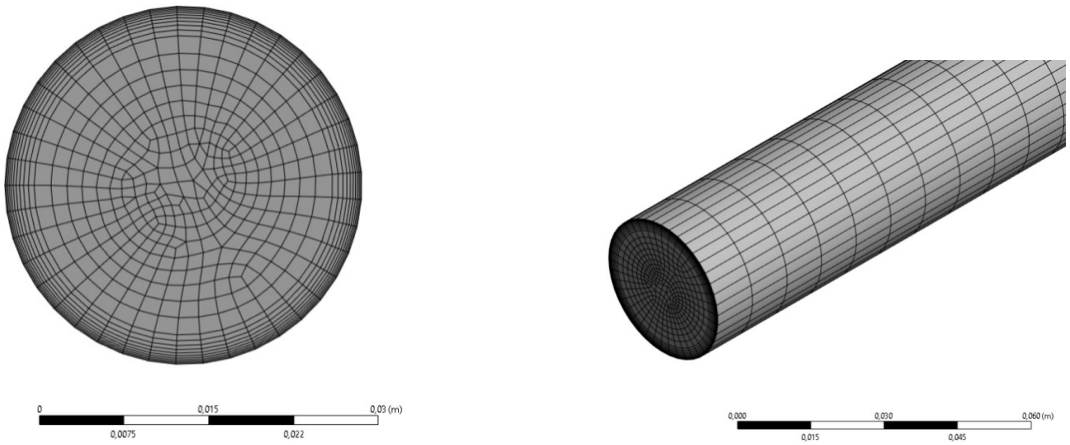

(a) Mesh view 1.

(b) Mesh view 2.

Figure 3.50: Detail of the hexahedral mesh of a pipe.

of minimum orthogonal quality and maximum skewness. Regarding the former, values greater than 0.15 are considered acceptable, while the latter is acceptable when values don't exceed 0.85. A detail of the mesh is reported in Figure 3.49 and Figure 3.50.

The incoming product flow rate as well as the initial temperature (65°C) was set on the inlet section by setting a velocity value and a temperature value, respectively. At the outlet section, on the other hand, a relative reference pressure of 0 Pa was set. A constant temperature of 72°C was set on the walls of the ascending pipes. The product was characterized based on what was described in section 2.2. Three different scenarios were simulated:

- CS1: using design data (flow rate 1'200 m3/h and Newtonian rheology, considering an apparent viscosity of 0.3 Pa s);
- CS2: using the design flow rate (1'200 m3/h) and actual rheology of the product (non-Newtonian as described in section 2.2);

- CS3: the same as CS2 but using the pump flow rate at actual pressure drops (obtained from CS2).

The SIMPLE scheme was used for pressure-velocity coupling; with reference to spatial discretization, second-order discretization was used for pressure, while second-order upwind was used for momentum, energy, and turbulent kinetic energy and specific dissipation rate of the $SSTk-\omega$ turbulence model.

Results and Discussion

First, the distribution of flow rates between the 369 pipes was assessed. On this aspect, the results obtained in the three case studies were overlapping: the distribution resulted fairly uniform, with maximum variations from the mean value (3.25 m^3/h) of -14% and +18% (Figure 3.51). These variations also affected temperature distribution: the average temperature increase calculated on the outlet section of the pipes varied in a range of ±5.7% for all the case studies considered.

Regarding the pressure drops, the results showed that an approach based on fixed apparent viscosity, in this specific case, leads to a substantial overestimation. Indeed, at the wall, where there are the highest shear rates, the apparent viscosity of the fluid is much lower in CS2 than in CS1 (Figure 3.52 and Figure 3.53), where the viscosity is independent of the shear rate and is considered equal to 0.3 Pa s over the entire section. Since this zone is the one that contributes the most to the pressure drops, the pressure drops in CS2 (190'162 Pa) are much lower than in CS1 (255'106 Pa).

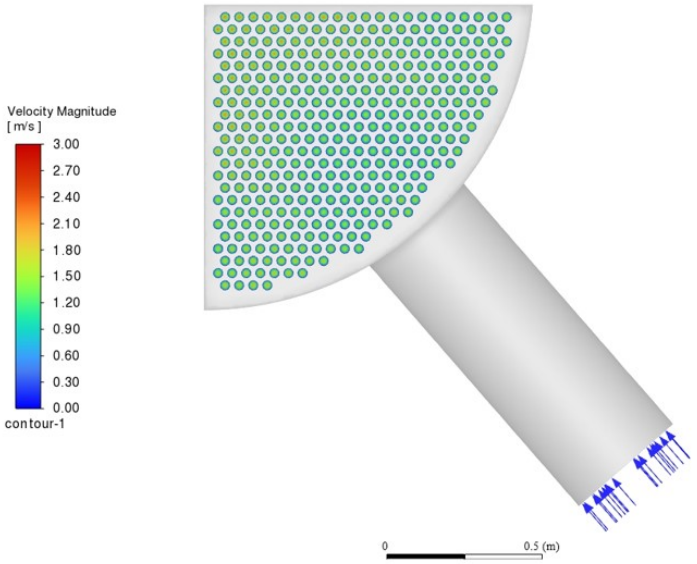

Figure 3.51: Flow distribution across the 369 pipes of the ascending heat exchange section.

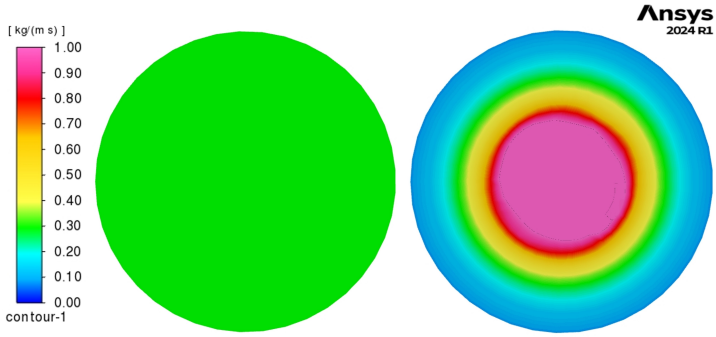

Figure 3.52: Viscosity across the pipe section when modeled with a fixed value (left) and the actual viscosity calculated based on the shear rate and temperature (right) limited between 0 and 1 kg/m s.

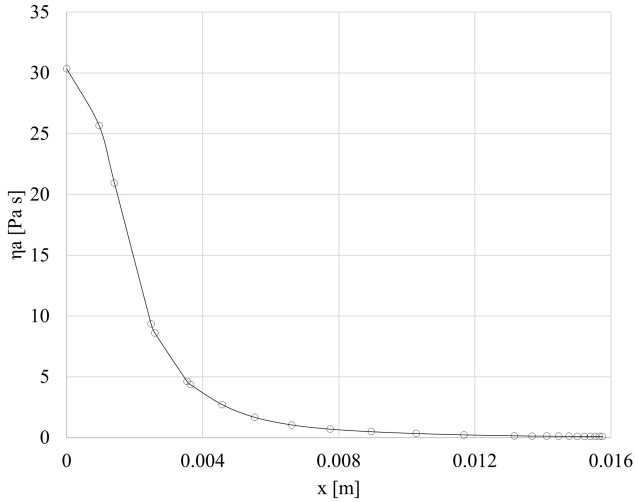

Figure 3.53: Apparent viscosity trend along the radius of the outlet section in CS2.

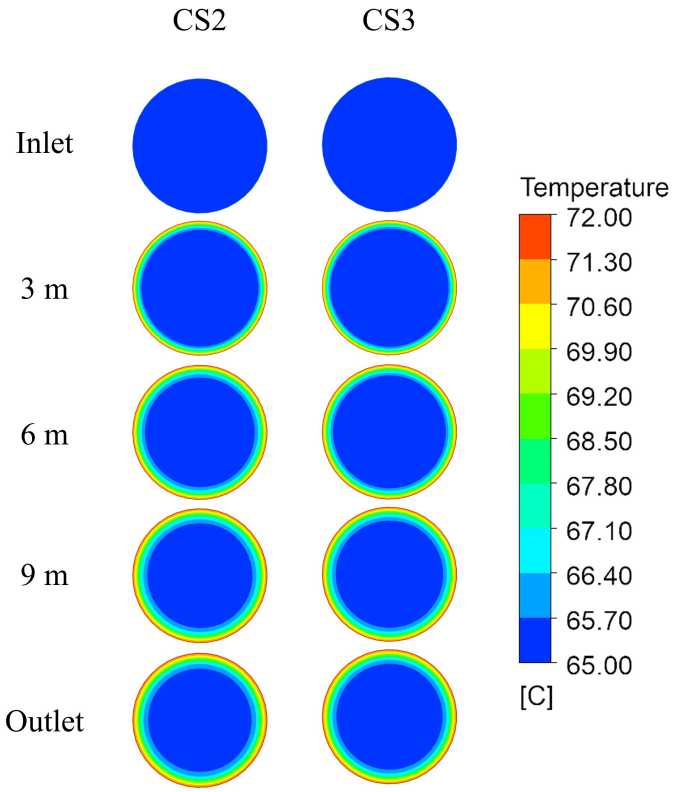

Figure 3.54: Temperature evolution in 5 different sections between inlet and outlet in CS2 and CS3.

As a consequence, it follows that, with respect to the design data (CS1), the pump operates at a lower head. Under these conditions, a higher flow rate can therefore be processed. Based on the characteristic curve of the pump, it is obtained that to guarantee the head calculated in CS2, the pump operates at a flow rate of 1'500 m3/h. This latter is therefore the flow rate which, under actual operating conditions, is recirculated through the heat exchanger. These operating conditions were those considered in CS3.

As can be expected, the temperature resulted being significantly influenced by both the rheological characteristics of the product and the flow rate. The average temperature increase calculated on the outlet section resulted to be 1.56°C, 1.39°C, and 1.28°C for CS1, CS2, and CS3, respectively. Figure 3.54 shows the temperature evolution on a pipe section in CS2 and CS3, at five distances from the inlet section (0m, 3m, 6m, 9m, 12m), considering a flow rate equal to the mean value of 3.25 m3/h and the product rheology modeled with a power law. Figure 3.55 shows the temperature trend along the duct radius at four different distances from the inlet section (3m, 6m, 9m, and 12m) in the three case studies analyzed. It can be observed that the Newtonian approximation leads to an overestimation of the product temperature rise by 11%.

By comparing the design condition (CS2) with the actual condition (CS3), it can be seen that the increase in the flow rate causes a lower increase in product temperature. This is partially counterbalanced by the higher number of recirculations of the product

per unit of time. Since all energy supplied in the form of heat results in the evaporation of water, it is possible to estimate the amount of water evaporated in the unit of time based on the calculated temperature increases. Since the descending heat transfer section is characterized by a greater number of pipes, which results in a 24% increase in the volume involved, it can be assumed that the residence time, and thus the temperature increase, also increases in a directly proportional manner. In view of this, taking into account the latent heat of vaporization of saturated steam at 65°C (2'344 kJ/kg), it can be deduced that, in real operating conditions, the considered system evaporates 7'900 kg/h of water, equal to 79% of the planned quantity (10'000 kg/h). By reducing the flow rate to 1'200 m3/h, the thermal jump provided by the single pipe increases (+8.5%) but, on the other hand, the number of recirculations decreases (-20%). As a result, the amount of water that the system can evaporate increases (8'580 kg/h), but not enough. Further reducing the product flow rate, or increasing the temperature of the steam at the compressor discharge, could cause the product in contact with the pipe walls to overheat, causing damage. It follows that the approach used in the design phase, with the related assumptions, resulted in an incorrect sizing of the system which, in operating conditions, even with adjustments, is unable to achieve the desired performance. The feedback from the industrial application actually confirms these results, as the product obtained does not reach the expected concentration and has a lower consistency than required, even after repeated regulation attempts.

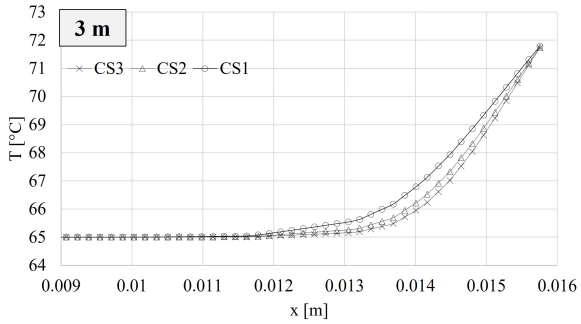

(a) Temperature profile at 3m.

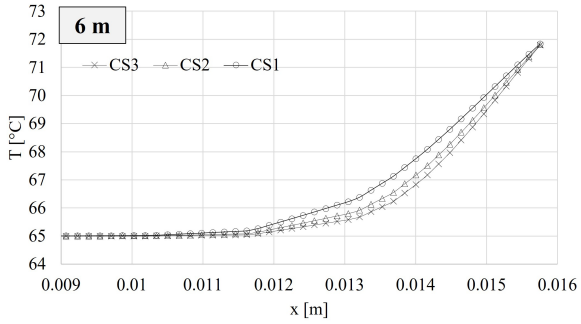

(b) Temperature profile at 6m.

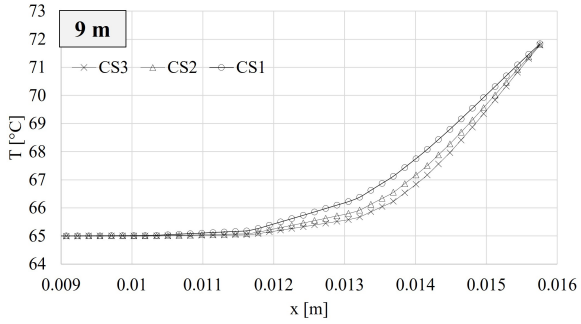

(c) Temperature profile at 9m.

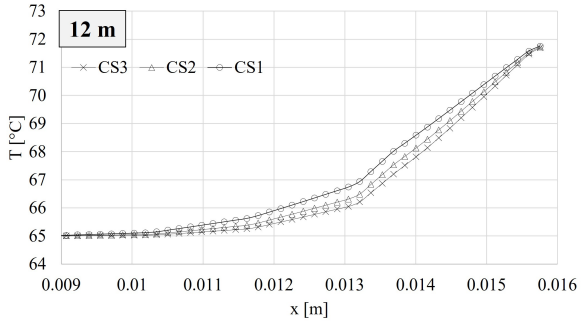

(d) Temperature profile at 12m.

Figure 3.55: Temperature evolution along the radius of the section at four different heights.

Conclusions

The results obtained show that the actual working conditions of the plant are significantly different from those expected. In fact, since the Newtonian fluid approximation led to overestimation of pressure drop, the pump actually works at a higher flow rate than the design data (1500 m3/h vs. 1200 m3/h); as a consequence, the performance of the system resulted to be different from what was expected.

Computational Fluid Dynamics simulations allow to reproduce the real operating conditions of the plant, highlighting the main critical issues in the system and evaluating the effect of some corrective actions.

From the results obtained, it was evident that the assumptions that were made in the design phase, above all that of Newtonian behavior of the fluid, caused incorrect design choices that do not allow, even in the face of adjustments, the desired performance to be achieved.

Future research will focus on analyzing in detail the other heat exchange sections, as well as on studying plant revamping solutions aimed at achieving the desired performance. In conclusion, fluid-dynamic simulation has proven to be an essential tool that can help plant designers and plant users make more informed choices, reducing the number of assumptions needed compared to traditional approaches.

3.4.2 Design of an industrial device for the UV-C treatment of fruit and vegetables

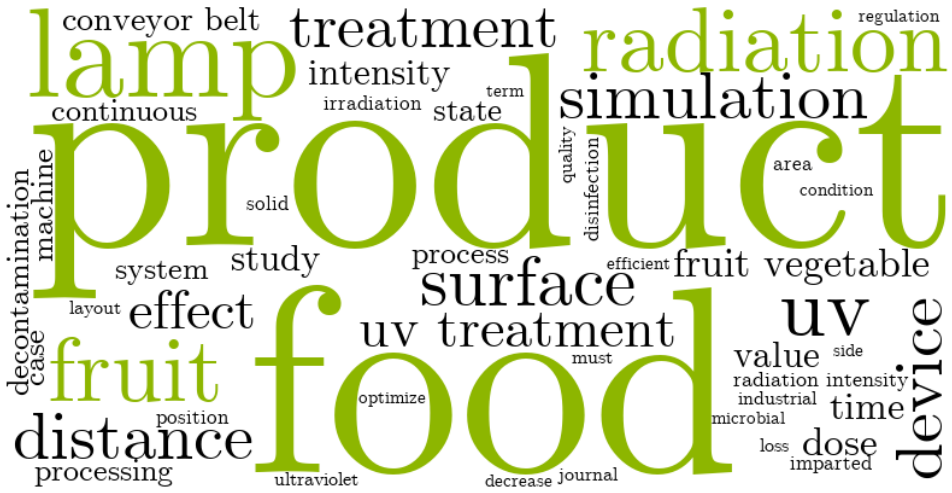

The research in this chapter has been included in the peer-reviewed article [177] *Lysova, N., Solari, F., Bocelli, M., Volpi, A., and Montanari, R. (2024). Industrial device for the continuous UV-C treatment of fruit and vegetables: simulation-aided design and model validation. International Journal of Food Engineering. https://doi.org/10.1515/ijfe-2023-0065*

and in the conference paper [178] *Volpi A., Solari F., Lysova N., and Bocelli M. (2022) Design and optimization through simulation of an industrial system for the continuous UV-C treatment of fruits and vegetables. (2022). Proceedings of the 8th International Food Operations and Processing Simulation Workshop (FoodOPS 2022). https://doi.org/10.46354/i3m.2022.foodops.011.*

Abstract

The irradiation of foods with UV-C light is a non-thermal and non-chemical treatment that allows for achieving several benefits, from surface decontamination to hormetic effects on biological matrices. Nowadays, even if its effects have been extensively proven and discussed, UV-C radiation is not widespread on an industrial level for the treatment of solid and liquid foods, mainly due to technical limitations and the non-uniformity of legislation for different products and among different countries.

In this study, numerical simulation was adopted as a tool for the design and optimization of a device for the UV-C treatment of fruits and vegetables. After validating the modelling approach, the radiation treatment was evaluated for different product configurations. The proposed approach aims to facilitate the implementation and the scale-up of the UV-C treatment in the food industry, as it allows for assessing its effects under different operating conditions, prior to the physical prototyping stages.

Introduction

It is globally acknowledged that food waste and food loss are critical issues: in a recent report, FAO estimated that approximately one-third of the food produced is lost during the supply chain and consumption phases [179]. The reduction of food waste and loss has been addressed by one of the UN Sustainable Development Goals - SDG 12 "Responsible Consumption and Production" - [180], which has set a target for its reduction to be achieved by 2030.

As plant-based diets emerge as a more sustainable alternative to the consumption of meat and animal-based products [181], efficient agricultural and processing techniques are required to guarantee the quality of fruits, vegetables, and legumes, while ensuring food safety and minimizing the use of resources, e.g., water, soil, energy and chemical reactants. While efficient agricultural and processing techniques have historically always been pursued by researchers and practitioners, the focus nowadays is gradually switching towards production techniques based on environmentally friendly and sustainable technologies. This is due both to the need to limit the use of resources and to the growing customers' demand for minimally treated and sustainable products.

Horticultural products, however, are particularly prone to rapid decay, especially due to fungal and microbial contamination. Surface treatments based on chemical disinfection are commonly used to reduce the contamination of fruits and vegetables and limit their decay. These treatments are performed by washing the products with water and disinfectants, often adopting chlorine-based preparations. Besides requiring high volumes of process water, which however could be reused, these treatments may lead to the accumulation of chemical residuals on the product surfaces and even to the absorption and formation of by-products harmful to human health [182].

Within this context, the treatment of fruits and vegetables with ultraviolet radiation in the UV-C region (200-280 nm) has emerged as a promising alternative methodology. The effectiveness of the UV-C, with maximal germicidal activity at 253.7nm, is generally recognized: indeed, UV-C rays have been adopted for a long time for the disinfection of air, water, and surfaces [183–185]. Exposure to ultraviolet radiation destroys the ability of the microorganisms to reproduce, as it causes photochemical changes in their nucleic acids [186]. The inactivation process, in the case of surface treatments, is based on the provision of a certain radiation dose, defined as the amount of energy supplied to a point over time. When UV-C is applied to treat liquid matrices, on the other hand, other aspects must be taken into account including, among others, the absorbance and turbidity of the sample, the presence of particulate and/or fibres, the possible presence of UV-absorbing compounds, the design of the reactor and the flow regime of the treated product. The radiation doses necessary to inactivate the most relevant pathogens, yeasts, and moulds in different media are reported in the literature [77].

In recent years, the use of UV-C rays in the food industry has drawn increasing attention, as it allows for treating both solid and liquid foods and presents several advantages compared to the techniques commonly adopted [187]. This treatment, indeed, is non-thermal and non-chemical, thus it is energy-efficient [50], and it does not pose the risk of leaving chemical residuals and by-products on the food surfaces. This disinfecting methodology can be applied to a broad variety of edible products, e.g., fruits and vegetables [188], meat [189], fish [190], cheese [191], milk [192], juices [193], liquid foods [194] and more. The technology has proved to be cheap and easy to implement, as its requirements generally narrow down to the source of the UV-C radiation, e.g., lamps, and an enclosed treatment space. One of the main disadvantages of the treatment with UV-C is its scarce penetration ability: in the case of solid products the useful effect is limited only to the irradiated parts of the surface. In the case of liquids, on the other hand, the treatment characteristics and the geometry of the reactor in terms of, e.g., reactor length and number of sections, bends, thickness of the thin fluid film, flow rates elaborated and flow conditions, must be appropriately defined based on the physical, optical and compositional characteristics of the treated product, aiming to ensure that each point receives a sufficient radiation dose for the intended level of microbial inactivation. Furthermore. it is essential to constraint the radiation to a confined environment to protect the operators, since exposure to UV-C rays can cause extensive damage to human health, affecting mainly the skin and the eyes [195].

With reference to fruits and vegetables, researchers have extensively studied the effects of UV-C radiation on the products' quality and safety. Several studies show how this postharvest treatment allows for the decontamination of the product surface, and the extension of the shelf-life and quality while minimizing losses, side effects and the use of resources [196–198]. Moreover, the exposure of the biological matrices to low radiation doses has been observed to induce beneficial effects based on hormesis [199–201]. This stress-induced biological phenomenon has shown great potential in enhancing the defence compounds and preventing early decay of the produce, thus leading to longer shelf-life and higher nutritional quality.

The implementation of the UV-C treatment on an industrial scale level, however, is not widespread. This is due mainly to the current regulations and technological aspects. While in the USA the FDA has authorized the use of UV-C rays for water and fruit juices for food preservation purposes [180], and in Canada its use has been approved for treating apple juice and cider with commercial devices [202], in Europe to date there is not a harmonized legislation, with authorization being granted on a product-by-product basis [203]. Moreover, to date, the technology has been implemented mainly on a laboratory scale, as its industrial scale-up may be complex to design. The main requirements that an industrial system for irradiating fresh produce should satisfy, besides obviously being allowed by the local regulations, have been outlined in [201]: (i) the radiation dose

supplied to the products must be easily measurable and tunable; (ii) the process must be economically efficient; (iii) it must be possible to use the device for treating a wide variety of products, with (iv) a high throughput and (v) the least possible mechanical damage. Moreover, the radiation dose provided must be as uniform as possible, to prevent over-treating some regions of the products and under-treating others, generating the risk of a rapid recontamination of the surface. To facilitate the scale-up and the implementation of the treatment in industrial processing lines, both the device and the process must be appropriately designed and optimized. To this end, numerical simulation can be used: in the last decades, indeed it has allowed for optimizing a multitude of industrial plants and operations [92, 131, 132]. Simulation has been used in the last years for evaluating, designing and enhancing the performances of devices using UV-C radiation to treat both liquid [36, 67] and solid products; the studies on the latter subjects, however, are very few. In [178] simulation has been used to evaluate the distribution of incident radiation in the case of a system performing continuous UV-C treatment with different product displacements. In [6, 204] the authors have simulated a machine for the continuous treatment of strawberries on a polymeric tray to optimize the system geometry, as well as the number and position of lamps and reflectors.

In this paper, a simulation model for the design and optimization of an industrial device for the continuous surface treatment of fruits and vegetables was developed. In this device, the UV lamps are intended to be displaced both above and under the products, so the most appropriate geometry of the conveyor belt must be selected to optimize the dose provided. To this end, experimental tests have been conducted to determine the radiation passing through the metallic mesh belt and validate the simulation model and settings. Finally, the validated model was used to evaluate the intensity and the uniformity of the radiation provided to the products' surface in the case of different distances between the solids, i.e., belt filling rates.

Materials and methods

After defining a preliminary geometry of the industrial device for the continuous UV-C treatment of fruits and vegetables, a first simulation was performed with Ansys® Release 2022 R2 [34, 71] to evaluate the radiation field generated by a single lamp. The model was validated with experimental tests using a sensor that measured the irradiation intensity. The measurements were then repeated with two different conveyor belt geometries positioned between the sensor and the lamp to determine the one that allowed for the highest amount of radiation to pass through.

Finally, a simulation model of the industrial device was developed based on the geometrical features and the characteristics of the UV-C lamps. The model was used to evaluate the distribution of radiation intensities on the product surfaces as the distances

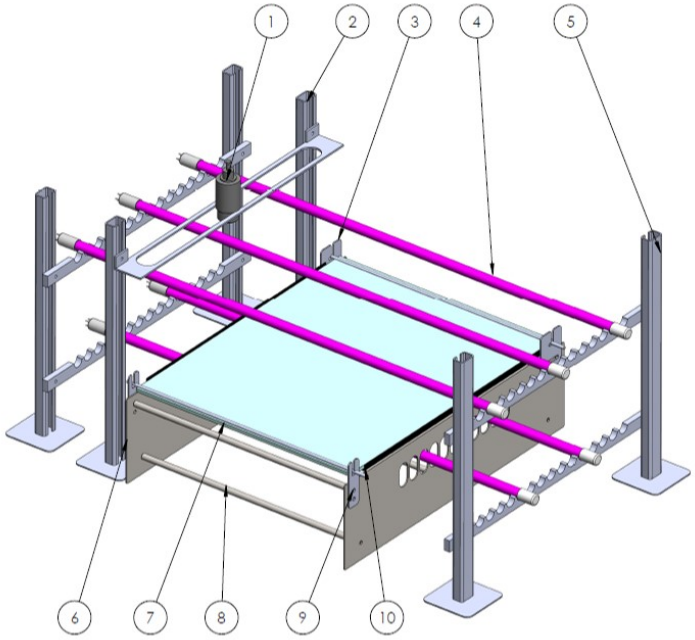

Figure 3.56: Proposed configuration of the pilot device for the UV-C treatment of fruits and vegetables.

between them varied, thus reproducing different degrees of filling rate of the belt.

Device for UV-C treatment of solid foods

While the final aim is to design an industrial device with a continuously running conveyor belt, the first design phases focus on building a pilot device for the initial experimental tests, featuring a fixed and static conveyor belt. In this section, a first configuration of the pilot device, consisting of a single UV-C module and still in the design stage, is presented and described (Figure 3.56). The geometry of the device was defined according to the characteristics of the treatment with UV-C radiation and of the products to irradiate.

In particular, the pilot device consists of the following elements:

- A stainless steel conveyor belt on which the products will be positioned. The width of the conveyor belt was selected to be smaller than the length of the lamps so that even the fruits placed at the ends of the belt would not be affected by edge effects.
- One row of lamps at a defined height above the belt displaced orthogonally to the product flow direction. Thanks to the configuration of the lamp support, it is possible to adjust the distance between the lamp, and between the lamps and the belt.
- One row of lamps below the belt, orthogonal to the product flow and positioned offset to the upper lamps. As for the top lamps, it is possible to adjust the position of the bottom lamps and test different configurations.
- A UV-C sensor, positioned above the top lamps at a given distance. It is possible to

move the sensor along the belt length direction, to evaluate the radiation intensity at different points and the superposition of effects of different lamps.

- A safety system to screen the operators and protect them from coming into contact with harmful UV-C radiation. Later development stages will include an external stainless-steel tunnel for this purpose.

The two rows of lamps were included to provide a uniform radiation dose to the whole product surface, as the UV-C rays have poor penetration ability and can achieve only surface decontamination.

In this study, a device layout with a mesh conveyor belt and two rows of lamps has been preferred to a commonly adopted belt with rotating bars (with one row of lamps) to generalize the application range in terms of treated products. Fruits and vegetables, indeed, are characterized by a broad range of dimensions and mechanical resistances. In most cases, mechanical damage to the product surface would result in bruises, decreased quality and enhanced predisposition to microbial proliferation. To this end, the implementation of a mesh belt, with openings that would allow the handling of small and sensitive products, but also for the radiation to pass through, was deemed to be the best choice. Furthermore, the possibility of irradiating the product from two sides is expected to give better control over the supplied dose, in this first explorative design stage. Indeed, in an industrial application of this technology, it will be possible to tune the radiation dose by adjusting the exposure time (total length of the device and the speed of the conveyor belt) and the radiation intensity (distance between lamps, number of lamps, distance between lamps and product) according to the specific application.

With the practical industrial implementation in mind, the lamps are positioned transversally to the direction of the conveyor belt for two main reasons:

- Enhance the ease of maintenance: the lamps oriented transversely to the conveyor belt can be easily extracted from the side of the machine and replaced when needed.

- Flexibility in the length of the device: if the lamps were placed in the running direction of the conveyor belt, the length of the device would be constrained to the length of the lamps.

With regard to the device presented in Figure 3.19, the bill of materials used to implement the assembly is reported in Table 3.19. To carry out the first experimental tests after building the pilot device, the assembly will be positioned inside an enclosed space to screen the operators from the radiation.

UV-C Lamps

In the device designed, the sources of the radiation are commercial amalgam UV-C lamps. The characteristics of the lamps are reported in Table 3.20.

Table 3.19: Bill of materials for the first configuration of the UV-C machine.

n°	Description	Quantity	Material	Notes
1	UV-C Sensor	1	N/A	Commercial component
2	Floating sensor support	1	AISI 304	Custom part
3	Tape tensioner, fixed part	1	AISI 304	Custom part
4	UV-C lamp	6	N/A	Commercial component
5	Floating UV-C lamps support	2	AISI 304	Custom part
6	Conveyor sidewall	2	AISI 304	Custom part
7	Conveyor belt	1	AISI 304	Width = 410 mm; Length = 500 mm
8	Round conveyor support	5	AISI 304	Custom part
9	Belt tensioner, moving part	1	AISI 304	Custom part
10	Belt support "Z" profile	2	Polymer	UV-C resistant

Table 3.20: Characteristics of the UV-C lamps.

Term	Description	Value	Units
D_L	Diameter	15	mm
L_L	Length	843	mm
P_L	Lamp power	105	W
$P_{L,254}$	UV output at 254 nm	31.5	W

The effectiveness and efficiency of the UV-C treatments depend strongly on their uniformity: it is essential to guarantee that the surface of the product is irradiated in the most uniform way possible. The product, indeed, should be subjected to an adequate dose distribution, sufficient to achieve the intended effects even in the least irradiated points.

$$D = \int I dt \tag{3.19}$$

$$I \propto \frac{I_0}{r^2} \cdot \exp(-\alpha_{254} \cdot r) \tag{3.20}$$

The radiation dose D, defined as the energy provided to a point over time, is calculated with Eq. 3.19, where I is the intensity of the radiation at a generic distance from the lamp, and t is time. I is inversely proportional to the square of the distance from the radiation source. Furthermore, it decreases depending on the medium it passes through – in this case air – according to a negative exponential law (Eq. 3.19). I_0 is the intensity of the radiation at the source; r is the distance from the source; α_{254} is the absorption coefficient of the medium at 254 nm.

Conveyor belts

As stated, UV radiation has a very low penetration ability, so the optimal geometry of the conveyor belt should be determined based on the amount of radiation that is

able to reach the products from the bottom lamps. The design of the belt, therefore, should include large open areas to allow for the radiation to pass through. Two different geometries of belt, made of stainless steel wire, were considered to this end. The first geometry consisted of a triangular mesh (Figure 3.57a), while the second one was a rectangular bar conveyor belt (Figure 3.57b). The characteristics of the belts are reported in Table 3.21.

Belt	**Dimensions**		
	A [mm]	B [mm]	Belt thickness [mm]
Triangular mesh	7.80	4.90	6.00
Rectangular bar	5.00	55.00	1.50

Table 3.21: Characteristics of the evaluated belt geometries

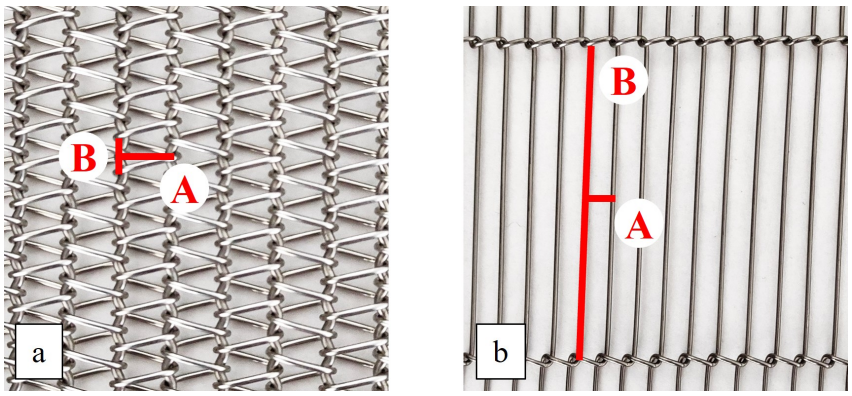

Figure 3.57: Triangular (a) mesh and rectangular bar (b) conveyor belts.

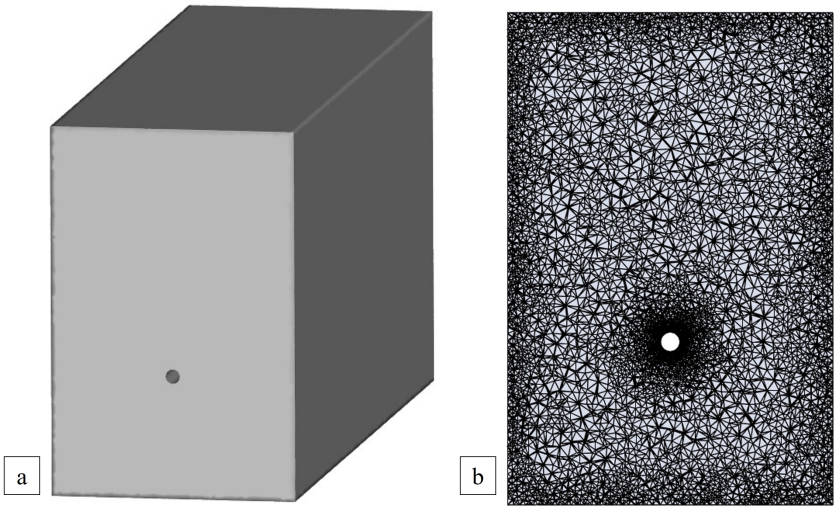

Figure 3.58: Geometry (a) and mesh (b) of the domain used to evaluate the radiation field of one UV lamp.

Simulation of the radiation field

A first simulation was carried out with Ansys® Fluent 2022 R2 [34, 71]. The simulated domain included a UV lamp, with the characteristics of the commercial lamps used, and a volume of air surrounding it (Figure 3.58a). The domain was discretized according to the finite volume method, and a finer mesh was generated near the lamp to precisely calculate the magnitude and the gradient of the radiation field (Figure 3.58b). Discrete Ordinates (DO) model, which is based on the Beer-Lambert law [72], was used for the solution, to calculate how the radiation propagates from the lamp inside the volume of air. DO radiation model solves the equations within a number of solid angles obtained by discretizing each octant of the angular space along the two angular directions (theta divisions and phi divisions respectively). Each solid angle thus obtained is further discretized according to pixelation settings to increase the accuracy of the results. In this study, angular discretization of 5 x 5 for the theta and phi divisions, and 3 x 3 for theta and phi pixels were set up.

Experimental tests and validation of the radiation model

Experimental tests were performed with two main goals: (*i*) validation of the DO model used to simulate the radiation field, as well as its discretization settings; (*ii*) determination of the radiation intensity passing through the two different geometries of belt; this allowed to select the best belt configuration for the specific application, i.e., the one that allowed for the highest radiation to pass through, and derive the "damping" multiplying coefficient to assume when setting the radiation intensity of the bottom lamps, thus avoiding the need of modelling the geometry of the belt.

The experimental tests were performed by turning on the lamp and keeping it on for a time of approximately 15 minutes for each configuration, i.e., without a belt and with the two selected belt geometries. Of the total test duration, a period following the conclusion of the startup transient phase, characterized by steady operating conditions, was recorded as it was considered representative of the lamp's standard functioning. During this period of approximately 4 minutes, the intensity of radiation was registered.

First, the configuration without any belt between the lamp and the sensor was replicated, to validate the simulation model. Then, the two different belt geometries were positioned between the UV lamp and the sensor (Figure 3.59). The distance between the lamp and the sensor was kept unaltered to allow for the comparison with the first measurement. The measured radiation intensities were divided by the value obtained during the first test, i.e., without the conveyor belt, to determine the percentage of radiation passing through the belt in each case. The following component setup was adopted during the execution of the tests (Figure 3.60):

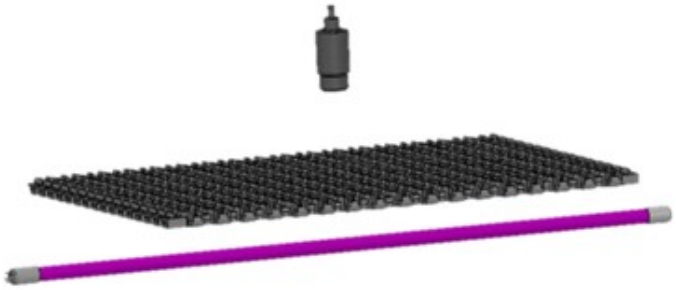

Figure 3.59: Schematic representation of the set-up during the experimental tests.

Figure 3.60: UV sensor SUV 20.2 and measurement window FUV 38.

- lamp - sensor distance: 160 mm;
- sensor – belt distance: 95 mm;
- lamp – belt distance: 65 mm.

The model of the UV sensor is SUV 20.2 by UV-Technik Speziallampen GmbH, with a viewing angle of 160° and a current output at 4–20 mA. During the tests, the sensor was placed inside a measurement window model FUV 38, by UV-Technik Speziallampen GmbH, built following the DVGW standards (Figure 3.60).

Simulation of the different product configurations

Once validated, the simulation model was used to simulate the treatment of products inside the industrial device represented in Figure 1.

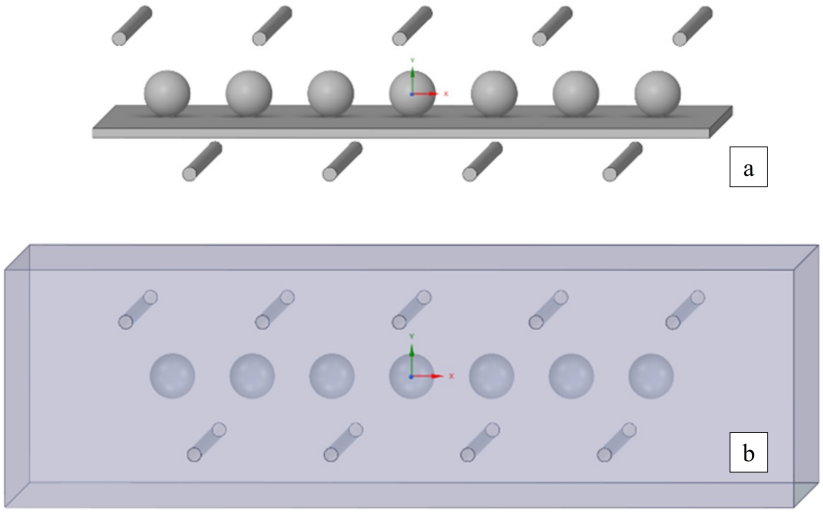

Figure 3.61: 3D model (a) of the components inside the pilot device and simulated domain (b).

The 3D model of the device geometry was created by generating a row of products, modelled at this initial stage with spheres, having a diameter of 50 mm. Five lamps were positioned at a distance $d_{LF,y}$ above the fruits, and four lamps were inserted below the fruits at the same distance $d_{LF,y}$ from the fruit surfaces, positioned offset to the upper lamps. Compared to the device depicted in Figure 3.56, two lamps were added to both the row of lamps above the conveyor belt and the row of lamps below the belt. In this way, it is considered that this device will be placed within a modular system which will be both preceded and followed by identical UV-C modules. The addition of these lamps makes it possible to reduce edge effects and to make an accurate assessment of the dosage provided by the individual module when inserted within a modular industrial apparatus.

The geometry is presented in Figure 3.61a, including the geometry of the conveyor belt for reference. To model the radiation field inside the device an enclosure was generated around the bodies to simulate the volume of air surrounding the lamps and the fruits. The geometry of the belt was not included in the simulation: instead, to account for the interference of the conveyor belt, the intensity of radiation emitted by the bottom lamps was multiplied by a "damping" coefficient, based on the experimental measurements. The influence of the device walls on the radiation field was neglected. The final geometry of the system was generated by subtracting the bodies of the lamps and of the fruits from the enclosure: the simulated domain, therefore, consisted only of the volume of air (Figure 3.61b).

As described in the dedicated section, DO model was used to solve the equations of the radiation field inside the device. Radiation boundary conditions were defined on the external surfaces of both the lamps and the fruits. The fruits were defined as "opaque" bodies, while the lamps were set as "semi-transparent", with uniform diffusion in all directions. The radiation intensity emitted per unit area was calculated as the

ratio between the output of the lamp at the wavelength of 254 nm and its total surface area. Three different product configurations were considered by modifying the distance between the fruits. In this way, it was possible to estimate the effect of different filling rates of the conveyor belt on the treatment. The geometric features considered during the simulations are reported in Table 4. The values of distance between lamps (d_{LL}), and distance between the lamps and fruit surfaces ($d_{LF,y}$) were chosen based on the results of the radiation field calculation, to have uniform incident radiation on the surface of the fruits at the various positions occupied by the fruits with respect to the lamps. The optimal value of these distances obviously depends on both the size and shape of the fruit. Therefore, depending on the product to be processed, they will have to be adjusted to optimize treatment effectiveness and uniformity. For each configuration, to account for more relative positions of the fruits with respect to the lamps, several simulations were carried out after moving the rows of fruits along the x direction. In particular, 13 different positions of the fruits with respect to the lamps in the longitudinal direction were considered (each one obtained by moving the fruit along the x direction by a distance equal to $(D_F + d_{FF})/2$). For each of these positions, the UV radiation field on the surface of the fruits was calculated and the results at all intermediate points were then obtained by interpolation. The simulations were carried out under steady-state conditions. Finally, the intensity of the radiation on the surfaces of the products was calculated to evaluate the maximum, average and minimum values registered; these three values, jointly considered, allow the assessment of both treatment intensity and uniformity.

Term	Description	Value	Units
D_F	diameter of the fruits	50	mm
$n_{L,TOP}$	number of top lamps	5	-
$n_{L,BOTTOM}$	number of bottom lamps	4	-
d_{LL}	distance between lamps	150	mm
$d_{LF,y}$	vertical distance between the lamp and fruit surfaces	40	mm
$d_{FF,1}$	distance between fruits 1	25	mm
$d_{FF,2}$	distance between fruits 2	37.5	mm
$d_{FF,3}$	distance between fruits 3	50	mm

Table 3.22: Geometrical features of the simulated conditions

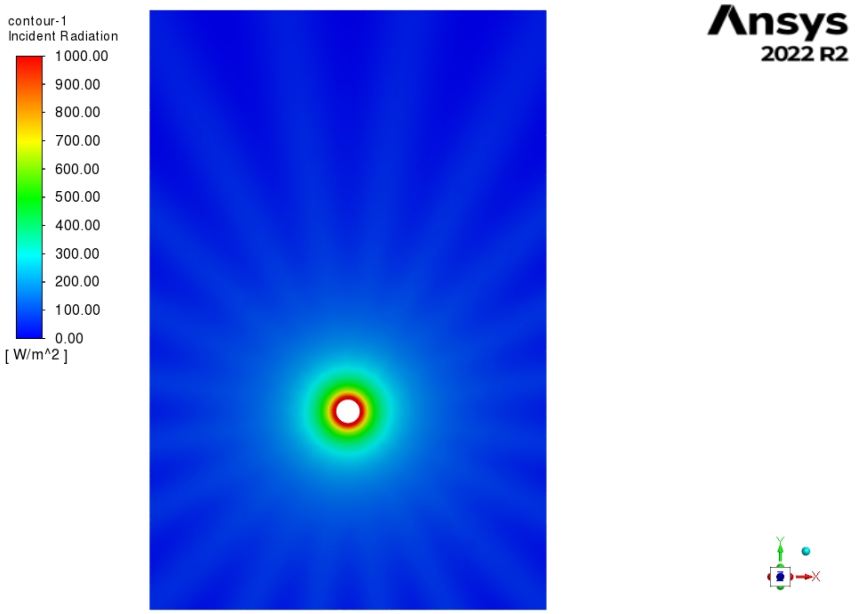

Figure 3.62: Contours of incident radiation inside the simulated volume.

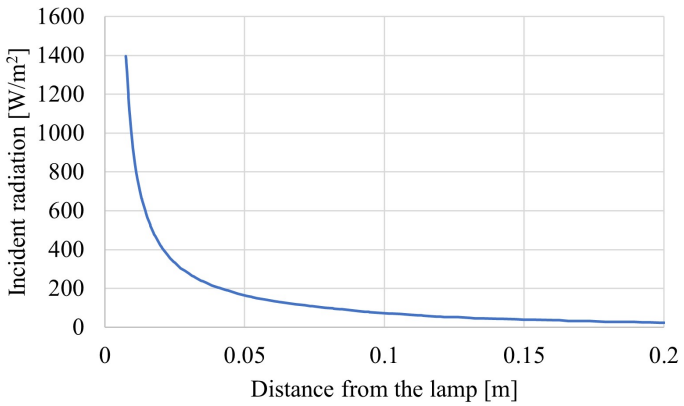

Figure 3.63: Value of incident radiation at increasing distance from the lamp.

Results and discussion

Simulation of a single UV lamp

The calculated contours of incident radiation are presented in Figure 3.62. It can be observed how the radiation rapidly decreases as the distance from the lamp increases. This trend is confirmed by the values of incident radiation presented in Figure 3.63, calculated on a vertical line starting from the lamp surface.

Experimental tests and model validation

The results of the experimental campaign are presented in Figure 3.64. Average, maximum, minimum, and standard deviation values of the measured radiation intensities were calculated for each configuration. The two belt geometries were characterized in terms of the radiation passing through them as described previously. The results are reported in Table 3.23. The measured radiation intensity without the belt (26.27 ± 0.09 W/m^2) was in good agreement with the calculated value of 29.7 W/m^2 at 0.16 m from the lamp. It is important to highlight that the difference between the values may be partly due to the difficulty of accurately measuring the distance between the sensor and the lamp.

The optimal belt geometry turned out to be the rectangular bar belt, as it allowed for 82% of the radiation to pass through. This percentage was considered as a "damping" multiplying coefficient of the total radiation intensity emitted by the lamp during the simulation of the bottom lamps to account for the presence of the conveyor belt without having to simulate its geometry, thus strongly reducing the computational time and resources required.

Belt	**Average [W/m^2]**	**Min [W/m^2]**	**Max [W/m^2]**	**St. Dev [W/m^2]**	**Percentage of transmitted radiation**
No belt	26.27	26.04	26.50	0.09	-
Triangular mesh	12.31	12.00	12.58	0.12	46%
Rectangular bar	21.61	21.33	21.87	0.10	82%

Table 3.23: Experimental results

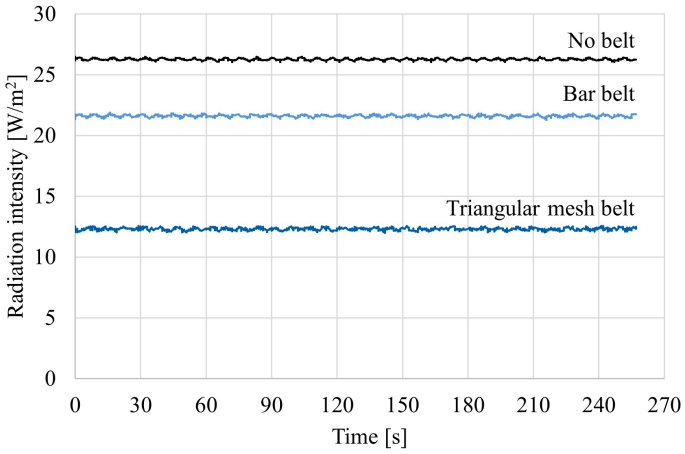

Figure 3.64: Results of the experimental tests with no belt between the lamp and the sensor, and with two belt geometries.

Simulation of the industrial device for the UV-C treatment

Simulation results, in terms of radiation intensity on the product surface, are presented in Figure 3.65. It can be appreciated how the radiation strongly depends on the position of the product relative to the lamps. In Figure 3.66 a comparison between the radiation intensity on the top side and the bottom side of the fruits is represented. It is observed that in the bottom part, due to the presence of the conveyor belt which absorbs part of the radiation, the intensity is lower. The most irradiated areas are generally located in the upper part of the product, while the least irradiated zones are located on the sides of the fruit, where the radiation from the lamps arrives only partially, as it is affected by the shadow generated by the other products.

To assess the performance of the machine in both the most irradiated and the least irradiated areas, i.e., the maximum dosage and the minimum dosage absorbed by the fruit, it is necessary to monitor the evolution of radiation on the fruit surface throughout the whole process. To this aim, the minimum and maximum dose was calculated on the surface of each fruit, so that the evolution of these quantities as the position of the fruit within the machine changed was known.

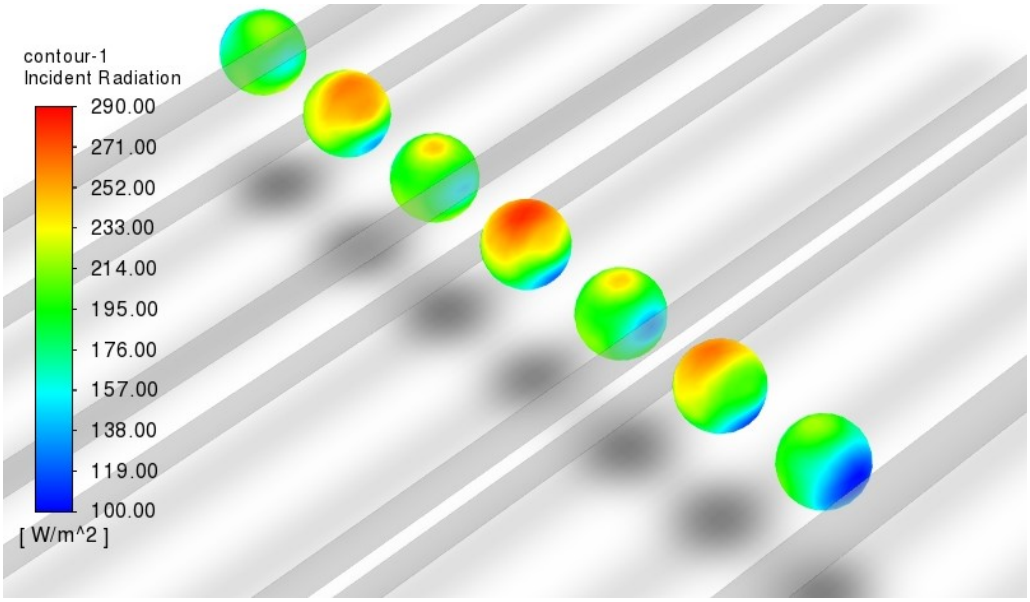

Figure 3.65: Contours of incident radiation on the fruit surfaces.

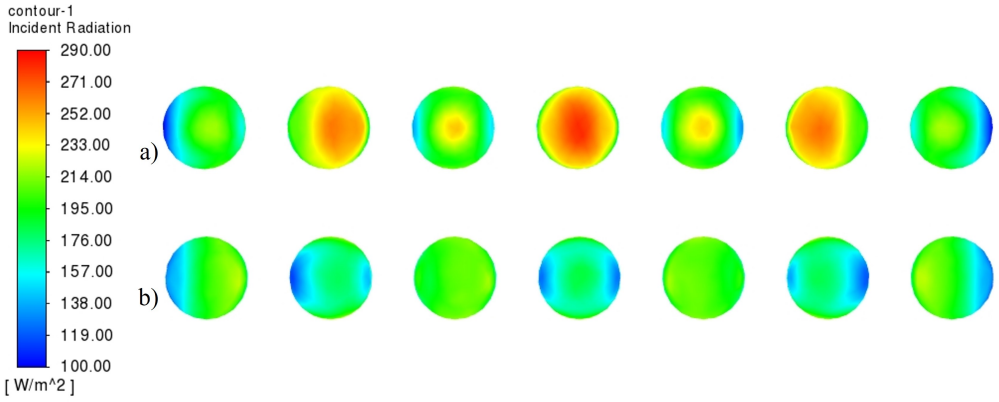

Figure 3.66: Contours of incident radiation on the top and bottom sides of the fruits.

In Figure 3.67, the maximum and minimum radiation on the surface of the fruit as the position of the fruit inside a single module of the machine varies are reported for the configuration with a 25 mm distance between the fruits. In the graph, the solid black lines represent the positions of the top lamps, while the dashed black lines indicate the bottom lamps. It can be seen that the highest values of radiation intensity are recorded in the central zone where the overlapping effects of multiple lamps occur; for the same reason, the dose values tend to decrease when approaching the ends of the module as the lamps contributing to the irradiation of the fruit are fewer. The lowest intensity values are recorded when the fruit is exactly above or exactly below a lamp. This is because the area where the lowest value is recorded is on the side of the fruit, and when the fruit is exactly above or exactly below a lamp, this area receives no radiation from the nearest lamp.

The maximum dose and the minimum dose provided by a single UV-C module can be obtained by integrating the two curves over time. These doses will obviously depend on the speed of the conveyor belt. Table 3.24 shows the maximum and minimum dose provided by the single module as the conveyor belt speed changes.

	Conveyor belt speed [m/min]				
	0.5	1	1.5	2	5
Maximum dose [J/m^2]	9575	4788	3192	2394	958
Minimum dose [J/m^2]	4946	2473	1649	1236	495

Table 3.24: Maximum and minimum dose provided by the single module as the conveyor belt speed changes

Such results, depending on the product to be processed and the target microorganism to be abated, allow at the design stage to choose the number of modules and the conveyor belt speed to achieve the desired treatment. It can be seen from the results that the maximum dose provided, regardless of belt speed, is approximately twice the minimum dose. This could cause overexposure of some zones of the products. To increase the treatment uniformity, in an experimental phase, the inclusion of turning bars to rotate products during the process could be considered, in particular for those products less prone to mechanical damage.

Finally, Figure 3.68 and Figure 3.69 show the trend of minimum and maximum intensity as the distance between the fruits changes. It is observed that as the distance increases, both the minimum and the maximum intensity tend to increase. Since the dose absorbed by the fruit is linked to the radiation intensity supplied during the exposure time, as the distance between the fruits decreases, to keep the doses unchanged, it is necessary to increase the exposure time, and thus reduce the conveyor belt speed. To maximize the productivity of the machine, ensuring the minimum required dose, it is then necessary to determine the optimal trade-off between the filling degree of the conveyor belt and its velocity.

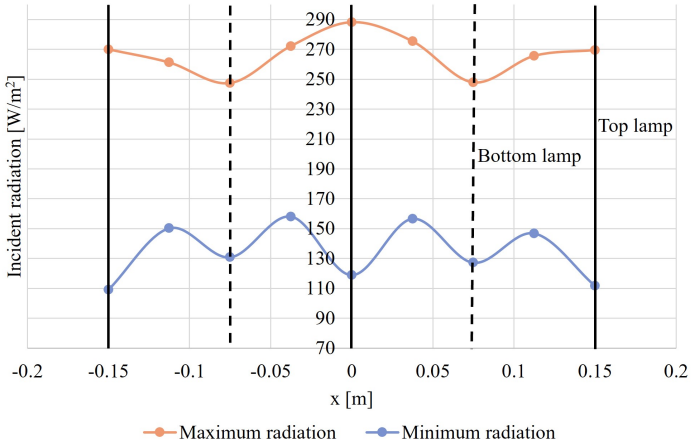

Figure 3.67: Maximum and minimum radiation intensity for the configuration with 25 mm distance between the fruits.

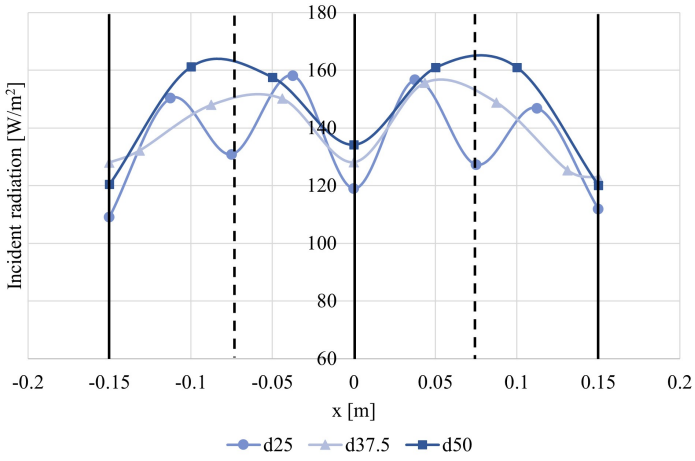

Figure 3.68: Minimum radiation intensity for the three different fruit layout configurations.

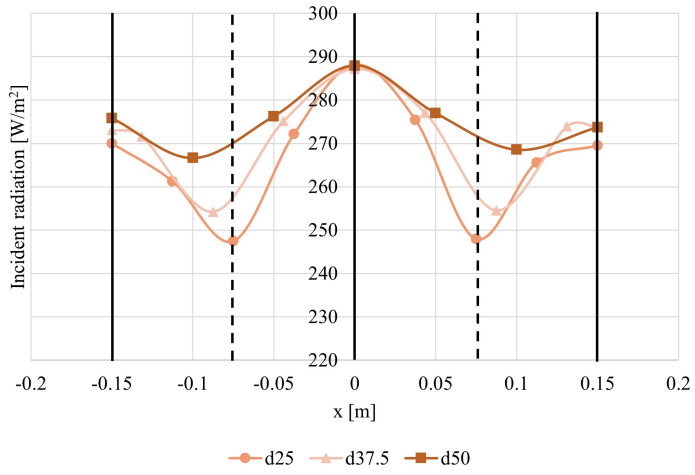

Figure 3.69: Maximum radiation for the three fruit layouts.

Conclusions

A numerical simulation model was developed to design and optimize a machine for the surface treatment of fruits and vegetables with UV-C radiation. This type of treatment has been attracting considerable interest in recent years because it allows decontamination of the products and can induce beneficial hormetic phenomena, limiting energy consumption, and avoiding the production and the accumulation of unwanted chemical by-products.

The final goal of the research is to design an industrial device, for the continuous UV-C treatment of fruits and vegetables. In this study, a first design of a pilot configuration, consisting of one module of the industrial machine is proposed. The device consists of a conveyor belt positioned between two rows of UV-C lamps. The arrangement and the number of lamps were selected to maximize the treatment uniformity and to reduce, as much as possible, the constructive constraints of the machine.

All the stages of the device design will be supported by numerical simulation. To this end, the radiation emitted by a single lamp was first simulated with Ansys Fluent using the DO radiation model. The numerical model and the settings used to simulate the radiation field, were validated with experimental tests. The test also allowed to select the best belt geometry and derive useful insights for further simulations.

Once validated, the simulation model was used to simulate the treatment inside a single module of the UV-C device, to identify the areas on the fruits' surface subject to the highest and lowest radiation intensity. Based on the results, the device performance, in terms of the evolution of maximum and minimum radiation on the fruit surface was assessed.

Three different product arrangements were evaluated to quantify the impact that the spacing between the fruit, i.e., the belt filling rate, has on device performance. As the distance between the fruits decreased, i.e., the degree of filling of the conveyor belt increased, the radiation intensity on the fruit surface overall decreased, due to the occurrence of shadow effects caused by the neighbouring fruits.

This work significantly contributes to the state of the art of the food irradiation sector, by implementing numerical simulation as a tool to support the design and optimization of an industrial device for the UV-C treatment of food products. Indeed, due to the characteristics of UV radiation, it is essential to optimize the device and the process to ensure an adequate and uniform irradiation of the products.

Future research activities will include the construction and the experimental evaluation of the designed pilot device, focusing both on the microbiological reduction achieved and the increase in the product shelf life. Then, a scale-up will be performed, to design and build an industrial device with a given number of UV-C modules and a running conveyor belt.

Chapter 4

Integration of simulation results and digital technologies for the control of industrial plants

Contents

4.1 Development of Digital Twin frameworks

Effective and efficient control of industrial plants is essential to achieve target productivity levels, while also guaranteeing adequate quality and safety standards, minimising the use of resources and the production of waste.

Standard industrial controls were historically based on manual regulations, based on the know-how and experience of the operators, or, more recently, on more or less precise *feedback* approaches.

In these cases, regulations are performed in response to deviations of the measured values from the set point. In PID (Proportional-Integral-Derivative) control systems, the extent of the adjustment is based on the error magnitude, the trend of measurements over previous time steps, and the rate at which the signal changes. While the effectiveness and efficiency of such controls can be very high when correctly designed, the process is treated as a black box.

Nowadays, more advanced control systems techniques do not rely only on *feedback* techniques but sometimes can also feature a *feedforward* approach.

In particular, *feedforward* control is a proactive strategy that predicts and anticipates the effects of disturbances on system outputs by using a model of said system. Based on this model, *feedforward* control adjusts inputs and operating conditions in advance to maintain the desired output, thus preventing deviations before they occur or at least limiting their impact. Since the adjustments rely on model predictions, the effectiveness and precision of the control depend heavily on model accuracy. To this end, to ensure both responsiveness and stability in the system, *feedforward* is often paired with *feedback* control, which has the objective to fine-tune the regulation and correct any residual errors.

The logic behind *feedforward* control is one of the foundations of Digital Twin technology [110]. As stated in the Introduction (Section 1.1), Digital Twins (DTs) are integrated, data-driven representations of dynamic entities - such as, but not limited to, industrial plants and devices.

DTs rely on three main components: (i) a physical entity defined as "physical twin", (ii) its virtual model, referred to as "digital shadow", and (iii) a continuous real-time communication between the two. In DTs, real-time data and the models are combined to anticipate and respond to the changes in a system proactively. A review of DT applications and studies in the literature is presented in the two included articles.

The capabilities to perform real-time monitoring, predictive modelling and proactive adjustments make DTs highly effective for real-time decision-making, process optimization, and predictive maintenance, among other applications.

To build an effective DT, however, one must have a clear understanding of its purpose and of the operation of the target system. Indeed, it is crucial to correctly define input

and output parameters, including the choice and the development of the right digital model.

The data used to generate the digital models can be of various nature: historical and experimental data, as well as the results of analytical or numerical modelling campaigns.

In the present thesis, two studies are included that aim to generate digital models of industrial plants based on experimental data and results of CFD simulations, in order to formulate *DT* frameworks for plant monitoring and control.

The two case studies concern two pilot plants installed at the University of Parma (Italy):

1. application in air-filtration domains, where the operation of the cyclone bag filter considered evolves over time as the clogging of the filtering devices increases;

2. application in the sector of thermal treatment of food fluids, where a constant outlet product temperature must be guaranteed to achieve food safety and quality.

At the moment, both frameworks include the experimentally validated digital models of the plants and the control logic designed to achieve the target outcomes of interest.

The next steps of the research projects will include the deployment of the developed control systems on the pilot plants, to test their effectiveness, before further extending the investigated approach.

4.1.1 Real-time optimization with 1D CFD: Control of industrial air-filtering plants under evolving clogging conditions

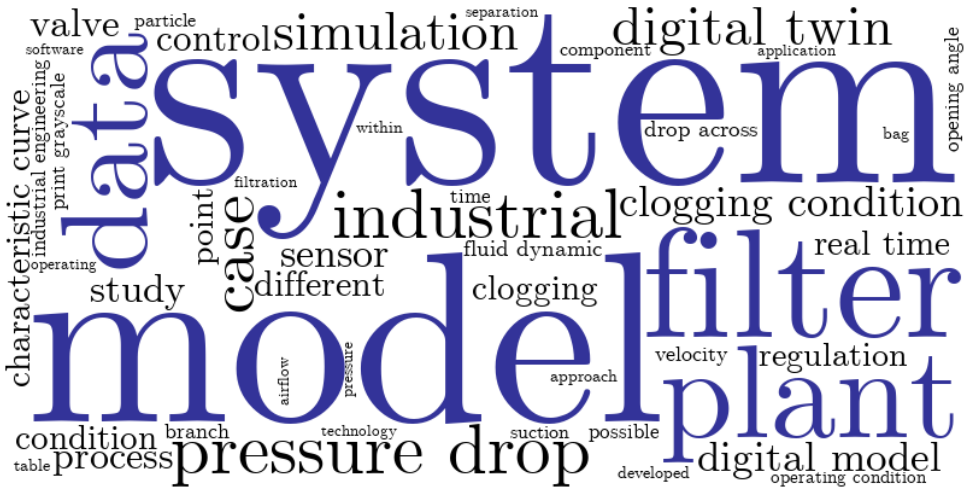

The research in this chapter has been included in the peer-reviewed article [205] *Solari, F., Lysova, N., and Montanari, R. (2024). Monitoring and control of air filtration systems: Digital twin based on 1D computational fluid dynamics simulation and experimental data. Computers & Industrial Engineering, 197, 110607. https://doi.org/10.1016/j.cie.2024.110607*

The authors would like to express their gratitude to the company OCRIM Spa for the crucial support in conducting the analysis and in preparing the present article.

Abstract

This study presents the development of a digital model based on one-dimensional computational fluid dynamics for the monitoring and control of filtering systems used for removing flour, dust, and other particulates from the airflow arriving from various sections of industrial production plants. Focusing on a pilot plant equipped with a cyclone bag filter, historical experimental data was integrated with the results of a one-dimensional fluid dynamics simulation model to create a digital twin capable of real-time control and regulation of industrial plants. In particular, measured pressure drop data under different clogging conditions were interpolated to generate the characteristic curves of the filter under various clogging conditions, to be implemented within the digital model of the plant. The generated model, validated through a dedicated experimental campaign, accurately predicted the airflow rate and pressure distribution across the plant. The system's capability to adapt to changing operational conditions, such as clogging, was demonstrated through simulation, highlighting the model's usefulness in maintaining the desired operation levels while minimizing the need for extensive sensor networks. The analyzed case study in the field of air filtration systems aims to fill the gap in the scientific literature related to the application of Digital Twin technology to the control of industrial manufacturing plants. The findings highlight the potential of Digital Twins in monitoring and control, as well as predictive maintenance, of industrial systems. Future research activities will explore the model's applicability in failure and anomaly detection, to further enhance predictive maintenance of air filtering systems.

Introduction

The separation of heterogeneous mixtures is a widely used process in many industrial sectors [206]. In some cases, such separation is achieved by exploiting the action of a force field which, when phases have different densities, tends to separate them. When the applied force field is the gravitational one, it is referred to as sedimentation or settling [207, 208]; in this case, the process rate, being the magnitude of the force field fixed, is mainly driven by the difference in density between the phases. When, on the other hand, a centrifugal force is applied, it is referred to as centrifugal or cyclonic separation [100, 102]. In this case, the efficiency of the process and its rate can be influenced by acting directly on the force field and therefore on the operating and design parameters of the process.

In other cases, i.e., when phase densities are very similar, or when the size of the particles to be separated is very small, separation is achieved by passing the mixture through a porous media that traps suspended or dissolved particles, based on a cut-off dimension or chemical affinity. In the first case, the process is referred to as "filtration" [101, 103]. In the latter case, when separation is achieved by exploiting the chemical-physical interactions (i.e., Van der Waals forces or intermolecular chemical bonds) that occur between the filter matrix and the species to be separated, the process is referred to as "adsorption" [209]. In both filtration and adsorption, the filter matrix tends to become saturated over time and therefore must be periodically regenerated. Regeneration allows the matrix itself to be partially cleaned to extend its useful life. In the case of filtration, regeneration is carried out by flushing a countercurrent flow of fluid through the porous media to remove part of the trapped substances [104–106]. In the case of adsorption, on the other hand, desorption cycles are carried out, to renew the filter matrix by purifying it from the adsorbed solute, either using a solvent [210, 211], by thermal treatment [212], or by a pressure decrease [213].

After a certain period, regeneration cycles are no longer effective, and the filter matrix must be replaced. Preventive maintenance techniques are generally adopted to schedule such substitution interventions by constantly monitoring the performance of the process. Generally, pressure drops at the ends of the filter are used as reference parameters to identify when regeneration is no longer able to re-establish acceptable operating conditions, i.e., when the reference parameter remains above a certain threshold value. This approach makes it possible to promptly intervene whenever the filter's performance is no longer acceptable, thus allowing it to always work under conditions of good efficiency. In some cases, however, for example in the presence of particularly abrasive materials or when non-homogeneous clogging of the filter matrix occurs, deviations from standard operating conditions could develop that could lead to sudden and premature failure of the filter matrix. In these cases, therefore, reactive, unscheduled maintenance must be carried out, resulting in considerably higher costs compared to a scheduled inter-

vention. To avoid these situations, it is necessary to switch from preventive to predictive maintenance. To this end, it is necessary to develop analytical or numerical models, i.e., virtual representations based on the integration of real-time data, historical data, and data resulting from analytical or numerical sub-models [92,115,117]. In [97], the authors have described a predictive maintenance model for a cyclonic bag filter based on a digital model, built from both historical data and fluid-dynamic simulation results. By integrating pressure drop measurement with velocity measurements at a specific point within the filter, the authors developed a model that can detect in real-time both failures and malfunctions. The authors hence have focused on conditions internal to the filter to make predictions about the filter's remaining useful life, but they have not evaluated how the operating conditions of the filter impact the behavior of the whole system. Indeed, the filter is generally embedded within a more complex plant, and its operating conditions impact the overall fluid dynamic behavior [214]. Thus, it may happen that, while the clogging conditions of the filter are not yet sufficient to demand a replacement of the filter matrix, the behavior of the entire system does not reflect the desired one in terms, for example, of air flow rate; a tuning intervention would hence be necessary.

Since the clogging conditions of the filter and, as a consequence, the operating conditions of the system, are continuously changing, a continuous control and regulation system would be needed. In industrial settings, however, it is often difficult to monitor the actual operating conditions of the system because of specific process conditions which make it challenging to install sensors. This happens, for example, when the mixtures are highly heterogeneous, or there is a high percentage of suspended solid particles. It is therefore extremely difficult to detect deviations from the desired operating conditions and to develop automated adjustments based on standard feedback control.

In many studies, Computational Fluid Dynamics (CFD) has been adopted to accurately characterize both air suction systems and separation processes under different operating conditions, allowing for the monitoring of the parameters of interest at each point of the plant, even where the measurement with physical sensors is not possible [134,137]. Simulation results can be indeed used, in addition to, or in substitution, to real data, to evaluate corrective actions for the adjustment or improvement of the operating conditions. In [215] the authors have combined CFD simulations with field measurements to analyze dust pollution diffusion under different operating conditions and by varying suction port positions. The optimized parameters for air suction volume and suction port position were then applied to a construction site, leading to a significant improvement in dust control within the tunnel environment. However, traditional three-dimensional fluid dynamic simulations are very time-consuming and can not be used for real-time control. Many studies can be found in the scientific literature that have addressed this issue, to make the results of fluid dynamic simulations available more rapidly, thus making them more compatible with the development of real-time control systems and the implementa-

tion of digital twins. To this end, some of the existing studies adopted traditional 3D fluid dynamic simulation integrated with reduced-order models. [216] have presented a novel approach for the optimization of the design of cyclone separators for the separation of oil aerosols from gas streams. Starting from validated CFD simulations, the authors have developed a reduced-order model able to predict velocity profiles, pressure drops and separations efficiency with good agreement to experimental data. Although the main objective of the proposed approach was to reduce the computational time required by CFD simulation, the final aim of the authors was to speed up the design phase of cyclone separators and not to develop a model for real-time process control.

Some other studies have adopted simplified fluid dynamic models, such as [217], where the authors have developed a simplified calculation model based on CFD simulations, to rapidly calculate the dynamic process of particle capture, contributing to extending the service life of filter media and reducing the energy consumption in air purification systems. The authors have succeeded in reproducing the dynamics of particle deposition on a single fiber and the results appeared promising. However, being the method developed by assuming a single fiber and approximating it with a two-dimensional domain, it can hardly be applied with acceptable results in a much more complex industrial context. In both of the above cases, there is no connection between the real and the virtual system.

When a virtual model receives input from the real system and uses its results to provide feedback and maintain control over the real system, it is referred to as "Digital Twin" [110]. Digital Twin technology is increasingly transforming various industries by creating connected virtual replicas of physical assets, processes, or systems. A recent study [218] has highlighted how the main applications of the Digital Twin can be found in the manufacturing sector, especially in the management of planning and scheduling phases of job shop activities and assembly processes. In another study, [219] the authors have confirmed this evidence by highlighting how most of the studies focus on the pilot testing, monitoring, and improvement phases of the single machine or process. The application of the digital twin for industrial plant control appears to be an unexplored area of research.

In a recent study, [220] have demonstrated that one-dimensional lumped-parameters fluid-dynamics simulation could be adopted to develop a Digital Twin of a complex system (i.e. an irrigation network) aiming to minimize water consumption and detect possible failures and malfunctions. Indeed, while 3D CFD simulations allow for detailed modeling of complex geometries and flow patterns, they can be notoriously very time- and resource-extensive. Furthermore, such a high level of detail may not be necessary for the development of Digital Twins and, more in general, for applications intended for real-time control of industrial plants. In contrast, 1D CFD simulations, offer a more computationally-efficient alternative by simplifying the system through lumped param-

eters. This type of simulation tends to reduce the overall computational cost, limiting the level of detail by simplifying the assumptions and averaging the system's parameters, variables, and flow characteristics. While this can reduce the accuracy of the results, as well as the applicability and flexibility of the method in particular contexts (e.g., complex geometries or turbulent flows), in several cases of industrial interest, 1D CFD simulation allows to optimize the trade-off between the information required to control the plants, the time available for the computation and the allocatable resources.

The present study focuses on an industrial air suction plant with a cyclonic bag filter, like that described in [97]. In this device, an air stream with suspended solid particles is treated and separated by combining centrifugal separation and filtration on polyester filter bags. The adopted approach consists of integrating real data with one-dimensional fluid dynamics simulation to develop a digital twin for real-time control and regulation of an air suction system, which is commonly adopted in many industrial sectors.

After a characterization of the filter at different flow rates and under different clogging conditions, a 1D CFD lumped-parameter model of the entire system was developed. The digital model, validated with dedicated experimental measurements, accurately reproduces the system's behavior in terms of pressure and flow rate at each point when compared to the values detected by the field sensors. These values can be fed in real-time as input data into the digital model, which can then be considered a digital shadow of the plant. Specifically, it predicts in real-time the velocity and pressure ranges throughout the system and evaluates deviations from the desired operating conditions.

The proposed approach leverages modern computational capabilities for industrial applications and could be considered the base for future research and development in the field. Indeed, in future research activities, the digital shadow could be connected, via an application programming interface (API), to the actuators installed on the plant (i.e., the butterfly valves for flow regulation), allowing the use of the resulting digital twin for regulation purposes, aiming to maintain the deviations from the set-points within the expected limits. An in-depth economic analysis could also be performed, to assess the cost savings from reduced maintenance and improved efficiency.

Materials and methods

Description of the plant

The filtering device, installed at the University of Parma, Italy, consists of a cyclonic separator mounting 31 filtering bags, and it is characterized by a standard industrial scale (Figure 4.2, Table 4.1). The cyclonic body allows for the separation of the bigger, heavier, particles, while the filtering bags trap the finer particulate. The bags are made of non-woven polyester needlefelt, with casual fiber orientation, thermally treated to lock all the fibers in place, and singed to ensure an appropriate surface finish (Figure 4.3).

The characteristics of the polyester needlefelt are reported in Table 4.2. The polyester fabric bags are mounted over a metallic structure (Figure 4.3) to ensure the correct shape throughout the filter's operation. The separator functions as follows: the particle-laden air from the processing line, drawn by a fan located after the filter, enters the system tangentially and proceeds towards the conical bottom of the cyclonic body in a spiraling motion. In this process, the heavier particles are separated from the airflow and collected in the conical bottom of the cyclone, from which they are periodically discharged. Afterward, the airflow is forced to pass through the filtering bags. While passing through the filtering material, the residual smaller particulate remains trapped in the fabric due to several phenomena ranging from inertial impaction, interception, and diffusion to electrostatic forces, and accumulates over time despite the periodic cleaning measures usually adopted.

Since the analyzed pilot plant is not connected to a real industrial line, the fan draws air from the external environment; after passing through the separation system, the filtered air is released back into the atmosphere. The total flow rate circulating in the system can be regulated by acting on the inverter of the fan through a PLC panel through a human-machine interface, and by adjusting the opening angle of valve V_1. In particular, by acting on the inverter it is possible to change the frequency of the electrical supply: by modifying the speed at which the motor's magnetic field rotates, this variation allows for more precise control over the speed of the fan blades. The adjustment in the opening angle of the valve, on the other hand, allows to regulate the processed flow rate. Figure 4.1 illustrates three characteristic curves of the fan used in the pilot plant, each corresponding to a different inverter frequency, that show the relationship between the processed flow rate and the total head provided by the fan.

In this pilot plant, it is possible to draw air either exclusively from the main pipe section or also from a secondary branch by adjusting the opening angle of a secondary valve V_2. The valve opening angles can be regulated through the StepControl software, acting on dedicated stepper motors (aec M60SH86-TO0512P24C).

Table 4.1: Characteristics of the cyclonic body.

Dimension	**Value**	**Units**
Total separator height	5.308	m
Separator diameter	1.300	m
Height of the conical bottom	1.550	m

Several sensors are installed across the pilot plant to monitor the system's operation. The data are acquired every 0.5 s with a Data Acquisition Module (DAQ) connected to a NI LabVIEW project that allows to continuously log the data and write it to a file for further elaborations and analyses. In particular, the KIMO differential pressure device, equipped with a Debimo air flow measuring blade, measures the flow rate in the system.

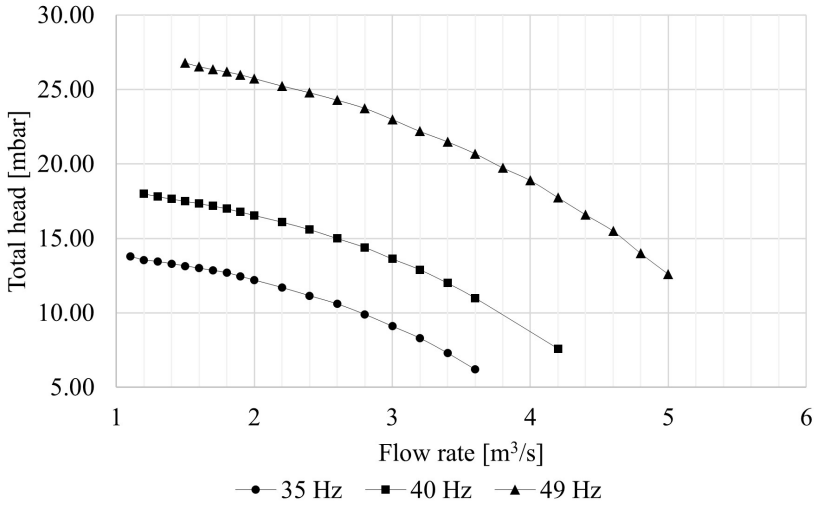

Figure 4.1: Characteristic curves of the fan at different frequencies, which can be modified by means of an inverter.

Figure 4.2: Pilot plant with a cyclonic bag separator installed at the University of Parma, Italy.

Table 4.2: Characteristics of the polyester bags.

Characteristic	**Value**	**Units**
Length	3.000	m
Diameter	0.123	m
Thickness	1.4	mm
Weight	350	g/m^2
Density	0.26	g/cm^3
Pore volume	81%	-
Air permeability	320	l/dm^2 min

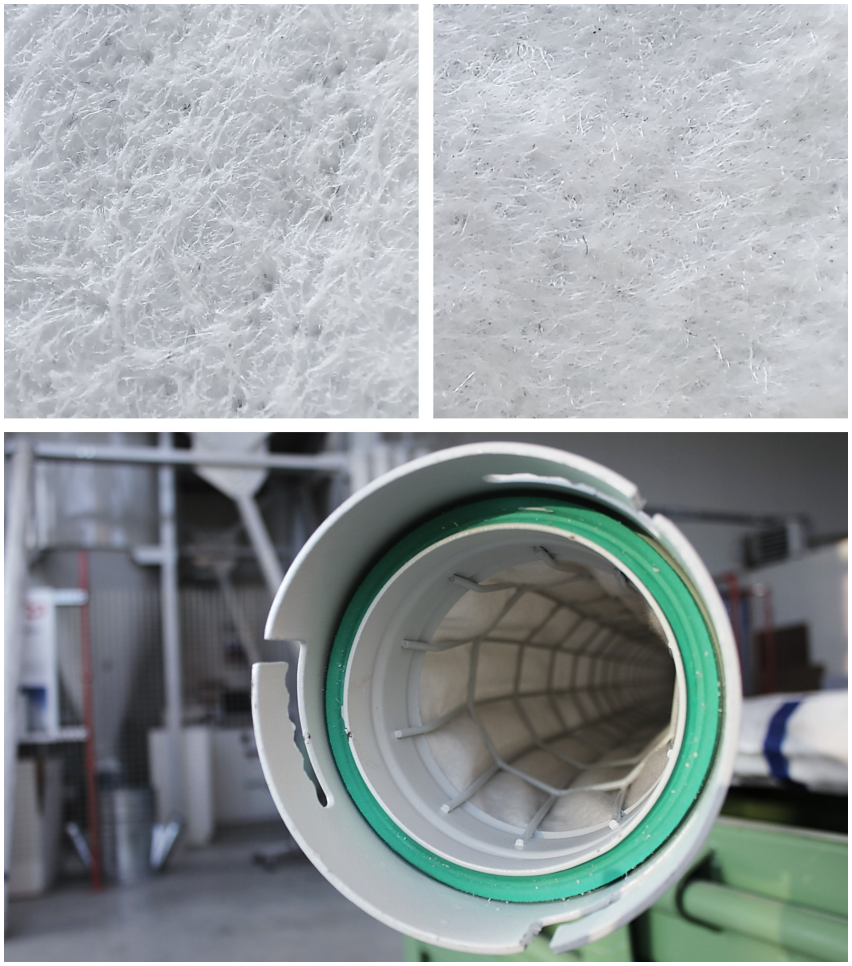

Figure 4.3: Top (a) and bottom (b) sides of the filtering material. Inside of a filtering bag, showing the metallic support structure (c).

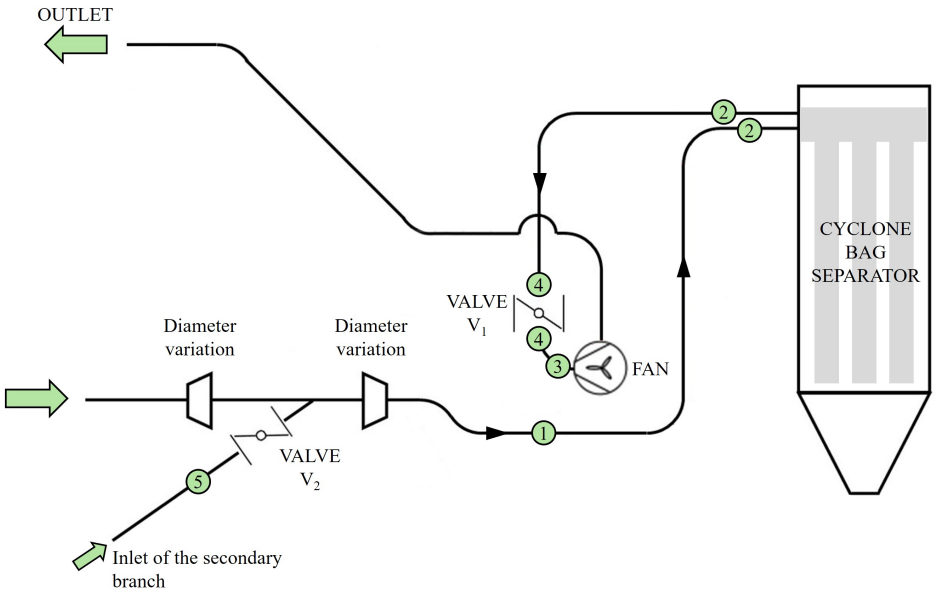

Figure 4.4: Schematic representation of the pilot plant. The green numbered circles indicate the sensors described in Table 4.3.

This device, installed on a straight pipe section after the inlet of the secondary branch and before the filter, generates a differential pressure, the square root of which is proportional to the flow rate according to Eq. 4.1 provided by the manufacturer, where C_M is a conversion coefficient which depends on the blade geometry and installation.

$$v = C_M \sqrt{\frac{2 \cdot \Delta p}{\rho}} \tag{4.1}$$

The pressure drop across the filter, and that across valve V_1, are measured with differential pressure sensors, while the pressure at the suction section of the fan is measured by a barometric pressure transmitter. Finally, a hot-wire anemometer is used to measure the air velocity in the secondary inlet branch. The locations of all the sensors, detailed in Table 4.3, are presented in Figure 4.4.

Bags and clogging

During the standard operation of filtering devices, the porous material tends to become progressively more obstructed with particulate over time. Indeed, although compressed air systems are usually implemented to clean the bags by periodically injecting compressed air jets counter-current to the processed airflow, they are not able to completely remove all the particulate matter trapped in the fabric, besides the fact that their action is generally limited to the upper part of the bags.

This phenomenon takes the name of "clogging", and it is the main factor affecting the service life of filtering media. The effects of clogging at the macroscopic level can be

Table 4.3: Overview of the sensors installed on the plant.

Sensor	Model	Measured quantity	Range	Accuracy
1	KIMO CP212 differential pressure transmitter	Pressure, converted to the velocity of the airflow entering the filter	± 1000 Pa	± 0.5%
2	Endress Hauser Deltabar S PMD75 differential pressure transmitter	Pressure drop across the filter	± 10 mbar	± 0.05 %
3	Trafag Barometric Pressure Transmitter Absolute	Pressure at the suction section of the fan	800 – 1200 mbar a	± 0.3 %
4	DELTA OHM HD402T2 differential pressure transmitter	Pressure drop across the valve	0 – 10 mbar	± 0.75 %
5	EE650 hot-wire anemometer	Velocity of the airflow	0 – 20 m/s	± 3.0%

summarized as a reduction in the permeability of the fabric, which results in an increase in the pressure drop across the filter. This pressure drop is generally the only indicator of clogging monitored in industrial settings and used to schedule filter maintenance.

In fact, when the pressure drop across the filter exceeds a critical value (10-15 mbar), the bags are usually dismounted and replaced altogether with a new set. At the microscopic level, clogging can be observed as the accumulation of particulate matter in the fabric, in particular on the fibers (Figure 4.5 and 4.6).

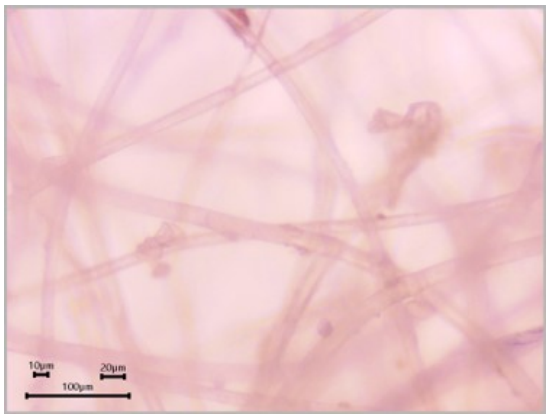

(a) Clean bags.

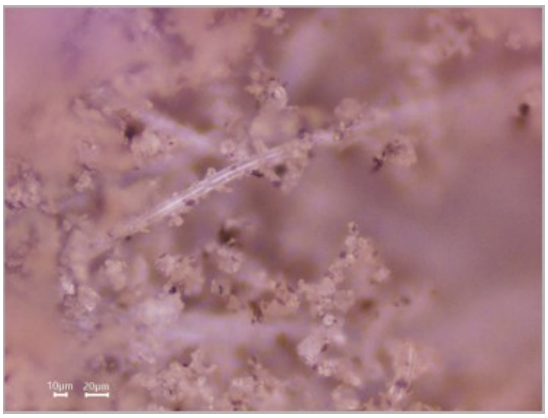

(b) Completely clogged bags.

Figure 4.5: Bags observed under optical microscope with 20x magnification.

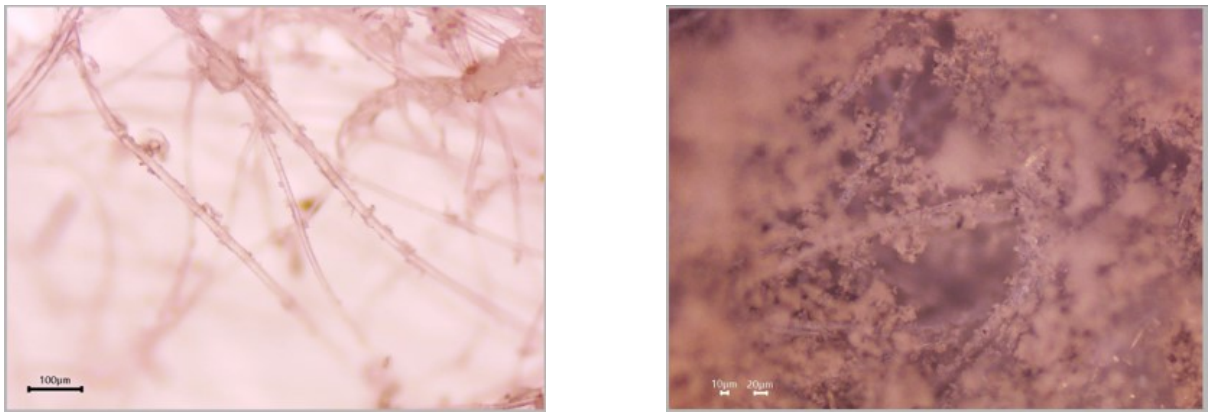

(a) Clean bags. (b) Completely clogged bags.

Figure 4.6: Bags observed under optical microscope with 10x magnification.

Experimental testing

Experimental tests were performed in order to characterize the cyclone bag separator under different clogging conditions and with different air flow rates. The flow rate processed in the pilot plant was changed by acting on the fan inverter. The clogging conditions, on the other hand, were reproduced by manually disassembling the clean bags from the separator and substituting them with a given number (Table 4.4) of completely clogged bags, provided by an industrial manufacturer for research and testing purposes after dismounting them from the industrial filter. In Figure 4.7, it is possible to qualitatively assess the difference between the two limit states of the bags, with clean filtering bags on the left side of the figure and completely clogged bags on the right side.

The characterization of clogging is based solely on the pressure drop across the separator, so it is assumed that, e.g., the presence of 40% of clogged bags corresponds to a clogging level of 40%. The clogging level, therefore, is calculated by dividing the number of clogged bags by the total number of bags (31). For each case, the range of inverter frequencies was determined based on the inlet air velocities commonly encountered under standard operating conditions, and the pressure drop across the filter, which had to be less than the upper measurement limit of the differential pressure sensor (10 mbar). The valve V_1 was left completely open (90°) for the two cases with clogged bags (Cases 2 and 3), while for Case 1 with clean bags, the opening angle was modified to have a comparable range of airflow rates.

Figure 4.7: Comparison between clean (on the left) and completely clogged filtering bags (right) disposed of by an industrial manufacturer.

Table 4.4: Clogging conditions reproduced during the experimental campaign.

Case	**1**	**2**	**3**	**4 (Validation)**	**Units**
Number of clogged bags	0	8	31	17	-
Clogging level	0%	26%	100%	55%	-
Range of inverter frequencies	35 – 50	35 – 45	35 – 41	35 – 45	Hz
Valve opening angle	55	90	90	90	°

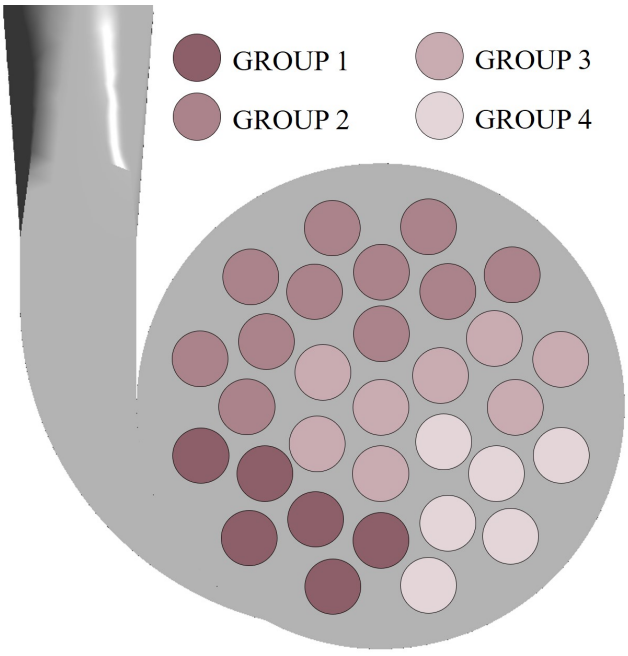

Figure 4.8: Division of the bags into four groups according to the expected clogging rate.

To insert the clogged bags, the clogging sequence identified by [97] was followed. In particular, the analysis allowed for the division of the 31 bags into 4 groups based on the airflow rates through them and thus the rapidity with which they tend to clog (Figure 4.8). Namely, the bags in Group 1 are expected to clog more rapidly, while those in Group 4 are characterized by a lower clogging rate. The experimentally evaluated clogging configurations, therefore, were reproduced by first substituting Group 1 with clogged bags, and then all four groups.

During the experimental runs, as previously stated, the sensor data were continuously acquired and logged by means of a Data acquisition (DAQ) module connected to a project created with LabVIEW software. The analysis of the data allowed to derive the characteristic curves of the filter at the tested clogging levels by interpolating the experimentally measured pressure drops across the device. Moreover, the results of the analysis were used to predict pressure drop at intermediate, not tested clogging levels, allowing to generalize system's functioning under different conditions. An additional clogging state was then experimentally reproduced on the pilot plant to validate the results obtained by substituting Group 1 and Group 2 with clogged bags (Case 4 in Table 4.4).

Modelling the effect of clogging on the pressure drop

The sensor data logged during the filter functioning were exported and analyzed with MS Excel. By analyzing the data from the experimental campaign it was possible to derive characteristic curves of the filter under the tested conditions. In particular, to fit the trend in the filter pressure drop at increasing air flow rates, the following steps were followed: (*i*) cleaning of the data, by removing the transient conditions represented by the measured values logged during the change of the fan operating point; (*ii*) evaluation of the general trend in the data; (*iii*) fitting of the data with an appropriate model, which resulted to be a linear regression. The results obtained made it possible to generate, for each clogging condition, an equation for the pressure drop in the general form of Eq. 4.2.

$$y = m \cdot x + q \tag{4.2}$$

The trend in the values of m and q were then observed and fitted with suitable models to generalize the system operation under different clogging conditions and predict the filter characteristic curves under non-tested conditions.

In industrial settings, the characteristic curves of the filter under different clogging conditions could be derived, for example, by monitoring and analyzing pressure drop value over the filter's useful life, or by characterizing it with 3D CFD simulations.

Digital model

The digital model of the plant was developed in Flownex, a one-dimensional lumped-

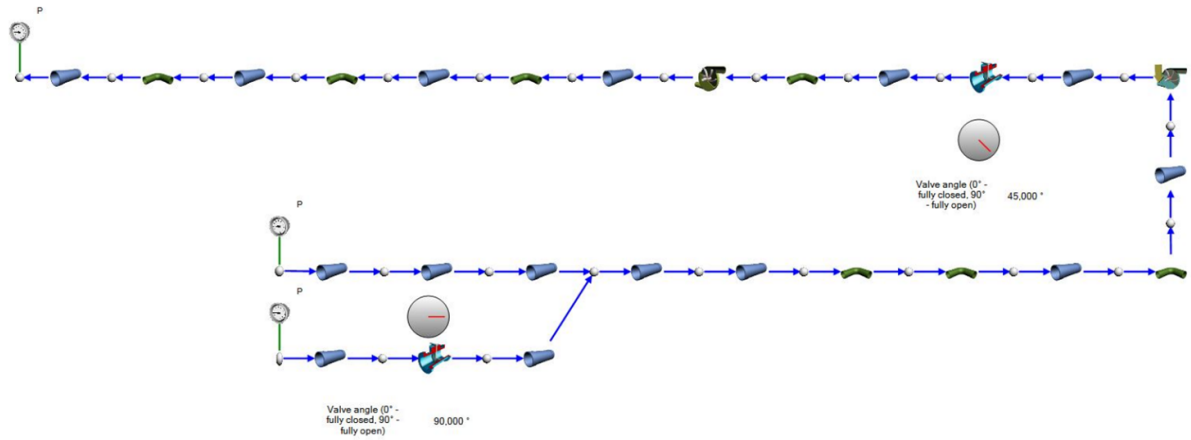

Figure 4.9: Digital model of the plant.

parameter fluid dynamics simulation software, typically used for the modeling of thermal-fluid networks and energy systems (Figure 4.9).

The numerical model must be defined by setting valuable boundary conditions and by characterizing all the elements and the nodes involved in the network. The fundamental differential equations (i.e. mass, momentum, and energy equation) are then solved through an iterative procedure. Unlike traditional three-dimensional models, lumped parameter models do not require domain discretization with a computational grid since it is given by the individual elements inserted into the system.

In this study, atmospheric pressure was set at both the inlet and the outlet sections of the plant. Standard components (i.e., piping, valves, connections) were characterized using the existing components from the software library. For piping, diameter, length, material (steel) and surface roughness (35 microns) were specified. For bends, the ratio between the radius of curvature and the internal diameter was also specified (1.5). The valve was represented using a standard butterfly valve, and the fan was characterized by its actual operating characteristic curves at different operating frequencies, provided by the manufacturer. The filter, which is not a standard component, was characterized by means of a proper experimental campaign. To have a characterization dependent on the clogging conditions, it was characterized at different clogging levels, which were reproduced by replacing a number of sleeves with fully clogged sleeves. Three different clogging conditions were reproduced based on which intermediate clogging conditions can be inferred by interpolation, as described in the previous sections.

In this work, the simulation model developed with Flownex was used to determine, for each clogging condition, the opening angle of the valves V_1 and V_2, and the operating frequency of the fan (f_{fan}), that would allow maintaining a constant airflow rate in the system. In particular, regulation is carried out by following the standard procedure generally adopted in industrial contexts: at first, regulation is carried out by acting on

the opening angle of the main valve (V_1); in a second step, if regulation with valve fails to reach the set point, the supply frequency of the fan is increased or decreased, depending on whether the air flow rate in the system is to be increased or decreased. After the supply frequency is changed, the valve opening angles have to be adjusted to obtain the desired airflow rates in the different sections of the system.

The simulation model is extremely flexible and could be adapted to many industrial scenarios to optimize the management and regulation of complex air distribution networks with several branches. It allows, on the one hand, to achieve real-time results regarding air distribution across the system based on the actual configuration, thus allowing prompt and effective regulation. On the other hand, since it assumes uniform flow properties along the length of the system, it does not give any detailed information about the flow patterns within the machines and components constituting the plant. To overcome this limitation, the 1D lumped-parameter model can be integrated with detailed three-dimensional models of the single components, which allow the behavior of individual components to be deeply investigated. Indeed, it is possible to connect the 1D simulation software (i.e. Flownex) with the 3D simulation software (i.e. ANSYS Fluent).

Digital model validation

The digital model was then validated with proper experimental tests in which, given the operating conditions of the fan (i.e., its characteristic operating curve), the valve V_1 opening was progressively changed and the overall flow rate and pressure values at various points in the system were monitored both in terms of mean values and standard deviation. In particular, the operating frequency of the inverter of the fan was set at 40 Hz, and four different valve openings were tested (fully opened, 60 degrees opened, 40 degrees opened, and 30 degrees opened) The same conditions were then reproduced on the digital model and the obtained results were compared. Regarding the pressure, the comparison was made based on the following values: (i) pressure drops across the valve V_1, (ii) pressure drops across the filter, and (iii) depression at the fan intake section.

Flow rate values and the air distribution among the branches were validated through two measurements: (i) air velocity in the main duct, upstream of the filter, and (ii) flow rate percentage of air drawn through the secondary duct.

Proposed Digital Twin framework

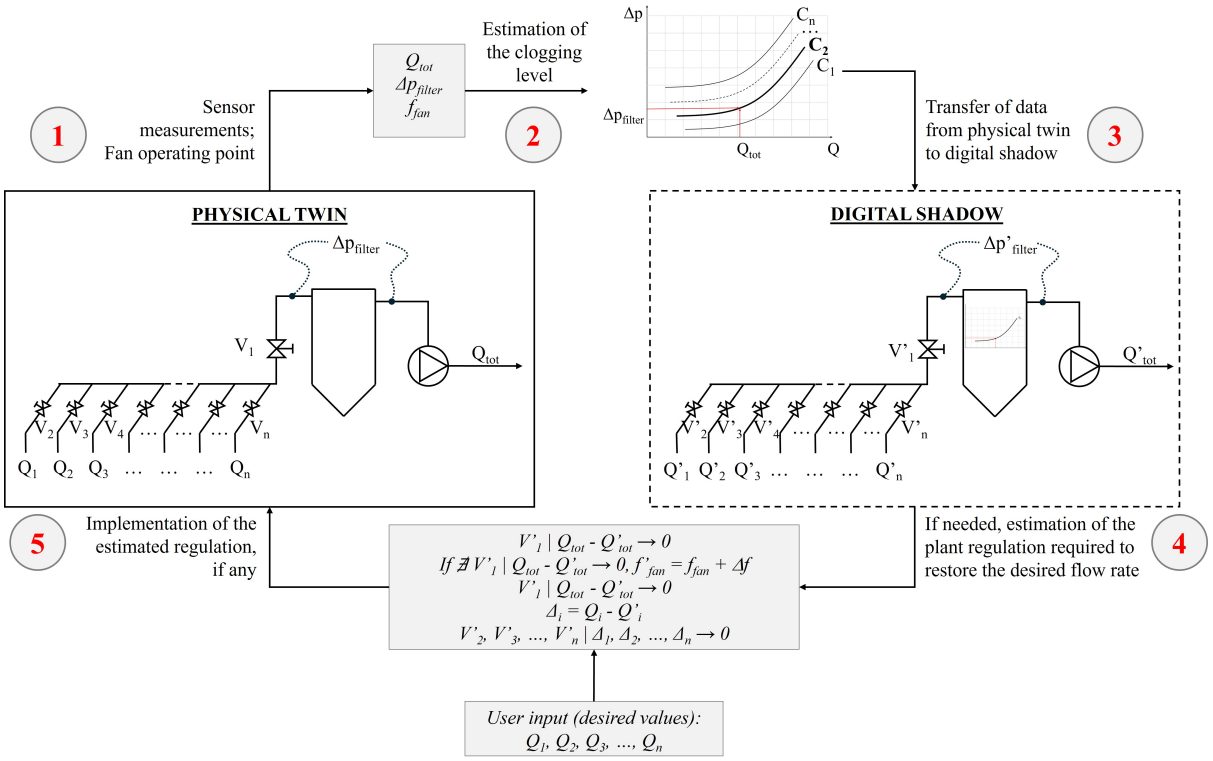

Figure 4.10: Proposed digital twin framework.

Once validated, the model, i.e., digital shadow, can be connected to the physical twin, i.e., real plant, through an API to generate a digital twin (Figure 4.10).

Results and discussion

Experimental testing

The sensor measurements logged during the experimental tests summarized in Table 4.5 were cleaned from the transient data and interpolated with a linear regression to generate the characteristic curve of the filter for each case in the form $dp = m \cdot v + q$, where dp is the pressure drop across the filter and v is the inlet air velocity (Figure 4.11). The coefficients of the linear model were then interpolated with appropriate models to generalize the effect of clogging and derive characteristic curves of the non-tested conditions. In the case of q, the fitting was performed on its negative, $-q$, and 0% clogging value was approximated with 1e-9 to use a power law model (Figure 4.12).

Table 4.5: Overview of the filter operation under the reproduced clogging states.

Case	**1**	**2**	**3**	**4 (Validation)**	**Units**
Number of clogged bags	0	8	31	17	-
Clogging level	0%	26%	100%	55%	-
Range of inverter frequencies	35 – 50	35 – 45	35 – 41	35 – 45	Hz
Valve opening angle	55	90	90	90	°
Measured inlet air velocities	15.6 – 23.3	17.7 – 23.6	14.2 – 17.7	17.0 – 22.8	m/s
Air flow rates	117.6 – 176.0	133.4 – 179.1	107.2 – 133.7	128.5 – 172.1	m^3/min

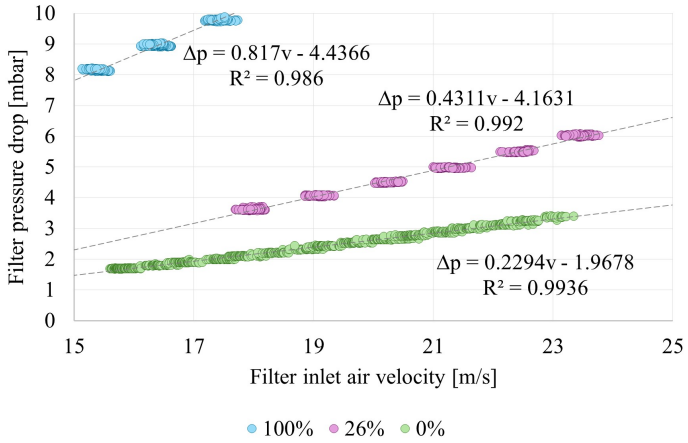

Figure 4.11: Plot of filter pressure drop against inlet velocity with 100%, 26% and 0% of clogging, and fitting with a linear model.

The generated model was then validated by reproducing an additional clogging condition, by mounting the clogged bag into the locations of Group 1 and Group 2, thus resulting in a 55% clogging condition; the generated model had an average error on the pressure drop value of 4.8% (approximately 0.3 mbar), and a maximum error of 9% (0.5 mbar) (Figure 4.13a). For a given clogging condition, therefore, the linear model of the characteristic curve in the form of $dp = m \cdot v + q$, can be estimated by solving Eq. 4.3 and Eq. 4.4 where c is the clogging level ranging from 0 (clean bags) to 1 (100% clogging). The trend in the filter pressure drop against filter inlet air velocity, calculated with the generated model, is reported in Figure 4.13b for different clogging levels, while the coefficients are reported in Table 4.6.

$$m = 0.5726 \cdot c + 0.2524 \tag{4.3}$$

$$q = 4.4135 \cdot c^{0.039} \tag{4.4}$$

Table 4.6: Coefficients of the characteristic filter curves under different clogging conditions.

Clogging level	**m**	**q**
100%	0.825	-4.414
55%	0.566	-4.311
26%	0.400	-4.186
0%	0.252	-1.967

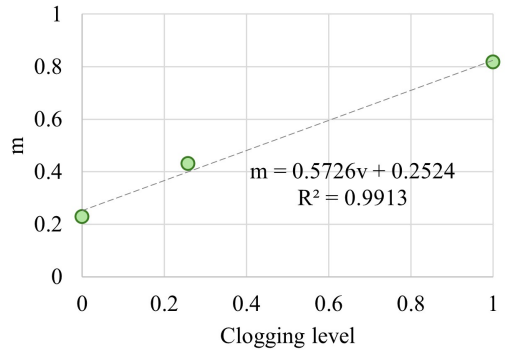

(a) Regression model for m.

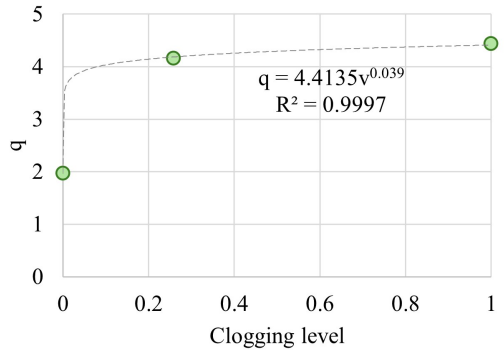

(b) Regression model for q.

Figure 4.12: Regression models for m and q coefficients of the characteristic curves of the filter under different clogging conditions.

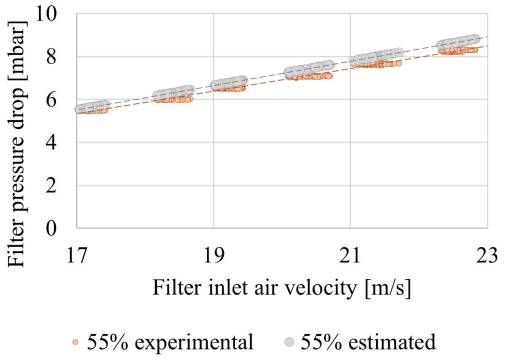

(a) Validation of the predictive model of filter pressure drop based on the clogging level.

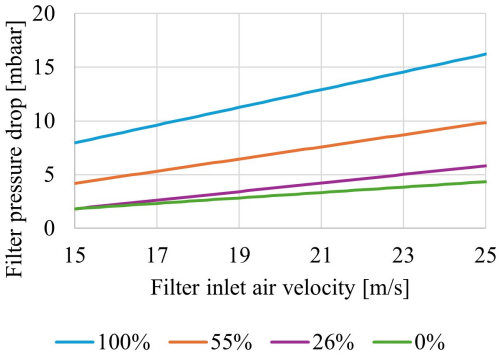

(b) Characteristic curves of the filter calculated with the generated model based on experimental data.

Figure 4.13: Pressure drop modelling under progressive clogging conditions.

Digital model

The digital model was used to assess velocity and pressure distribution across the plant (Figure 4.14).

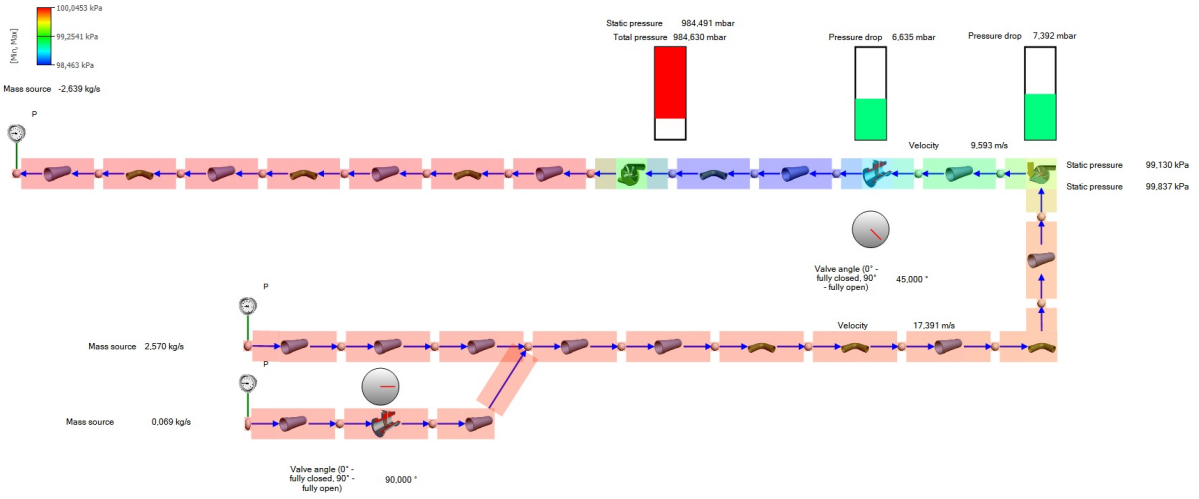

Figure 4.14: Pressure drop distribution along the plant computed with the digital model.

Digital model validation

In the following graphs, the comparison between the results of the digital model and the experimental data is reported (Figure 4.15). The pressure drops across the valve, as well as the pressure drop across the filter, are accurately predicted by the model. Regarding the depression at the suction section of the fan, there is a difference in the range of 0.65 mbar and 1.79 mbar between the experimental and simulated data.

This deviation, which increases as the valve opening changes, may be caused by the non-ideal installation of the sensor, which is located immediately after a bend and immediately before the fan. Turbulence, which increases at higher air velocity values, may therefore exist and significantly affect the measurement.

Regarding the air velocity in the main duct, the velocity measured by the sensor is always lower than that predicted by the model. To deeply explain this difference and identify which one of the two data is more reliable, a check can be made by analyzing the fan operating curve.

Within the considered range of total head (between 1400 and 1800 Pa), the fan provides a flow rate between 1.2 and 2.9 m3/s, which, at the sensor location, corresponds to velocity values between 10 and 20 m/s. It can therefore be concluded that the velocity predicted by the model is more realistic than that measured by the sensor, which, probably due to a velocity profile that is not fully developed or slightly disturbed by the presence of bends in the vicinity, constantly underestimates air velocity.

For all configurations tested, the digital model predicts an air flow rate in the secondary branch equal, on average, to 2.63% of the overall value. This result is confirmed by the experimental measurements ($2.6 \pm 0.045\%$).

In light of these considerations, even considering the fact that measurements for air flows always suffer a certain degree of uncertainty, the fact that experimental data and

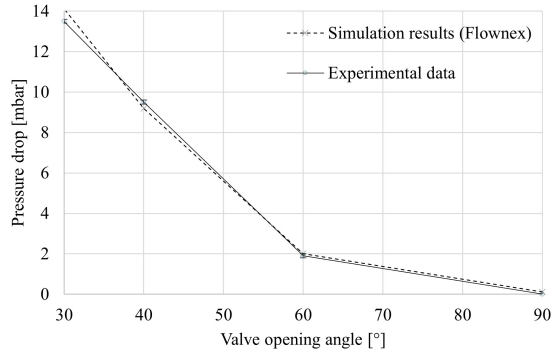

(a) Pressure drop across the valve.

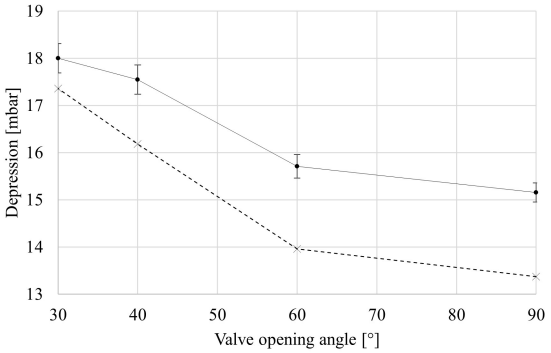

(b) Depression at the suction section of the fan.

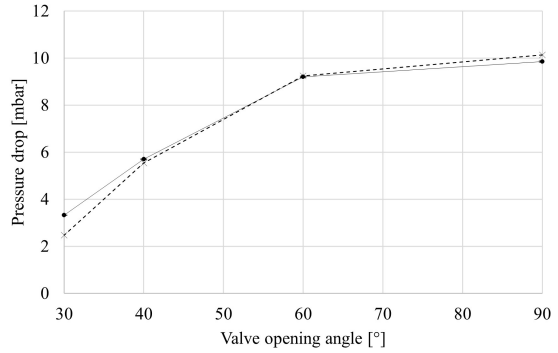

(c) Pressure drop across the filter.

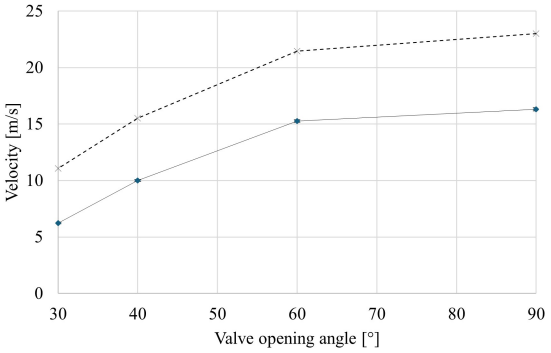

(d) Air velocity in the main duct.

Figure 4.15: Comparison between the results of the digital model and the experimental data.

simulated data show the same behavior and are also similar in terms of absolute value, it can be concluded that the model accurately reproduces the behavior of the real system. In a way, model-based assessments can even be considered more reliable, since they do not suffer the uncertainties that, naturally and inevitably, affect experimental measurements. As a conclusion, a digital model-based control can therefore be considered more reliable and more stable.

Finally, since the calculation times are very fast (less than 1 second), the developed model can be used for real-time evaluations.

Simulation of a real operating cycle

A working cycle was simulated using the virtual model, from clean filter conditions (0% clogging) to fully clogged conditions (100% clogging) (Figure 4.16a and Figure 4.16b). Within this range, the clogging evolution was discretized by considering three intermediate clogging conditions: 25%, 50% and 75%. Within this scenario, the filter characteristic curve is considered to be updated at discrete intervals, when the threshold clogging percentages are reached. Whenever the filter characteristic curve is updated, the

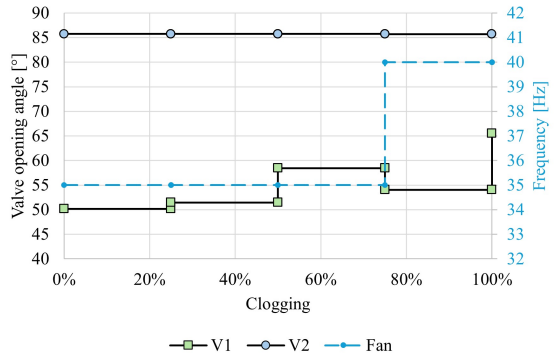

(a) Regulation of the valve opening angles and fan inverter frequency.

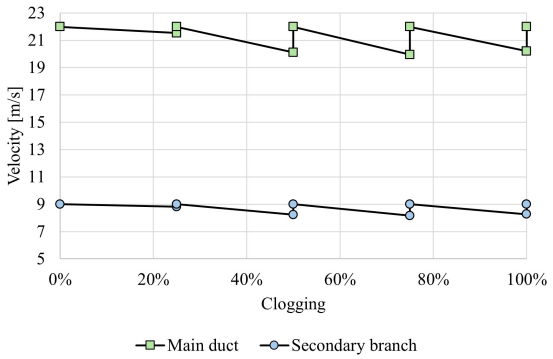

(b) The resulting velocities is the main and secondary ducts.

Figure 4.16: Simulation of the regulation during a production cycle.

system must be adjusted, both in terms of valve opening angles and fan supply frequency.

The set point values of velocity in the main duct and secondary branch were set, considering values that are generally adopted in industrial applications (22 m/s and 9 m/s, respectively). Three frequency values were considered, namely 35, 40 and 49 Hz. At the initial time, under clean bag conditions, the fan frequency was set at 35 Hz.

As the filter clogging increased, the digital model calculated the opening angles of valves V_1 and V_2, and the operating frequency of the fan, to keep the velocity values close to the set-point values. The calculation procedure for opening angle regulation is an iterative procedure with a maximum number of iterations of 25 and a convergence criterion of 0.001. In all configurations tested, the solution converged before reaching the maximum number of iterations.

Up to a clogging condition of 50%, the set-point values can be guaranteed by simply regulating (opening) the valves (V_1 in particular). As clogging of 75% is reached, at an operating frequency of 35Hz, the fan was no longer able to reach the desired set-point, even by fully opening the valves, so the operating frequency was increased to 40 Hz and, at the same time, an adjustment of the valves was also performed. As clogging further increased, V_1 had to be further opened to keep the flow rate unchanged (Figure 4.16a). In the case considered, the adjustments on V_2 are undetectable because, as the flow rate on the main duct is kept constant, the flow rate in the secondary branch also remains unchanged. A more marked adjustment would be observed when, for instance, the set-point values are changed. It is observed from Figure 4.16a that the velocity in both pipes progressively decreases as clogging increases and, when adjusting, the set-point value is restored. To keep the velocity values closer to the set-point values, a higher regulation frequency would be required.

Managerial Insights

Industry 4.0 technologies and paradigms can be of great support to industrial stakeholders in the pursuit of increasingly high-efficiency levels required by today's competitive market. To ensure efficiency, high quality, and optimized production, first of all, it is necessary to have deep knowledge of the system components and effective control over the plant. Indeed, the management of the system should be as much as possible informed and data-driven. In some industrial contexts, however, it is challenging to obtain useful and meaningful data to leverage for decision-making purposes.

The application discussed in this paper is one of these cases: the main issue affecting the optimal functioning of the plant, i.e., clogging of the filtering bags, can be only estimated indirectly through the value of pressure drop, and its effects on the plant and the distribution of flow rates across the system are generally unknown. Indeed, usually, there are no flow rate sensors on the different secondary branches of the plant, so it is not possible to directly assess whether the drawn flow rate is the one required for the correct system functioning. To overcome the complexities due to the nature of the specific application, the Digital Twin paradigm can be implemented in this context, supporting efficient control and management of the plant based on the availability of a digital model connected to the physical plant, that employs both historical and real-time sensor data.

First of all, it is necessary to characterize the critical component, in this case the filter, during its functioning, to generate its characteristic curves. This can be carried out in a few ways: it is possible to analyze historical data related to one life cycle of a set of bags, perform dedicated experimental campaigns like in the present study, or carry out simulation campaigns with a validated model replicating different clogging conditions. In the latter case, 3D Computational Fluid Dynamics (CFD) simulation can be adopted. This approach has the advantage of providing detailed insights into the functioning of the device but requires significant know-how, computational resources, and time. All three methods allow for the generation of characteristic curves of the filter under different clogging conditions, that can be then leveraged for the control of the whole plant.

With regards to the modeling of the whole system, 3D CFD simulation is not directly implementable: it would be highly impractical to simulate the whole distribution network, due to the resources and time required; besides, the added value of this approach would be extremely limited for the intended purpose.

1D CFD (lumped parameter CFD) simulation, on the other hand, appears to be the optimal approach in this case. By considering the overall behavior of the network components, it still reproduces the fluid dynamics inside the plant, allowing to quantify the flow rates in every branch of the system while at the same time neglecting the details not necessary for the application of interest. These details can however be included when needed by coupling 1D simulation of the entire system with 3D simulation of individual

components Moreover, as demonstrated by the results of the study, the calculated values can be more precise and reliable compared to the measures of real sensors installed improperly or in non-optimal positions.

The lumped parameter CFD simulations can be performed with both open source and commercial software, with the latter ones featuring more user-friendly interfaces and less steep learning curves. These simulation models "evolve" over time based on the measured sensor data, aiming to faithfully reproduce the actual plant under different operating and clogging conditions. The commercial software used in this study, i.e., Flownex, can communicate with the plant in two ways: it receives the data measured by the sensors and sends back to the actuators the details about the regulations to be performed to ensure the intended functioning of the plant. Indeed, in this case, the software is equipped with an optimization tool that allows to rapidly estimate the valve openings that would ensure the correct flow rate in the system based on the operating conditions.

The presented approach is not limited to the case under examination: the same general approach can be extended to several industrial applications and is particularly relevant in contexts where few data are directly available to assess and control the functioning of the plant.

Conclusions

In this study, a digital model, based on 1D lumped-parameters computational fluid dynamics, was developed for the simulation and monitoring of industrial air suction systems. These systems draw air at different locations within a production plant, to remove dust and other volatile substances. To ensure that such systems efficiently fulfill their function, the correct amount of air must be aspirated from each branch.

It is therefore necessary, on the one hand, that the fan supply the required total head, to aspire the required air flow rate. On the other hand, it is necessary to ensure that the flow rate is distributed correctly among the various branches of the system. This balancing should be done frequently since the operating conditions of such systems are constantly changing. For example, the continuous accumulation of solid particles on the filtration elements of the bag filter causes the pressure to drop and, consequently, the flow rate, to change continuously.

Such regulation is particularly complicated because these systems generally consist of a very high number of branches, since, typically, there are many suction locations within a production plant; adjustment made in one branch, therefore, impacts all other branches in the system, and vice versa. It is therefore necessary to perform an overall balancing of the system by adopting an iterative approach. Furthermore, this regulation is made even more difficult by the fact that it is difficult to monitor the actual operating

conditions at the different points because, in the presence of dust, traditional velocity measurement systems (pitot tubes and hot-wire anemometers), are difficult to apply. Thus, the regulation of these systems represents a very challenging issue that still appears to be poorly investigated in the scientific literature.

In this study, a digital model was developed by reproducing an industrial-scale pilot plant installed at the University of Parma, which was subsequently used for testing and validation. The developed model resulted in accurate and real-time calculation of the airflow rate aspirated by different branches of the system, considering the real filter clogging conditions and the fan operating curve, both obtained based on real-time measured data. The model can thus be considered a digital shadow of the system. This developed model proved to be much more reliable in regulating the system than data measured with sensors, which are very sensitive to the installation position as well as to the flow conditions.

The digital shadow, through an application program interface (API), can then communicate with the physical counterpart and act on some components of the plant, thus effectively becoming a digital twin. As an example, depending on the results obtained, to keep the flow rates aspirated by each branch within the desired limits, the digital twin can be used to adjust with a feed-forward logic both the operating frequency of the fan and the opening degree of all the valves of the system.

The proposed approach can be applied for reliable and immediate regulation of very complex suction systems without installing sensors on all the secondary branches: the only sensors required would be a flow rate sensor on the main duct and a differential pressure sensor at the ends of the filter. By optimizing air suction systems, the proposed approach could directly contribute to reducing the environmental footprint of industrial operations as well as improving safety and workplace conditions.

The study presents some limitations, mainly related to the simulation approach. First of all, the presence of the particles (flour, dust, etc,) is not accounted for in the model. While this assumption is acceptable when the concentration of particles in the flow is low, in applications where it becomes significant some adjustments to the model should be made. In addition, the 1D simulation model is based on the reproduction of the system with standardized components; in the case of non-standard components and devices, like the functioning of the filter under different clogging conditions in the present study, these should be characterized by the end-user. While this may represent a limitation of the presented approach, it is also a sign of its flexibility, as it is always possible to include in the model personalized components with the level of detail tuned to the intended use.

Future research activities may focus on the development of models for failures and operating anomalies identification, thus targeting system predictive maintenance which could significantly impact the industry by reducing downtime and operational costs. Fur-

ther exploration could also be done regarding the scalability of the model, its economic benefits, and environmental sustainability which could boost its applicability and relevance to industry.

4.1.2 RSM approach: Thermal treatment of viscous products with a tube-in-tube heat exchanger

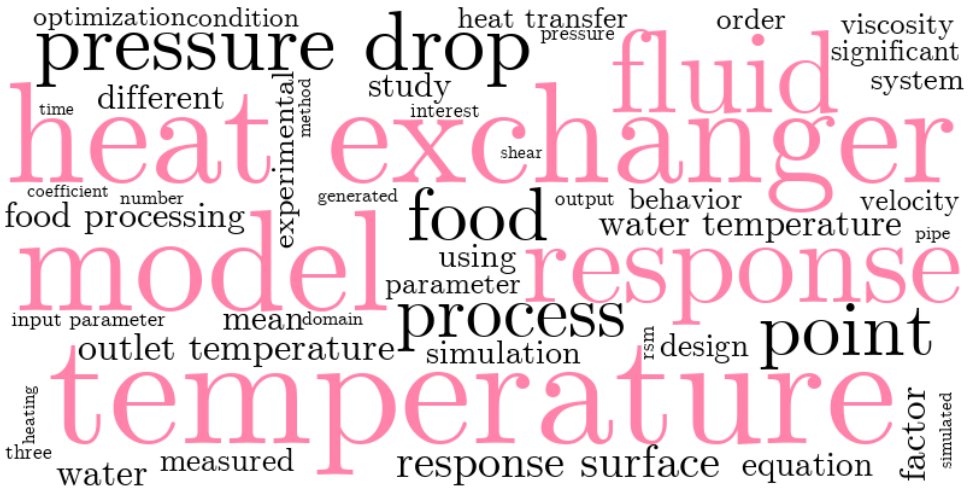

The research in this chapter has been included in the peer-reviewed article [92] *Lysova, N., Solari, F., and Vignali, G. (2022). Optimization of an indirect heating process for food fluids through the combined use of CFD and Response Surface Methodology. Food and Bioproducts Processing, 131, 60–76. https://doi.org/10.1016/j.fbp.2021.10.010.*

Abstract

The behavior of a counter-current tube-in-tube heat exchanger for fluid foods, was simulated under different operating conditions with a Computational Fluid Dynamics (CFD) parametric study. Three input parameters (product velocity vp,in, inlet product temperature Tp,in and inlet water temperature Tw,in) and two output parameters (outlet product temperature Tp,out and pressure drop across the heat exchanger Δp) were chosen. The results highlighted that the relative impact of vp,in on Δp was positive (93%), while higher Tp,in and Tw,in yielded lower pressure drop values (-3% and -4%, respectively). Tp,out was influenced positively by inlet product (62%) and water (22%) temperatures, and negatively by vp,in (-16%). A Response Surface (RS) was then generated and validated with a suitable experimental campaign. A good agreement was found between the simulated and the experimental results: Tp,out and Δp have been calculated with mean errors of 0.85 K and 628 Pa, respectively, thereby confirming the potential value of the RS as a Reduced Order Model, which could be used to develop a digital twin of the device. This modelling approach leads to a significant state-of-the-art improvement, allowing m the results of the CFD simulations to be ready-to-use, and granting deeper knowledge and finer control of the system.

Introduction

One of the biggest challenges in defining heat treatment for a food product is to guarantee food safety by preserving the organoleptic characteristics of the product itself as much as possible. In particular, in thermal treatment of fluid products the geometric features of the heating device and the process parameter settings are crucial to reaching the desired temperatures in the most rapid and uniform way. To achieve this goal, it is essential to have a deep understanding of the rheological behaviour of the product and its dependence on the process parameters, since it can strongly influence the flow patterns, thereby affecting system pressure drop and heat transfer performance [221]. Moreover, most of the fluid foods are non-Newtonian and their viscosity strongly depends not only on the temperature but also on the shear rate. The rheological behaviour of these fluids can be described through mathematical models, such as Power Law, Bingham, Herschel-Bulkley, Cross and Carreu models [3]. In industrial applications, the desired pasteurization or sterilization temperature of the fluid food can be reached using a heating medium or electric current. In the former case, the heat transfer can be either direct, with the water vapour being directly injected or infused into the product, or indirect, where the product does not come into contact with the heating medium, since they are separated by a metallic wall [222]. In the case of electric ohmic heating, heat is internally generated within the material being processed due to its natural electrical resistance, thanks to an electric current passing through it [223]. In the case of viscous food products, the flow regime inside conventional heat transfer devices is usually laminar, leading to a low heat transfer coefficient. In order to achieve a more efficient heat treatment, many enhancement methods have been developed, consisting in various techniques aiming to reduce the thermal resistance by increasing the effective heat transfer surface area or by generating turbulence [224]. However, most passive heat transfer enhancement techniques cannot be applied when the fluid is highly viscous or when it contains large solid pieces, because the inserts would damage the particles and the corrugation would make the heat exchanger surface difficult to clean. To avoid these problems and achieve an efficient thermal treatment, ohmic heating is sometimes preferred for high viscous and heat-sensitive fluids, low flow rates and food containing large particulates. For all other applications the conventional heating with heat exchangers is adopted because of its cost-effectiveness, flexibility, ease of use and management. Many studies on heat exchangers based on Computational Fluid Dynamics (CFD) can be found in the literature. The numerical simulations allow detailed insight into the flow patterns and distributions of the physical properties in every point of the simulated domain. Moreover, this approach allows the assessment of what-if scenarios by changing both geometric and operating parameters in order to optimize the overall performance of the process and reduce waste and costs, without the need for an expensive and time-consuming experimental campaign. CFD applications in the sector of food thermal

treatment include studies on pasteurization of fruit puree containing pieces [225], thermal treatment of a commercial juice inside a tube with a curved elbow [226], sterilization process, and subsequent nutrient degradation, of blackberry juice [5], and enhancement of the olive oil extraction process by thermal conditioning of olive paste [227]. Although the CFD is widely used, it appears to be extremely time-consuming and requires an intensive computational resource; for this reason, there have been few applications of CFD for real-time control of industrial processes to date. Nowadays, however, increasing attention is being paid to the design of digital twins of food processes, which allow monitoring and controlling the production systems [228, 229]. Response Surface Methodology (RSM) could be effectively adopted for the results of CFD simulations to be ready to use within an industrial control process [230]. Response surfaces can also be used to optimize the performances of devices and processes by modifying the values of input parameters of the CFD simulations and evaluating their effects on the output responses of interest. Applications of RSM in food industry include formulation procedures, drying and blanching processes, and production of microbial enzymes and other metabolites [231]. In [232] RSM has been used to evaluate the effects of different gums (Gellan, Xanthan and Quince seed gums) on the stability, probiotic viability and qualitative properties of a drinkable dairy product. In [233], RS methods have been applied to investigate the effects of the extraction conditions on the antioxidant activity and the functional properties of quince seed mucilage. In [234] the authors have adopted RSM to determine the combination of conditions and operations that allowed optimization of Gorgon nut processing. In [5] the authors have generated a Response Surface starting from a mathematical model of a double pipe heat exchanger in order to illustrate the dependence of microbiological and nutritional quality on product flow rate and heating medium temperature. In the case of heat exchangers, RSM has been used to optimize heat transfer coefficients and friction factors by modifying the geometric features of pipes and inserts and the operating parameters. Some authors (Han et al., 2015) modelled different pipe corrugation geometries, while others simulated twisted tape inserts by varying the features of sinusoidal tape [235], modifying cut geometries [236] or modelling new configurations of combined vortex generators [237]. Finally, [238] evaluated the performance of a coiled tube-in-tube heat exchanger with different coil configurations. In this study the thermal treatment of a non-Newtonian product flowing through a counter-current tube-in-tube heat exchanger [239] has been evaluated using a CFD simulation. The product tested was a mixture of 0.1 wt % Gellan gum powder [240] and water, whose rheological behavior was assessed at different temperatures and resulted to be pseudo-plastic. A parametric study was defined to characterize the device under different operating conditions. Product flow rate and inlet temperature, along with inlet water temperature, were defined as input parameters, while outlet product temperature and pressure drop across the heat exchanger were defined as output parameters. The simulation results were finally validated with a

suitable experimental campaign on the pilot plant. The Response Surface obtained from the parametric study aims to be used to develop a Digital Twin of the system, and to rapidly predict the behavior of the device as a function of the input operating conditions. This approach could improve the current state-of-the-art, since it would allow using the results of CFD simulations for advanced control of industrial plants.

Materials and methods

Equipment

Figure 4.17: Pilot plant set-up.

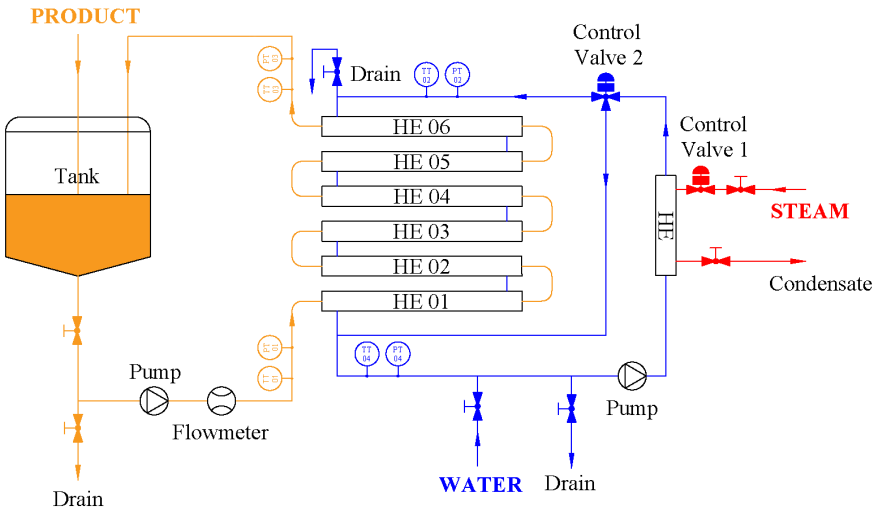

Figure 4.18: Schematic representation of the pilot plant configuration.

The pilot plant consists in a tubular heat exchanger for pre-heating of fluid foods that can process up to 2,500 l/h of viscous products containing particles with a size up to 10 mm. The plant is equipped with auxiliary systems that supply steam, electricity, water and compressed air to each machine. The system is controlled by a Programmable Logic Controller (PLC) and the process settings can be adjusted from the control panel by means of a Human-Machine Interface (Figure 4.17).

As stated before, this study focuses on modeling the heating of a fluid food achieved through a tube-in-tube heat exchanger where the product flows through the inner tube, while the water flows counter-current in the outer shell tube. The machine consists of six horizontal linear heating modules, each approximately 4 m long, arranged in a vertical configuration. The inner pipes of consecutive modules are connected with 180° bends, while the outer shell pipes are connected with vertical flange connections. Both inner and outer pipes are made of stainless steel.

The product, initially stored in a stainless steel storage tank equipped with a mixer, is moved by means of a twin-screw volumetric pump, whose flow rate is measured through a mass flowmeter and can be adjusted by regulating the frequency of the power supply with an inverter. The product enters the heat exchanger from the lower section, flows through the inner pipe and exits from the upper section, before being finally recirculated to the storage tank.

The water is moved by means of a centrifugal pump: it enters the tubular heat exchanger from the upper section and flows in the opposite direction to the product. The temperature of the water is raised by indirect contact with steam inside a dedicated heat exchanger.

Both steam and water flow rates can be regulated by means of two control valves (respectively Control Valve 1 and Control Valve 2 in Figure 4.18). Valve positions can either be adjusted automatically, by using a Proportional-Integral (PI) controller, so that product and water temperatures remain close to user-defined set-point values, or manually defined by setting a fixed opening percentage. Pressure and temperature of both product and water are evaluated through dedicated sensors at the inlet and outlet sections of the heat exchanger: temperatures are measured with resistance temperature detectors, while pressures are measured using pressure transmitters with flush diaphragm. The main data of the heat exchanger geometry are reported in Table 4.7. The main processing parameters of the pilot plant are summarized in Table 4.8.

Materials

The product used in this study is a mixture of 0.1 wt % Gellan gum powder and water. Gellan gum is a high molecular weight exopolysaccharide produced via aerobic fermentation by *Sphingomonas elodea*, commonly used as a thickening, stabilizing and emulsifying agent in food industry with European food additive E-number E418 . To prepare the mixture, 200 g of biopolymer were added to 200 l of water contained in the storage tank.

Table 4.7: Geometrical data of the heat exchanger

Description	**Value**	**Unit**
Number of heating modules	6	-
Total linear section length	3950	mm
Heating section length	3770	mm
Distance between water inlet and outlet axes	3600	mm
Inner pipe diameter	39.8	mm
Inner pipe bends r/D	1.5	-
Outer pipe diameter	73.2	mm
Inner and outer pipe thickness	1.5	mm
Water pipe diameter	57.1	mm

Table 4.8: Main processing parameters of the pilot plant

		Unit	**Value**	
			min	**max**
Product pump	*Twin-screw pump*			
	Operating pressure	bar	0	5
	Flow rate	m^3/h	0	5
	Viscosity	Pa s	0	0.5
	Particle size	mm	0	10
Water pump	*Centrifugal pump*			
	Flow rate	m^3/h	0	12
	Prevalence	m	25.5	27.5
	Product density	kg/m^3	1000	
	Product viscosity	Pa s	0.001	

The content of the tank was continuously agitated by means of a mixer and the product pump was running to incorporate the powder gradually and homogeneously.

Density, thermal conductivity and specific heat were assumed to be similar to those of water, while viscosity was determined thanks to experimental measurements. In food processing applications involving pipe flow, shear rate values generally range from 100 to 103 s-1 [3], with the lowest values at the center of the pipe and the maximum values at the walls. In this study the rheological characterization was performed using a concentric cylinder geometry (Couette cell) mounted on an ARES rheometer (Ta Instruments, New Castle, DE, USA). The dimensions of the geometry were 34 mm cup diameter, 32 mm bob diameter, and 33 mm height. Eight ml of the product were transferred to the rheometer cup using a graduate cylinder and a sample was equilibrated for 2 min before being analyzed [241]. The measurements were conducted under isothermal conditions, evaluating the shear stress at three temperatures (293.15 K, 313.15 K and 333.15 K), with shear rates ranging from 10 to 300 s-1, with 30 points in logarithmic distribution (Figures 4.19a and 4.19b.

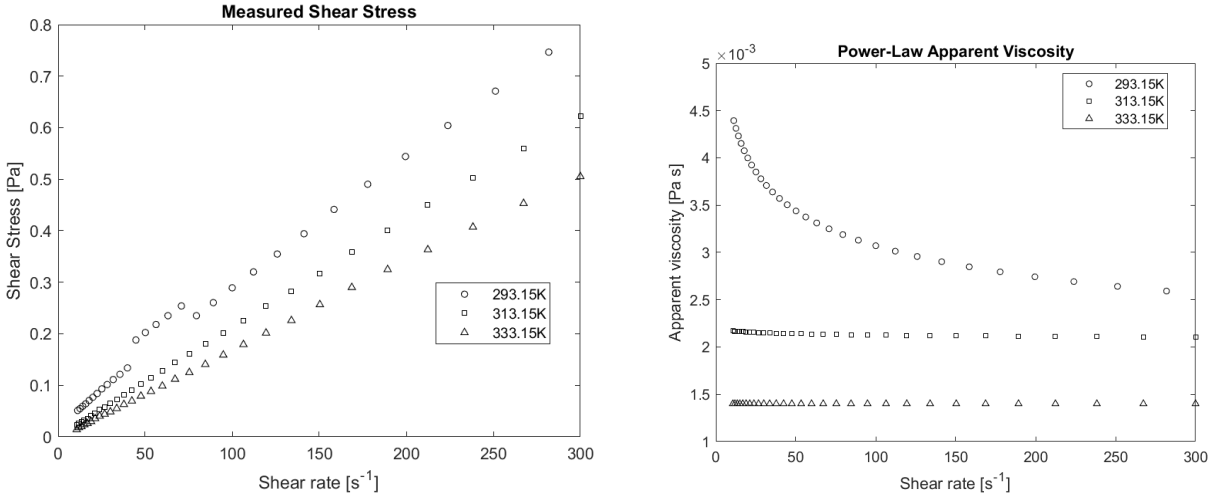

(a) Experimentally measured shear stress at three different temperatures.

(b) Apparent viscosity at the three evaluated temperatures.

Figure 4.19: Rheological characterization of the product.

It can be observed that, especially at low temperatures, the fluid had a slightly non-Newtonian, shear thinning behavior, which can be described by means of a Power-law model (eq. 4.5), where τ is the shear stress, $\dot{\gamma}$ is the shear rate, and K and n are consistency and flow behavior indexes, respectively. Apparent viscosity η of the fluid can be calculated from the shear stress, by means of eq.4.6.

$$\tau = K\dot{\gamma}^n \tag{4.5}$$

$$\eta = \frac{\tau}{\dot{\gamma}} = K\dot{\gamma}^{n-1} \tag{4.6}$$

A logarithmic transformation of eq. 4.5 was performed to evaluate K and n(eq. 4.7). Eq. 4.7 represents a linear model describing a straight line in the form of eq. 4.8, where:

$$\ln(\tau) = \ln(K) + n\ln(\dot{\gamma}) \tag{4.7}$$

$$y = a + bx \tag{4.8}$$

$$y = \ln(\tau) \tag{4.9}$$

$$a = \ln(K) \tag{4.10}$$

$$b = n \tag{4.11}$$

Parameters and are obtained by means of a linear regression aiming to define the least squares regression line by solving the following system of normal equations (eq. 4.12 and 4.13):

$$\sum_i y_i = aN_m + b\sum_i x_i \tag{4.12}$$

$$\sum_i x_i y_i = a\sum_i x_i + b\sum_i x_i^2 \tag{4.13}$$

where N_m is the number of experimental measurements, y_i values are the natural logarithms of the measured shear stress values, and x_i values are log-transformed values of shear rate (eq. 4.9). Once the system of equations is solved for a and b, consistency index K can be calculated from eq. 4.10 with eq. 4.14, while the flow behavior index n is equal to b (eq. 4.11).

$$K = \exp(a) \tag{4.14}$$

The same procedure was used to calculate K and n coefficients at all temperatures considered, resulting in values reported in Table 4.9.

Table 4.9: Calculated Power-law coefficients

Term	**Unit**	**293.15K**	**313.15K**	**333.15K**
K	Pa s^n	0.0065	0.0022	0.0014
n	-	0.84	0.99	1.00

Results show that the product's behavior varies with the temperature: it has a non-Newtonian behavior at low temperatures, while at higher temperatures it behaves like a Newtonian fluid with a viscosity value very close to that of water. Since the temperature values change significantly within the domain, it is important to consider the temperature dependence of apparent viscosity. The influence of temperature was taken into account using the Arrhenius relationship (eq. 4.15), where η_α and T_α are reference values, E_a is the energy of activation for viscosity, and R is the universal gas constant. The magnitude of $\frac{E_a}{R}$ was evaluated considering apparent viscosity values at a shear rate of $100s^{-1}$ with eq. 4.16.

$$\frac{\eta}{\eta_\alpha} = \exp\left(\frac{E_\alpha}{R}\left(\frac{1}{T} - \frac{1}{T_\alpha}\right)\right) \tag{4.15}$$

$$\frac{E_\alpha}{R} = \frac{\ln\left(\frac{\eta}{\eta_\alpha}\right)}{\frac{1}{T} - \frac{1}{T_\alpha}} \tag{4.16}$$

$$R^2 = 1 - \frac{\sum_i (y_i - \hat{y}_i)^2}{\sum_i (y_i - \bar{y})^2} \tag{4.17}$$

$$\hat{y}_i = \ln K + n \ln \dot{\gamma} + \frac{E_\alpha}{R}\left(\frac{1}{T} - \frac{1}{T_\alpha}\right) \tag{4.18}$$

The accuracy of the model was assessed by means of the coefficient of determination R^2, calculated with eq. 4.17, where y_i are the log-transformed values of shear stress, $\bar{y}$ is the mean of y_i values, and $\hat{y}_i$ are the predicted values, calculated with eq. 4.18. R^2 coefficients were calculated by considering different reference temperatures (Table 4), to determine the combination of temperature values that would grant the best accuracy.

The reference temperature chosen in this study was 313.15 K, while the temperature of 293.15 K is used to calculate the value of $\frac{E_a}{R}$. The calculated model fits the experimental data well, as shown in the plots in Figure 4.20.

The temperature-dependent shear stress, calculated on the basis of K and n coefficients, fits the measured data as illustrated in Figure 4.21. The model appears to be more accurate at higher temperatures ($T \geq 313.15$ K).

For the CFD simulations, water and steel too were characterized from a thermodynamic point of view. Materials properties are summarized in Table 5.

Table 4.10: Various R^2 values at different temperatures

T_α **[K]**	313.15	313.15	293.15	293.15	333.15	333.15
T **[K]**	293.15	333.15	313.15	333.15	293.15	313.15
E_α/R **[K]**	1703	1197	1703	1466	1466	1197
R^2 **at 293.15K**	0.9472	0.8999	0.9924	0.9924	0.9113	0.8518
R^2 **at 313.15K**	0.9999	0.9999	0.9682	0.9565	0.9973	0.9962
R^2 **at 333.15K**	0.9932	0.9955	0.9602	0.9472	0.9988	0.9988
Mean R^2	0.9801	0.9651	0.9736	0.9654	0.9691	0.9489

Table 4.11: Properties of water, stainless steel, and product

	Viscous product	**Water**	**Stainless Steel**
Thermodynamic state	Fluid	Fluid	Solid
Density	998.2 kg/m^3	998.2 kg/m^3	8030 kg/m^3
Specific Heat	4182 J/kg K	4182 J/kg K	502 J/kg K
Thermal Conductivity	0.6 W/m K	0.6 W/m K	16.3 W/m K
Dynamic Viscosity	-	0.001 Pa s	-
Consistency index (K)	0.0022 Pa s^n	-	-
Flow behavior index (n)	0.99	-	-
Energy of activation	14.2 kJ/mol	-	-
Reference temperature	313.15 K	-	-

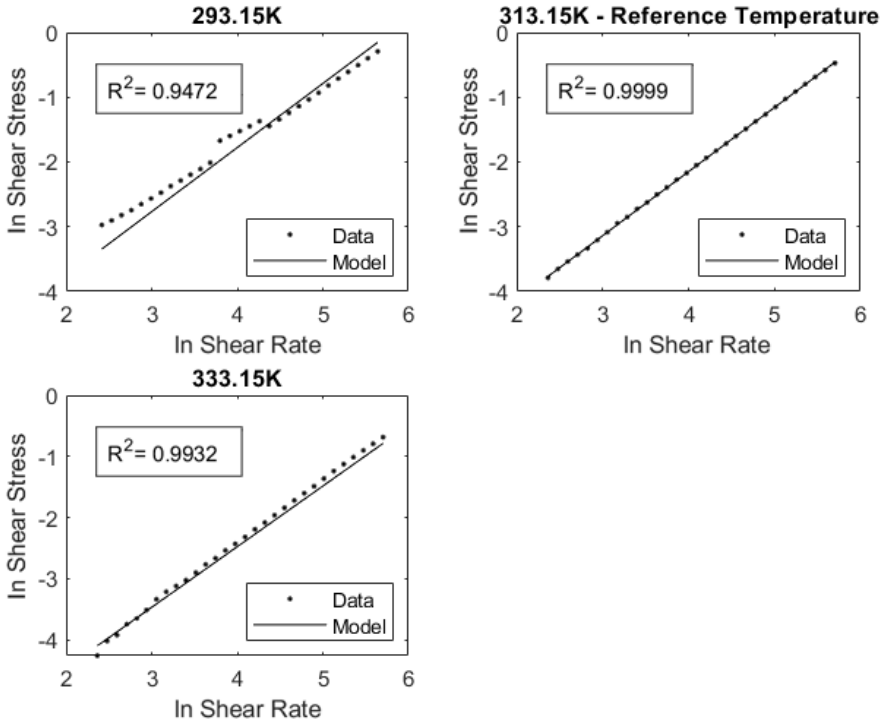

Figure 4.20: Log-transformed data, linear model and calculated coefficients of determination R^2.

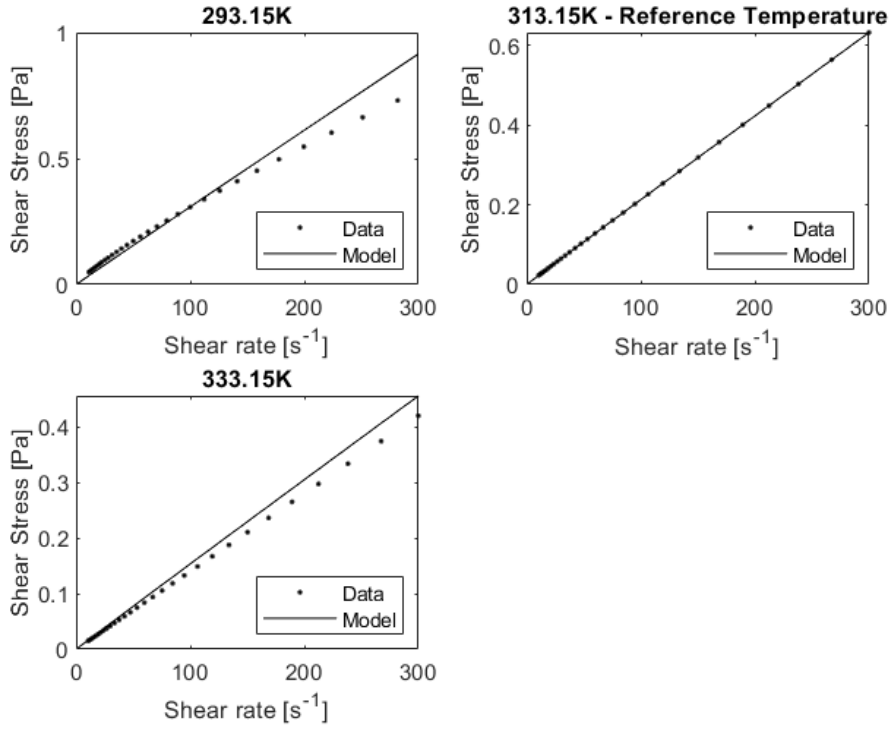

Figure 4.21: Experimental data and power-law temperature-dependent model.

Flow patterns

The flow regimes of the two fluids can be estimated by using the Reynolds number value. In the case of water, which is a Newtonian fluid, Reynolds number is calculated with eq. 4.19, where where ρ is the fluid density, v is the velocity, D is the hydraulic diameter of the pipe, and μ is the dynamic viscosity of the fluid. The flow pattern of the shear-thinning product can be evaluated by means of the generalized Reynolds number equation, proposed by Metzner and Reed [242] (eq. 4.20), where w is the mean velocity of the viscous product and R is the pipe radius.

$$Re = \frac{\rho u D}{\mu} \tag{4.19}$$

$$Re_{MR} = \frac{8\rho}{K} w^{2-n} \left(\frac{n}{3n+1} \right)^n R^n \tag{4.20}$$

For practical purposes, the flow pattern inside a pipe can be estimated on the basis of three ranges of Reynolds number: at Re<2000 the flow is laminar and has a parabolic profile; when Re ranges between 2,000 and 4,000 the flow is in an unstable transition region and can be either laminar or turbulent, with the critical Re_{CR} at which the transition begins to be influenced by fluid properties and geometric features of the pipe; at Re>4000 turbulent flow is dominant and the flow profile becomes fairly flat [243].

As for the processing parameters of the pilot plant, the Reynolds numbers calculated for the two fluids at different flow rates are reported in Table 4.12 (**mean water velocity on the annular area of the outer pipe*). It appears that the flow is turbulent for both product and water.

Table 4.12: Pump flow rate, velocity, and Reynolds numbers for water and product

	Pump flow rate [m^3/h]	**Uniform velocity on the section** [m/s]	**Reynolds number Re**	**Generalized Reynolds number** Re_{MR}
Water	12	1.16*	18519	-
Product	1	0.22	-	4164
	2	0.44	-	8386
	3	0.66	-	12630
	4	0.88	-	16888
	5	1.11	-	21157

Numerical simulation

Methods for solving heat transfer problems for non-Newtonian fluids in turbulent conditions can be found in the literature [244]. However, these methods are effectively applicable only if the boundary conditions and the rheological characteristics of the fluid are constant in space and time.

In our case, the rheological characteristics of the product resulted to be extremely sensitive to temperature, which, for both fluids considered, changes from point to point

across the heat exchanger. In this case, therefore, a numerical simulation can better reproduce the real situation.

Geometry and mesh

In order to perform the numerical simulation of the thermal treatment, a 3D model of the heat exchanger was generated with ANSYS SpaceClaim [70]. The model reproduced the entire machine's geometry and consisted of two distinct bodies: one for the inner fluid domain (product) and one for the outer fluid domain (water). The contribution of the solid domain (stainless steel pipe) was considered as the conductive resistance of a thin stainless steel wall at the interface between the two fluid domains. The following assumptions were made:

- In order to have fully developed flow profiles at the inlet areas of the heat exchanger, additional linear sections were modelled for inner pipes;
- The inner fluid domain (product) was split into several sections in order to set different boundary conditions for the heating zones and the bends;
- The outer fluid domain (water) was divided into linear sections and T-junction sections in order to facilitate the generation of the computational grid;
- A shared topology option was set for both inner and outer fluid domains in order to obtain matching grids on consecutive sections of the bodies.

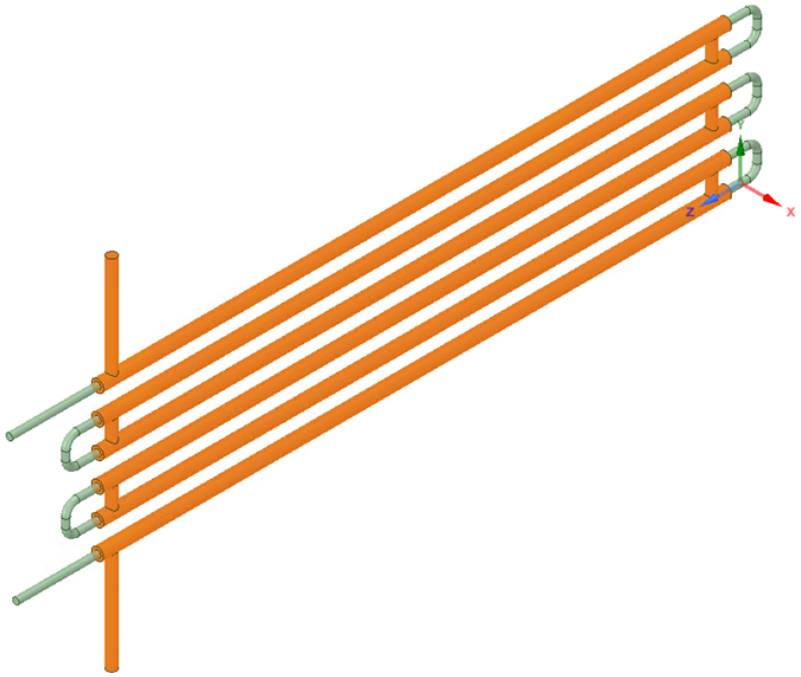

Figure 4.22: Geometry of the heat exchanger, with two separate bodies for the inner and outer pipes.

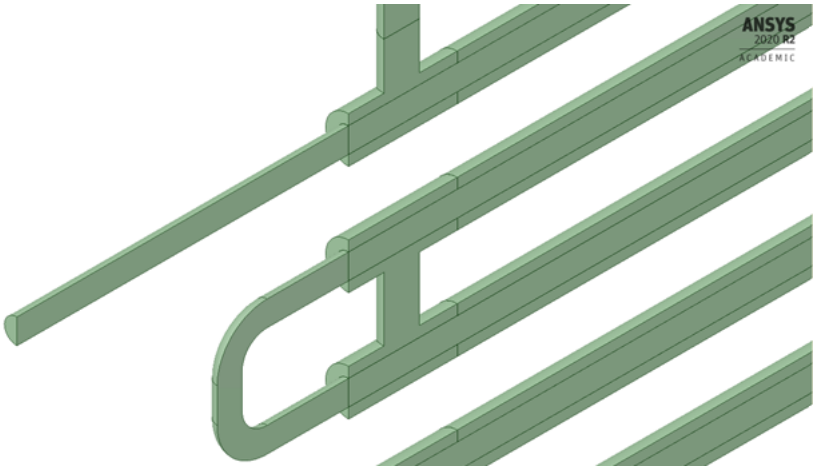

Figure 4.23: Heat exchanger geometry cut in half to reduce the computational cost of the simulations.

To reduce the computational cost of the simulation, the thermal treatment inside the heat exchanger was considered to be overall symmetrical, thereby allowing modelling only half of the device geometry.

The grid generation for the two fluid domains was performed with ANSYS Meshing in order to define a finite number of control volumes. A structured hexahedral mesh was created for the fluid product domain, while in the water domain a structured mesh was created in the linear sections, and an unstructured mesh was used within the T-junctions.

Special attention was paid to the near-wall regions in order to obtain accurate information about the heat transfer process. Ten inflation layers, with a first layer thickness of

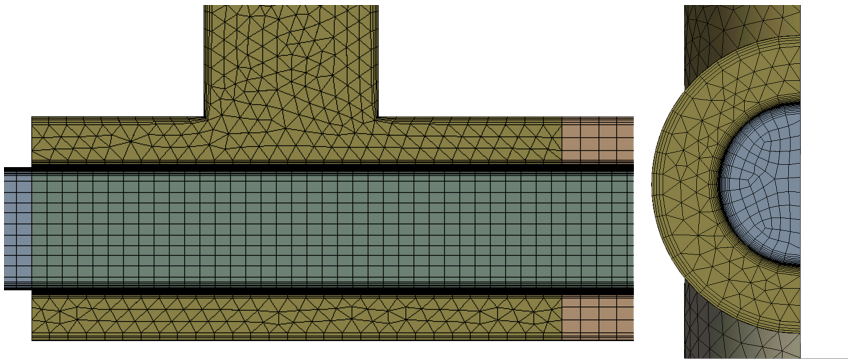

Figure 4.24: Details of the selected mesh.

10-4 m and 1.2 growth rate, were generated at each side of the interface for both product and water domains.

A grid sensitivity analysis was carried out to examine the influence of the mesh size on the simulation results. Five different grids with an increasing number of elements was tested, and the outlet product temperature and pressure drop values calculated were then compared. The differences in the results obtained, especially the outlet temperatures, were very small, so the grid for the study was determined on the basis of the pressure drop values and the computation time (Table 4.13). Mesh 3 resulted to be the best choice since a higher number of elements provided no significant improvement in the results, while strongly increasing computation time.

Table 4.13: Comparison of simulation results using different grids

Grid	**Element Size** [mm]	**Number of Elements** [mil]	**Computation Time** [h]	**Pressure Drop** [mbar]
1	7	1.5	3	150.02
2	6	2.2	5.5	149.84
3	5	3.5	7	149.71
4	4	4.6	10	149.70
5	3	7.8	17	149.69

Governing equations

In order to model the thermal treatment inside the heat exchanger, ANSYS Fluent 2020 R2 was used to solve the governing equations for the defined fluid domains [71]. According to ANSYS Fluent Theory Guide [34], the numerically solved Navier-Stokes equations are defined as follows. The continuity equation for mass conservation is presented in eq.4.21, where t is time, ρ is the density of the fluid, and $\vec{v}$ is the overall velocity vector. Conservation of momentum is described by eq.4.22, where p is the static pressure, $\rho\vec{g}$ is the gravitational body force, and $\vec{F}$ vector considers external body forces. The stress tensor $\overline{\overline{\tau}}$ is defined in eq.4.23, where μ is the molecular viscosity and I is the unit tensor. Since the problem includes heat transfer, the energy equation is solved and defined as expressed in eq.4.24, where the total energy E is defined as in eq.4.25, k is the thermal conductivity of the material and h is the enthalpy.

$$\frac{\partial \rho}{\partial t} + \nabla(\rho\vec{v}) = 0 \tag{4.21}$$

$$\frac{\partial}{\partial t}(\rho\vec{v}) + \nabla(\rho\vec{v}\vec{v}) = -\nabla p + \nabla(\overline{\overline{\tau}}) + \rho\vec{g} + \vec{F} \tag{4.22}$$

$$\overline{\overline{\tau}} = \mu\left[\left(\nabla\vec{v} + \nabla\vec{v}^{T}\right) - \frac{2}{3}\nabla(\vec{v}I)\right] \tag{4.23}$$

$$\frac{\partial}{\partial t}(\rho E) + \nabla(\vec{v}(\rho E + p)) = \nabla(k\nabla T) - \nabla\cdot(\overline{\overline{\tau}}\vec{v}) \tag{4.24}$$

$$E = h - \frac{p}{\rho} + \frac{v^2}{2} \tag{4.25}$$

Boundary conditions

The simulated three-dimensional flow was incompressible, so a pressure-based solver was used for the study, and the gravity option enabled. Uniform axial velocity and temperature values were defined on the inlet areas for both fluid domains. The outlet areas were defined as pressure outlets, with gauge pressure set to zero in order to calculate the pressure drop inside the heat exchanger. A symmetry boundary condition was applied to all the surfaces lying in the plane of symmetry. A no-slip condition was set at the walls. The interface between the two fluid domains was defined as a coupled two-sided wall made of steel, with wall thickness equal to 2 mm. The walls in contact with the external environment were considered to be adiabatic. The simulations were carried out in steady-state conditions and the convergence criterion was set at 10-6. A coupled scheme was used for pressure-velocity coupling during the numerical solution of the governing equations. The gradients were computed according to the Least Squares Cell-Based method. PRESTO! scheme was used to interpolate pressure since it is suitable for flows

in curved domains. A second-order upwind discretization scheme was used for energy and turbulent flow equations, while a first-order upwind was used for the momentum equation to improve the convergence of the solution. In addition, Shear-Stress Transport $SSTk-\omega$ turbulence model was used to solve the turbulent flow numerically. $SSTk-\omega$ model is a linear combination of $k-\epsilon$ and $k-\omega$ models activated for the free stream regions and near-wall zones, respectively, in order to overcome the limits of both models [144].

Parametric study

A parametric study was defined as shown in Table 4.14 to model the behavior of the heat exchanger under different operating conditions. Product flow rate, and inlet product and water temperatures were selected as input parameters. Outlet product temperature and pressure drop through the heat exchanger were chosen as output parameters. The results of the parametric study, calculated in a finite number of Design Points (DPs), were used to generate a Response Surface to estimate the values of the output variables (responses) in all the points of the simulated domain.

Table 4.14: Input and output parameters of the parametric study

Parameter	**Name**	**Variable**	**Description**	**Unit**
Input	P1	x_1	Inlet product temperature	K
Input	P2	x_2	Product velocity on the inlet area	m/s
Input	P3	x_3	Inlet water temperature	K
Output	P4	y_1	Outlet product temperature	K
Output	P5	y_2	Pressure drop	Pa

Response surface generation

Response Surface Methodology (RSM) is a collection of mathematical and statistical techniques used to model and analyze problems in which a dependent response of interest (y_k) is a function of a set of independent explanatory factors (x_i) [245]. In this study there are three independent factors (x_1, x_2, x_3), so a generic estimated response could be expressed with eq.4.26, where ϵ is the error observed in the response y_k. The graphical three-dimensional representation of the response, plotted against two independent factors of choice, is called "Response Surface".

The simulated *DPs* where the responses should be numerically evaluated were defined by means of a proper Design of Experiments (DOE). The first step was the definition of the experimental domain, performed by choosing the range for each input factor as summarized in Table 4.15. Five levels of coded factors cf were defined in a dimensionless range from $-\alpha$ to α, and the actual values of the input parameters were then calculated using eq.4.27. Coded and actual input factor values are reported in Table 4.16. α value is equal to 1.23 and was calculated by minimizing a measure of non-orthogonality, known as the Variance Inflation Factor (VIF) [34].

$$y_k = f(x_1, x_2, x_3) + \epsilon \tag{4.26}$$

$$x_i = \frac{cf(x_{i,1} - x_{i,-1})}{2} + \bar{x}_l \tag{4.27}$$

$$N_r = 2^f + 2f + c_p \tag{4.28}$$

Table 4.15: Ranges of the three input factors that define the experimental domain

Factors		**Natural variables**	
Name	**Unit**	**min**	**max**
x_1	K	293.15	333.15
x_2	m/s	0.221	1.105
x_3	K	323.15	373.15

Table 4.16: Five-level coded input variables

Factors	**Coded factors**				
Name	**-α**	**-1**	**0**	**1**	α
x_1	293.15	296.90	313.15	329.41	333.15
x_2	0.22	0.30	0.66	1.02	1.11
x_3	323.15	327.82	348.15	368.48	373.15

The Central Composite Design model (CCD) was selected to define the experimental design for this study since it required fewer simulation runs compared to the Full Factorial Design (FFD) and provided higher accuracy at the extremes of the experimental domain

Table 4.17: Design points of the parametric study based on face-centered CCD model

Design Point	**Input factors**			**Point type**
	x_1	x_2	x_3	
1	0	0	0	Central point
2	-α	0	0	Axial points
3	α	0	0	
4	0	-α	0	
5	0	α	0	
6	0	0	-α	
7	0	0	α	
8	-1	-1	-1	Factorial points
9	1	-1	-1	
10	-1	1	-1	
11	1	1	-1	
12	-1	-1	1	
13	1	-1	1	
14	-1	1	1	
15	1	1	1	

compared to the Box-Behnken Design (BBD). CCD is a second-order polynomial model developed by Box and Wilson [246], consisting in three-point types: a centre point, two-level factorial points, and axial points at a distance α from the central point. Factorial points estimate linear effects and two-factor interactions, while axial and central points evaluate quadratic effects. The number of experimental runs N_r can be estimated with eq. 4.28, where f is the number of factors and c_p is the central point. The experimental matrix, with the definition of the simulated design points in terms of coded factors, is reported in Table 4.17. The experimental 3D domain, defined by the evaluated design points, is shown in Figure 4.25.

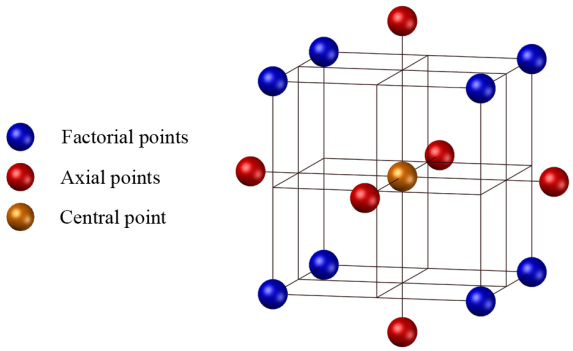

Figure 4.25: Three factor Central Composite Design (CCD) model with five-level variables.

Experimental method

An experimental campaign was conducted on the pilot plant to validate the simulated results. A set-point value for water temperature was defined in the dedicated control panel section after the product was prepared. Automatic regulation of the opening percentage of Control Valve 1 was enabled to raise water temperature to the set-point value and then maintain it stable at that level during the treatment. The opening percentage of Control Valve 2 was set manually at 100% to allow the whole volume of water to flow in the outer pipes of the heat exchanger.

Since the product was continuously recirculated, its temperature at the inlet section of the heat exchanger changed constantly under the influence of the water temperature (see Figure 4.18). Therefore, during the experimental validation, the only manually-set parameter was product flow rate, which was changed by adjusting the frequency of the power supply of the pump with an inverter. Different values were tested to verify the reliability of the model under different operating conditions. Phases with constant flow rate, and with sudden and significant changes in flow rate were tested to verify whether the model's responses followed those of the real system, and to assess the extent of any deviations and delays.

Results and discussion

Simulation results

The simulation results for the outputs of interest, evaluated at operating conditions defined by the DPs examined, are summarized in Table 4.18. Contours of temperature, pressure, shear rate and viscosity, with input parameter values corresponding to the central point of the experimental domain (DP1) are presented in the following figures.

Table 4.18: Simulation results for the output parameters of interest

	Input parameters			**Output parameters**	
DP	**P1**	**P2**	**P3**	**P4**	**P5**
	$v_{p,in}$ [m s^{-1}]	$T_{p,in}$ [K]	$T_{w,in}$ [K]	Δp [Pa]	$T_{p,out}$ [K]
1	0.66	313.15	348.15	13287.52	337.58
2	0.22	313.15	348.15	9272.69	342.91
3	1.11	313.15	348.15	20504.08	333.68
4	0.66	293.15	348.15	13435.42	330.33
5	0.66	333.15	348.15	13160.27	345.17
6	0.66	313.15	323.15	13521.71	319.84
7	0.66	313.15	373.15	13086.98	356.48
8	0.66	313.15	327.82	9881.18	320.75
9	1.02	296.89	327.82	19557.34	314.66
10	0.30	329.41	327.82	9801.65	328.16
11	1.02	329.41	327.82	18943.92	328.45
12	0.30	296.89	368.48	9728.24	356.21
13	1.02	296.89	368.48	18901.04	340.21
14	0.30	329.41	368.48	9679.40	328.53
15	1.02	329.41	368.48	18445.31	353.90

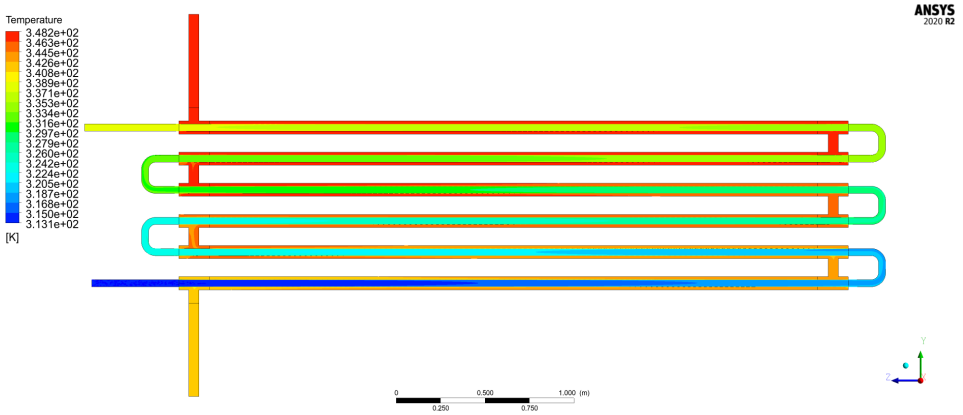

Figure 4.26: Temperature of product and water on the symmetry plane of the heat exchanger

Response surface

A Response Surface was generated starting from the results of the CFD simulations

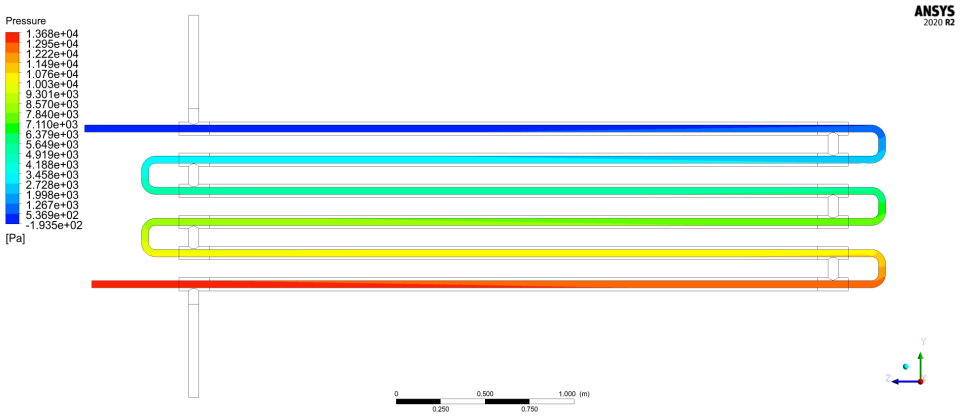

Figure 4.27: Profile of pressure across the heat exchanger.

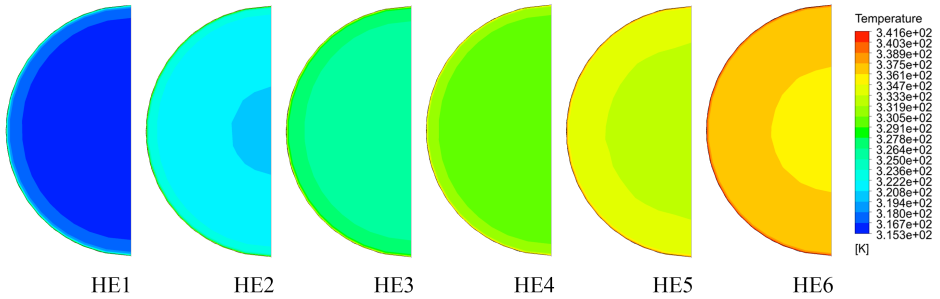

Figure 4.28: Product temperature profiles at the central transversal section of each Heat Exchanger (HE) module.

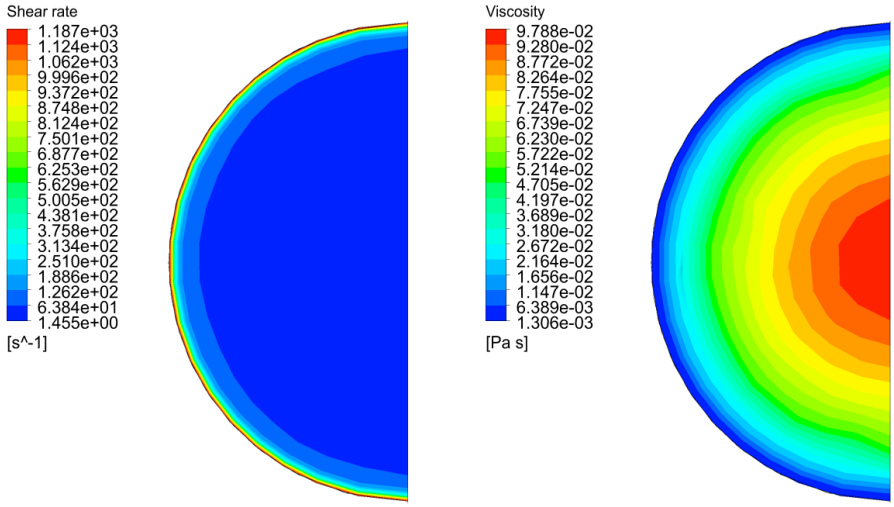

Figure 4.29: Contours of shear rate (left) and shear rate dependent viscosity (right) on a transversal section of the inner pipe.

reported in Table 4.18. RS generation, with relative Analysis of Variance (ANOVA), was carried out in the statistical analysis software Design Expert v.13. A quadratic model was used to fit the CFD data. As defined in eq.4.5, and considering $x_1 = v_{p,in}$, $x_2 = Tp, in$, $x_3 = Tw, in$, the equation for a generic response can be expressed as in eq. 4.29, where β_{ij} are the factor coefficients, and ϵ, as stated before, is the expected error. In the current study the responses of interest were the pressure drop ($y_1 = \Delta p$) and the outlet product temperature ($y_2 = T_{p,out}$). The ANOVA test was conducted to determine whether the model and its terms were significant for the evaluated responses.

$$y_k = \beta_0 + \beta_1 \cdot v_{p,in} + \beta_2 \cdot T_{p,in} + \beta_3 \cdot T_{w,in} + \beta_{12} \cdot v_{p,in} \cdot T_{p,in} + \beta_{13} \cdot v_{p,in} \cdot T_{w,in} + \\ + \beta_{23} \cdot T_{p,in} \cdot T_{w,in} + \beta_{11} \cdot v_{p,in}^2 + \beta_{22} \cdot T_{p,in}^2 + \beta_{33} \cdot T_{w,in}^2 + \epsilon \tag{4.29}$$

A term is considered to be significant if its *p-value* is less than 0.05. For both estimated responses, the generated quadratic model and all of its terms are significant, except for the product of the two inlet temperatures and their square values. The R^2 coefficients of determination values are very close to 1 for both responses ($R^2_{\Delta p}$=0.9999, $R^2_{T_{p,out}}$=0.9998), meaning that the quadratic model predicts the simulated values very well. The final equations for outlet product temperature and pressure drop can be expressed in terms of actual input parameters in their original units, using eq.4.29 and the calculated quadratic model coefficients summarized in Table 4.20. These equations can be used to estimate the system responses for given levels of input factors.

Table 4.19: ANOVA results for the quadratic model — p-values calculated for pressure drop and outlet product temperature responses

	Δp response		T_{out} response	
Source	**p-value**	**significant**	**p-value**	**significant**
Model	< 0.0001	yes	< 0.0001	yes
v_{in}	< 0.0001	yes	< 0.0001	yes
$T_{\text{p,in}}$	< 0.0001	yes	< 0.0001	yes
$T_{\text{w,in}}$	< 0.0001	yes	< 0.0001	yes
$v_{\text{in}} \cdot T_{\text{p,in}}$	0.0003	yes	< 0.0001	yes
$v_{\text{in}} \cdot T_{\text{w,in}}$	0.0004	yes	< 0.0001	yes
$T_{\text{p,in}} \cdot T_{\text{w,in}}$	0.1354	no	0.24	no
v_{in}^2	< 0.0001	yes	0.028	yes
$T_{\text{p,in}}^2$	0.6476	no	0.087	no
$T_{\text{w,in}}^2$	0.499	no	0.057	no

A Local Sensitivity (LS) analysis was performed to understand the relative impact that each input factor has on the estimated response. For a single input parameter (x_i), response (R) sensitivity is calculated with eq.4.30, where $R(max) - R(min)$ is the maximum response variation and $max(R(x_i)) - min(R(x_i))$ is the maximum response variation due to the changing of factor x_i, with the other input parameters being held

Table 4.20: Estimated coefficients for the quadratic model of pressure drop and outlet product temperature.

Coefficient	**Factor**	**Pressure Drop [Pa]**	**Outlet product temperature [K]**
β_0	-	21257.31	-86.24
β_1	v_{in}	13422.97	5.26
β_2	$T_{\text{p,in}}$	-40.41	1.05
β_3	$T_{\text{w,in}}$	-42.84	0.47
β_{12}	$v_{\text{in}} \cdot T_{\text{p,in}}$	-20.12	0.29
β_{13}	$v_{\text{in}} \cdot T_{\text{w,in}}$	-15.05	-0.32
β_{23}	$T_{\text{p,in}} \cdot T_{\text{w,in}}$	0.07	-4.58e-04
β_{11}	v_{in}^2	8208.07	3.59
β_{22}	$T_{\text{p,in}}^2$	0.03	-1.22e-03
β_{33}	$T_{\text{w,in}}^2$	0.03	9.03e-04

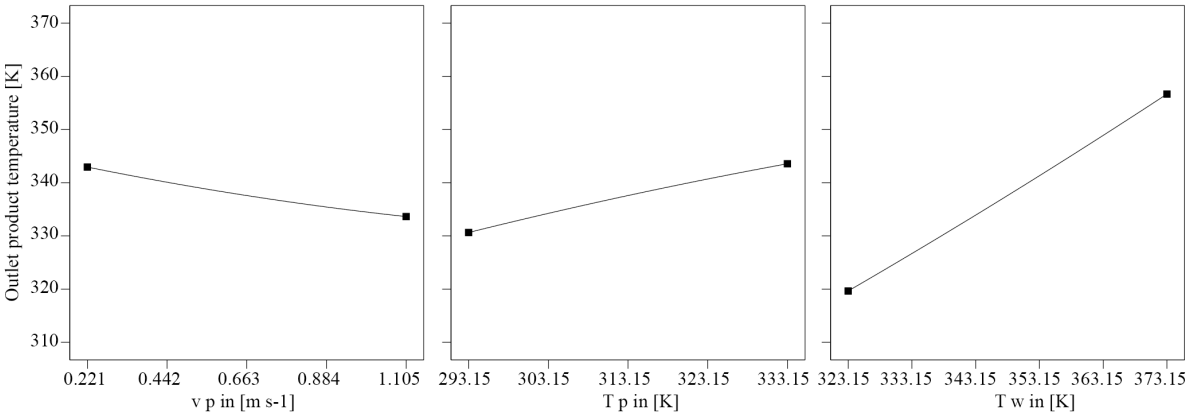

Figure 4.30: $T_{p,out}$ one-factor response charts showing the sensitivity of the response and the effects of modifying one parameter at a time.

constant. If the response value rises as the factor value increases, LS is a positive number, otherwise it is negative.

As shown in Figure 4.31, the pressure drop is mostly influenced by product velocity, while product and water temperatures result to have a lower impact. The strongest positive effect on outlet temperature of the product is given by the water temperature, while an increase in product velocity yields a lower product temperature raise, since the residence time of the fluid inside the heat exchanger decreases.

$$LS(R, x_i) = \frac{\max(R(x_i)) - \min(R(x_i))}{\max(R) - \min(R)} \tag{4.30}$$

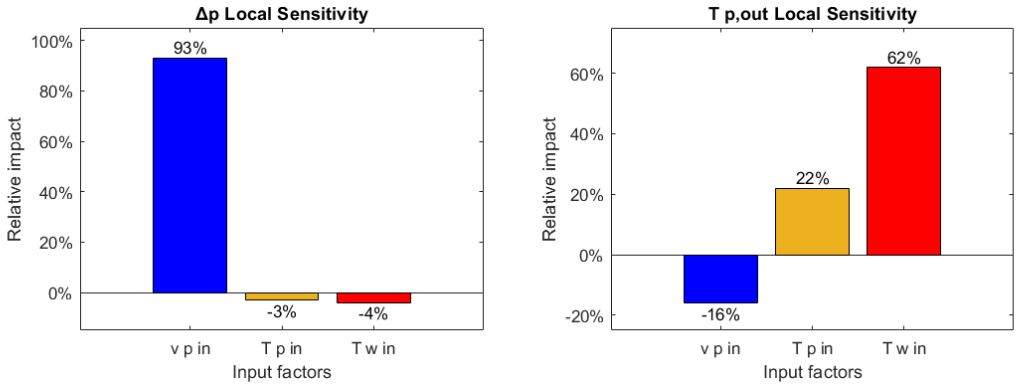

Figure 4.31: Relative impact of the input factors on the analyzed responses.

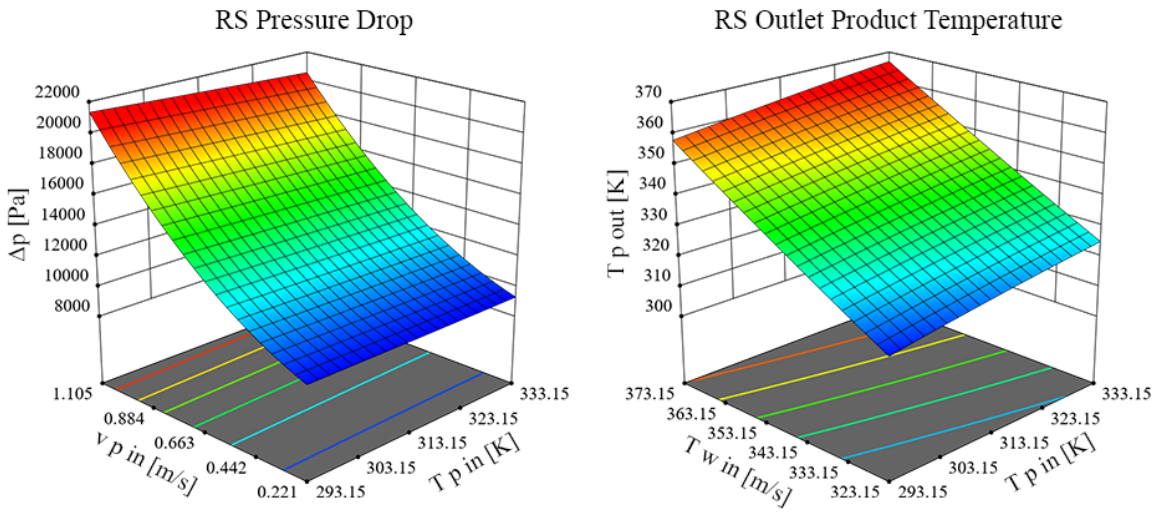

Figure 4.32: Response surfaces for pressure drop and outlet product temperature responses.

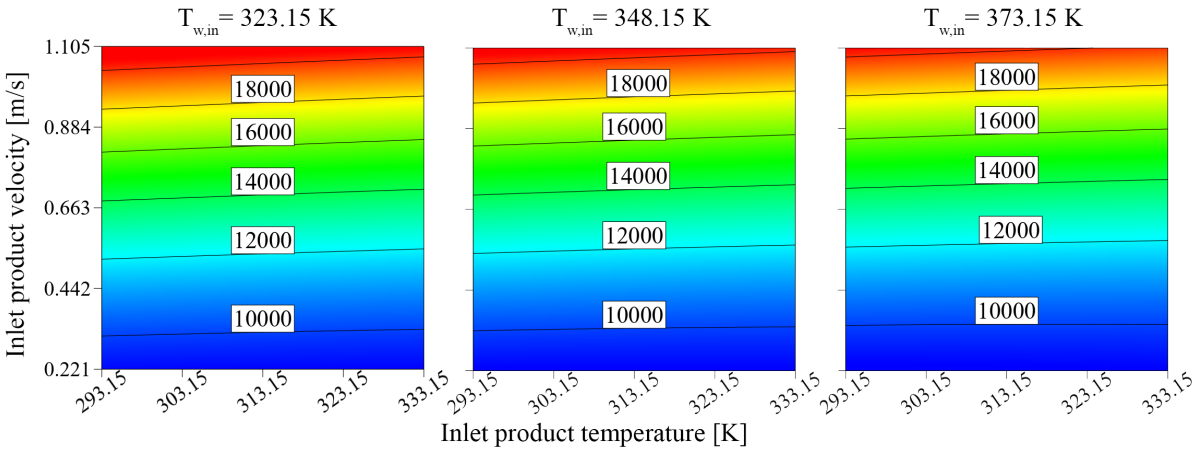

Figure 4.33: Response surface contour plots for pressure drop [Pa]

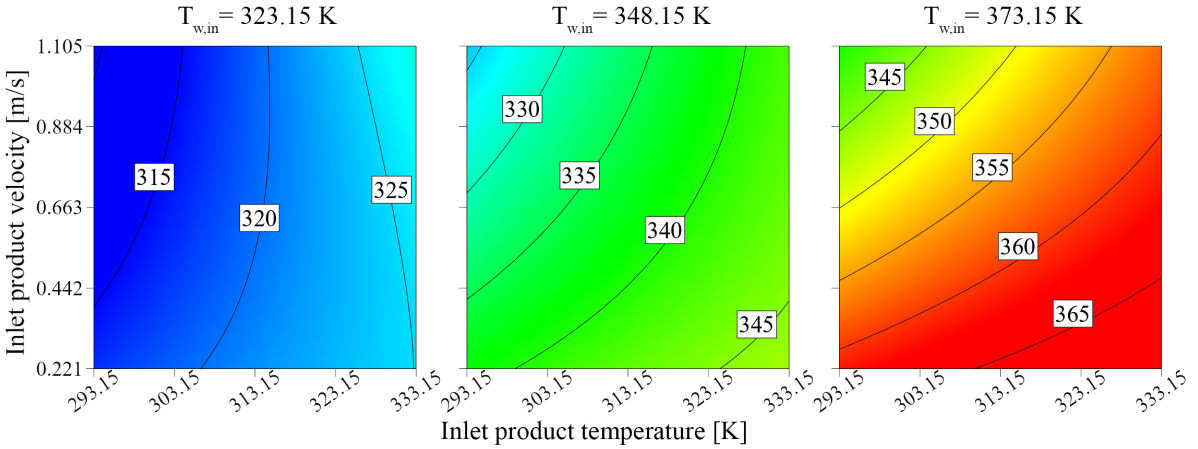

Figure 4.34: Response surface contour plots for outlet product temperature [K], as a combination of different levels of inlet product temperature and velocity.

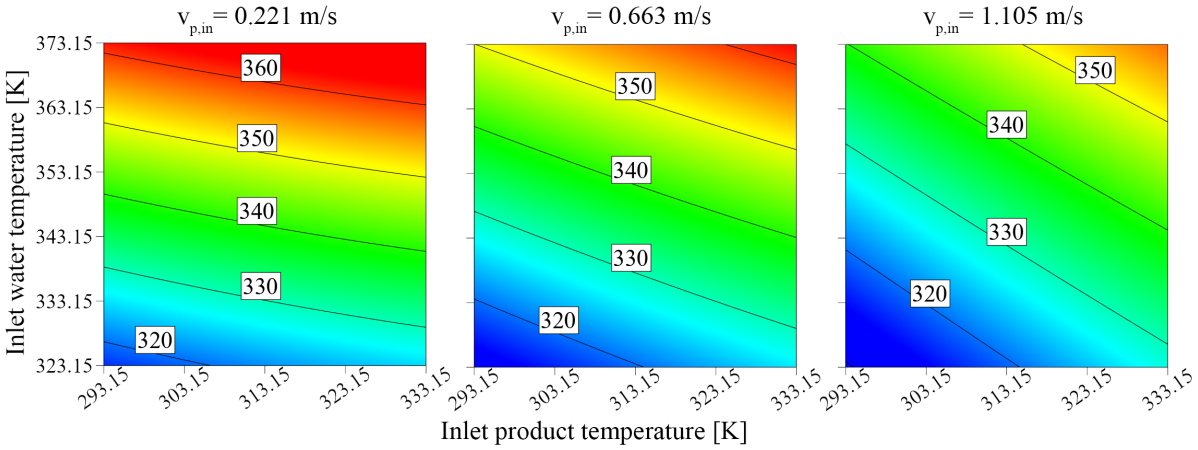

Figure 4.35: Response surface contour plots for outlet product temperature, as a combination of different levels of inlet product and water temperatures.

A graphical representation of the estimated responses can be seen in Figure 4.32: the pressure drop response is plotted as a function of inlet product temperature and velocity, while the outlet product temperature is represented as a function of the inlet temperatures of water and product. Contour plots of the estimated response for pressure drop, expressed in Pa, are shown in Figure 4.33, for different combinations of $T_{p,in}$ and vp, in. The third factor, specifically $T_{w,in}$, is fixed at three values corresponding to $-\alpha$, 0 and α coded levels. The strong dependence of the pressure drop on the product flow rate is once again evident.

Response surfaces for outlet product temperature, expressed in K, are generated as a function of $T_{p,in}$ and $v_{p,in}$, at 3 fixed values of $T_{w,in}$ (Figure 4.34). On the right-hand side of the first contour plot the fluid is considered to flow counter-current to water at a lower temperature, so it is subjected to cooling. It is important to notice that the response presents curvature, which is considered thanks to the choice of a second-order model. The estimated responses for outlet product temperature are also represented as a function of $T_{p,in}$ and $T_{w,in}$, with $v_{p,in}$ values fixed at minimum, mean and maximum values (Figure 4.35). As the flow rate increases, the product temperature increment tends to decrease, and its dependence on the inlet product temperature becomes stronger.

Experimental validation

The results of the CFD simulations, and the generated Response Surface, were validated with an experimental campaign on the pilot plant. Measured and RS-estimated outputs of interest are compared in Figure 4.36 and Figure 4.37. Plots of measured values of pressure and temperature are based on sensor readings that were acquired every 2 seconds with a Data Acquisition (DAQ) module and stored in a spreadsheet. RS estimated values were calculated with the final equations of the estimated response in terms of actual factors by multiplying the measured input factor readings by the coefficients of the quadratic model. The model was validated by comparing the measured outputs with the calculated ones.

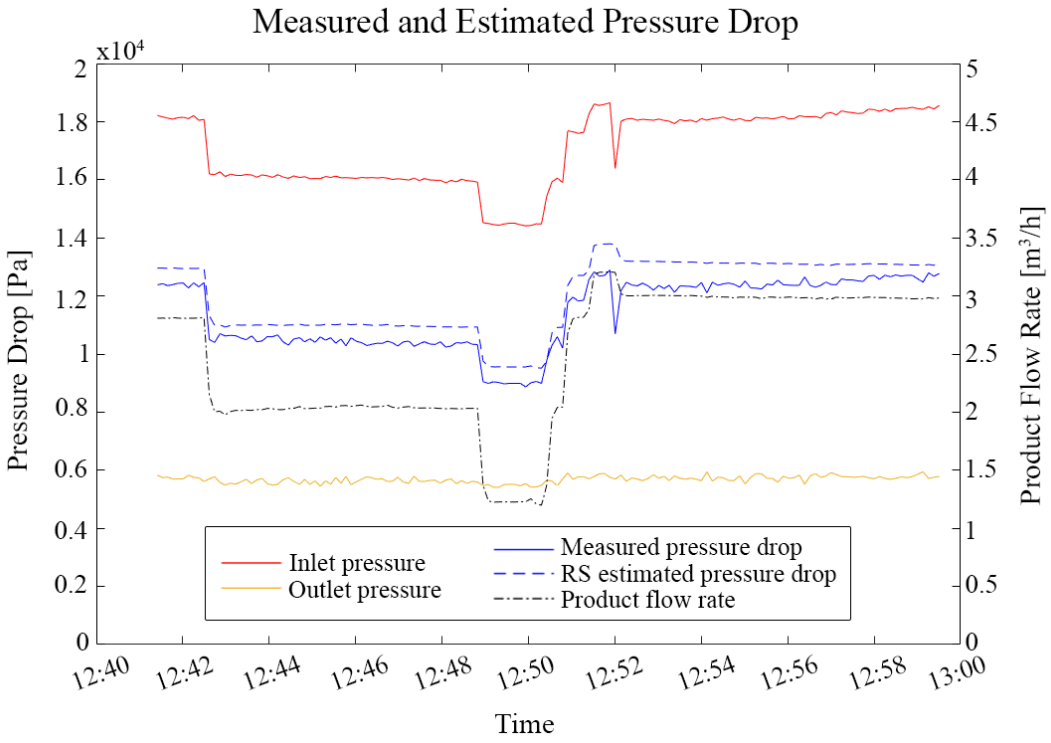

Figure 4.36: Experimental validation of the estimated pressure drop response.

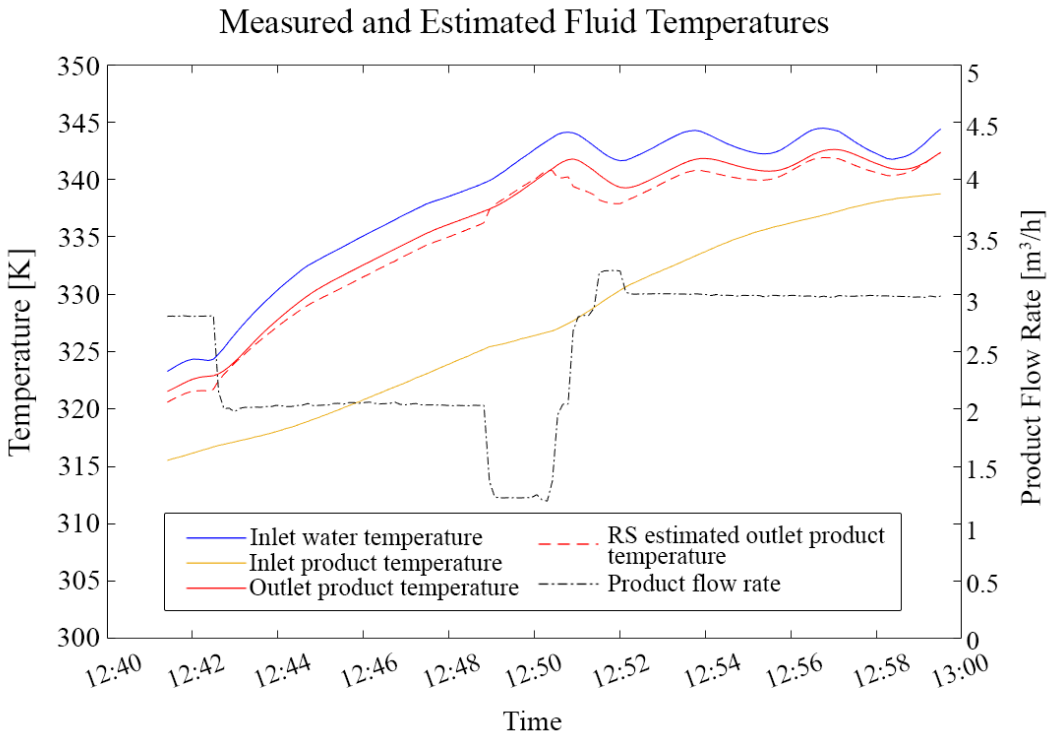

Figure 4.37: Experimental validation of the estimated outlet product temperature response.

Thanks to the continuous acquisition of experimental data the comparison with the simulated results can be performed in every operating point where the input values lie within the considered range, rather than in a few selected validation points. As stated in section previously, the fluid was continuously recirculated, so the only manually-set parameter was the product flow rate. A set-point value was established for the water temperature, which, therefore, tended to reach the desired value thanks to the automatic regulation of the opening percentage of the steam control valve. Due to the recirculating configuration the inlet product temperature rose continuously under the influence of the water temperature.

The experimental campaign was divided into three phases:

- 12:43-12:48 Constant flow rate (2 m3/h), and constantly rising water and product temperatures. In accordance with the sensitivity analysis, the pressure drop appeared to be mainly influenced by flow rate and, therefore remained fairly constant throughout the entire phase.

- 12:48-12:52 Sudden significant changes in flow rate were induced to verify whether the reactivity of the real system was comparable to that of the model. Since the water temperature had not yet reached the defined set-point, the temperatures of both fluids were still increasing. The behavior of the real system was in agreement with the digital model, without significant delays or adaptation times.

- 12:52-13:00 Constant product flow rate (3 m3/h) and water temperature oscillating around the set-point value. The temperature of the recirculated product approached the water temperature. Unlike the behavior observed in the first part of the test, a slight increase in pressure drop was observed in this phase. This can be explained by the onset of a time-dependent behavior of the Gellan gum solution. Time-dependent behavior of thickening agents under particular conditions has been investigated in the literature [247, 248]. Further studies are necessary to investigate this aspect, which, however, is not strictly relevant to the objectives of this research.

The Mean error, defined as the mean of punctual errors between the actual values and the estimated ones, was calculated to numerically evaluate the accuracy of the model with eq.4.31 and eq.4.32. The Mean error was chosen for this purpose, since, as can be seen from Figure 4.36 and Figure 4.37, the difference between measured and estimated responses remains almost constant as the operating parameters vary. In the equations, N is the number of sensor readings. Results are reported in Table 4.21.

$$e_{\Delta p} = \frac{\sum_{i=1}^{N} \left(p_{in,measured,i} - p_{out,measured,i}\right) - \Delta p_{RS,i}}{N} \tag{4.31}$$

$$e_{\Delta T} = \frac{\sum_{i=1}^{N} \left(T_{out,measured,i} - T_{in,measured,i}\right) - \left(T_{out,RS,i} - T_{in,measured,i}\right)}{N} \tag{4.32}$$

Table 4.21: Mean errors between measured and estimated outputs

	$e_{\Delta p}$	$e_{\Delta T}$
e_{mean}	-628 Pa	0.85 K

The model, as can also be seen from Figure 4.36 and Figure 4.37, tends to overestimate the pressure drop by an average of 628 Pa, and to underestimate outlet product temperature by an average of 0.85 K.

In order to further improve the accuracy of this particular model, the calculated mean error values could be included in the final equations, as expected errors for the two responses. The final quadratic model equation for the estimation of outlet product temperature, therefore, would be expressed as in eq.4.33, while the expected value of system pressure drop could be calculated with eq.4.34.

$$\begin{aligned} T_{p,out} = &-86.24\,K + 5.26 \cdot v_{p,in} + 1.05 \cdot T_{p,in} + 0.47 \cdot T_{w,in} + 0.29 \cdot v_{p,in} \cdot T_{p,in} + \\ &- 0.32 \cdot v_{p,in} \cdot T_{w,in} - (4.58 \times 10^{-4}) \cdot T_{p,in} \cdot T_{w,in} + 3.59 \cdot v_{p,in}^2 + \\ &- (1.22 \times 10^{-3}) \cdot T_{p,in}^2 + (9.03 \times 10^{-4}) \cdot T_{w,in}^2 + 0.85\,K \end{aligned} \tag{4.33}$$

$$\begin{aligned} \Delta p = &\,21257.31\,\text{Pa} + 13422.97 \cdot v_{p,\text{in}} - 40.41 \cdot T_{p,\text{in}} - 42.84 \cdot T_{w,\text{in}} - 20.12 \cdot v_{p,\text{in}} \cdot T_{p,\text{in}} + \\ &- 15.05 \cdot v_{p,\text{in}} \cdot T_{w,\text{in}} + 0.07 \cdot T_{p,\text{in}} \cdot T_{w,\text{in}} + 8208.07 \cdot v_{p,\text{in}}^2 + \\ &+ 0.03 \cdot T_{p,\text{in}}^2 + 0.03 \cdot T_{w,\text{in}}^2 - 628\,\text{Pa} \end{aligned} \tag{4.34}$$

Discussion

Once the generated model is validated, RSM could be very useful in both predictive and operating phases as a support in the design and control of the plant respectively, allowing optimization of the process according to a series of goals and constraints. In a predictive phase, in order to optimize the design of the plant and of the thermal process, it can be used to predict how the input parameter variations would affect the output variables. During the operating phase it allows identifying the possible operating points, defined as combinations of input processing parameters, that enable reaching a defined value for output of interest. The case in which the inlet product temperature is known and a desired outlet product temperature has been defined is reported as an example. $T_{p,in}$ is set at 303.15 K, while the set-point $T_{p,out}$ is a pasteurization temperature of 348.15 K. A contour plot of the case is reported in Figure 4.38, with $v_{p,in}$ and $T_{w,in}$ on the x and y axes, respectively. The colour range covers temperature values from a minimum of 315 K to a maximum of 363 K. The chosen output temperature value is highlighted on the contour plot by an iso-level that identifies all the possible couples of inputs leading to the result

requested. Some of the possible operating points, calculated by means of a numeric optimization of the response surface, are reported in Table 4.22. In this optimization problem there is one goal ($T_{p,out}$=348.15 K) and one constraint ($T_{p,in}$=303.15 K).

If, in addition to the goal of reaching a target temperature, we aim to minimize the system pressure drop, the operating point that meets these requests can be calculated by means of a response optimization with two goals ($T_{p,out}$=348.15 K; $\Delta p_{opt} = min(\Delta p)$) and one constraint ($T_{p,in}$=303.15 K). The optimum operating point is defined as a combination of input parameters as reported in Table 4.23.

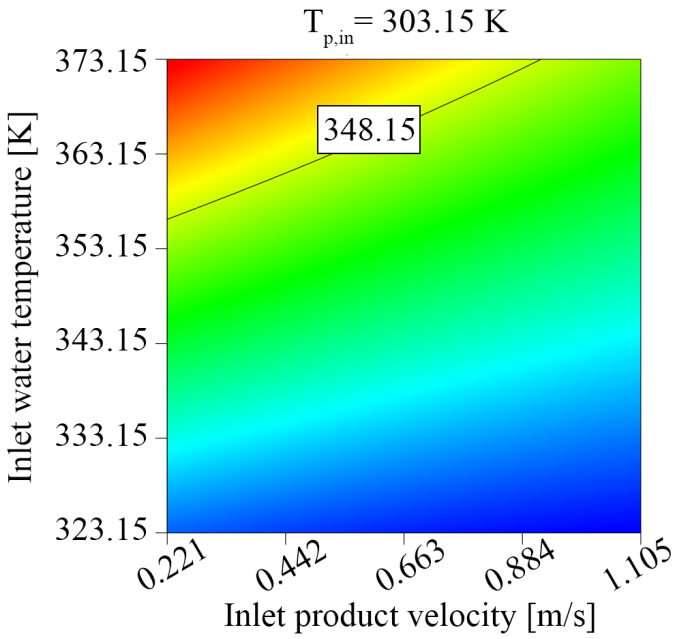

Figure 4.38: Outlet product temperature contour plot, with a highlighted iso-level at the desired pasteurization value.

Table 4.22: RS defined Operating Points (OP) that allow obtaining the desired output product temperature.

	constraint				**target**
	$v_{p,\text{in}}$ [m s^{-1}]	$T_{p,\text{in}}$ [K]	$T_{w,\text{in}}$ [K]	Δp [Pa]	$T_{p,\text{out}}$ [K]
OP 1	0.30	303.15	358.1	9740.72	348.15
OP 2	0.45	303.15	361.3	10897.11	348.15
OP 3	0.60	303.15	364.9	12491.70	348.15
OP 4	0.80	303.15	370.0	15159.22	348.15
OP 5	0.90	303.15	373.1	16867.94	348.15

Table 4.23: Operating point that allows reaching the set-point temperature, while minimizing system pressure drop.

	constraint			**minimize**	**target**
	$v_{p,\text{in}}$ [m s^{-1}]	$T_{p,\text{in}}$ [K]	$T_{w,\text{in}}$ [K]	Δp [Pa]	$T_{p,\text{out}}$ [K]
OP 6	0.22	303.15	356.3	9235.95	348.15

Any constraint on the input parameters that could be due to plant or product characteristics can be included in the optimization set-up so as to better adapt the solution to the real-life situation. Once they have been calculated, the product velocity and water temperature values obtained can be used to define the processing parameters of the pilot plant by setting the corresponding product flow rate and water temperature set-points on the control panel.

Conclusions

In this study, the behavior of a tubular heat exchanger has been reproduced by means of CFD simulations under different operating conditions thanks to a parametric study. Product flow rate, and inlet product and water temperatures were chosen as input parameters, while outlet product temperature and pressure drop across the heat exchanger were chosen as output parameters. The product used in the study was characterized from a rheological point of view and its viscosity was modeled with a Power-law model, considering the temperature dependence through the Arrhenius equation. The rheological model appears to be more accurate at high temperatures ($T \geq 313.15$ K), because at low temperatures the pseudo-plastic behavior of the product changes and becomes more significant than at high temperatures. A Response Surface was generated using a quadratic model, starting from the results of the parametric study. The results highlighted that the relative impact of vp,in on Δp was positive (93%), while higher $T_{p,in}$ and $T_{w,in}$ yielded lower pressure drop values across the heat exchanger (-3% and -4%, respectively). $T_{p,out}$ appeared to be positively influenced by inlet product (62%) and water (22%) temperatures, and negatively by $v_{p,in}$ (-16%). An ANOVA test showed that the quadratic model and the selected independent factors resulted to be significant for the estimation of both responses of interest. The RS was validated through to a suitable experimental campaign. The Mean errors, defined as the mean of punctual errors between the actual values and the estimated ones, were calculated to numerically verify the model for the two responses of interest. Mean error values of 628 Pa and 0.85 K were obtained for pressure drop and outlet product temperature, respectively. These errors can be considered acceptable since, generally, in industrial applications, heat exchangers work with significant pressure drop and temperature variation so, in these conditions, the calculated mean error values become negligible. It is crucial, however, that the measured input data be accurate and reliable, otherwise incorrect information about the independent variables would lead to highly erroneous estimated results. The results obtained can have significant implications in industrial applications as the method investigated allows generating a response surface that could be used as a Reduced-Order-Model of the plant, and which could be implemented to develop a Digital Twin (DT) of the heat exchanger when connected to its real-world counter-part by sensor measurements. The fact that the model was generated

on the basis of steady-state simulations could reduce its accuracy in transient conditions which, however, are not the operating standard for this type of plant in common industrial applications characterized by stationary regime conditions. Further studies will have to be conducted to verify and investigate the applicability of the method to processes with more significant transients. The implementation of the DT would allow knowing how the system would behave at the measured conditions, evaluating any deviations and then making suitable adjustments to guarantee optimal performance. The model could also be used as a design tool, by setting a goal for the output values and calculating the possible combinations of inputs that lead to the desired result. As stated in the Introduction, this modelling methodology could significantly improve the current state-of-the-art, since it would allow the results of the CFD simulations to be ready-to-use, thereby granting deeper knowledge and finer control of the system.

4.2 Introduction to “virtual sensors”

The topic presented in this section concerns the development of data-based "virtual sensors", aimed at providing insights about points of interest where real sensors are not available or could be impossible to install.

This approach was currently investigated focusing on a heat exchanger for the continuous thermal treatment of viscous food products. The device analyzed in this study is the same one discussed in Section 4.1.2, where a detailed description of the plant and the modelling approach was given.

For quality and safety purposes, it would be necessary to have uniform temperature distribution on the outlet section of the heat exchanger. This ideal condition could be easily obtained with water-like products. In most food industry applications, however, products are highly viscous and present a complex rheological behaviour, that results in non-uniform temperature distributions. The risk, in this case, is that the product flowing in the centre of the pipe receives an insufficient thermal treatment and reaches a lower temperature than required (potentially affecting food safety), while the product at the walls could be over-treated (potentially affecting food quality).

While it is fundamental to monitor the thermal treatment, it does not make sense, neither from technical nor economical points of view, to install multiple temperature sensors at different depths at the outlet of the device. Also, in the case of fluids containing solid particles or pieces, it would not be possible to insert temperature probes to measure the temperature in the centre of the pipe without damaging the product.

One possible application of "virtual sensors" in this case could be, knowing the operating conditions and the temperature in one point from sensor measurements, for example near the wall, the estimation of the temperature in the centre of the pipe. The data about the temperature distribution inside the domain could be obtained from CFD simulation, through an appropriately defined simulation campaign.

This application would be in line with that proposed by Guzmán et al. [126]. The study focused on greenhouse temperature monitoring using virtual sensors based on CFD and control techniques. The study demonstrates that virtual sensors can effectively monitor temperature with only one physical reference sensor, significantly reducing the cost and maintenance needs associated with numerous physical sensors.

Another interesting application of the "virtual sensor" concept is presented in [127]. The study explores the use of virtual sensors to monitor multiphase flow patterns within microfluidic devices to support zero-defect manufacturing, which is critical for high-quality and cost-efficient production. After modelling the multiphase behaviour inside the microfluidic chip with CFD, the authors have processed the obtained results to generate a reduced-order model (ROM), able to calculate fluid interface positions within the device in extremely short times (approximately one millisecond), obtaining results match-

ing those of the CFD simulations that obvious require considerably longer computational times (approximately one week).

Using simulation results to develop virtual sensors would allow to further extend the value of the CFD simulations beyond characterization purposes, effectively using them to develop advanced tools for plant monitoring and control.

An application, among those discussed in the thesis, that could extensively benefit from virtual sensing is continuous ohmic heating (Section 3.3.2). In that case, heating is achieved thanks to the passage of electrical current through the product. Due to the presence of a strong electrical field, conventional sensors can not be installed inside the device.

Given the common application of ohmic heaters to sensible products, like those with high protein content, that could be strongly damaged by non-uniform heating and the possible formation of hot points, it appears essential to have a clear idea of what is happening inside the device. CFD results provide an essential contribution to this need but alone could be used just for process characterization. Also, in this case, developing simulation-driven virtual sensors could greatly benefit monitoring and control of the system.

Another approach currently under evaluation is related to the use of machine and computer vision techniques. A bibliometric analysis of the literature, aiming at identifying applications and fields currently investigated is presented in Section 2.2. Nowadays, in the food industry, these techniques are used mainly for spot-on quality checks, and applications concerning sorting, grading, and defect identification. Often, the result of this evaluation is the classification of product categories or the removal of defected or unsuitable ones.

Based on the industrial collaborations carried out over the last year of the Doctoral project, involving the application of vision techniques in food processing lines, a research question that emerged was: *Is it possible to go beyond the current application of vision-based techniques, integrating them in plant monitoring and control applications?* In this way, the evaluations would overcome "black or white" grading, or simple classifications. Indeed, they could communicate with the control system and allow for better management of the plant, resulting in greater quality and efficiency, in line with zero-defect manufacturing concepts.

The topic of including vision-based data in the control system of industrial plants and processes has been discussed in the recent paper by Konstantinidis et al. [31], which focused in particular on the dairy industry. Specifically, the authors have proposed a "Dairy 4.0" framework, integrating Industry 4.0 principles to achieve zero-defect manufacturing, thus enhancing product quality, reducing waste, and improving process sustainability in dairy operations.

The architecture of the proposed framework consists of a four-level structure, including (*i*) the physical layer (farming, manufacturing, logistics), (*ii*) the machine vision layer to monitor various production aspects, from animal health to product quality and facility hygiene, (*iii*) the Digital Twin layer, integrating data from the machine vision layer and the physical systems to create virtual representations for real-time analytics and predictive maintenance, and finally (*iv*) the zero-defect manufacturing layer, that leverages data from the digital twin and machine vision layers to detect, predict, and prevent defects.

The topic of data-driven virtual sensors, based on simulation results, experimental data, or machine vision applications, represents a promising topic of great interest, that will definitely be explored in future research activities.

4.2.1 Analysis of temperature distributions during thermal treatment of different product concentrations, and proposal of a modelling approach for virtual sensor development.

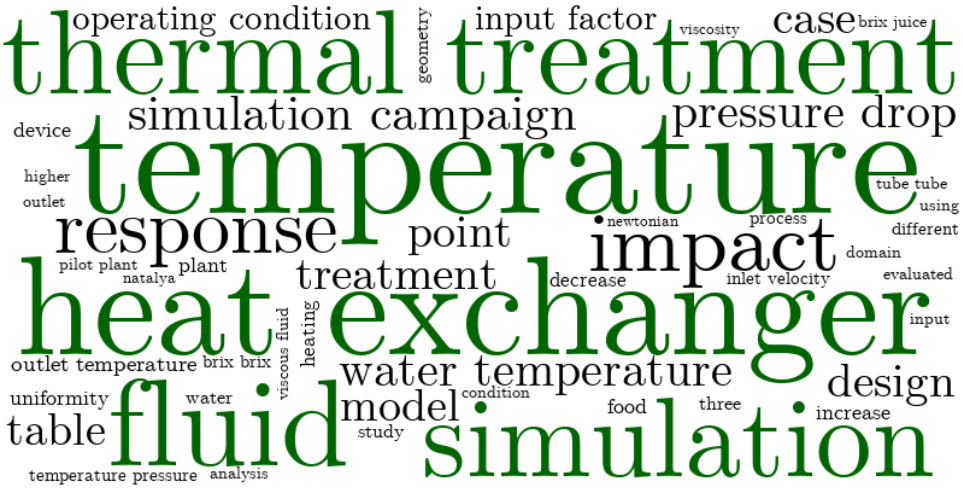

The research in this chapter has been included in the peer-reviewed conference paper [175] *Lysova, N., Solari, F., Bocelli, M., Rizzi, A., and Montanari, R. (2024). Exploring the impact of the process parameters on the thermal treatment of viscous food fluids in a tube-in-tube heat exchanger. Procedia Computer Science, 232, 2347–2357. https://doi.org/10.1016/j.procs.2024.02.053.*

Abstract

Thermal treatments are essential to abate the microbial load in food matrices and ensure food safety. Heat exchangers (HEs) are commonly adopted for the pasteurization of liquid foods, thanks to their simple structure and ease of use. In particular, tubular HEs are often employed with viscous fluids and products containing fibres and pieces. The aim of pasteurization is to ensure that every point of the product reaches and maintains the target temperature for an adequate amount of time. To this end, it is essential to guarantee uniformity and prevent portions of fluid from reaching an insufficient temperature, and others from being overheated.

To evaluate the thermal treatment inside a tube-in-tube HE, computational fluid dynamics (CFD) was used to simulate a pilot plant. Three different fluids with shear-thinning temperature-dependent non-Newtonian behaviour were evaluated. A CFD simulation campaign was carried out reproducing, for each juice, the thermal treatment under different operating conditions. Then, the results were analysed with statistical techniques to evaluate the impact of each operating parameter on the treatment, highlighting how high viscosity greatly impacts the thermal treatment, resulting in lower average temperature and temperature uniformity, while causing an increase in the pressure drop. The results of the simulation campaign were also used to generate a reduced order model (ROM) of the device, that could be exploited to estimate the outcomes of a treatment both as averaged values on a section or at a specific point like "virtual sensors". The ROM could be also adopted to design and evaluate alternative treatments by performing numerical optimization based on given objectives and constraints. Finally, as the ROM can be implemented in real-time, it could be used to monitor and control the functioning of food plants, detecting deviations from the expected conditions and possible failure conditions.

Introduction

The heating process is one of the most important in the food industry: it is essential for performing thermal treatments or as a pre-heating stage of several unit operations. It is often carried out using heat exchangers, where a service medium supplies heat to the treated product through a separating wall. A very important aspect of heating is the uniformity of the treatment: in the case of pasteurization and sterilization, indeed, every point of the product must reach, and maintain, a target temperature for a defined amount of time. Not complying with these requirements, e.g., if some areas of the product do not reach the target temperature, would lead to an insufficient thermal treatment, which may result in recontamination of the product and a hazard to human health. On the other hand, overheating must be avoided, as it decreases the product quality and may cause the formation of harmful by-products.

The type of product treated strongly impacts the geometry and the type of heat exchanger that is most suitable for the scope: food products, indeed, can be highly viscous and contain fibres or even dispersed particles or solid pieces. In these cases, tube-in-tube heat exchangers are usually adopted. These devices present a simple structure, consisting of an inner tube dedicated to the product and an outer tube where the hot medium flows releasing heat. The simple geometry and structure of the device allow to efficiently heat the product to the desired temperature while avoiding causing mechanical damage to the particles contained in the fluid. Furthermore, contrary to what would happen in the case of plate heat exchangers or devices with small passage areas, tube-in-tube heat exchangers reduce the risk of fouling and obstruction with fibres or solid pieces. While tube-in-tube heat exchangers are generally very simple devices that have been extensively studied and described in the literature, their functioning may become less straightforward to evaluate in the case of complex fluids. Indeed, the non-Newtonian rheological behaviour, mostly shear-thinning and temperature-dependent, of most food fluids [3] makes the analysis of the heat exchange performances considerably more difficult to achieve with traditional analytic methods. To this end, numerical simulation methods become convenient, as they allow to iteratively solve the governing equations, calculating the physical quantities of interest at, ideally, any location inside the domain. This allows to gain a deep understanding of a treatment, assess its weaknesses and identify possible safety hazards. Computational fluid dynamics (CFD) simulation has been extensively applied for the simulation of a multitude of industrial devices over the last decades, allowing for reliable evaluation of the processes even in the case of complex geometries, fluids and boundary conditions [1, 131]. It is also widespread for preventively evaluating geometry modifications and testing alternative what-if scenarios [236,238]. CFD has been extensively applied to study the pasteurization process [1, 249]. In the literature, several studies are available that use CFD for the simulation and evaluation of the efficiency of

different categories of heat exchangers. Also, studies that simulate the thermal treatments of food fluids in tube-in-tube heat exchangers have been published in the past years [226].

In some studies, the authors have applied statistical techniques to evaluate the performance and yield of food industry processes [231]. CFD simulation has been leveraged, in combination with modelling and statistical techniques, to generate virtual sensors and gain insights about data of interest at locations where physical sensors could not be installed [126, 127]. Response surface methodology (RSM) has been used in combination with simulation, also for the evaluation and optimization of food processes [250]. In [5] the authors applied RSM to evaluate the performance of a decontamination process in a tubular heat exchanger in terms of microbial inactivation and nutritional quality. In [92] CFD was combined with RSM to assess the impact of the operating conditions on the treatment and generate predictive models of the process outcomes to be implemented in a real-time control of the plant. In this study, it was highlighted how the change in the product temperature highly impacted its rheological behaviour. To the best of our knowledge, no studies in the literature have evaluated how the characteristics of a product impact the efficiency and the uniformity of thermal treatment, while keeping constant the operating parameters and the geometry of the device.

To this end, in this study we have considered three different concentrations of a non-Newtonian fruit juice, presenting different rheological behaviours. The characteristics of the fluids were retrieved from the literature. Then, three parallel simulation campaigns, one for each fluid, were carried out using a previously validated CFD model of a pilot plant heat exchanger for viscous fluids [92]. The simulation campaigns were designed based on RSM central composite design (CCD). The results obtained were then analysed with statistical methods, to evaluate the impact of each operating parameter on the thermal treatment, and analyse how these impacts changed as the fluid characteristics varied. The analysis allows to gain an in-depth understanding of the thermal treatment of food products, in the perspective of "informed" and smart manufacturing and the pursuit of food safety.

Materials and methods

Pilot plant

The evaluated plant consists of a tubular heat exchanger for viscous fluids installed at the University of Parma (Fig.4.39) [92,251]. The plant is equipped with auxiliary services that provide water, steam, compressed air and electricity to each component of the plant. The heat exchanger consists of an inner tube, where the product flows, and an outer tube, where the hot water flows counter-current to the product, yielding heat to it through a metallic wall. The plant can process from 1 m^3/h to 5 m^3/h of product, even containing dispersed particles or pieces up to 10 mm. Due to the particular structure of the product

treated, the walls of the inner tube are smooth, so as not to cause mechanical damage to it. The main geometrical features of the plant are summarised in Table 4.24.

Table 4.24: Overview of the geometrical features of the heat exchanger pilot plant

Description	**Value**	**Unit**	**Description**	**Value**	**Unit**
Number of linear heating sections	6	units	Ratio of the bend radius to the inner tube diameter	1.5	-
Length of the linear sections	3950	mm	Outer tube diameter	73.2	mm
Length of the heating section	3700	mm	Tube wall thickness	1.5	mm
Inner tube diameter	39.8	mm			

Figure 4.39: Pilot plant for the thermal treatment of viscous fluids installed at the University of Parma.

The product that must be heated, initially stored in a stainless steel tank equipped with a mixer, is pumped with a screw pump towards the inlet of the first heating section, located at the lowest level of the heat exchanger; from there, the fluid proceeds to flow across six linear heating sections connected by 180° bends where no heat exchange occurs, as the outer tube with the hot water is connected to the next heating section with a straight pipe segment; after exiting from the outlet section, the fluid is recirculated in the pilot plant. The heating service medium, i.e., water from the supply network, is pumped at a fixed flow rate of 12 m^3/h with a centrifugal pump towards the inlet of a dedicated heat exchanger where it is heated to a target temperature with the steam provided by a steam generator; the heated water then proceeds towards the top section of the heat exchanger and flows counter-current to the product and it is finally recirculated in the plant. The by-pass flow rates of both steam and hot water can be regulated with positioner valves to achieve the desired set points of water and product temperature.

Fluid characterization

The simulation campaign was performed by simulating the thermal treatment of three food fluids, namely juices, at different concentrations. The physical and rheological properties were retrieved from a study in the literature that reported experimentally determined thermo-physical and rheological properties of several concentrations of blackberry juice at different temperatures [252]. The concentration of the juices is represented by their Brix degree, which quantifies the grams of solute, usually sugar, in 100 grams of solution. The juices at 20.0, 29.4 and 40.2 Brix were selected for this study. As can

be observed in Table 4.25, based on the value of the flow behaviour index n, the three fluids were non-Newtonian (n≠1) with a shear-thinning behaviour ($n < 1$). The flow behaviour index n remains overall constant for the three fluids, while the consistency index K increases at higher juice concentrations.

The expressions for the thermo-physical quantities, i.e., density, specific heat and thermal conductivity, in function of temperature, were derived by performing a linear regression of the available experimental data at different temperatures. The rheological behaviour has been modelled according to the Arrhenius law, in the form reported in Eq.4.35 (Table 4.25). In particular, η is the apparent viscosity of the non-Newtonian fluid at a generic temperature T, η_α is the apparent viscosity at the reference temperature T_α, E_a is the activation energy and R is the universal gas constant. η_α can be calculated according to the power law equation (Eq. 4.36), where $\dot{\gamma}$ is the shear rate, which for pipe flow conditions is usually assumed to be in the range of 0 – 1000 s^{-}1 [3]. The reference temperature T_α was considered to be 273.65 K for every fluid, and the reference values of K and n were retrieved in [252] at the temperature T_α. To account for the temperature-dependent behaviour of the fluid, it is necessary to calculate the value of the Arrhenius slope $alpha_Arr = \frac{E_a}{R}$. To this end, the apparent viscosity must be evaluated at a second temperature point. In this case, one of the other temperature points available in [15], equal to 295.55 K, was selected for the calculation of η according to Eq. 4.36, and α was then derived using Eq.4.35.

$$\frac{\eta}{\eta_\alpha} = \exp\left(\frac{E_a}{R} \cdot \left(\frac{1}{T} - \frac{1}{T_\alpha}\right)\right) \tag{4.35}$$

$$\eta_\alpha = K \cdot \dot{\gamma}^{n-1} \tag{4.36}$$

System modelling and simulation

Table 4.25: Thermo-physical and rheological properties of the three concentrations of blackberry juice considered, obtained by modelling the experimental data from [252]

Symbol	Unit	Description	20.0 Brix	29.4 Brix	40.2 Brix
ρ	kg/m^3	Density	$-0.6168T+$ 1244	$-0.5738T+$ 1275	$-0.4558T+$ 1303
c_p	J/(kg K)	Specific heat	$3.7952T$ + 2553	$3.943T$ + 2200	$3.486T$ + 1997
λ	W/(m K)	Thermal conductivity	$0.0012T$ + 0.2029	$0.001125T+$ 0.1779	$0.001008T+$ 0.1753
K	Pa s^n	Consistency index	0.216	1.069	6.705
n	-	Flow index	0.609	0.629	0.624
T_α	K	Reference temperature	273.65	273.65	273.65
α_{Arr}	K	Arrhenius slope	5896.20	6139.10	6890.40

The pilot plant functioning was reproduced with CFD simulations based on the model validated in [92] with a shear-thinning fluid at different temperatures and flow rates. The 3D model of the heat exchanger was generated in ANSYS SpaceClaim reproducing the real shape and dimensions of the device (Fig. 4.40a). In particular, the modelled domain reproduced the volume of fluid inside the inner and outer pipes. The wall separating the product from the hot water was not modelled to reduce the computation time required: it was however accounted for in the simulation settings, as described below. Finally, exploiting the symmetry of the system, half geometry was cut to reduce the computational weight of the simulation and, consequently, the simulation time (Fig. 4.40b).

The geometry was then discretised with ANSYS Meshing into an adequate number of cells, to achieve precision of the calculated solution while optimizing the calculation time based on the sensitivity analysis carried out in [92]. The final mesh consisted of 3.5 million elements, with hexahedral elements in the product domain and both tetrahedral and hexahedral elements in the water domain.

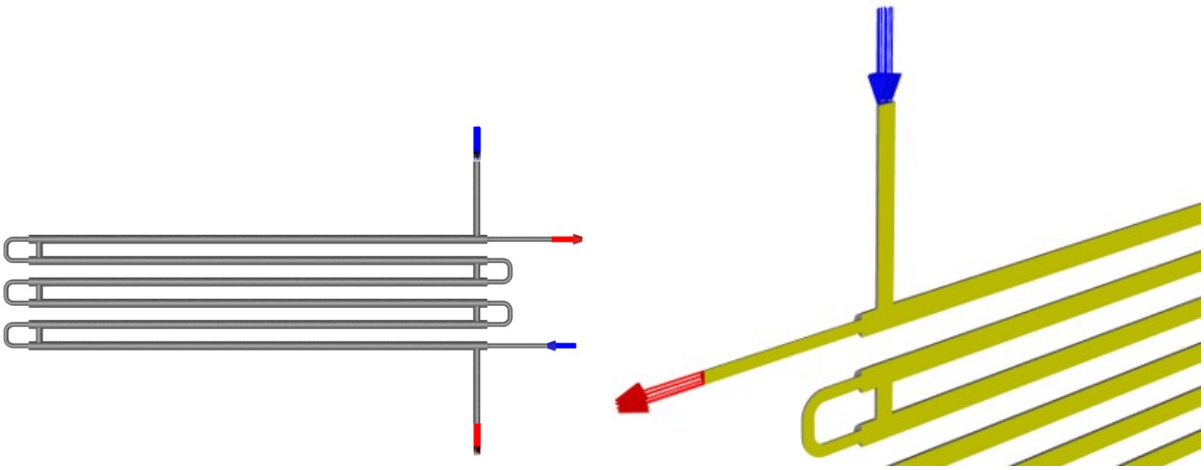

(a) Modelled geometry of the heat exchanger, with the indication of the inlets and outlets of the two fluids, i.e., product and hot water.

(b) Detail of the new geometry after its division in half across the symmetry plane (in yellow).

Figure 4.40: 3D geometry of the simulated device.

To accurately account for the heat exchange, ten inflation layers were generated near the wall for both the product and water domains. The mesh was then imported into ANSYS Fluent [71], to simulate the heating process by numerically solving the Navier-Stokes equations in the discretised fluid domain based on a set of boundary conditions. The inlet product velocity and the temperature of the hot water were considered input parameters, and their values were varied during the simulation campaign as described in previously. The physical presence of the metallic pipe was accounted for by defining an interface wall with known material and thickness between the two fluid domains. The main settings of the simulation are summarised in Table 4.26.

Table 4.26: Main simulation settings.

General settings	Solver	Pressure-based
	Gravity	Enabled
	Simulation conditions	Steady-state
	Turbulence model	k-ω SST
Boundary conditions	Product inlet	Velocity inlet; the velocity value is an input factor of the simulation campaign; the temperature is fixed at 303.15 K
	Water inlet	Velocity inlet; the velocity value is equal to 1.3 m/s; the temperature is an input factor of the simulation campaign
	Product and water exit sections	Pressure outlet
	Faces on the cut plane	Symmetry condition
	Pipe walls	No-slip condition
	Interface between water and product	Coupled two-sided steel wall with known thickness (Table 4.24)

Simulation campaign

The simulation campaign was designed with design of experiments (DOE) methodology, according to the RSM CCD design [245], a second-order polynomial design, consisting of central, factorial and axial design points, that allows for the estimation of the effects of k input parameters on i output responses. Factorial points are used for the estimation of linear effects, while central and axial points estimate the quadratic effects. Two key operating parameters, i.e., the product flow rate and the water temperature were selected as inputs for the analysis. For the CFD simulations, the product flow rate was converted into the mean velocity on the inlet section. The input parameters of the study, therefore, were the product inlet velocity and the inlet water temperature. To design the experimental campaign, m levels of input factors were considered; in this case, m was equal to 5 according to the standard, not face-centred, CCD design requirements. The output responses were the outlet product temperature (average, minimum and maximum), the outlet water temperature and the pressure drop on the product side (Table 4.27).

Table 4.28: Actual values of the input parameters corresponding to the coded levels used in the experimental design.

Input factor	**Coded factors**				
	-1 $(-\delta)$	-0.81	0	0.81	1 (δ)
$x_{1,act}$ [m/s]	0.22	0.30	0.66	1.02	1.11
$x_{2,act}$ [K]	323.15	327.82	348.15	368.48	373.15

Table 4.27: Input factors and responses of the present study.

Parameter	**Var.**	**Description**	**Unit**	**Parameter**	**Var.**	**Description**	**Unit**
Input	x_1	Inlet product velocity	m/s	Response	y_3	Minimum outlet temperature	K
Input	x_2	Inlet water temperature	K	Response	y_4	Outlet water temperature	K
Response	y_1	Average outlet product temperature	K	Response	y_5	Pressure drop (product side)	Pa
Response	y_2	Maximum outlet temperature	K				

Table 4.29: DPs of the simulation campaign.

DP	x_1	x_2	$x_{1,act}$ [m/s]	$x_{2,act}$ [K]	**Point**
1	0	0	0.66	348.15	Central
2	1	0	1.11	348.15	Axial
3	-1	0	0.22	348.15	Axial
4	0	1	0.66	373.15	Axial
5	0	-1	0.66	323.15	Axial
6	0.81	-0.81	1.02	327.82	Factorial
7	0.81	0.81	1.02	368.48	Factorial
8	-0.81	-0.81	0.30	327.82	Factorial
9	-0.81	0.81	0.30	368.48	Factorial

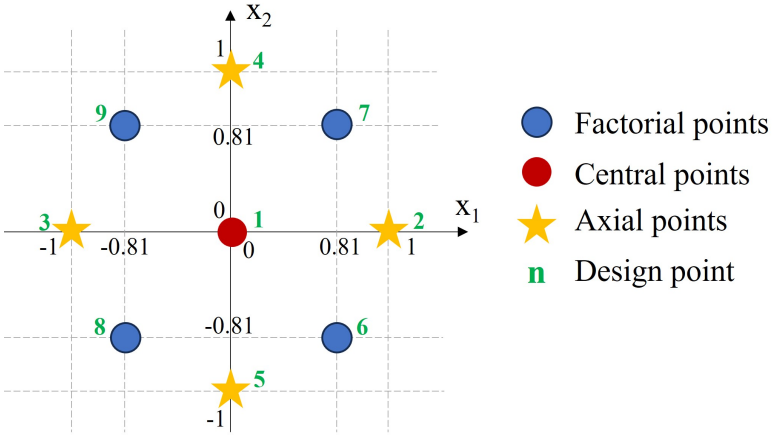

Figure 4.41: Schematic representation of the experimental domain.

First, the ranges of variation, i.e., the limits of the experimental domain, for the two input variables were established. By normalizing the real, "actual", values based on the variation range defined, it was possible to define a "coded" range for each input factor, where the level -1 corresponded to the minimum, 1 to the maximum, and 0 to the average value. Then, to consider two more input factor levels, the coded distance of the axial points from the centre of the experimental domain, δ, was calculated according to [34] to minimise the variance inflation factor, a measure of non-orthogonality, resulting equal to 1.23, thus representing values slightly outside of the variation range [-1 1] and generating a circumscribed design. As the variation range defined was a real process constraint, mostly with regard to the product flow rate, there was no practical use in investigating axial points located outside of it. An inscribed design was therefore generated by dividing all the coded levels by δ: the non-0 coordinates of the axial points took the value of -1 and 1, and the factorial points were adjusted accordingly. The actual values of the input factors, calculated with Eq. 4.37, are reported in Table 4.28. The number of design points (DPs) evaluated (n_{DP}), i.e., simulation runs, is calculated with Eq. 4.38. As the analysis involves only simulation experiments, with results that are not subject to replication errors, the number of central points replications, cp, is 1. In this case, 9 simulation runs were performed for each fluid, resulting in a total of 27 simulations (Table 4.29, Fig. 4.41).

$$x_{k,act,m} = \frac{cf_m \cdot (x_{k,act,max} - x_{k,act,min})}{2} + \overline{x_{k,act}} \tag{4.37}$$

$$n_{DP} = 2^k + 2 \cdot k + cp \tag{4.38}$$

Statistical analysis

The results of the simulation campaign were evaluated using Design Expert statistical software. First, an ANOVA test was performed to assess the significance of the input parameters. Then, their impact I_{y_i,x_k} was quantified through a local sensitivity analysis, by dividing the variation in the response due to a single parameter by its total variation range (Eq. 4.39). Finally, the statistical results were compared to evaluate the effect of the fluid viscosity on the treatment.

$$I_{y_i:x_k} = \frac{\max(y_i(x_k)) - \min(y_i(x_k))}{\max(y_i) - \min(y_i)} \tag{4.39}$$

Results and discussion

The results of the three simulation campaigns, in terms of average product temperature and pressure drop for the 9 simulated DPs are presented in Fig. 4.42a and 4.42b. The

calculated average product temperature on the outlet section, y_1, as well as the minimum and maximum temperature values, y_2 and y_3, are presented in Fig. 4.43.

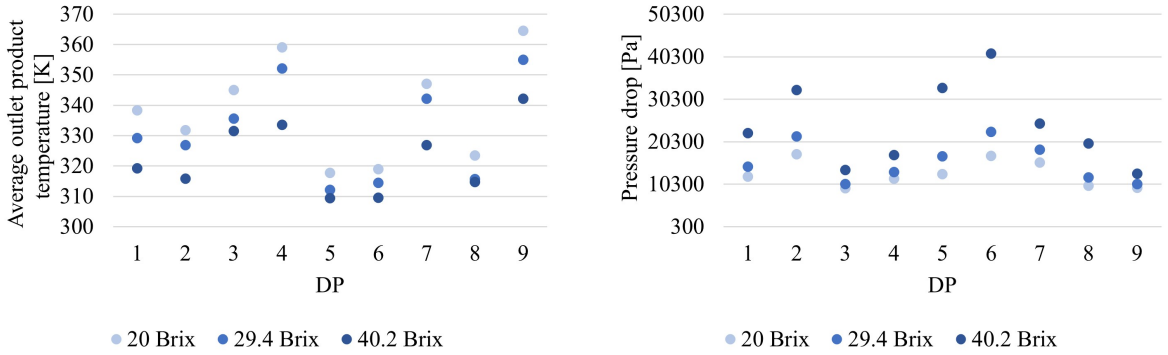

(a) Average outlet product temperature.

(b) Pressure drop, product side.

Figure 4.42: Results for different concentrations of juice in the 9 DP simulated.

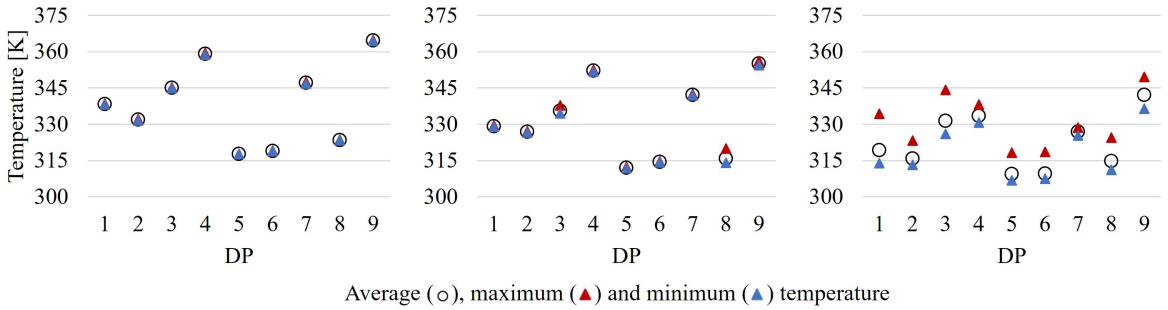

Figure 4.43: (a) Average outlet product temperature and (b) Pressure drop, product side, for different concentrations of juice in the 9 DP simulated

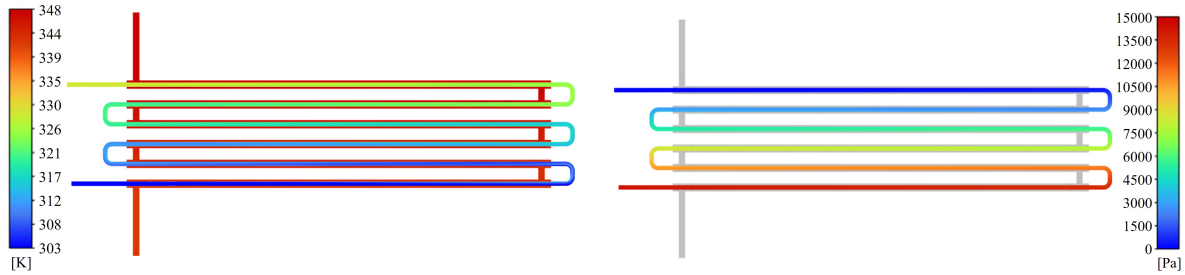

(a) Contours of temperature.

(b) Contours of pressure.

Figure 4.44: Contours on the symmetry plane for 29.4 Brix juice and DP 1.

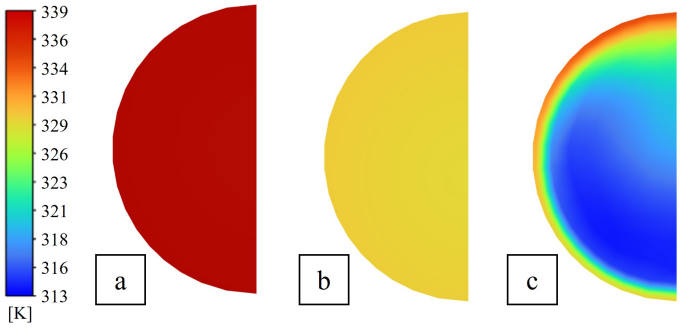

Figure 4.45: DP 1 contours of temperature on the outlet section for the juices at 20.0 (a), 29.4 (b) and 40.2 (c) Brix.

The results of the CFD simulations are shown in Fig. 4.44a and 4.44b for $DP1$ and blackberry juice at 29.4 Brix, representing the temperature and the pressure on the symmetry plane, respectively. Fig. 4.45 represents the contour plot of the outlet temperature reached in $DP1$ for the three juices evaluated, highlighting the difference in the treatment uniformity.

Responses y_1 (area-averaged outlet product temperature) and y_5 (pressure drop, product side) were analysed using Design Expert. In particular, y_1 was modelled with two-factor-interaction models, while y_5 with quadratic models, based on the software suggestions. Both the single input factors (inlet product velocity x_1 and inlet water temperature x_2) and their interactions were significant ($p < 0.05$) for y_1 in the case of 20.0 and 29.4 Brix juices, while the interaction between the factors was slightly above the significance range for 40.2 Brix juice ($p = 0.067$). Regarding y_5, both the input factors and their interaction were significant in all cases. With regards to the quadratic terms, x_1^2 was significant for 20 Brix juice, x_2^2 was significant for 40.2 Brix juice, and both x_1^2 and x_2^2 were significant for 29.4 Brix juice.

The impacts of the input parameters x_1 and x_2 on the two responses y_1 and y_5 are reported in Table 4.30. Negative impacts indicate that an increase in the input factor value generates a decrease in the response, while a positive impact leads to an increase in the response when the input increases. It should be noted that the differences in the significance of the quadratic terms, as well as the slight deviations in the calculated impacts, may be ascribed to the experimental characterization of the fluids used as input data. A visual representation of how these impacts change for the three products can be observed in the contour plots of the response surfaces in Fig. 4.46 and 4.47.

With regards to y_1, it can be observed in Fig. 4.42a that the average temperature at the outlet section decreases while going from 20 Brix to 40.2 Brix. Furthermore, in Fig. 4.43 and Fig. 4.45, it can be observed how the uniformity in the temperature strongly decreases for higher product concentrations, with portions of fluid near the wall receiving a higher thermal treatment compared to the central areas. Under the same operating conditions, therefore, more viscous products reach overall lower average temperatures,

and the uniformity of the treatment decreases. The former can be confirmed by observing the results for $DP4-7-9$ in Fig. 4.42a, characterised by the highest water temperature values, where the average temperature reached by the 40.2 Brix juice deviates the most from the other two products. The latter results in a practical insight: when treating viscous fluids, the value of the temperature measured by sensors may change considerably based on the position of the probe.

Table 4.30: Impact of the input operating parameters on the average product temperature and the pressure drop for the three products considered.

Concentration	**Impact on y_1**		**Impact on y_5**	
	x_1	x_2	x_1	x_2
20.0 Brix	-24%	+76%	87%	-13%
29.4 Brix	-18%	+82%	76%	-24%
40.2 Brix	-36%	+64%	57%	-43%

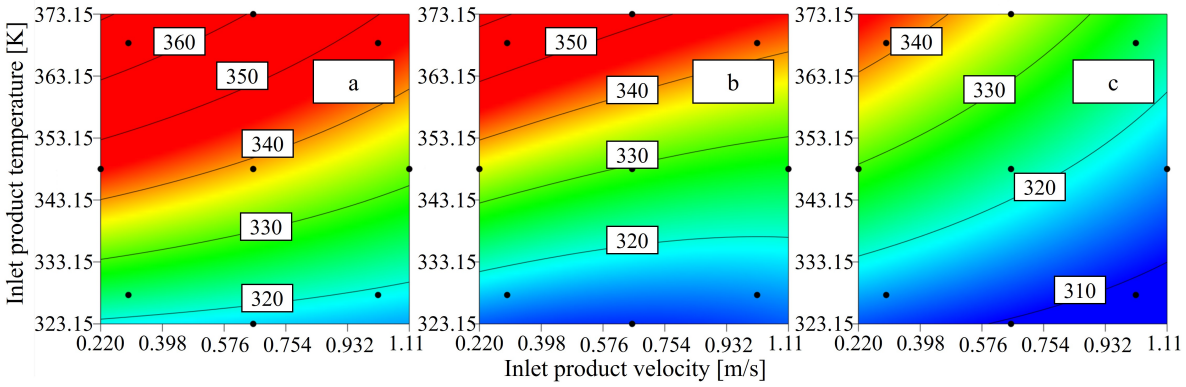

Figure 4.46: Contour plots of y_1 for blackberry juice at 20.0 (a), 29.4 (b), and 40.2 Brix (c)

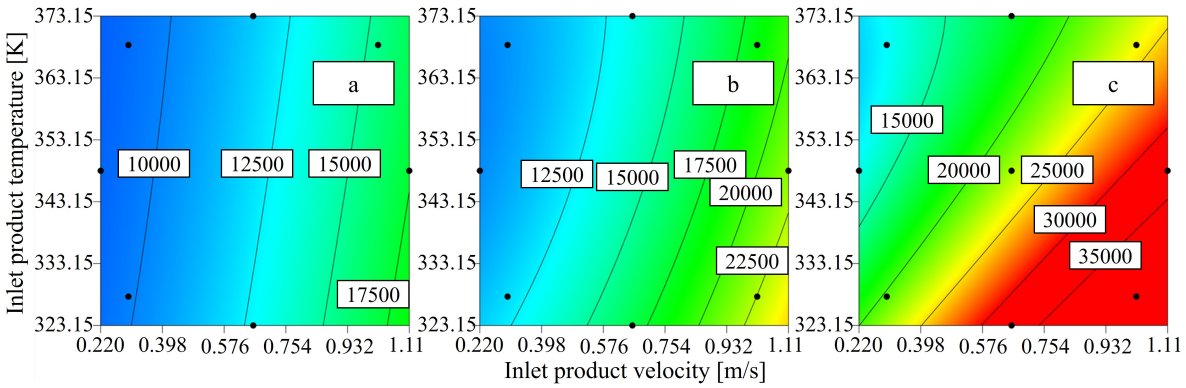

Figure 4.47: Contour plots of y_5 for blackberry juice at 20.0 (a), 29.4 (b), and 40.2 Brix (c)

From Table 4.30 and Fig. 4.46, it can be noted how the impact of the operating conditions on the outlet product temperature changes at higher viscosity values, with the

impact of the product flow rate becoming stronger and, at the same time, that of the water temperature decreasing: to achieve the desired thermal treatment of products with different rheological characteristics, the same operating conditions can not be applied. Furthermore, just increasing the water temperature would not produce the desired effect, as it would affect mainly the portion of the fluid near the pipe wall. To reach the necessary temperature and ensure the desired level of uniformity, products with higher viscosity would require lower flow rates, thus longer treatment times, and the introduction of turbulence and mixing in the system.

The calculated pressure drop, as expected, became higher as the concentration of the product increased (Fig. 4.42b). However, in Table 4.30 and Fig. 4.47 it can be observed how the impact of the operating conditions significantly changes in the three cases: while the product flow rate remains the main parameter affecting the pressure drop, the impact of the inlet water temperature strongly increases for highly viscous products: this is due to the temperature-dependence of the viscosity. Indeed, as the temperature of the product increases, its apparent viscosity decreases, resulting in a decrease in the pressure drop. This can be seen in Fig. 4.42b for the results for $DP8-9$ and $1-4-5$ where, while operating with the same product flow rate, the pressure drop decreases when the temperature of the water increases. Furthermore, observing the decrease in the pressure drop due only to an increase in the water temperature in $DP6-7$ compared to $DP8-9$ (Fig. 4.42b), as well as the contour plot in Fig. 4.47, it can be seen how the impact of the water temperature becomes stronger at higher flow rates in the case of 40.2 Brix juice.

By applying RSM techniques it is possible to generate reduced order models (ROMs) for the estimation of the responses for given values of input factors within the experimental domain. Examples of models for the expected area-averaged outlet temperature ($\hat{y_1}$) and the pressure drop ($\hat{y_5}$) are reported for blackberry juice at 40.2 Brix in Eq. 4.40 and 4.41, respectively. The same approach can be used to generate models for the estimation of the minimum and maximum product temperatures, to evaluate the efficiency of the thermal treatment and its uniformity.

$$\hat{y_1} = 71.66 + 105.46 \cdot x_{1,act} + 0.75 \cdot x_{2,act} - 0.35 \cdot x_{1,act} \cdot x_{2,act} \tag{4.40}$$

$$\hat{y_5} = 5.78 \cdot 10^5 + 1.29 \cdot x_{1,act} - 3181 \cdot x_{2,act} - 318.08 \cdot x_{1,act} \cdot x_{2,act} + 3015.68 \cdot x_{1,act}^2 + 4.44 \cdot x_{2,act}^2 \tag{4.41}$$

After modelling the values calculated with simulation through RSM, furthermore, these can be leveraged to determine the most suitable operating conditions to achieve the desired treatment. For example, numerical optimization can be applied to define an operating condition that would allow the product to reach the required temperature, by setting the desired minimum outlet temperature ($y_2 = constant$), while minimizing the

risk of overheating the fluid near the walls ($min(y_3)$).

Practical implications

The analysis allowed for evaluating how, for a given plant, the product characteristics affect the thermal treatment. The results highlighted how the heating achieved in a tube-in-tube heat exchanger and the impact of the operating conditions are strongly influenced by the change in viscosity. Overall, more viscous fluids displayed a decrease in the average temperature on the outlet section, an increase in the pressure drop and a lower heating uniformity, pointing out how the thermal treatment of different products needs a careful definition of the appropriate operating conditions. In particular, in the case of highly viscous fluids, higher treatment time and an increase in the mixing of the product would be necessary to reach the required temperature and uniformity. The mixing could be achieved by increasing the number of bends and/or randomly varying their orientation, or by switching to a coiled pipe heat exchanger.

Models such as those presented in Eq.4.40 and Eq.4.41 that estimate the expected outputs, e.g., product temperature and pressure drop, based on the input operating conditions, allow to verify the correspondence between the expected standard conditions and the actual measured ones. These ROMs, overcoming the limitations of CFD simulation in terms of time and resource requirements, can be implemented in real-time monitoring and control of industrial plants, promptly highlighting deviations from the expected operating conditions. After a preliminary evaluation phase, the deviations could be linked to potential failures: in the case of highly viscous products, for example, a decrease in the outlet product temperature under the same operating conditions could be a sign of the onset of fouling on the pipe walls. In addition, numerical optimization of the responses can be implemented during the design phase to tune the treatment based on a series of objectives and constraints.

The issue of poor temperature uniformity as the viscosity of the product increases results in the risk of insufficient heating of some portions of the fluid. It is also difficult to univocally assess the outlet temperature of the product, as its value appears to strongly change depending on the location of the temperature probe. To this end, numerical simulation combined with statistical techniques, as in the presented approach, could be an essential tool as it is possible to estimate the physical quantities of interest at every point of the device, even where sensors could not be installed, resulting in virtual sensors. As CFD results convey information about the temperature distribution in every point of the domain, based on the value experimentally measured by the physical probe and its position, it is possible to model and derive the temperatures in critical points of interest. For example, with the probe inserted at a given distance from the pipe wall, it would be possible to derive the temperature at the wall and in the centre of the pipe.

Conclusions

A simulation campaign was designed according to DOE methodology and performed with CFD simulation to replicate the functioning of a heat exchanger for viscous food fluids with three different juices at several operating points, defined by changing the inlet product velocity and inlet water temperature. By carrying out three parallel simulation campaigns for three fluids, a total of 27 simulations were run. The results were evaluated with statistical methods to assess the impact of the input factors on the thermal treatment and obtain practical operational insights.

The novelty of the present work is threefold. Firstly, the CFD results are the starting point for an exploratory sensitivity analysis of the thermal treatment of different food products with a given device. This evaluation should be carried out by practitioners while designing a treatment or introducing new products, as it clearly emerges how the same device can not perform effectively and efficiently with different product concentrations. Secondly, we aim to promote the implementation of the presented approach, which combines CFD and statistical modelling, in a sector such as the food industry, that often relies on few physical sensors displaced across the plant. As can be seen in the results for the most viscous fluid, knowing a single value of outlet temperature is not enough to characterise what is happening inside the device. Being able to derive a temperature profile, by leveraging virtual sensors, would be essential in aiming to achieve increased food safety and quality, in the perspective of an "informed" and smart manufacturing. Finally, we aim to encourage the implementation of ROMs built on simulation data for the real-time monitoring and control of food industry plants, as they allow to estimate the process outputs, even with complex fluids and geometries, highlighting the deviations from the expected conditions that may be linked to the onset of failures.

The present study is based on a numerical model already validated in real-time with a non-Newtonian fluid at different flow rates and water temperatures. However, in view of a practical application with a specific viscous food fluid, possibly containing suspended solids, future activities involving additional experimental validations would be required to finely tune the simulation settings and the parameters of the rheological model.

Chapter 5

Simulation approaches for management and optimization of warehouse systems

Contents

5.1 Simulation of inventory systems for perishables

Almost every system that produces physical items is characterized by an inventory, whose primary aim is to decouple supply and demand. The discipline that studies how to effectively and efficiently design and operate inventory systems is referred to as "*inventory management*". The main goals of an inventory management system include economic optimization, achieving a target service level (defined as the fraction of customer demand that is met), and minimizing wastes.

Depending on the source of the stored products, that can be bought or self-produced, for a given inventory it is necessary to correctly size the operating leverages of the replenishment policy. If products are sourced externally, optimizing reorder policies is crucial, including defining optimal levels for operational decisions operating leverages, which can be summarised as *when to order*, and *how much to order*. The main policies in this context include, among others:

- Periodic Review Policies: Products are ordered at fixed intervals, with each order bringing stock up to a target order-up-to level ($OUTL$).
- Continuous Review Policies: Stock levels are continuously monitored, and orders are placed when levels drop below a safety threshold. Orders may be of a fixed size or bring stock back to the $OUTL$.

While basic cases can often be optimized using classical analytical approaches, the complexities of real-world conditions make more flexible tools necessary. In this context, simulation becomes of great value, as it allows understanding complex dynamics and improving decision-making in inventory management.

In these types of applications, one of main simulation techniques applied are Discrete-Event Simulation (DES) and Discrete-Time Simulation (DTS).

- DES is a method used to model systems where changes occur at distinct points in time, triggered by specific events, such as arrivals, departures, or reordering. This type of modelling is often applied for applications where events happen irregularly but impact the system state, like manufacturing or queuing systems.
- DTS, on the other hand, model systems by updating them at regular, fixed intervals, for example every week, day, or hour. DTS is a simple simulation approach that is commonly used in systems where periodic updates are suitable, such as inventory levels or financial forecasting. This approach is very flexible, and allows to model the effects of different replenishment strategies in a controlled, replicable digital environment. The discrete intervals used for the simulation must be chosen based on the typical operational frequencies of the modelled system, intended as time intervals that pass between critical events like order arrivals and demand fulfilment.

In the studies presented in the following sections, DTS has been applied to model inventory management systems for perishables. In addition to standard inputs like demand parameters, lead time, and operating costs, this applications requires considering product shelf life, which heavily impacts the approach to inventory management. A daily time step has been used; at the start of each day, operations such as demand fulfilment, order processing, and disposal of expired products are performed and recorded.

A key feature of inventory management for perishables is the modelling of demand. In B2C (business-to-consumer) scenarios, demand for items with expiration dates is highly age-dependent. Consumers prefer fresher products for their higher perceived quality and longer usability. If inventories are not managed properly, this can lead to significant food waste, which is a well-known and critical issue.

Some of the studies included in the following sections evaluate strategies to optimize inventory management and reduce food waste in retail. One of these targets consumers through discounts on expiring products, while another targets retailers by evaluating the impact of penalties on disposed goods. In both cases, the studies highlight that modelling demand as age- and/or price-dependent is essential to accurately reflect real conditions and produce meaningful results. Regarding the first study, the simulation model will be enhanced with insights from a survey about actual consumer behaviour in presence of discounts on expiring items, bringing the model even closer to real-world conditions.

5.2 Warehouse management of perishable products: overview of the literature on modelling approaches

The content of this chapter is part of the article "*Simulation of reordering policies for perishable products under service level constraints: sensitivity analysis based on DOE and RSM*", by Solari F., Lysova N., Volpi A., Montanari R. and Bottani E., submitted and currently under review at the journal International Journal of Systems Science: Operations & Logistics.

"Perishable" products are items whose characteristics decay or deteriorate over time. These products, indeed, can be subject to depletion, decay, and spoilage, or even experience a decrease in their value due to reduced functionality [253]. The length of the time in which a perishable item remains fit for consumption and sale is defined as "shelf life", which represents the key difference between perishable and non-perishable items [254]. Generally, the condition of perishability applies to products with a shelf life shorter than two weeks [255].

Modelling techniques can be extensively leveraged to analyze inventory management systems for perishable products and optimize their operation. Generally, the approaches to model and optimize inventory management policies can be divided into analytical and numerical, e.g., simulation-based.

This section provides a brief literature overview of the analytical and numerical inventory models for perishable products, possibly coupled with statistical methods for sensitivity analysis, and of the service parameters typically considered.

In the following Section of the thesis, based on the literature review presented, a sensitivity analysis is carried out in the case of periodic review inventory management for perishable product under service level constraints, to evaluate the impact of the operating condition on the optimal levels of the operating leverages that allow to minimize the total management costs.

Modelling approaches

Analytical methods

When modelling perishable item inventory systems, analytical approaches often require simplifying assumptions, mostly relating to the demand distribution, the procurement lead time and the deterioration rate or shelf life of items. Tuan, Hung, and Yang [256] have described an economic order quantity (EOQ) model for perishable items, hypothesising fixed shelf life and non-increasing generalized demand, while neglecting the lead-time effect. The authors start from the consideration that as opposed to stable products, perishable items feature a limited time range in which they can be sold and gradually lose their value over time. However, before the expiry date is reached, these products do not necessarily change their characteristics; this justifies the assumption of fixed shelf life. Yadav and Khanna [257] have taken a different perspective, assuming, instead, that the continuous decay in product characteristics has an adverse effect on the customer's demand. In the study, the authors have developed an inventory model for perishable products with a price-sensitive demand and zero lead-time. Berk and Gürler [258] have developed an analytical model for the optimization of inventory management in the case of perishable products, assuming positive lead time and lost sales. The goal of the study was to provide insights for effective inventory strategies, to minimize the occurrence of stockouts and maximize profitability. Chen et al. [142] have proposed an analytical approach for the minimization of the total cost assuming zero lead time, First In Firs Out (FIFO) issuing policy, two-period shelf life and a replenishment cycle equal to the shelf-life time of the perishable product. They have also included the possibility of adjusting inventory in the middle of the selling cycle, including a mid-cycle expedited order, a mid-cycle returns plan or a combination of expedited orders and returns. They demonstrated that the expedited order plan is more effective in controlling wastage risk but increases shortage risk compared to the returns plan. A combined plan of both strategies offers a balance, lowering total costs and optimizing resource allocation. Kouki et al. (2020) have considered a base stock inventory system for perishables and derived explicit expressions for the stationary distribution of the system state and the total expected cost by employing a queuing network approach to investigate a positive replenishment lead time together with a general lifetime distribution. Gutierrez-Alcoba et al. [259] have analyzed a periodic review inventory system with service level constraints and a reorder period of one day, including a fixed ordering cost; they have derived an approximate analytical model to compute the expected value of inventory in the case of finite and discrete shelf life. They have finally compared the results of the analytical approximation with two extensions of Silver's heuristic, and they have demonstrated that the proposed heuristics generally outperform the analytical approximation.

Simulation approaches

As opposed to analytic models, simulation-based approaches allow for obtaining solutions characterized by good accuracy, even in complex contexts with numerous uncertainty factors, and as such, they are frequently applied to supply chain or inventory management problems [260]. Montanari et al. [261] have adopted a simulation approach to reproduce an Economic Order Interval (EOI) inventory control model for perishable items under different operating conditions. Haijema, Van Der Wal, and Van Dijk [262] have optimized a double-level order-up-to rule applied to a Poisson demand distribution, by combining Markov dynamic programming and simulation. Haijema and Minner [263] have conducted a simulation analysis to compare the performance of standard single-parameter policies, i.e., base-stock-policies (BSP) and constant order policies (COP) and hybrid COP-BSP policies, with the number of operating parameters ranging between two and four. These additional parameters were introduced to improve the performance of single-parameter policies in the management of perishables, with the aim of preventing overstocking and reducing the number of expiring products. The authors have instead chosen to neglect the cost of order issuing and have assumed a fixed review period of one day. Other assumptions of this study include constant and deterministic shelf life and lead time, and static, normally distributed demand, divided into two fractions: one satisfied according to a FIFO policy and the other satisfied according to a last in first out (LIFO) policy. The authors have evaluated the system performance, in terms of the average cost, under different operating conditions. Again, Haijema and Minner [2] have developed a simulation-based optimization for perishable items handled at supermarkets, focusing on age-dependent order policies. The assumptions of their model include short and fixed shelf life of items, stochastic demand (with a fraction satisfied following FIFO policy and the other satisfied following a LIFO policy) and fixed lead time. Lowalekar, Nilakantan, and Ravichandran [264] have instead modelled a periodic review policy for perishables, assuming random issuing of items from the inventory, so that neither the FIFO nor LIFO logic is strictly followed. The rationale behind this choice is that the FIFO policy does not fit all real scenarios; rather, it is typically observed in those contexts in which the supplier has sufficient control over the inventory and order preparation. Kouki et al. [265] have used a Markov renewal process to develop an algorithm for the optimization of the expected total cost in the case of a periodic review inventory system with both lost sales and backorders, and perishable products with a random lifetime distributed exponentially. The authors have shown that in many cases the order issuing cost cannot be neglected, and, in these situations, it is more convenient to adopt reorder periods longer than one day. They have compared their results with those obtained with a classical periodic review model in which the perishability is neglected, and with a model in which the perishability is modelled using a deterministic shelf life. The results have shown that neglecting the perishability of the products leads to an underestimate of the

expected operating costs by 34% and 30% in the case of lost sales and backorders, respectively. Moreover, ignoring the randomness of the shelf life resulted in an underestimate of costs of up to 15% and 13% for lost sales and backorders, respectively. The authors have made no remarks about the service levels achieved with their model.

Replenishment policies

Another classification can be made according to the reordering policy considered: because of their ease of application, periodic review policies in the context of perishable items are relatively popular [264]; nonetheless, in the literature, there are also studies adopting and comparing other inventory management policies. Montanari et al. [266] have developed a simulation model for perishables under an EOQ policy. Wei and Chen [267] have extended the newsvendor problem to a multiperiod scenario in the case of a supply chain of perishable items, assuming a demand with normal distribution and price dependence. A comparison of different reorder policies for perishable items, supported by simulation, has been conducted by Piva et al. [268] in the specific case of an Italian company.

Service levels

When managing inventories, the decision maker will certainly consider the economic suitability of the policy (cost minimization or profit maximization), but in practice, the achievement of a target service level will also be required; this is exacerbated in the case of perishable items, because of the risk involved by uncertain demand and decay in the product properties in time [269]. Popular definitions of the service level constraints have been made in terms of the non-stockout probability, inventory fill rate or backordered product/lost sales; these parameters have been applied to general inventory management studies (see, e.g., [270–272], as well as in some studies targeting perishable products (e.g., [265, 269]. Minner and Transchel [269] have described a periodic review policy for perishable products under random demand, assuming deterministic lead time and shelf life. They have developed a numerical dynamic model assuming that orders were issued at the beginning of each day with a negligible order cost. They have compared different replenishment policies under service level constraints based on the average inventory level and the average amount of products disposed of, and have demonstrated that, in these conditions, a dynamic replenishment model outperforms the two simpler BSP and COP policies. Gutierrez-Alcoba et al. [259], as described in the introduction, modeled a similar scenario while including a fixed ordering cost. Pauls-Worm et al. [273] have modelled analytically an EOI policy for a manufacturer of perishable items, facing uncertain demand and having to meet a given service level at the minimum cost, including setup cost, production cost, cost of holding stocks and cost of disposal. The model assumes zero lead time and backlogging of shortage; the service level is measured as the probability of not being out-of-stock. Balugani et al. [274] analyzed a periodic inventory control system of perishable products with fixed lifetime and intermittent demand and proposed a method to assess the order-up-to-level to satisfy a target fill rate service level.

They demonstrated that considering both intermittent demand and product perishability significantly improves inventory management strategies. Babaï et al. [275] focused on a dynamic re-order point inventory policy considering both demand and lead time variability. They derived the operating parameters to meet a given target service level and they demonstrated that the dynamic policy outperforms the static policy allowing a considerable cost reduction.

Statistical evaluation

Finally, concerning the analysis of the results, many authors have performed statistical evaluations to assess the impact of the variations in the input parameters on the monitored outputs. [276] have developed an inventory control model, again supported by simulation, for perishable items with a demand rate that is variable (in an attempt to reproduce the uncertain behaviour due to the pandemic emergency), and dependent on the inventory rate. The model also considers backlogging and lost sales, while deterioration of items is modelled as a time-dependent variable. A sensitivity analysis is finally carried out to study the impact of the key problem variables on the resulting inventory policy parameters (i.e., the lot size in particular) and total cost. Some additional examples of studies that have applied sensitivity analyses to inventory management policies include the studies [172, 277, 278]. All these studies make use of RSM as the tool for conducting sensitivity analyses [279] and for modelling and evaluating the extent to which the response of interest depends on a set of input factors [245]; however, none of these studies refers to the context of perishable items. Indeed, Tang et al. [**?**, 277] have combined system dynamics simulation, Taguchi method, and RSM to model a multi-echelon supply chain and optimize the total profit and customer service level. Wang, Dang, and Nguyen [278] have leveraged RSM to determine the optimal levels of some key factors, such as order quantity, reorder point, target stock, and inventory review policy, for minimizing inventory holding cost and penalty cost due to backlog in an (S,s) replenishment policy. Finally, Yang et al. [172] have proposed RSM as a tool to analyze the optimal inventory policy as a function of different risk preferences of decision-makers, in a multi-echelon supply chain.

5.2.1 Discrete-time simulation of inventory management policies for perishable items: definition of the simulation approach and sensitivity analysis in a B2B scenario

The content of this chapter is part of the article "*Simulation of reordering policies for perishable products under service level constraints: sensitivity analysis based on DOE and RSM*", submitted and currently under review at the journal International Journal of Systems Science: Operations & Logistics.

The supplementary material of this study is available at DOI 10.17632/dg6n8mbypm.1.

Abstract

A multi-period inventory management model for perishable products is developed using a simulation approach. A single-product scenario is modelled under both continuous and periodic review policies, considering Weibull demand, non-null deterministic lead time, a combination of lost sales and backorders, fixed product shelf life and service constraints. Eight inputs, including managerial aspects and product's characteristics, and six outputs, i.e. the minimum cost and the operating leverages of the two policies, are evaluated based on Design of Experiments. Discrete-time simulation is used to determine, for each design point, the optimal operating leverages, namely target stock level, reorder period and base stock, which minimize the total cost with service constraints. The outcomes were then analysed, according to ANOVA and Response Surface Methodology, to assess the impact of each input parameter on the selected responses. Results show that the optimal operating leverages mainly depend on demand features, some unitary costs (order issuing in particular), shelf life and lost sales fraction. The shelf life results to be significant only below a given value, which mainly depends on the shape factor of the demand distribution; for greater shelf life values the products could be managed as non-perishable, from an inventory point of view.

Introduction

The physical and organoleptic properties of some categories of products, such as fruits, vegetables, or blood, decay constantly during the storage period. For these products, the shelf life is assumed to be stochastic and to vary depending on numerous factors, including storage conditions, product characteristics, and origin. For other categories of products, like canned food and beverages, the shelf life is instead determined by the expiry date, and thus it is deterministic. The properties and the commercial value of these products remain stable during the storage period; on the contrary, when the items reach the expiry date, they lose their value altogether and must be disposed of.

The challenging issue of managing inventory of perishable products has been addressed in the literature with increasingly complex models, to account for the many uncertainty factors that could arise. A typical goal of inventory management models is to minimize the system's cost while ensuring an adequate level of customer demand satisfaction. These aspects, however, can be somewhat conflicting: higher stock levels, that would allow for meeting the customer demand in full, could lead to excessively high costs for holding the product in stock; in the case of perishable items, further costs could arise for disposing of the expired product. On the other hand, reducing the inventory level would cause the operating costs to decrease but will expose a company to the risk of not being able to satisfy the customer demand in full, involving possible stock-out situations, with consequent costs and penalties. Hence, it is not always true that the best solution from an economic perspective corresponds to a high service level, but at the same time, focusing on the service factors only could lead to selecting configurations with very high operating costs. For the management of the inventory system to be cost-effective while ensuring the reliability of the company towards the clients, both economic and service aspects must necessarily be evaluated together, and an optimal trade-off between them must be achieved.

Service level measures are widely adopted by companies practice, since service agreements are often signed between suppliers and customers, and service level constraints are commonly applied in practical settings [272]. Agreements can also be set between manufacturers and customers [280], with the purpose of coping with stock out situations instead of quantifying a penalty cost, which could be challenging. Looking at the inventory cost, both analytical and numerical approaches have been applied in the literature to optimize inventory management from an economic point of view. However, to be able to solve the problem analytically, it is often necessary to make simplifying assumptions. Simulation approaches have therefore been introduced as valid alternatives to analytical methods, as they allow for obtaining solutions of good accuracy, even in complex contexts characterized by numerous uncertainty factors. These models can also be empowered by coupling them with heuristic and metaheuristic methods, thus decreasing the computational time

required to return effective solutions [281, 282], or, as observed recently, with big data analysis techniques, reducing the number of assumptions required [283, 284].

This study starts from an analysis of the scientific literature, reported in Section 5.1. This analysis was conducted to provide a comprehensive and exhaustive overview of the state of the art on the topic and to focus the study on the most unexplored aspects.

This preliminary analysis not only highlights the innovative aspects of this study but also allows the identification of other gaps that are worth considering in future research activities. This comprehensive analysis reveals that, to date, no studies have simultaneously considered the economic optimization of inventory management systems for perishable products with service level constraints.

This study aims to fill this gap, using an integrated approach that makes use of simulation, Design of Experiments (DOE) coupled with a variance-based sensitivity analysis (ANOVA), and finally Response Surface Methodology (RSM). A discrete-time simulation model for a warehouse handling perishable items was first developed, and two inventory policies (periodic and continuous review) were then reproduced in a multi-period environment, to make a quantitative comparison between the two scenarios. The model returns, as output, the total cost of the inventory system and some relevant service parameters, assuming Weibull demand distribution, non-zero deterministic lead time, deterministic product shelf life, and a combination of lost sales and backorders.

After defining the appropriate input factors and their variation range, a simulation campaign is launched, covering a finite number of system configurations (design points), according to the DOE methodology. Each configuration is optimized, in terms of the minimization of the total cost, through simulation. This allows for determining the values of the operating leverages of each inventory policy that minimise the total system cost while ensuring that a target service level is reached. ANOVA is then applied on the outcomes obtained to evaluate the statistical significance of each input parameter on the observed output; the impact of the operating parameters and of the product shelf life on the system cost under optimal conditions is also evaluated. RSM is finally used following the approach previously adopted and validated in [92].

Novelty and contribution of this work

This study contributes to the literature in several ways. First, the review above highlights that research papers focusing on the context of this study have in general optimized the inventory management of perishable items by considering either the economic effectiveness [265] or the service level constraints [269], but both aspects have rarely been evaluated simultaneously. The only exceptions are the studies [272] and [273]; however, while the former study does not focus on the context of perishable products, the second has not integrated backlogging and shortage in the analysis. Also, typical inventory management studies on perishable products have dealt with modelling and optimizing

one selected policy, while one study only has compared more policies for perishables (i.e., [268]); in this last paper, however, the analysis made is in the form of a case study and therefore results are specific to the context analysed. The model developed in this study is more general in nature. Indeed, it embodies two inventory policies (periodic review and continuous review), which are optimised in economic terms (minimum cost), by simultaneously taking into account service level constraints; comparative results among the different policies are thus offered. Looking expressively at the economic analysis, the model takes into account numerous cost components of the inventory system, resulting in a comprehensive evaluation. Second, the methodological approach used in this study is more structured compared to the existing ones, as it consists in a combination of various tools; in particular, it exploits RSM, which, although sometimes implemented for the optimization of inventory management policies [277, 278], has never been applied to the context of perishable products. Using this technique to elaborate the simulation results could help identify the factors that affect the inventory management performance to the greatest extent, including the typical characteristics of perishable items (e.g., shelf life). Finally, in this study, a detailed analysis of the impact of shelf life on inventory management is presented; in particular, the shelf life value below which perishability is a significant factor is highlighted.

Research methods

Simulation model formulation

The scenario reproduced by the model is a business-to-business context of the retail sector. The central player of the system, for which the inventory policies are evaluated, could be, e.g., a distribution centre, which delivers perishable products to its customers, e.g., retail stores; the case in which final consumers issue orders directly to the central player is neglected in this scenario. The inventory model, and therefore the analysis, focuses on a single type of perishable product. The product type is not specified a priori, because in the set of analyses made, the shelf life can vary (and this prevents the possibility of defining a unique product). The central player issues orders to its supplier and uses its on-hand inventory to satisfy the daily demand of the customers' d_i (Figure 5.1); this latter is modelled using a Weibull distribution, characterized by two parameters, namely the scale factor (D_a) and shape factor (D_b), thus fitting many real distributions, even non-symmetrical and with small samples of historical data [285]. Table 5.1 provides a brief overview of the assumptions adopted in this study.

The commercial value of the product remains constant until the last day of shelf life (SL), which marks the expiry date. The expired product loses its value altogether, as it is assumed to be completely deteriorated and therefore it has no potential to be longer sold. At the beginning of each working day i ($i = 1, \ldots, N$), therefore, the warehouse

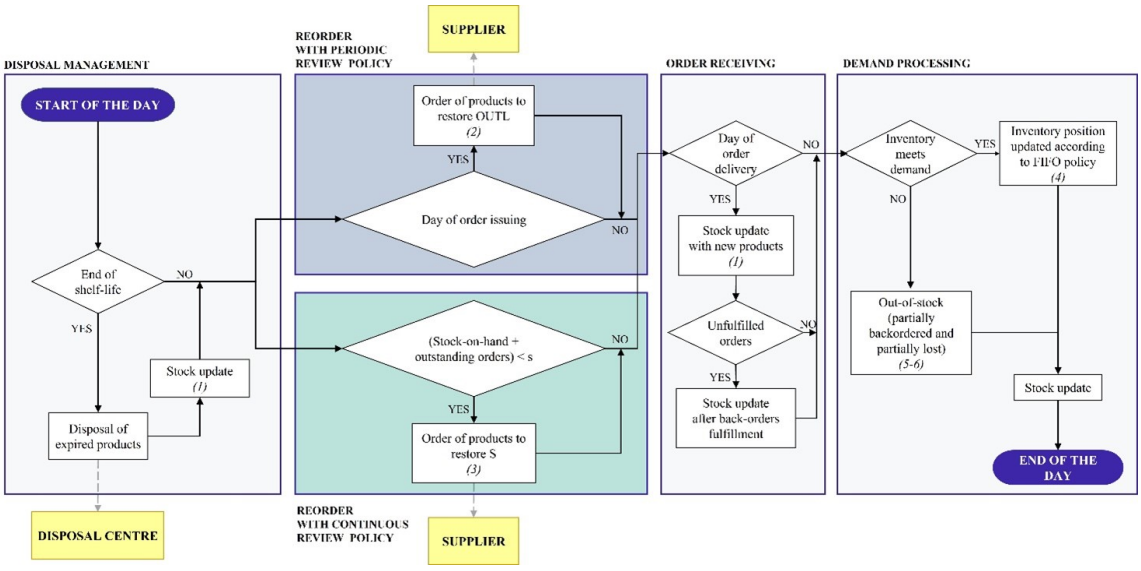

Figure 5.1: Flowchart of the proposed approach.

manager must review the stock-on-hand (OH_i) to check for expired items (Q_exp, i) that should be disposed of.

According to the periodic review (PR) policy, orders are issued at regular time intervals (DT), while in the continuous review (CR) policy, orders are issued when the stock-on-hand added to outstanding orders is lower than a base stock (s). In both cases, a variable quantity is ordered such as to restore the target stock level ($OUTL$ and S respectively). At any moment in time, there can be at most one replenishment order; also, no interactions occur between the ordering period and procurement lead time (LT), which is assumed to be deterministic and set at 1. In line with the fact that the central player of the system is a distribution centre, the volume of items handled is expected to be high, and thus, some parameters are assumed to have discrete values only, multiple of 500 product units; this is the case for $OUTL$, S and s. This assumption fits, for sure, the case for the PR policy, in which orders are placed at regular time intervals, resulting in the aggregation of numerous items; to ensure uniformity in the model and results obtained, the same conditions are also assumed for the CR policy. The unitary order-issuing cost is fixed and independent of the quantity ordered, as it mainly refers to administrative procedures and transport fees. The batches of products ordered (O_i) are shipped by the supplier and delivered to the warehouse after a fixed and deterministic LT; the products shipped or received together are assumed to have the same SL. The products start decreasing their SL as soon as they are shipped by the supplier. Hence, inventory management is age-dependent, and the age of each product stored is monitored and continuously updated as described later.

Anytime the demand is fulfilled using the available inventory, a strict FIFO logic is followed; this assumption is in line with Lowalekar et al. (2016), who stated that the FIFO policy is typically applied by players having sufficient control over the inventory and

order preparation, which could certainly be the case for a distribution center. Although the FIFO policy is not exactly the same as the first expiring first out (FEFO) policy - which could sound even more appropriate for perishable items - in most real contexts, the two logics coincide. Indeed, if a product is received at the retail store on a given day, it is implicit that its expiry date must be subsequently compared to a product received yesterday; this means that the distribution centre has followed a FIFO policy when fulfilling the order. Hence, the FEFO policy implies the FIFO logic, as well. It follows that the oldest products are the first to be sold, as they were the first to arrive. If their amount is not sufficient, newer items can be used to meet the demand. In mathematical terms, the products delivered at time $i + LT$ are labelled as "New" until another lot of products is delivered at time $i + DT + LT$. These latter items will thus be labelled as "New", while the former will be classified as "$Old1$". When another order is received, the products will be labelled as "New"; the former "New" products will be labelled as "$Old1$"; the former "$Old1$" products, if there are any left, will be labelled as "$Old2$", and so on. The model developed is designed to handle up to ten levels of "Old" products, thus allowing to reproduce a wide variety of stock conditions of perishable items. For the sake of brevity, the "Old" label will be used in this article to refer to "Old" products of any level, to account for all the products stored in the inventory that are not "New". Looking at the service performance, if OH_i, i.e., the sum of "Old" and "New" products, does not meet the d_i, an out-of-stock is observed and the unmet demand is fully or partially back-ordered, according to the specific inventory conditions and customer contracts. The fraction of the customer demand lost due to out-of-stock is expressed as the percentage of lost sales ($\%LS$). Several conditions of $\%LS$ were simulated in this study, to capture different scenarios. As opposed to LS, the fraction of demand backordered (BO) is not lost; rather, it is recorded and cumulated until a new batch of products is delivered, so that the orders can be finally fulfilled. The economic losses due to the LS are included in the stock-out cost, while the delayed fulfilment of the customer demand (BO) does not result in penalties. Service levels α_i, β_i and γ_i are calculated for each day: (i) non-stockout probability at day i, α_i, is equal to 100% if d_i is completely met with OH_i, while it scores 0% if a shortage occurs; (ii) the fraction of di met with OH_i at day i, β_i ; (iii) the total quota of the customers' demand met, γ_i, which includes β_i and the demand fulfilled with BO, thus accounting for the incidence of the LS only.

According to the description above, in the model the following actions are taken for each day i:

1. The residual SL_i of the products in stock is decreased by 1;

2. Products with SL_i=0 are disposed of ($Q_{exp,i}$);

3. OH_i is updated based on $Q_{exp,i}$ and the orders placed LT days before ($O_i - LT$),

Table 5.1: Model assumptions

Topic	**Symbol**	**Assumption**
Daily demand	d_i	Stochastic, modelled with Weibull distribution with known scale factor D_a and shape factor D_b
Replenishment policies	PR, CR	Periodic review, Continuous review
Lead Time	LT	Deterministic, non-null, equal to 1 day
Reorder period	DT	(PR) Deterministic, discrete
Target stock level	$OUTL$	(PR) Deterministic, multiple of 500
Base stock level	s	(CR) Deterministic, multiple of 500
Target stock level	S	(CR) Deterministic, multiple of 500
Inventory composition		Single product
Shelf life	SL	Deterministic
Product commercial value		Constant during shelf life, null afterwards
Inventory management		Age-dependent
Stock-on-hand	OH	Sum of the "New" and "Old" products
Issuing policy	$FIFO$	First-In-First-Out
Shortages	LS, BO	Lost sales and/or back-orders, according to $\%LS$
Service level	α, β, γ	Non-stock-out probability, fill-rate, total fill rate

resulting in the following transition formula:

$$OH_i = OH_{i-1} - Q_{exp,i} + O_{i-LT} \tag{5.1}$$

4. The replenishment is managed according to either the PR (branch a) or theCR (branch b) policy: a) If an order was scheduled for day i, a batch of items useful to restore $OUTL$, including possible back-ordered quantities BO_i, is ordered:

$$O_i = (OUTL - OH)_i + BO_i \tag{5.2}$$

b) If OH_i is lower than a defined base stock s, an order is issued to restore the target stock level S, following the same logic as above:

$$O_i = (S - OH)_i + BO_i \tag{5.3}$$

5. d_i is fulfilled according to the FIFO policy;

6. If OH_i meets d_i, the stock is updated accordingly and α_i is set at 100

$$OH_i = OH_i - d_i \tag{5.4}$$

7. If OH_i does not meet d_i, LS_i and BO_i quantities are computed as follows, and α_i is set at 0

$$LS_i = (d_i - OH_i) \cdot \%LS \tag{5.5}$$

$$BO_i = (d_i - OH_i) \cdot (1 - \%LS) \tag{5.6}$$

8. The remaining service parameters are finally computed as follows:

$$\beta_i = \frac{min(OH_i, d_i)}{d_i} \tag{5.7}$$

$$\gamma_i = 1 - \frac{LS_i}{d_i} \tag{5.8}$$

Cost computation

The total inventory management cost is computed as the sum of the relevant cost items, which, for the case of perishable items, include inventory holding cost, order issuing cost, stock-out cost, and disposal costs.

1. Inventory holding cost [€/unit/day] ($C_{inv,i}$): it reflects the cost of keeping the products in stock. Generally, it is variable as it depends on the number of items stored. In this study, it is computed as:

$$C_{inv,i} = OH_i \cdot c_{inv} \tag{5.9}$$

2. Order issuing cost [€/order] ($C_{oi,i}$): the cost of generating an order includes, among others, the costs related to order invoicing, goods transportation, and receiving operations (unloading, control, allocation, etc.). Most authors (e.g., [286] or [256] have assumed the order issuing cost to be independent of the order entity. Other researchers, like Ozyoruk et al. [287], have instead assumed the cost to be composed of a fixed quota and a variable quota depending on the ordered quantity. In this study, the former approach is followed, and therefore, order issuing generates a cost (Coi, i) that is fixed and independent of O_i;

3. Stock-out cost [€/unit/day] ($C_{so,i}$): this cost is incurred in by a company when the demand is greater than the stock-on-hand. The stock-out cost is generally difficult to assess, as it must consider numerous aspects depending on the management context, such as the possibility of backorders, penalty cost, lost sales, substitution, purchase of products from an external supplier, and image damage of the company. Authors have taken different perspectives to model this cost: Luo [288] has assumed the shortages to be allowed, and the unitary stock-out costs to be known and fixed, while Vijayan and Kumaran [286] have introduced fuzziness in the cost parameters, including stock-out cost, to evaluate the impact of the impreciseness of the cost

components on the total cost. In this study, it is assumed that the unitary stock-out cost is known, so that $C_{so,i}$ is calculated by considering the fraction of lost sales multiplied by that unitary cost:

$$C_{so,i} = LS_i \cdot c_{so} \tag{5.10}$$

4. Disposal cost [€/unit/day] ($C_{disp,i}$): based on the product characteristics, this cost may be associated with the loss of value due to deterioration, to the disposal of the products that have reached the end of their shelf life, or to both aspects. Muriana [289] has introduced an outdating cost that occurs when the product remains unsold at the end of its life cycle. Other authors (e.g., Tuan et al. [256]) have instead considered the product shelf life to be fixed but have not included any disposal cost at the end of the product lifetime. Other authors have considered the value of the product to decrease during the lifetime, according to different decay models: Ghosh et al. [290] and Ahmadini et al. [291] have assumed a constant deterioration rate of the product during the shelf life, while Yang et al. [292] and Mahata [293] have applied an exponential decay function; finally Mondal et al. [294] and Dhaiban [295] have used a Weibull distribution to model deterioration. In this study, the value of the product is assumed to be constant throughout the shelf life, while at the end of the lifetime, the product suddenly loses its value and must be disposed of, generating a cost that was quantified based on a fixed unit disposal cost:

$$C_{disp,i} = Q_{exp,i} \cdot c_d isp \tag{5.11}$$

Design of experiments

As sketched in the Introduction, a sequential approach (Figure 5.2), which makes use of DOE, simulation, ANOVA, and RSM, is used in this paper to first reproduce the two reorder policies, then optimize their performance, and finally assess the significance of the operating conditions on system performance and on the operating leverages of both inventory policies.

A parametric study was designed based on k input and l output parameters, as listed in Table 5.2: 8 inputs (x_k) and 6 responses (R_l) were selected for the analysis. After defining the mean value for each input, their variation range was established to determine the experimental domain for the study (Table 5.3). The experimental design for the simulation campaign was defined according to the Central Composite Design (CCD) [246], which consists of central, two-level factorial, and axial points, with the latter located inside the experimental domain at a coded distance δ from the central point. Factorial points allow for an evaluation of linear effects and two-factor interactions,

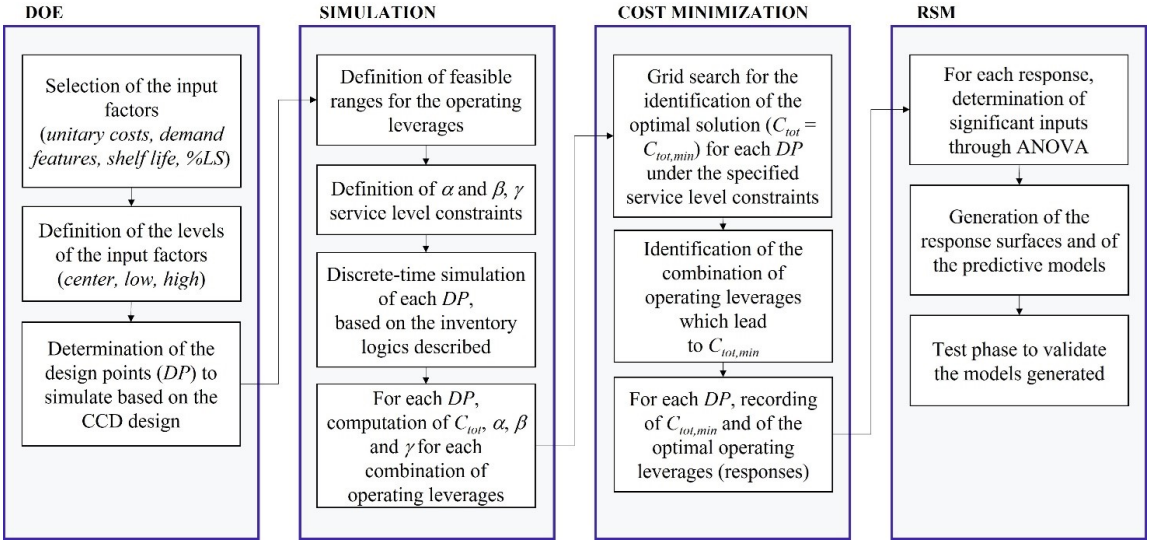

Figure 5.2: Steps of the methodology adopted for system simulation, optimization, and modelling.

while central and axial points estimate the quadratic effects. The coded factors cf were defined in a dimensionless range from -1 to 1 (-1, $-\delta$ 0, δ, 1). The coded value of δ was calculated using eq.5.12 [245], and the actual values of factors at δ and $-\delta$ coordinates were calculated using eq.5.13.

$$\delta = (2^k)^{\frac{1}{4}} \tag{5.12}$$

$$x_{k,\delta(1\leq k\leq 8)} = \frac{\delta(x_{k,1} - x_{k,-1})}{2} + \bar{x_k} \tag{5.13}$$

Finally, the number of simulation runs N_r was calculated based on eq.5.14, considering the number of central points cp=1, being the experiments digital with a null expected replication error.

$$N_r = 2^k + 2k + cp \tag{5.14}$$

Table 5.2: Input and output parameters of the study

Parameter	Name	Variable	Unit	Parameter	Name	Variable	Unit
Input	c_{inv}	x_1	€/units	Input	$\%LS$	x_8	%
Input	c_{so}	x_2	€/units	Output	$C_{tot,min,PR}$	R_1	€/day
Input	c_{oi}	x_3	€/order	Output	$C_{tot,min,CR}$	R_2	€/day
Input	c_{disp}	x_4	€/units	Output	DT_{opt}	R_3	days
Input	D_a	x_5	units	Output	$OUTL_{opt}$	R_4	units
Input	D_b	x_6	units	Output	s_{opt}	R_5	units
Input	SL	x_7	days	Output	S_{opt}	R_6	units

Based on the value set for D_b, the modelled distributions of the customers' demand are presented in Figure 5.3 (D_a is set at a fixed value of 2500 units, for simplicity).

Table 5.3: Ranges and values of the selected input factors

Factors			Numerical values			Actual values of factor levels				
Name	**Symbol**	**Unit**	**Min**	**Mean**	**Max**	**-1**	**-δ**	**0**	**δ**	**1**
c_{inv}	x_1	€/units	0	0.022	0.044	0	0.0165	0.022	0.0275	0.044
c_{so}	x_2	€/units	0.330	0.550	0.880	0.330	0.440	0.550	0.660	0.880
c_{oi}	x_3	€/order	900	1500	2200	900	1200	1500	1850	2200
c_{disp}	x_4	€/units	0.135	0.225	0.360	0.135	0.180	0.225	0.270	0.360
D_a	x_5	units	1000	2500	4000	1000	2125	2500	3125	4000
D_b	x_6	-	0.5	3	5.5	0.5	2.4	3.6	4.5	5.5
SL	x_7	days	3	6	9	3	5	6	7	9
$\%LS$	x_8	%	0	50	100	0	38	50	63	100

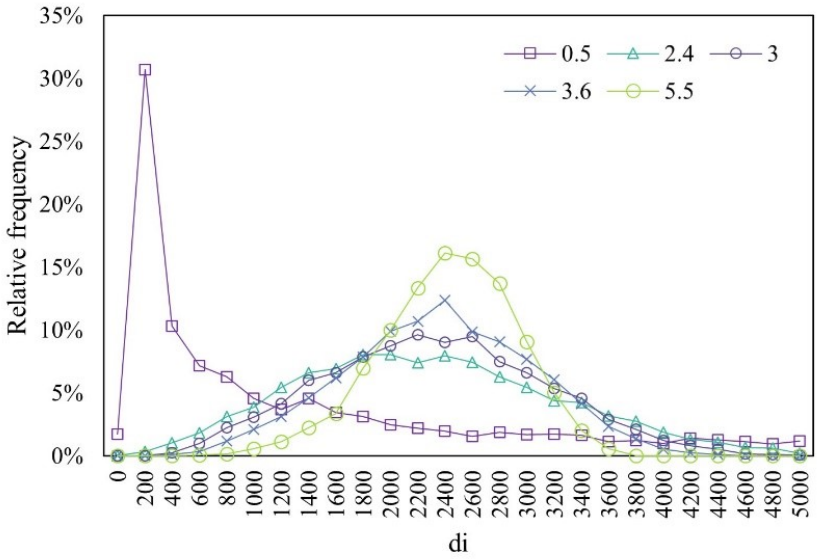

Figure 5.3: Example of distributions of the daily demand based on the value of the shape factor D_b.

Simulation outcomes and optimization

A discrete-time simulation model was developed using MS ExcelTM to reproduce the reorder process described in previous sections and related formulae (eq.5.1 - 5.11). A total of 273 design points were simulated for each policy to thoroughly explore the behaviour of the proposed inventory management system, as well as to evaluate the impact of the input parameters and of possible interactions between them. The total number of days simulated was set at N=50'000 to derive statistically consolidated results. The system cost and the service levels α, β, and γ are derived by averaging the outcomes on the simulation duration (eq.5.15 and 5.16). The total system cost is finally calculated with eq.5.17.

$$C_{inv} = \frac{\sum C_{inv,i}}{N}, C_{so} = \frac{\sum C_{so,i}}{N}, C_{oi} = \frac{\sum C_{oi,i}}{N}, C_{disp} = \frac{\sum C_{disp,i}}{N} \tag{5.15}$$

$$\alpha = \frac{\sum \alpha_i}{N}, \beta = \frac{\sum \beta_i}{N}, \gamma = \frac{\sum \gamma_i}{N} \tag{5.16}$$

$$C_{tot} = C_{inv} + C_{so} + C_{disp} \tag{5.17}$$

For each design point, the values of C_{tot}, α, β, and γ were calculated for each combination of operating leverages of the two inventory policies. Then, an optimization by grid-search was performed as the last step of the simulation, to determine the "optimal" settings of each inventory management policy. By optimal, it means the parameters that allowed for the minimization of $C_{tot,min}$ of the policy, while meeting target service level values; these latter were set at α=90%, β=90%, and γ=99%. An adequate number of configurations, approximately 300 combinations of operating leverages, were simulated to find a robust solution, that consistently determines the optimal operating conditions. The supplementary material of this study, at DOI 10.17632/dg6n8mbypm.1, lists the optimal values resulting from the DOE.

RSM modelling

The results of the simulations were processed using RSM to assess the impact of each input parameter on the selected responses, such as the minimum cost ($C_{tot,min,PR}$ and $C_{tot,min,CR}$) and the operating leverages of the two policies (DT_{opt} and $OUTL_{opt}$; s_{opt} and S_{opt}), using Design Expert v.13 software package. When necessary, preliminary transformations of the responses were performed via the functions suggested by the software, with the purpose of enhancing the model fit. More precisely, the (transformed) responses were analyzed using linear, quadratic, two-factor interaction, and cubic models. For each response, the adjusted R^2 coefficient was calculated to evaluate the goodness-of-fit of the models taking into account the significance of the input terms. Indeed, the value of adjusted R^2 would decrease if some of the terms included did not improve its fit. For each response, the model with the highest adjusted R^2 value was chosen. ANOVA tests were then performed to evaluate whether the models and the selected factors were significant, that is, $p - value$ was less than 0.05. Finally, a sensitivity analysis was carried out to evaluate the impact of the input factors on the responses. The effect of an input parameter x_k on a response R_l is calculated using eq.5.18 dividing the variation in R_l caused by the change in the factor x_k by the maximum variation in the response. If R_l increases as x_k increases, $I_{R_{lx_k}}$ is assumed to be positive; otherwise, it is negative.

$$I_{R_l,x_k} = \frac{max(R_{lx_k}) - min(R_{lx_k})}{max(R_l) - min(R_l)} \tag{5.18}$$

Results and discussion

Sensitivity analysis of the optimal cost of inventory management

To best fit $Ctot, min$, in both PR and CR policies, a square root transformation was

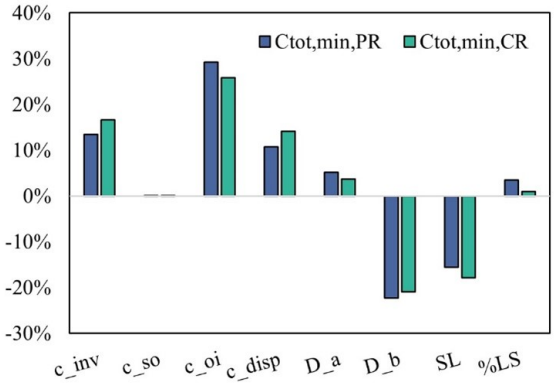

Figure 5.4: Graphical representation of the impact of the significant factors on $C_{tot,min}$

performed and the functions obtained were fitted with a quadratic model. According to the ANOVA test, both models turned out to be significant and adjusted R^2 of 0.94 and 0.96 were obtained in PR and CR, respectively. Most of the model terms also emerged as significant, which means that the choice of the model was appropriate. In contrast, because the service level constraints tend to minimize the occurrence of out-of-stock situations, c_{so} was found to be non-significant in both cases. As regards the lost sales, they result to be significant only for PR policy. In fact, in CR policy, the occurrence of shortages and consequently lost sales is limited by the presence of a base stock (s). PR, on the other hand, having a fixed reorder period, not adjusted according to demand variability, has a high shortage probability. The impact of each factor on $C_{tot,min,PR}$ and $C_{tot,min,CR}$ under service level constraints is presented in Figure 5.4.

The factors that exhibit the greatest impact on $C_{tot,min}$ are, in decreasing order of importance, c_{oi}, D_b, SL, c_{disp} and c_{inv}. In particular c_{inv}, c_{oi}, and c_{disp} resulted to be positively correlated with $C_{tot,min}$. SL and D_b on the other hand, resulted to be negatively correlated with $C_{tot,min}$: higher perishability rates and lower D_b cause an increase in inventory management costs. Furthermore, it can be appreciated that c_inv and c_{disp} have a greater impact in the case ofCR policy. In this case, the presence of a base stock (s) increases the average quantity of stock on hand, with a consequent increase in the inventory holding cost and a higher disposal cost, when these products reach the end of their useful life unsold. Also, the SL has a relevant impact in the case of CR, while c_{oi} impacts more on the PR policy, as the number of orders is predefined and independent of the demand trends. On the contrary, in the case of CR policy, the number of orders can be adjusted and optimized according to demand behaviour. Finally, the demand shape factor turned out to have a similar impact on both policies. The quadratic model used for both $C_{tot,min,PR}$ and $C_{tot,min,CR}$ allowed for evaluating the two-factor effects and detecting curvatures. The contour plots in Figures 5.5 and 5.6 show the values of $C_{tot,min,PR}$ and $C_{tot,min,CR}$ as a function of two of the most impacting costs, namely c_{inv} and c_{oi}. The interaction of these two factors was investigated by including different levels of product

SL (3, 6, and 9 days). It can be observed that with shorter SL, $C_{tot,min}$ depends mainly on c_{oi}. However, with longer SL periods, the impact of the order-issuing cost becomes comparable to the cost of holding the stock on hand. These considerations hold true for both the PR and CR policies. In the latter case, the total cost is lower than for PR, and the difference is stronger for low shelf life values.

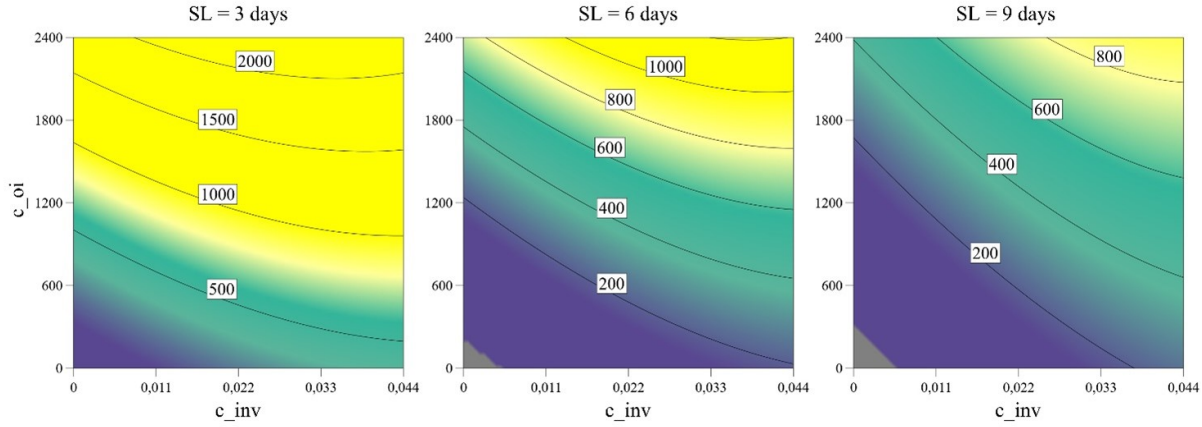

Figure 5.5: Contour plots of $C_{tot,min}$ as a function of c_{inv} and c_{oi} at 3 SL values (PR)

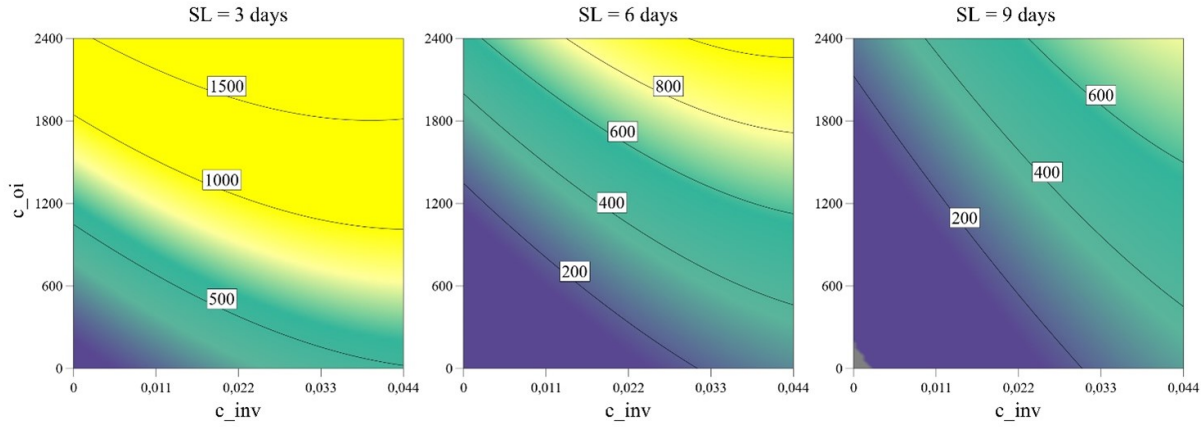

Figure 5.6: Contour plots of $C_{tot,min}$ as a function of c_{inv} and c_{oi} at 3 SL values (CR)

Sensitivity analysis of the optimal operating leverages

DT_{opt} and s_{opt} values were preliminarily transformed via the square root of their inverse function. The resulting functions were then interpolated, in both cases, with a quadratic model. According to the ANOVA test, the models turned out to be significant, with adjusted R^2 of 0.92 and 0.99 respectively. A linear model, including all interactions between input factors, was used to interpolate the natural logarithmic transformation of $OUTL_{opt}$ and S_{opt}. Both models turned out to be significant, with adjusted R^2 of 0.95 for both them. In all models, c_{so} was found to be not significant, once again because out-of-stock situations are almost null when working under optimal operating conditions. In the case of PR, inventory and disposal costs also appear not to have a significant effect on operating parameters.

The impacts of the input factors on the operating leverages are shown in Figure 5.6: c_{oi} turns out to have a greater impact on PR compared toCR, particularly on DT_{opt}, on which a positive correlation is observed with an impact of more than 40%. This means that higher c_{oi} values increase the suitability of decreasing the frequency of order

issuing. In contrast, the impact on s_{opt} is much lower, less than 10%. On $OUTL_{opt}$ and S_{opt}, finally, the impact of c_{oi} is around +20%: an increase in order issuing costs favours triggering less frequent orders, of bigger size.CR emerges as being much more sensitive to the demand parameters: s and S turn out to be very much impacted by both D_a (+34% and +21% respectively) and Db (-52% and -34% respectively); while the impact on DT_{opt} and $OUTL_{opt}$, though still evident, is lower. In this latter case, it can be observed that higher variability (uncertainty) in customer demand, in general, increases the suitability of placing orders frequently, as this could help prevent stock-out situations. In contrast, the PR policy is more sensitive to SL, whose change has a 20% impact on DT_{opt} value; the correlation is positive, which means that higher SL values result in longer storage periods, which makes it more profitable to increase the length of the reorder interval. Lost sales also have a greater impact in the case of PR, due to the absence of safety stocks that can absorb possible demand peaks.

Impact of the product shelf life

A specific analysis was conducted onSL to assess whether, and to what extent, the key characteristic of perishable products affects the economic and operational aspects of inventory management. Five different scenarios were considered. As already stated, perishable items generally have aSL of less than 2 weeks. Thus, for each scenario,SL was varied continuously from 3 to 20 days and the corresponding operating parameters (i.e., DT_{opt} and $OUTL_{opt}$ for PR policy; s_{opt} and S_{opt} for CR policy) have been calculated.

Results in Figure 5.7a highlight that DT_{opt} changes as a function ofSL, and specifically asSL decreases, DT_{opt} decreases as well (and vice versa); this behaviour is observed untilSL reaches a critical value (threshold), while for higher values, DT_{opt} doesn't vary anymore. This threshold appears to be higher when the demand is strongly asymmetrical (Scenario 2), and progressively lower as demand approximates the normal distribution (Scenarios 3 and 4). As regards s_{opt} (Figure 5.8b), this outcome turns out to be higher when Db is lower than 1 (Scenario 2); moreover, in this condition, it appears to be more influenced bySL than in the remaining case studies. Indeed, for all the other case studies, s_{opt} slightly decreases asSL increases. Again, an asymptotic value is reached above a certain SL value.

A similar trend is observed for $OUTL_{opt}$ and S_{opt} (Figure 5.8): when the demand distribution is skewed, the values tend to be higher and more influenced by theSL. Again, above a certain threshold ofSL, which is lower when the demand has a normal-like pattern, $OUTL_{opt}$ and S_{opt} no longer vary. An evaluation of the impact ofSL on $C_{tot,min}$, under service level constraints is shown in Figure 5.9.

CR, as could be expected, is generally more cost-effective than PR. In both cases,

the trend of $C_{tot,min}$ confirms an asymptotic behavior: above a certain SL threshold, $C_{tot,min}$ is no longer affected by the product perishability. When demand is symmetric and tends to assume a normal distribution (Scenarios 3 and 4), the asymptotic value is reached with lower shelf life values (around 7-8), while when demand is strongly asymmetrical (e.g., exponential-like, see Scenario 2), this shelf life threshold is higher (18).

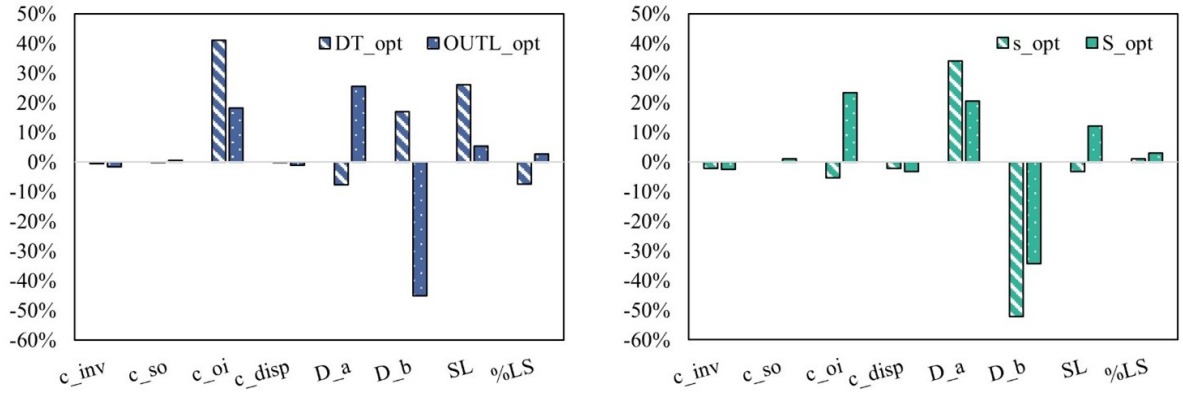

(a) Impacts in the case of PR.

(b) Impacts in the case of CR.

Figure 5.7: Graphical representation of the impact of the significant factors.

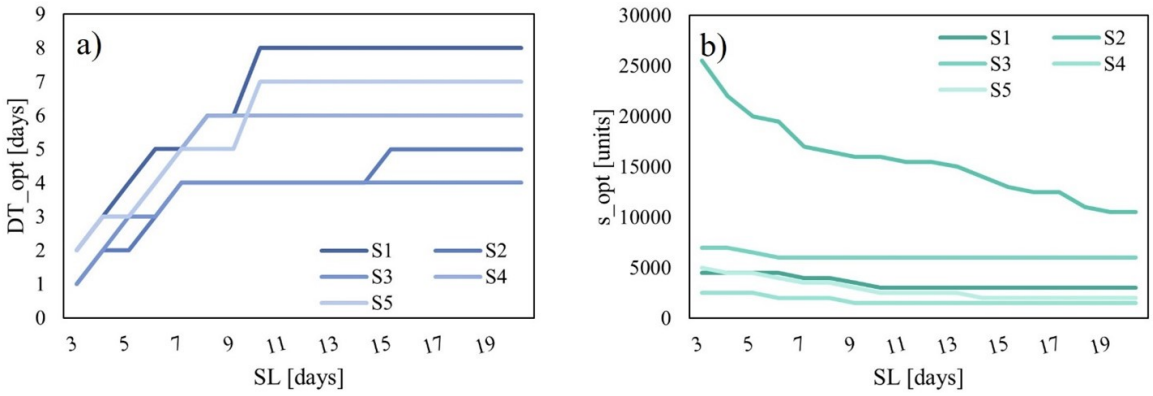

(a) Results of DT_{opt} (PR).

(b) Results of s_{opt} (CR)

Figure 5.8: DT_{opt} and s_{opt} variation as a function of SL, for the case studies evaluated

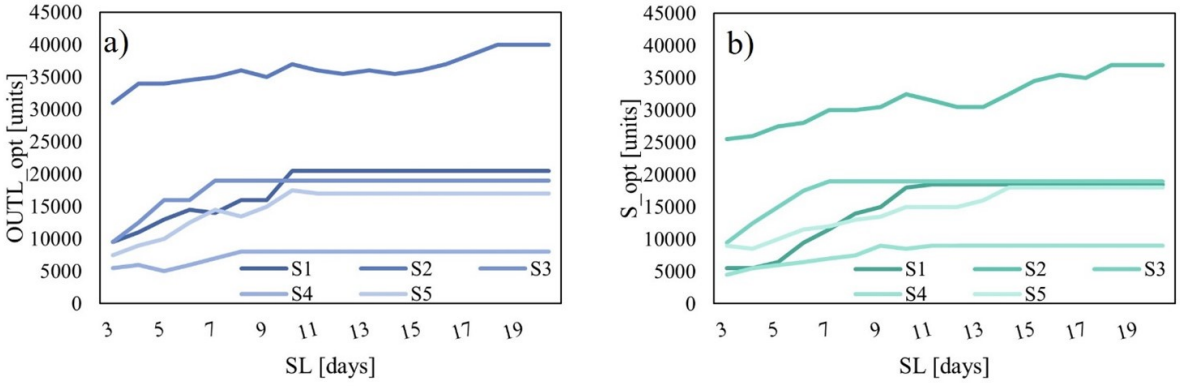

(a) PR policy.

(b) CR policy.

Figure 5.9: Trend of $C_{tot,min}$ for different product SL values.

Conclusions

In this study, a simulation model of an inventory system for perishable items in a business-to-business scenario was developed, considering a single-product multi-period scenario and two different replenishment policies, under the hypothesis of positive non-null lead time and stochastic demand with a Weibull distribution. Grid search optimization was performed to identify, among all the possible combinations, the values of the operating leverages of the policies ($OUTL_{opt}$-DT_{opt} and s_{opt}-S_{opt}) that allowed to reach the required service levels at the lowest possible cost ($C_{tot,min}$), thus considering simultaneously the economic suitability of the policy and the customer satisfaction. After defining the range of variation of the selected input parameters, an appropriate discrete-time simulation campaign was set up according to the DOE methodology. The results obtained proved that to identify the system configuration that meets given service level constraints at the lowest possible cost, several parameters must be taken into account. The optimal operating leverages, indeed, resulted to be strongly influenced by the demand features, operating cost items, and product characteristics. The unitary stock-out cost turned out to be not significant in defining the optimal policy, because under the desired optimal conditions, a high service level should always be guaranteed, and inefficiencies should be minimized. A detailed analysis was carried out to investigate the impact of the product SL. As expected, since the focus was on perishable products, SL turned out to be significant both for $C_{tot,min}$ and the optimal operating leverages. An interesting insight derived from the analysis, however, is that SL affects the reordering policies only up to a critical value. For higher SL values, instead, the behavior of the system, in terms of operating costs and optimal conditions, is stable and no longer influenced by the perishability of the products. The items managed, therefore, could be considered as non-perishable, from the point of view of inventory management, meaning that their decay and consequent disposal could be neglected, and the standard models for non-perishable products could be adopted for their optimization. Another interesting insight is that this critical value was found to be influenced by demand features, in particular the shape factor of demand: when demand is highly skewed, the critical value tends to increase, which means that product perishability has a greater impact on inventory management. Furthermore, the results highlighted how the CR policy appears to be overall more cost-effective than PR policy. Simulation outcomes were analyzed through ANOVA and RSM to investigate the significance of each input parameter. The results obtained represent a novelty in the scientific literature, as the inventory model developed in this paper embodies a set of features (i.e., periodic/continuous review policies, service level constraints, product perishability, Weibull demand distribution, cost analysis and so on) which have never been considered simultaneously in the available literature. It is therefore not immediate to make a direct comparison of the outcomes of this paper

with other studies; comparative analyses can be made in future studies. Moreover, some limitations of this work can be found as regards the assumptions of the model. As an example, in real contexts the rigorous implementation of the FIFO policy could not always be ensured, resulting in a hybrid LIFO/FIFO logic. That environment does not reflect the logic modelled in this paper and therefore the results of this paper could not be generalised to those cases in which such a hybrid logic is applied. Also, the model fits a business-to-business scenario, while its application to other contexts is to be preliminarily checked. Also, future activities could focus on investigating the impact of procurement lead times on the management policies and related costs, including also the case of stochastic lead time. Other factors that can be considered to make the analysis even more realistic could include constraints on the order size and the reorder interval, as well as multi-product warehouse scenarios.

5.2.2 Perishable product inventory management in the case of discount policies and price-sensitive demand

The research in this chapter has been included in the peer-reviewed conference papers [296] *Solari, F., Lysova, N., Bocelli, M., Volpi, A., and Montanari, R. (2024). Perishable Product Inventory Management In The Case Of Discount Policies And Price-Sensitive Demand: Discrete Time Simulation And Sensitivity Analysis. Procedia Computer Science, 232, 1233–1241. https://doi.org/10.1016/j.procs.2024.01.121*
and [297] *Lysova, N., Solari, F., Bottani, E., and Montanari, R. (2024). Impact of the Discount Policies on the Purchasing Behaviour of Perishable Items. IFAC-PapersOnLine, 58(19), 433–438. https://doi.org/10.1016/j.ifacol.2024.09.250.*

Abstract

In B2C contexts, the demand is normally shifted towards products with higher residual shelf life (LEFO policy). In such contexts, the risk is that products closer to the expiration date could not be picked up by consumers, thus reaching the end of their shelf life unsold, with the need to be disposed of. To reduce the extent of this phenomenon, retailers can promote the sale of expiring products by introducing appropriate discount policies. In this paper, a multi-period discrete-time simulation model is developed considering perishable products, having a fixed and deterministic shelf life, issued according to a periodic review policy. A mixed LEFO-FEFO issuing policy was considered. Specifically, in the absence of discount policies, the demand is fulfilled according to LEFO logic. When a discount policy is applied, a portion of the demand, proportional to the discount, shifts to discounted expiring products and is handled according to FEFO logic. The discount policy was defined as a percentage discount, applied to products with a residual shelf life of less than a defined number of days. The presented model was applied to a specific case study and a sensitivity analysis was performed to assess the impact of both the discount policy and other contour variables, such as demand parameters (mean and standard deviation), lead time (LT) and product shelf life (SL), on average daily profit ($\bar{P}$). The results show that, for the context analysed, the introduction of a proper discount policy leads to an increase in ($\bar{P}$) of between 0.31% and 2.45%. Moreover, it was obtained that demand variability positively affects the impact of discount policies. Sensitivity analysis finally showed that ($\bar{P}$) is negatively correlated with LT and positively correlated with SL.

Introduction

One of the 17 Sustainable Development Goals that the United Nations are targeting for 2030, specifically Goal 12.3, is to halve global per capita food waste at the retail and consumer level and reduce food losses during production and supply chains, including post-harvest losses. In fact, it is estimated that about one-third of all food produced for human consumption is wasted each year [298] and, with it, all the resources that were needed to produce it. According to the Food and Agriculture Organization, it is necessary to make a distinction between food loss and food waste. The former represents the waste that occurs in the first links of the production chain, while the latter refers to the last links of the chain i.e. retail and consumption. In developing countries, most food is wasted during the intermediate stages of production or due to storage problems; in rich countries, on the other hand, a large proportion of food is wasted in the last stages of the distribution chain, namely by consumers and retailers. It is estimated that 13.8% of food is wasted between collection and retail, the latter excluded, and 17% of food is wasted between retail, food services, and consumption [179, 299].

In retailing and distribution, the main causes of perishable product waste are overstocking, consumer behaviour, and inappropriate quality control and product handling [300]. Both stockout and the disposal of perishable products resulting from overstocking, as well as posing a problem in terms of sustainability, involve a cost for the retailer: reducing waste in this area is, therefore, a goal to be pursued, both for environmental and profit reasons. It is therefore necessary to identify an inventory management strategy that can optimise profit while minimizing waste. Several studies can be found in the literature that have addressed this issue. In [269], the authors focused on the level of service while neglecting the economic aspect of a periodic review policy. They assumed fixed and deterministic procurement lead time and shelf life, negligible order issuing cost, variable demand, and reorder interval equal to one day. In this context, the authors demonstrated that a dynamic reorder policy yields better results, in terms of service level, than two simpler heuristic policies (base stock and constant order). In a subsequent study [265], the authors showed that in cases where the order issuing cost cannot be neglected, a reorder interval greater than one day is economically advantageous. In both above studies, demand is considered independent of the selling price and the age of the products. In [301] authors conducted a stochastic dynamic optimization to identify the optimal joint pricing and production schedule which maximise the total discounted profit of an inventory control policy of perishable products. Similarly, in [302] the authors assumed the per unit selling price and the length of the replenishment cycle as decision variables to maximise the profit of an inventory system for deteriorating items with price-sensitive demand. In [303] the authors considered a price and time-dependent ramp-type demand function and developed a mathematical model to maximise the profit

based on the number of price changes and the length of the replenishment cycle. In all these latter studies, it is assumed that customers do not differentiate between products of different ages. In [304] the authors evaluate the performance of two replenishment policies by considering differential demand according to product age and assessing the impact of substitution when the requested product is not available (i.e., satisfying demand with a product having a different age than the requested one). To the best of our knowledge, there are still no studies in the literature that refer to the specific context of the retail store, where demand is highly dependent both on the selling price but also on the presence of products having different ages. Indeed, in the retail environment, it is well known that products with a close expiration date are perceived by consumers as having lower quality, demand therefore tends to prefer products having a longer remaining shelf life [305]. Products closer to expiration, therefore, remain on the shelves and, as they reach the end of their shelf life, must be disposed of. The application of discounts has been found in the literature to have an important effect on consumer behaviour [306]. The application of discounting policies helps to bring the consumer's attention back to products closer to expiration by reducing waste and contributing to profit [255].

In this paper, a discrete-time simulation model was built to simulate the operating cycle of a warehouse for perishable products, which involves a periodic review inventory policy, i.e., orders are issued at regular time intervals (T) and a quantity of products is ordered such that a maximum level (S) is restored. A single-product scenario was considered, and demand, having normal distribution, was assumed to be fulfilled according to a mixed Last-Expired-First-Out (LEFO)—First-Expired-First-Out (FEFO) logic. Specifically, in the absence of discount policies, all demand is met according to LEFO logic. When a discount policy is applied, a portion of the daily demand, proportional to the discount applied, shifts to discounted expiring products and is handled according to FEFO logic. The discount policy was defined based on two parameters: a discount percentage (%D) and a residual shelf life (RSL), from which, the product is sold at a discounted price, until the end of its useful life.

The model was then applied to some case studies characterised by different values of the mean (μ) and standard deviation (σ) of demand, procurement lead time (LT), and product shelf life (SL). The optimal configuration, defined as a combination of the operating parameters (T, S, %D and RSL) that maximises average daily profit, was identified through a grid-search optimization method. The impact that discounting policies have on average daily profit was evaluated, and a sensitivity analysis was also conducted to assess the impact that procurement lead time and product shelf life have on system performance.

Many works can be found in the literature on the identification of the optimal discount policy to maximise profit, and comprehensive reviews on this topic can be found as well [306, 307]. Authors in [255] focused on the combined effect that discount policies

Table 5.4: Nomenclature

Symbol	Description
i	i-th day (i=1....n)
d_i	Daily demand
μ_i	Average daily demand
σ_i	Standard deviation of daily demand
LT	Procurement Lead Time
T	Reorder period
S	Target stock level
SL	Shelf life
OH_i	Stock level at day i
O_i	Quantity purchased at day i
OOS_i	Out-of-stock at day i
c_{inv}	Unitary inventory holding cost
c_{so}	Unitary stock-out cost
c_{disp}	Unitary disposal cost
c_p	Unitary purchase cost
C_{oi}	Order issuing cost
p	Selling price
R	Sales revenue
P	Profit
$\bar{P}$	Average daily profit
RSL	Residual shelf life value from which a discount is applied
$\%D$	Discount percentage
$Q_{disp,i}$	Disposed quantity at day i
$Q_{exp,i}$	Expired quantity at day i
$Q_{s,i}$	Quantity sold at full price at day i
$q_{s,i}$	Quantity sold at a discounted price at day i

and dynamic shelf life have on performance in terms of waste reduction, profit, shortages, and product quality. None of the studies mentioned assessed how a change in demand parameters, supply lead time or product shelf life impacted the system performance. The proposed work therefore aims to fill this gap by assessing the impact that variable parameters have on optimal operational parameters and management policy performance.

The outline of the article is as follows: Section 2 describes the methodology and the assumptions adopted and introduces the case study analysed with the relative optimization procedure. In Section 3, the results obtained are presented and discussed. In Section 4 some managerial insights are reported, and in Section 5 the conclusions, limitations of the work and some insights for future activities are presented.

Materials and methods

Overview and assumptions

The context studied is a retail store that manages the stock of perishable products, having a deterministic shelf life, by means of a periodic reorder policy, considering a

positive, deterministic procurement lead time. A multi-period, single-product, discrete-time simulation model was developed that reproduces the warehouse working cycle. A single day was chosen as the reference period and 5000 periods were considered, during which the flows of products in the warehouse were observed. The main assumptions are as follows: Products are characterised by normally distributed demand, having known mean and standard deviation; Demand is satisfied according to the LEFO logic, which is transformed into a mixed LEFO-FEFO logic when a certain discount percentage is applied on products having a remaining shelf life equal to or lower than a certain residual shelf life (RSL).In particular, when a discount is applied, a percentage of demand, equal to the discount applied, shifted shifts to discounted expiring products and is handled according to FEFO logic. Products are characterised by a positive and deterministic shelf life; Products retain their value until the end of their useful life; A maximum warehouse capacity of 24000 units is assumed; Orders are issued at regular periods and, at each reorder, a quantity of products is ordered to reestablish a given level of stock in the warehouse; The target stock level is assumed to be a multiple of 500; The reorder period is assumed to be shorter than the shelf life; All products belonging to the same order have the same shelf life value, which begins to decrease the moment the product is shipped; The procurement lead time is considered positive and deterministic; Within the warehouse, products are grouped according to the order in which they arrive at the warehouse, and then according to their residual shelf life; Shortages are admitted and fully back-ordered;

Finally, the following economic aspects are accounted for within the model: inventory holding cost, stock-out cost, order issuing cost, disposal cost, purchasing cost, sales revenue, and profit. The order issuing cost is assumed to be independent of the ordered quantity.

Fig. 1 shows the logic of the developed model, which are described as follows: for each period i the following activities are performed (Fig. 1):

- products that have reached the end of their shelf life ($Q_{exp,i}$) are disposed of and the stock-on-hand (OH_i) is updated accordingly;

$$OH_i = OH_{i-1} - Q_{exp,i} \tag{5.19}$$

- products that may have been ordered LT days in advance are received in stock and the stock-on-hand is updated accordingly;

$$OH_i = OH_i + O_{i-LT} \tag{5.20}$$

- Any unfulfilled demand from previous days, if sufficient stock is available, is fulfilled (backorder);

$$OH_i = OH_i - OOS_{i-1} \tag{5.21}$$

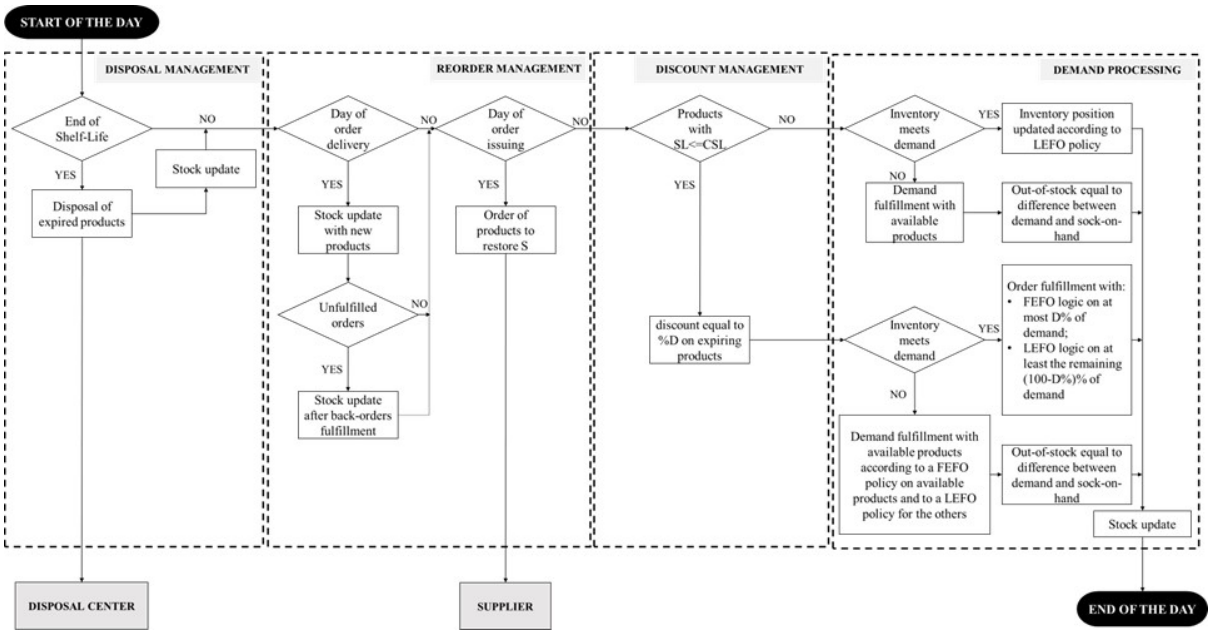

Figure 5.10: Flowchart of the proposed modelling approach.

- According to the periodic review policy, if an order is scheduled for period i, a quantity such as to restore a stock level equal to S is issued. The related cost ($C_{oi,i}$) which is fixed and independent of O_i is computed;

$$O_i = S - OH_i \tag{5.22}$$

- For products in stock having a remaining shelf life equal or lower than RSL, a discount equal to %D is applied;
- If discounted products are present in stock, a percentage of daily demand, equal to %D, shifts towards these products. The remaining portion of demand, on the other hand, remains oriented to products with the longest remaining shelf life;
- In both cases, if the stock-on-hand doesn't meet the demand an out-of-stock arises.

$$OOS_i = OOS_{i-1} + d_i - OH_i \tag{5.23}$$

The main cost items were then computed according to the following equations:

$$C_{inv,i} = c_{inv} \cdot OH_i \tag{5.24}$$

$$C_{so,i} = c_{so} \cdot OOS_i \tag{5.25}$$

$$C_{disp,i} = c_{disp} \cdot Q_{exp,i} \tag{5.26}$$

$$C_{p,i} = c_p \cdot O_i \tag{5.27}$$

$$C_{tot,i} = C_{inv,i} + C_{so,i} + C_{disp,i} + C_{oi,i} + C_{p,i} \tag{5.28}$$

$$R_i = Q_{s,i} \cdot p + q_{s,i} \cdot p \cdot \%D \tag{5.29}$$

$$P_i = R_i - C_{tot,i} \tag{5.30}$$

By repeating this process for a sufficiently large number of periods (5000 in this study), the expected outcomes that the inventory management policy achieves can be calculated. In this study, the average daily profit was considered as the main result:

$$\bar{P} = \frac{\sum_{i=1}^{N} P_i}{N} \tag{5.31}$$

Numerical case study and sensitivity analysis

To quantify the impact that some of the variables involved have on system performance, a sensitivity analysis was performed. As variables were selected those over which the inventory manager has limited influence, but which influence his choices: demand parameters, procurement lead time and product shelf life. For each variable three levels were considered, then both the minimum, the maximum and the mean value to be investigated were defined. The unitary costs as well as the selling price were considered to be fixed (c_{inv}= 0.024 €/unit, c_{so}= 0.47 €/unit, c_{disp}= 0.163 €/unit, c_p= 5 €/unit, C_{oi}= 550 €/order, p= 8 €/unit). A total of nine case studies, as summarised in Table 5.5, were considered.

Table 5.5: Case studies analysed.

Parameter	**CS 1**	**CS 2**	**CS 3**	**CS 4**	**CS 5**	**CS 6**	**CS 7**	**CS 8**	**CS 9**	**Unit**
μ_i	2500	2000	3000	2500	2500	2500	2500	2500	2500	Units
σ_i	500	500	500	400	600	500	500	500	500	units
LT	2	2	2	2	2	1	3	2	2	Days
SL	10	10	10	10	10	10	8	8	12	Days

Optimization procedure

The optimization procedure was performed in two successive steps. In the first step, the reorder policy was optimised by identifying the combination of parameters T and S that would minimise the total daily cost. Next, the optimal discount policy was identified, defined as the combination of %D and RSL that maximised the average daily profit. A

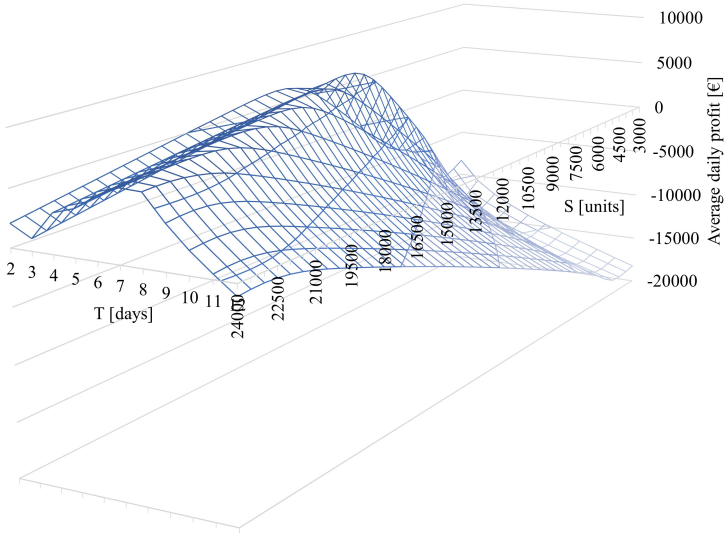

Figure 5.11: Average daily profit in function of T and S, without considering any discount policy.

grid search-based optimization method was used. In Table 5.6, the variation ranges of each operational parameter were defined. Each parameter was then varied within that range and all possible combinations were evaluated to identify the optimal one.

Results and discussion

Figure 5.11 shows the results related to the policy optimization without considering any discount policy, i.e., as if it were a standard reorder period policy, in the case of SL=10 and LT=2. The maximum average daily profit, equal to 6674.80 €, is obtained at T=4 and S=13500.

Results highlight that, for the case study considered, applying a discount at the last day of useful life has a less significant impact than applying it with 2 or 3 days of residual shelf life (Figure 5.12. It can also be seen that for high discount percentages, the average daily profit trends downward: in this area, the lost profits caused by selling at a discounted price outweigh the reduction in the disposal and stock-out costs. Table 5.7 displays the results related to the optimal discount policies of the nine investigated case

Table 5.6: Variation ranges of the operating parameters.

Parameter	**Min value**	**Max value**	**Increase step**
T	2	SL	1
S	8000	24000	500
CSL	1	3	1
%D	0	0.5	0.1

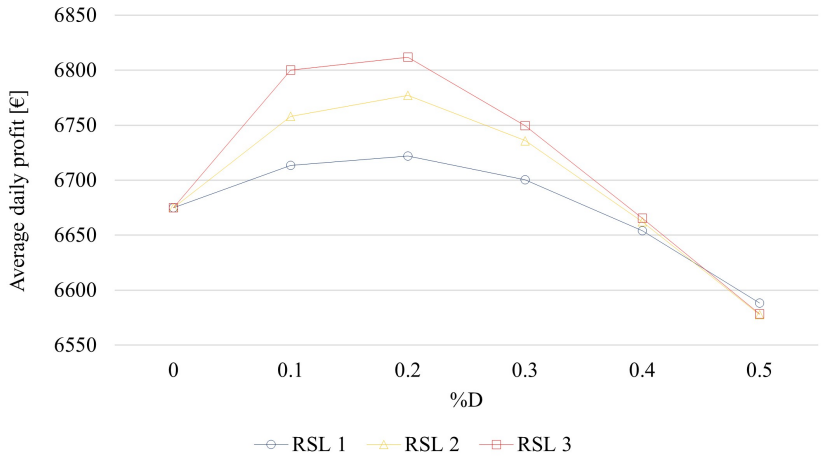

Figure 5.12: Impact of the discount policy on the average daily profit.

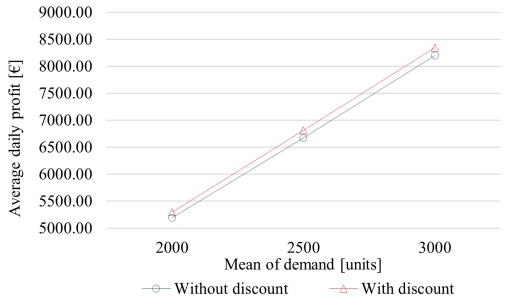

(a) Impact of the mean of demand.

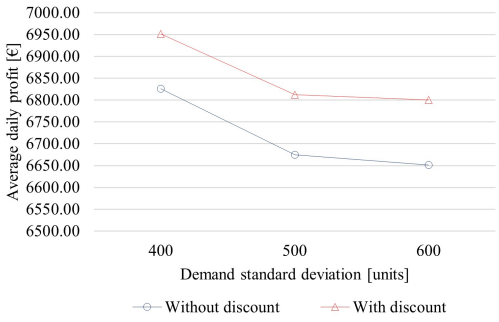

(b) Impact of the standard deviation of demand.

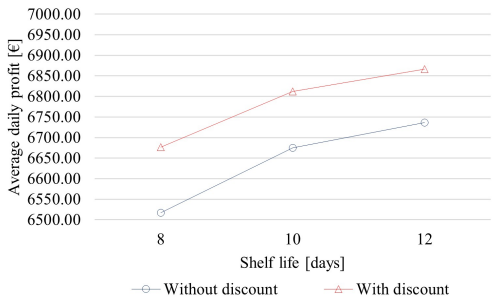

(c) Impact of the product shelf life.

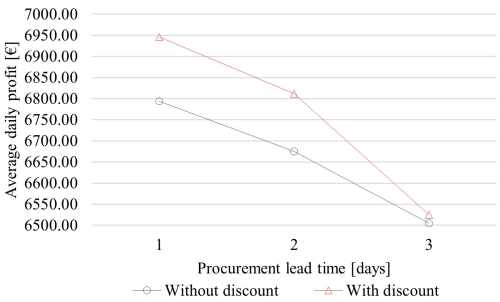

(d) Impact of the procurement lead time.

Figure 5.13: Impact of the variables with (in red) and without (in blue) discount policy.

Table 5.7: Optimal reordering policies and optimal discount policies for the nine case studies analysed.

Case study	**T [days]**	**S [units]**	**%D**	**Average daily profit without discount [€]**	**Average daily profit with discount [€]**	**Impact of discount**
CS 1	4	13500	20%	6674,80	6811,83	2,05%
CS 2	4	11000	20%	5190,05	5293,15	1,99%
CS 3	4	16000	20%	8202,91	8347,56	1,77%
CS 4	4	13500	20%	6825,90	6951,29	1,84%
CS 5	4	14000	20%	6651,25	6800,13	2,24%
CS 6	2	6000	10%	6793,82	6946,10	2,24%
CS 7	6	21000	10%	6504,74	6524,94	0,31%
CS 8	3	11000	10%	6516,92	6676,31	2,45%
CS 9	5	16500	20%	6736,17	6866,16	1,93%

studies. Finally, the impacts that the parameters considered have on system performance with and without discount policy were evaluated. The results are depicted in Figure 5.13.

As might be expected, lead time is negatively correlated with profit, i.e., an increase in LT causes a decrease in ($\bar{P}$), and vice versa. On the other hand, the correlation between SL and ($\bar{P}$) is positive and the impact of the discount policy is higher the shorter is SL. Moreover, as average demand increases, the impact of the discount policy slightly increases: the percentage increase in profit therefore is greater when, in the presence of discounting, average demand is higher. Regarding demand variability, it emerges how the impact of discount policy increases as the standard deviation of demand increases. Finally, the impact of discounting decreases as the procurement lead time increases, because for longer lead times, the on-shelf exposure time of the product decreases.

Managerial insights

The following managerial insights can be deduced from the study conducted:

- The impact of discount policy, in terms of increasing average daily profit, varies with system parameters.
- The increase in daily profit is between 0.31% and 2.45% (without considering any additional demand generated by the introduction of the discount).
- The impact of the discount is greatest when the variability of demand is high.
- The impact of the discount is highest when the supply lead time is short.

Conclusions

In B2C contexts, the shelf-picking process, in the absence of discount policies, follows a LEFO logic, as consumers believe that products which are farther from expiration

have higher quality. This means that the more time passes, the greater the probability that products with shorter residual shelf lives remain on the shelf. The risk that such products will have to be disposed of therefore increases. To reduce this risk, the retailer can introduce discounts to encourage consumers to purchase expiring products.

In this study, a discrete-time simulation model to evaluate the impact of discount policies in a B2C context is presented. The model was applied to nine case studies and a sensitivity analysis was performed to assess the impact that both the discount policy as well as other contour variables, such as demand features, lead time and shelf life of products, have on average daily profit. It was found that, for the case studies investigated, the introduction of an appropriate discount policy can lead to an increase in average daily profit between 0.31% and 2.45%. It was also found that the optimal discount percentage depends on the remaining shelf life value from which the discount is applied. In most cases considered, the optimal discount policy was found to be the one consisting of a 20% discount applied to products having a remaining shelf life of three days.

In future research, it might be interesting to further investigate the sensitivity analysis by designing a simulative campaign using the Design of Experiments methodology and performing a statistical analysis of the results to quantify the relationships that exist among the variables in the system. Also, the discount percentage could be correlated to the product's residual shelf life. The presented model has limitations that can be addressed in future research activities. For example, the demand is assumed to have a fixed statistical distribution. Other demand characteristics can be studied such as seasonality and multi-modality, as well as demand trends can be derived through data mining techniques based on time series. The assumption that shortages are fully backordered can also be considered a limitation, since in a B2C context, product shortages often result in lost sales. A context in which shortages are partly lost and partly back-ordered may be considered in future research activities. Moreover the assumption, already found in the literature, that the percentage discount introduced displaces a percentage of demand, equal to the percentage of discount applied, on expiring products, also represents a limitation. This assumption will need to be investigated with dedicated studies to further explore the relationship that exists between discount policies and consumer behaviour, also depending on the context.

As emerged from the previous study, the introduction of appropriate discounting policies could strongly reduce food waste and support economic convenience of retailers of perishable products. To assess how consumer behavior towards perishable items is affected by discount policies and promotional strategies, a survey was designed and submitted to a sample of 496 consumers, randomly selected among the Italian population. From the results obtained, practical suggestions for the development of analytical and numerical models can be derived, thus allowing simulation and optimization of inventory management policies for perishable items, coupled with pricing policies aimed to minimize waste and maximise profit. In particular, the results will support the development of the previously presented simulation model, allowing to relax several simplifying assumptions.

The following contents, dealing with the development of the survey and its results, can be found in the peer-reviewed conference paper [297] *Lysova, N., Solari, F., Bottani, E., and Montanari, R. (2024). Impact of the Discount Policies on the Purchasing Behaviour of Perishable Items. IFAC-PapersOnLine, 58(19), 433–438. https://doi.org/10.1016/j.ifacol.2024.09.250.*

Introduction

The food waste problem is one of the most widely addressed issues by both the scientific community and the world's major institutions. It is estimated that each year, 1.3 billion tons of food, accounting for one-third of production, are discarded [308]. To address the problem, the United Nations, within the 12th Sustainable Development Goal, Target 12.3, has defined the goal to "halve per capita global food waste at the retail and consumer level, and reduce food losses along production and supply chains by 2030".

Over the past 5 years, an average of 13.9% of the wasted food has been discarded at the retail stage [309]. According to [310], 34% of food products are discarded at the retail stage because they have reached their expiry date. Adopting discount policies for products close to expiration is a common strategy to reduce food waste. Some studies, however, criticize marketing policies as inducing consumers to buy more than they need and thus waste again [311]. On the contrary, a recent study [312] has stated that households with the highest percentage of food purchased at a reduced price, waste less food. In line with this, in [255], based on a simulation-based optimization model, the authors have showed that by discounting old products or adopting a dynamic shelf life, the food discarded by retailers can be reduced.

To be effective, the price reduction should be large enough to be perceived by consumers as compensating for the decrease in freshness [313]. On the other hand, in defining discount policies, profit also must be considered: indeed, these policies involve a gradual reduction in profitability, which could reflect negatively on the company's economic performance. It is, therefore, necessary, on one hand, to make accurate forecasts to avoid overstocking to limit the number of products remaining unsold; on the other hand, however, it is also important to avoid shortages, which, depending on the case, may be backlogged, may result in lost sales or may cause loss of the customer. In any case, they represent additional costs for the company.

In addition to price, another way to affect consumer decisions is to work on the location of products on shelves: placing a product on the top shelf, for example, as opposed to the bottom shelf, can increase by 20% the likelihood that it will be chosen; placing it near the horizontal centre of a shelf, rather than on one of its ends, increases it by 17% [314].

Gathering the considerations above, it is crucial for a company handling perishable items to properly combine demand forecasting techniques, inventory management, discount policies and goods exposition strategies. Hence, these dynamics must be analyzed in depth by investigating the consumer reaction to them, and ultimately developing more efficient inventory management models.

To date, there are few studies in the literature that investigate this aspect from the perspective of inventory management and discount policy making. This study aims to

explore these issues based on a survey that was submitted to a random sample of nearly 500 consumers. The survey was designed to investigate the most significant aspects that affect consumers' choices, such as discount policies, brand, expiration date, food category, and other factors that were identified through an in-depth analysis of the scientific literature.

The article is structured as follows: Section 2 contains the literature review aimed at identifying the main factors that influence consumer choices. Based on the findings, Section 3 details the methodology adopted for the survey design, the platform used for its dissemination, and the methods adopted for the analysis and processing of the results, which are presented and discussed in Section 4. Section 5 provides conclusions and suggestions for future research activities.

Literature review

Among the factors affecting consumers' purchasing decisions, the expiration date of items plays a very significant role. Even though it occupies less than 1% of the overall label size, it is a very important piece of information for consumers, especially for certain product categories, which can therefore influence their decisions [315]. It has been estimated that when the expiration date of a salad stored at 12°C was first reported, wastage increased from 12% to 27% since, in light of this additional information, people tend to throw the food away as soon as it reaches the expiry date, while its absence leads to fewer concerns and therefore less tendency to waste [316].

The expiration date on the product label can be denoted in two ways, depending mainly on the food category and the prescribed storage method. The first is "use by", which means that the food product if properly stored, is safe until the specified date. The second is "best before" and indicates that the food product, after the specified date, may lose quality and may not guarantee all nutrients, but, if stored properly, it can still be eaten without particular health risks. Generally, "best before" is associated with the level of freshness, food integrity and flavour of the product while "use by" is more related to safety, quality and potential health risks associated with the product consumption [317]. A survey, conducted in Europe, has explored whether participants were willing to consume products that have passed the deadline for consumption declared on the label [315]. Nearly half of the participants said they still considered a product that had gone beyond the "best before" date to be edible, linking it to decay mainly in terms of colour and flavour. In contrast, the percentage of participants willing to consume food that has gone beyond the date indicated by "use by" dropped to 28%.

The importance of the expiry date varies depending on the food category. In fact, for those products where the risk related to safety is perceived to be greater, such as meat, fish and dairy products, more emphasis is placed on the label information in general and

expiry date in particular, leading consumers to buy products with the longest possible residual shelf life. In [318], the authors have conducted a survey investigating whether consumers would refuse to consume products marked “use by” after their deadline. The data collected showed that 69% of participants are likely to throw away raw chicken that has passed that deadline; this percentage drops to 20% for breakfast cereals. In general, if the expiration date is close, consumers may decide to avoid buying the product, especially if it is perishable foods such as meat, fish, and dairy products. The issue is less evident for grains, fruits, or vegetables. On the contrary, if the expiration date is still far away, consumers would be more inclined to buy any kind of product.

Other factors that influence consumer choices are trust in a specific brand, its quality features, its appeal, or its exclusive availability [319]. Consumers, facing a brand with higher credibility, tend to buy related products paying less attention to whether (or not) they are sold through a sale promotion; they are also willing to pay more for a product of a well-known brand than one of a less-known brand, even if both products are close to the expiry date. Again, the relevance of the brand may change depending on the product category. In fact, for some kinds of products (e.g., fruit), when making purchasing decisions consumers pay more attention to the colour, shape, degree of ripeness, texture, smell and price than to the brand [320].

Other aspects that emerge as significant are the age and education level of consumers [318]. Older buyers, in fact, tend to be more sensitive to food quality and safety, as they may have greater health concerns. As a result, they generally pay more attention to labels and nutritional information on products and tend to choose those of higher quality. They also mainly base their purchasing preference on well-established habits and background knowledge. In contrast, younger consumers are more inclined toward food trends, such as ethnic cuisine, organic, and zero-mile products. They tend to choose products considered more "fashionable" and ethically produced, such as those with sustainability claims, organic products, or products with a high protein content. At the same time, they may be more influenced by advertising campaigns, promotions, special offers, and social media than older consumers. As a further point, consumers with higher levels of education may be more concerned about the price-quality ratio, but at the same time could be willing to pay more for higher quality and sustainability, opting to purchase organic, zero-mile, or locally sourced products. The information and claims on the label referring to ingredients, nutritional values, product healthfulness, and preservation methods also influence consumers’ behaviour and their purchasing attitude. Indeed, consumers in general prefer products with as few ingredients as possible, suggesting a high-quality and natural food, but also with few recommendations both from the perspective of allergens and the method of preservation [317, 321]. Adding claims referring to positive health effects can also increase the perceived healthiness of foods [322].

Along with the label, packaging itself can also influence consumer decisions. In su-

permarkets, the eye-shot effect is of outstanding importance: 85% of products seen first are purchased without further consideration of alternatives, and 90% of purchasing decisions are made just by taking a quick look at the front of a product. As a result, consumers make decisions by "visually purchasing" the products they see [323]. Visual attention, besides packaging, is also strongly influenced by the number of exhibited products and their location on the shelves [314].

Finally, price is a key determinant of consumer choices: the consumer willingness to pay for perishable items decreases as these items approach their expiry date; foods with longer remaining useful lives will be obviously preferred if no price reduction is offered for expiring products. Moreover, the price reduction must be large enough to balance the decrease in freshness [313]. Discounting strategies can be categorized into two classes: price reductions and quantity promotional offers (such as "buy two, pay one"). A study has been conducted to assess which of these policies influences consumers' behaviour to the greatest extent. Results show that people tend to prefer "two-for-one" offers against 50% price reductions [324]. In another study [325], it has been also demonstrated that the most effective discounting strategies are those consisting of limited-time offers, such as "today only", whether it is a quantity or price discount.

From the above analysis, it emerges that there is a quite large body of scientific literature on the factors influencing consumers' purchasing decisions and on their effectiveness for perishable items. The aim of this work is to start from this well-established state of the art to build a survey to gain a deeper understanding of how promotional strategies influence consumers' purchasing choices and how they can be leveraged to reduce food waste at the retail level. The study focused on the Italian context.

Methods

As can be seen from the literature review, the factors impacting the purchasing decision of perishable products are various. In the last years, it has gradually become common practice in Italy, mainly in distribution retailing, to offer discounts on products close to the expiry date: some stores prefer to maintain the expiring discounted products in their usual locations, while others display them in a dedicated location, for both visibility and marketing reasons.

In this context, to better understand the behaviour of the customers and gain useful insights about how discount policies can impact the purchase of perishable products, thus limiting food waste, a survey was designed and administered using the Microsoft Forms platform. The survey was evaluated and approved by the Research Ethics Board of the University of Parma. For the reasons mentioned above, the targeted respondents were people living in Italy, who are expected to have encountered, and potentially taken advantage, of discount policies on products close to the expiry date.

An invitation to complete the survey was then diffused by social media, QR codes, and mailing lists, ensuring the anonymity of the respondents. The diffusion of the survey via university mailing lists allowed to reach students, i.e., young consumers: their participation was deemed very important because, from the literature review, age turned out to be one of the most important factors driving the purchase decisions.

To enhance the usability and ease of completion, the survey was divided into three main sections. The first section focused on personal background data, to analyze the overall profiles of the participants. The second section focused on the interpretation and consideration of labelling information by the customers, while the third and last section dealt with consumers' behavior at the grocery stores, focusing on their purchase choices with regard to products close to the expiry date (Table 5.8).

The survey included several branches according to the answers of the participants, to better investigate specific topics, e.g., section 2 consisted of three different paths, based on the perceived importance that consumers assign to the expiry date, while section 3 had a dedicated path for customers that regularly buy products from a few brands due to loyalty and trust. Also, an option for early termination of the questionnaire was included after section 1 if the respondent was not directly responsible for grocery shopping.

The last question investigated the main reason driving the purchase of discounted products close to the expiry date, asking the participants about what attracts them the most between economic convenience and the opportunity to limit food waste. Given that the survey is fully anonymous, the results are expected to provide realistic feedback.

Table 5.8: Overview of the survey questions.

Sec.	Q	Item
1	1	Gender of the participants
	2	Age of the participants
	3	Education level
	4	Occupation
	5	Geographical origin of the respondents
	6	Frequency of grocery shopping (includes an option for early termination of the survey if the respondent is not personally responsible for grocery shopping)
	7	Reasons for grocery shopping
2	8	Importance and habit of checking the expiration date (1: I always check the expiration date; 2: I never check; 3: It depends on the product)
	9.1.1	Importance attributed to different wordings related to the expiration date on the labels
	9.1.2	Food categories that require the most attention with respect to the expiration date
	9.1.3	Perceived reasons to carefully check the expiration date for the selected food category
	9.2.1	Reasons why the consumer doesn't usually check the expiration dates
	9.3.1	Food categories that require the most attention with respect to the expiration date
	9.3.2	Perceived reasons to carefully check the expiration date for the selected food category
3	10	Criteria for the selection of the grocery store
	11	Approach to define the most economically convenient product
	12	Type of promotion that influences the most the purchase choice
	13	Reasons that drive the purchase choice (1: loyalty to one or few brands; 2: lowest price; 3: promotions; 4: other)
	14.1	Reasons to buy another product if the usual product of choice is available
	14.2	Reaction to the non-availability of the usual product of choice
	15	Willingness to purchase products nearing expiration but with a discount
	16	Preferred location of discounted products nearing expiration
	17	Willingness to visit and purchase from counters dedicated to discounted products nearing expiration
	18	Minimum discount percentage to take into consideration the purchase of products nearing expiration
	19	Days of residual shelf life up to which the respondent would purchase a non-discounted product
	20	Days of residual shelf life up to which the respondent would purchase a discounted product
	21	The main factor driving the purchase of discounted products close to the expiry date, between economic convenience and the opportunity to reduce food waste

Results

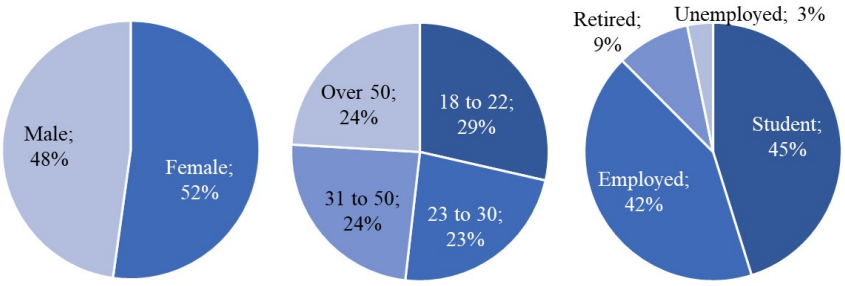

Figure 5.14: Participants' profiles, in terms of gender, age, and occupation.

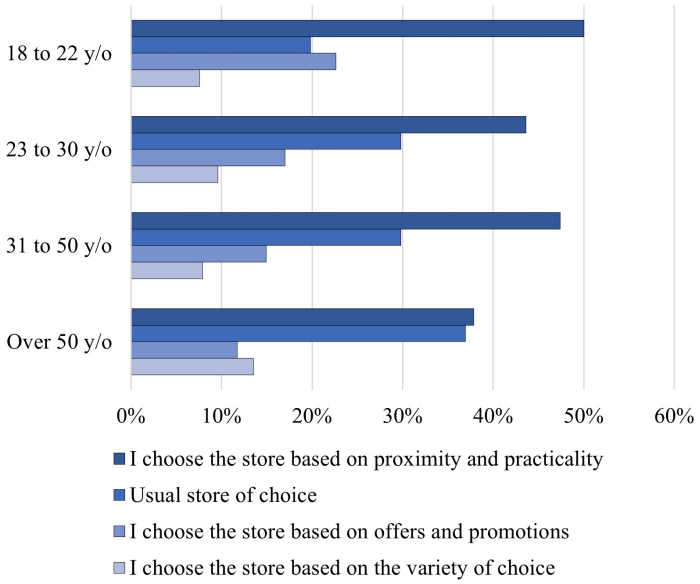

Figure 5.15: Reason for the usual store selection vs. age of the respondents.

A total of 496 answers to the survey were registered. Of these, 48 respondents (73% males and 27% females) ended the survey after section 1, as they declared to not be responsible for grocery shopping within their household. In view of this, the answers of 448 respondents were analyzed, with results presented in the following. Figure 5.14 shows an overview of the personal background data of the respondents: it can be observed that the sample was quite homogeneous in terms of gender and age. With regard to occupation, as expected, most participants were students or employees.

From a first aggregated analysis of the results, the following insights can be derived. A quota of 42% of the respondents declared to choose the grocery store based on proximity and practicality, 28% have a trusted store, while 16% of respondents select the grocery shop based on the promotions. The type of promotion that mostly attracts consumers

is the discount on single products (73%) rather than offers on the purchase of multiple units.

With respect to the purchase preferences, 42% of the participants declared to buy from one or a few trusted brands, regardless of the product category. Of these, when the usual product is available, 53% consider purchasing from other brands in case of discounts, while 22% do not usually contemplate trying different products. If the usual product of choice is instead unavailable, 68% of the respondents decide to substitute it with a similar product from a different brand, 16% look for the original product in another store, while the remaining 16% of consumers come back to look for the product in the same store on the following days.

A quota of 26% of the respondents declared to be willing to buy products close to their expiry date with a discount of at least 30%. The percentage increased to 56% in case of a minimum discount of 50%. Overall, 69% of participants declared buying discounted expiring products for economic convenience, while only 31% stated that their main reason is the opportunity to reduce food waste.

Some cross-analyses were performed by jointly evaluating the answers to different questions. As can be seen from Figure 5.15, younger consumers generally tend to select the store based on proximity and ease of reach. As the age level increases, the percentage of respondents having a trusted store becomes higher; on the other hand, consumers who choose the store based on the available promotions decrease. All these insights reflect the fact that as age increases, consumers tend to be more routine-oriented and generally have greater financial resources.

As can be observed in Figure 5.16a, the opportunity to decrease food waste is more important for consumers over 50 years old (39%), compared to the average of 29% of younger consumers. This represents an interesting and counterintuitive result, as it is generally thought that younger generations care more about sustainability compared to older generations. It appears, however, that due to their usually lower incomes, the economic aspect is dominant when it comes to grocery shopping.

As can be seen from Figure 5.16b, people who choose the shop based on the presence of promotions are more inclined to buy from counters dedicated to discounted expiring products. This result is in line with the high percentage of customers who declared to buy products close to the expiration date with discounts mostly because of economic reasons (69%). With respect to the preferred location of the discounted items, consumers who tend to always buy the same products from trusted brands (42%), as expected, prefer to find these products in their usual location, which they would have visited anyway. More budget-conscious consumers, on the other hand, who base their purchase choices on the lowest price (21%), consider it more convenient to find all the expiring items together at a dedicated counter (Figure 5.16c).

Finally, in Figure 5.16d the impact of the discount policy on the willingness to buy

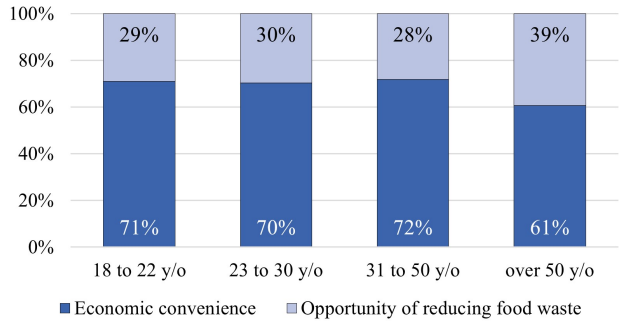

(a) "When you decide to buy discounted expiring products, are you more interested in the economic convenience or in the opportunity of reducing food waste?"; answers divided by age.

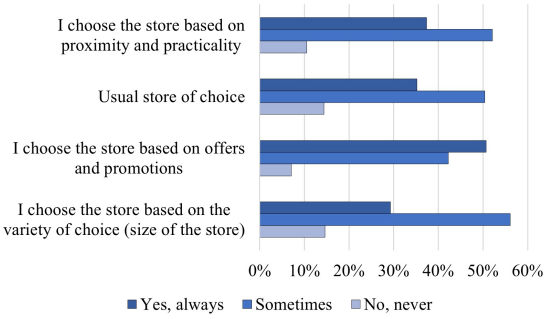

(b) . Inclination to purchase from the corners dedicated to discounted products vs. reasons for choosing the store.

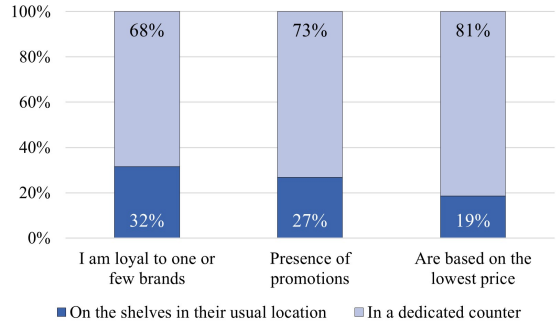

(c) Preferred position of the discounted products close to the expiry date vs. reasons driving the purchase choice.

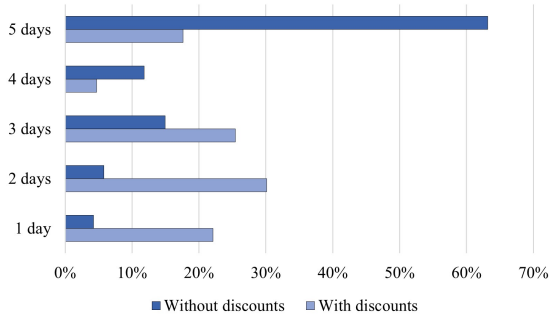

(d) Days of useful shelf life until which customers are willing to buy perishable products.

Figure 5.16: Some of the most relevant results of the survey.

expiring products is shown, for different levels of residual shelf life. It can be easily seen how economic convenience compensates for the lower useful shelf life: if no discount is available, 37% only of consumers are willing to buy products with a residual shelf life of less than 5 days; if a discount is instead applied, this percentage increases to 82%.

Conclusions

In the present study, through an analysis of scientific literature, all factors influencing consumer purchasing decisions were identified, focusing on products close to the expiry date. Based on the related findings, a survey was created and submitted to a random sample of 496 consumers. The purpose of the survey was to assess how consumer behaviour towards perishable items can be influenced by discount policies or promotional strategies, taking into account consumer purchasing habits, loyalty to one or more brands, age, and level of education.

The results obtained, referring to the Italian context, allowed to determine the percentage of consumers sensitive to discount policies or promotional strategies, the percent-

age of consumers loyal to a brand or a retail store, as well as to identify the discount policies to be adopted to effectively push consumers toward the purchase of expiring products.

From a scientific perspective, knowing these aspects is very useful for the development of analytical or numerical models aimed at simulating and optimizing inventory management policies for perishable items, combined with pricing strategies, with the ultimate goal of minimizing waste and maximizing profits. In Solari et al. (2023) authors described a discrete-time simulation model where discount policies were applied to expiring products. In the paper preliminary assumptions were made about the percentage of consumers willing to purchase discounted expiring products and about their behaviour in the case of shortages. The insights of the present survey can therefore be integrated into the simulation model for substantially relaxing the assumptions and making the model more representative of the real consumers' behaviour.

5.2.3 Importance of modelling the dependency of consumers' demand on the price and age of the products

The research in this chapter has been included in the peer-reviewed conference paper [326] *Lysova N., Solari F., Suppini C., Tebaldi L., Volpi A., and Montanari R. 2024. Leveraging economic sanctions to reduce food waste in retail: Insights from a discrete-time simulation approach. Proceedings of the XXIX Summer School "Francesco Turco" - Industrial Systems Engineering.*

Abstract

Food waste is universally recognized as a critical issue: one-third of the food produced ends up lost or wasted every year according to the 2019 FAO Report. Target 12.3 of the Sustainable Development Goals (SDGs) addresses this issue, urging the UN member states to halve by 2030 the per capita quota of food waste at retail and consumption stages and reduce food loss in production and supply chain. Specifically, food waste results in all the resources used in production, transportation, and storage being consumed in vain. The product wastage in retail amounts to 7% of the total food lost and wasted in Europe. While the percentage of domestic waste is significantly higher (54%), it can be argued that it would be easier to implement measures and regulations and, more importantly, monitor the results achieved, when it comes to commercial establishments, rather than private citizens. In this context, several approaches can be adopted: one is to apply sanctions on unsold products, to deter stores from over-stocking. This measure could be particularly significant in the case of highly perishable items, with high environmental impact and specific costs, such as beef and fish. In this study, the effect of the implementation of sanctions, defined in terms of percentages of the product purchase price from 0% to 100%, is investigated by evaluating the resulting difference in the quantity of products disposed of, and the variations in the optimal replenishment policy. To this end, a discrete-time simulation approach is adopted by modelling a B2C scenario with a single product, periodic review replenishment policy, uniform demand, and deterministic lead time. The results of the study will be of great support to policy-makers, by providing them with the results of a sensitivity analysis of a possible measure aimed at limiting food waste, in line with the SDGs.

Introduction

According to the 2019 FAO Report [179], one-third of the produced food ends up lost or wasted every year. Food production, meanwhile, is suitable for feeding a third of the world's population [327]. It is evident therefore that food waste is a complex and critical issue.

It has been years since researchers worked on this topic; just think that a query on the Scopus database having "*food waste*" as a keyword returns more than 19 million documents at the time of writing (i.e., the first trimester of the year 2024), with the scientific production on the topic starting in 1918 when Lucius P. Brown first wrote about some causes and remedies for food waste [328]. Well, after more than 100 years we have not solved this issue, but rather, the situation has worsened.

In numerical terms, most of the waste is generated in the domestic environment (approximately 54%) [329], meaning that consumers normally pay little attention to the way they store and consume food, to the expiry date of products, or to the number of goods they buy. However, it is evident that besides activating some awareness-raising campaigns, it is practically impossible to exert direct control over the behaviour of consumers in their homes.

Going backward, before the customer another actor comes into play, which is represented by the retail function (in other words, the entity allowing a person to buy food, which could be, for instance, a super-/iper- market or a grocery shop). At the retail level, food waste could derive for instance from the tendency of the retailer to have big amounts of displayed products for marketing purposes, inefficient product display policies, or non-optimized reorder policies, among others. Evidence shows that, at the European level, the wasted amount of food in retail accounts for approximately 7% of the total food lost [329]. This percentage is surely lower than the previously mentioned one, but the difference is that at the retail level, it could be easier to implement measures and regulations for reducing waste and to monitor the achieved results.

With reference to this attempt, several approaches have been proposed by the academic community, and recently IoT and Big Data technologies surely allowed making substantial progress with regard to this issue [330]. However, despite their high potential in reducing and preventing food waste, it was demonstrated that these solutions still must be economically feasible to be adopted by decision-makers in the food supply chain [331]. Some possible technical, logistical, and marketing interventions to reduce chilled-food waste at the retail outlet have been assessed in [332] using a simulation approach with a validated model. Concerning highly perishable products, other possible strategies to prevent food waste may be dynamic shelf life and discounting strategies [255]. Besides reducing food waste, appropriately defined discounting policies can allow for increasing daily profits in retail *B2C* scenarios [296].

Regardless of the enormous innovations and investments, the effectiveness of the introduced measures sometimes is not sufficient to effectively reduce food waste. There is something, however, to which everyone is sensitive: money. This is the ratio behind the study presented in this paper, which tries to address the following question: what would happen if the retailers were taxed/sanctioned depending on the food they waste, namely in terms of overstock or unsold products?

To reply, a discrete-time simulation approach is adopted by modelling a *B2C* scenario with a single product, periodic review replenishment policy, uniform demand, and deterministic lead time. The effect of sanctions, defined in terms of percentages of the product selling price from 0% to 100%, is then investigated by evaluating the resulting difference in the quantity of products disposed of, and the variations in the optimal replenishment policy.

This strategy could be particularly suitable for those categories of food having three specific peculiarities: (*i*) great economic value, (*ii*) high perishability, and (*iii*) great environmental impact. For example, this is the case of beef or fish (the readers are invited to refer to [333] or [334] for the outcomes of Life Cycle Assessments and Life Cycle Costing of pork and lamb meat production, by way of example, supporting the strong impact).

The results of this study can be of great support to policy-makers, by providing them with the results of a sensitivity analysis of a possible measure aimed at limiting food waste. Moreover, this contribution could support Target 12.3 of the SDGs, whose aim is to halve by 2030 the pro capita quota of food waste at retail and consumption stages and to reduce food loss in the production and supply chain.

Methodology

In the present study, the analysis focused on the inventory and reorder management of a perishable product in a retail store. Perishable products, e.g., food and beverages, differ from standard items in the fact that they are characterized by a period when they're adequate for consumption, called "shelf life". Usually, when given the chance, the consumers tend to buy fresher products, i.e., those with the highest residual shelf life; this is due to higher perceived and actual food quality, as well as a longer period available for food consumption. Some products present higher perishability than others, with shelf life periods only a few days long: this makes the management of the inventory more complex and increases the risk of wasting food.

Simulation model

The inventory management of a retail store was modelled with a discrete-time approach using MS Excel, focusing on the reorder policy of a single product. The simulated product was beef, as it is characterized by short shelf life and high environmental impact. Due

to the rapid decay of the products, periodic review reorder management was deemed appropriate to satisfy the customers' demand while maintaining an efficient and easily manageable order-issuing schedule. With this replenishment policy, orders are issued at fixed time intervals (DT) to restore a fixed order-up-to-level ($OUTL$).

- During the modelling of the inventory system, the following assumptions were made:
- B2C context (retail store);
- Periodic review inventory management;
- Single product scenario (beef);
- Orders are fulfilled according to Last-Expired-First-Out ($LEFO$) policy that, in this case, coincides with Last-In-First-Out ($LIFO$);
- Intended consumer demand follows a uniform distribution by default; it is however age-sensitive, so the actual demand depends on the age of the products on hand;
- In the case of shortages, the sale of the missing products is considered lost (LS);
- The last day available to sell an item is when its residual shelf life (SL) is 1;
- The items that remain unsold at the end of their shelf life must be disposed of;
- The cost sustained for order emission and transport of the goods from the supplier is fixed and independent of the ordered quantity;
- The ordered items (O) are delivered after a number of days equal to the lead time (LT); being the product highly perishable, a short supply chain with limited delivery time is assumed, with the products assumed to be delivered to the retail store on the next day following the order issuing;
- The products' SL starts to decrease when they are shipped from the supplier, i.e., LT days before arriving at the store;
- All the products in a single delivery are assumed to have the same SL;
- The whole available inventory is displayed to the customers, i.e., the newly delivered products are put on sale right away without waiting for the older ones to be sold first.

The simulated inventory system is age-dependent, and classifies the products based on their date of delivery, i.e., residual SL; in particular, there is the category of "*New*" products, that arrived within the last delivery, and up to 7 levels of "*Old*". In particular,

when one batch is delivered to the store, the items are classified as "*New*" until the following order is delivered; then, the former "*New*" products are classified as "*Old 1*" and the just delivered, fresher ones, as "*New*". If there are still "*Old 1*" products when the next bath is delivered, they will become "*Old 2*" and so on, potentially increasing the order of "*Old*" items with every delivery. The sum of all inventory age levels constitutes the stock-on-hand (OH).

If there is enough OH, consumer D will be satisfied with "*New*" products first, according to the $LEFO$ policy, proceeding to decrease the number of "*Old 1*" products if the "*New*" ones are not sufficient and use higher orders of "*Old*" products to follow. The stock-out is tracked in the highest order of "*Old*" products, as it is the last age level to be checked for product availability. If OH is not sufficient to fulfill D, the sale of the missing items is lost as stated.

Each row of the simulation model represents a day; in total, 10'000 days (N) were modelled. On each day i, characterized by a given customer demand D_i, the operations presented in Figure 5.17 are performed and computed as follows:

- (i) $OH_{i-1|SL_i-1=1}{}^{\smile}D_{i-1} = Q_{exp,i}$
- (ii) $O_i = OUTL - OH_i$
- (iii) $OH_i = OH_{i-1}{}^{\smile}Q_{exp,i} + O_{i-LT}$
- (iv) $if OH_i > D_i, OH_{i+1} = OH_i - D_i$
- (v) $else LS_i = D_i - OH_i$; $OH_{i+1} = 0 if O_{i-LT+1} = 0$

The modelled demand is age-sensitive demand, accounting for customers potentially interested in buying a product, but who may desist if it is not perceived as fresh enough.

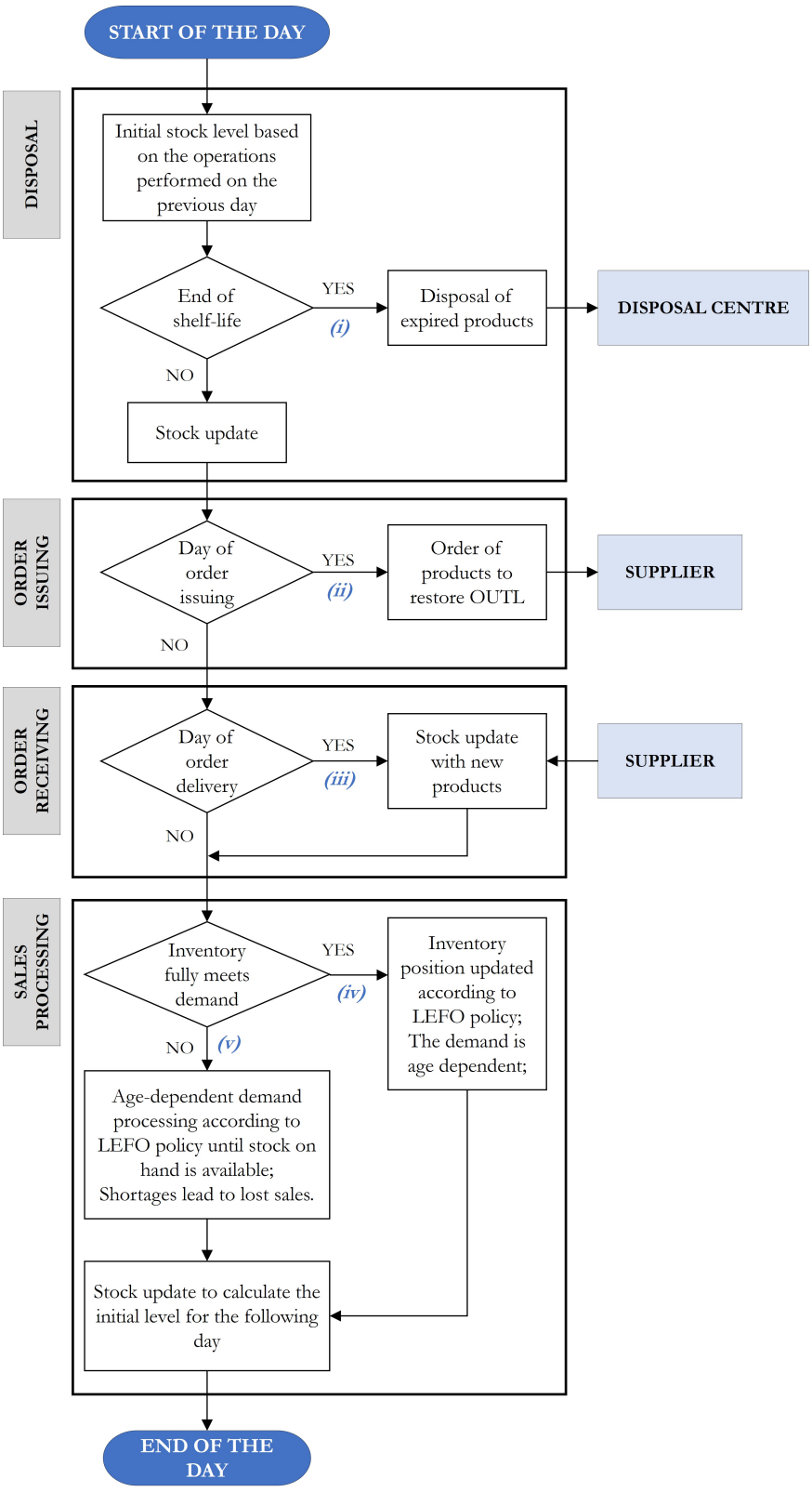

Figure 5.17: Flowchart of the operations performed each day.

Economic aspects

The management of the inventory obviously generates costs, which can be due to product purchase, order issuing and delivery, inventory holding, disposal of expired items, and costs associated with shortages. On the other hand, revenues are generated with the sale of each product unit.

- The purchase cost ($C_{p,i}$) [€] is calculated based on the unitary purchase cost c_p [€/kg] and the order dimension $O_i[kg] : C_{p,i} = c_p O_i$.
- The order issuing cost ($C_{oi,i}$) [€], includes order invoicing, administrative, transportation, and receiving costs; it is fixed and independent of the ordered quantity O_i.
- The inventory holding cost ($C_{inv,i}$) [€] includes the costs sustained by the retail management to keep the products in stock under the appropriate storing conditions; it is calculated by considering the cost of keeping one kg of product for a day (c_{inv}) [€/kg] and the level of stock-on-hand [kg]: $C_{inv,i} = c_{inv} OH_i$.
- The disposal cost ($C_{disp,i}$) [€] typically includes collection and transport fees, treatment expenses, disposal taxes and administrative costs (c_{disp}, [€/kg]); in this study, it is calculated based on the volume of produce disposed of [kg]: $C_{disp,i} = c_{disp} Q_{exp,i}$.
- The stock-out cost $C_{so,i}$) [€], associated with shortages, is generally difficult to estimate and it accounts for, among others, the lost sale revenues and the potential loss of customer trust; it is calculated as the unitary stock-out cost $c_s o$ [€/kg] multiplied by the volume of shortages [kg]: $C_{so,i} = c_{so} LS_i$.
- The packaging cost ($C_p k$) [€], associated with the packaging of trays with beef meat prepared by food operators at the retail store facilities when a new meet delivery arrives: $C_p k = c_p k O_{i-LT}$.
- The total daily management cost ($C_{tot,i}$) [€] is calculated as the sum of all the cost items detailed above: $C_{tot,i} = C_{p,i} + C_{oi,i} + C_{inv,i} + C_{disp,i} + C_{so,i} + C_{pk}$.
- The daily revenues (R_i) [€] are calculated by multiplying the unitary sale price p [€/kg] by the volume of produce sold [kg]: $R_i = pmin(D_i, OH_i)$.
- The daily profits (PR_i) [€], therefore, can be calculated as: $PR_i = R_i \breve{} C_{tot,i}$.

For optimization purposes, the average management costs ($Ctot$), revenues (R), and profits (PR), calculated over the simulated period, will be considered:

$$C_{\text{tot}} = \frac{\sum_{i=1}^{10000} C_{\text{tot},i}}{N} \tag{5.32}$$

$$R = \frac{\sum_{i=1}^{10000} R_i}{N} \tag{5.33}$$

$$PR = R - C_{\text{tot}} \tag{5.34}$$

Scenario set-up

After setting up the general simulation model, it was necessary to define the specifics of the investigated scenario, i.e., the sale of beef in retail stores. In particular, it was necessary to determine the costs and selling prices, as well as to make appropriate assumptions about the daily customer demand.

For this purpose, the data was derived from the ISMEA (Istituto di Servizi per il Mercato Agricolo Alimentare) "Value chain of the organic beef supply chain" report [335]. In particular, the authors considered data relating to the "non-integrated value chain", intended as an organizational model where farms operate independently from the subsequent processing and commercialization stages, i.e., slaughterhouses and wholesalers. This model is characterized by the separation between various stages of the supply chain and the lack of vertical integration. The value chain is summarized in Table 5.9.

With regard to the demand, the following considerations were made. The average beef consumption per capita amounts to 16.8 kg/year approximately [336]. Given the Italian population of 58'940'000 people, it can be estimated that 990'192'000 kg of beef are consumed in Italy every year, resulting in 2'712'855 kg/day.

In the same report, it is estimated that approximately 70% of beef is sold in retail stores other than butcher shops (1'898'998 kg/day); considering 25'082 retail outlets in Italy, it can be estimated that an average of 76 kg is sold in each store every day (D_m). It was assumed that, as often happens in retailing, the stores acquire cut meat from the processing company and package it into trays in dedicated store facilities.

The daily demand was assumed to be reasonably stable, following a uniform distribution ranging from $D_m \cdot (1 - 0.25)$ to $D_m \cdot (1 + 0.25)$. In particular, this demand can be defined as "intended", representing the intention of the customers to buy when they walk into the store. The demand for a highly perishable product like the one discussed in this study may decrease based on the product's age, in this study, therefore, it is modelled as age-sensitive.

The product SL was assumed to have an average value of 5 days at the moment of shipping from the processing company to the retail store; with an average $LT = 1$, the products are characterized by a maximum SL of 4 days when they arrive on the store shelves. When a customer who intends to buy beef finds a tray with the highest possible SL (4 days), he always proceeds with the purchase; when $SL = 3$ days, 75% of the intended demand ends up in a sale, 50% when $SL = 2$ days, and only 25% on the last day before expiration. In this scenario, coupled with the $LEFO$ policy, several

product units risk remaining unsold and being disposed of. Due to the strong economic variability in retailing, the unitary costs were estimated as fractions of the gross margin (11.29 €): 10% for the stock-out costs, 0.5% for the daily inventory holding cost, 0.5% for the baseline disposal cost; furthermore, three order issuing costs were evaluated, equal to 50, 75, and 150 €per order. The characteristics of the demand and costs are reported in Table 5.10. The disposal cost was investigated by applying progressively higher sanctions to the baseline c_{disp}. The aim of the study was to investigate how the introduction of penalties could mitigate the waste of food; to this end, it was decided to perform a sensitivity analysis by gradually incrementing the value of the sanctions from 0% to 100% of the retail purchase price. For each evaluated case the simulation model was used to determine the optimal operating leverages (DT, $OUTL$) of the reorder policy, aiming to maximize the system profits.

Table 5.9: Unitary prices of beef at different stages of the value chain (2022)

Prices at different production stages	**€/kg**
Selling price from farmer	6.53
Selling price from slaughterhouse	8.63
Selling price from the meat processing company	10.14
Selling price from packaging company	14.61
Retail selling price to the final consumer	21.43

Table 5.10: Summary of the demand and economic features

Item	**Value**	**Unit**	**Description**
$D_{i,mean}$	76	kg	Average daily demand
r	19	kg	Half range of daily demand
C_{oi}	50/75/150	€	Order issuing cost
c_{inv}	0.0565	€/kg	Unitary daily inventory holding cost
c_{disp}	0.0565	€/kg	Unitary baseline disposal cost
c_{so}	1.129	€/kg	Unitary stock-out cost
c_{pk}	1.129	€/kg	Unitary packaging cost
c_p	10.14	€	Unitary purchase cost
p	21.43	€	Selling price

The variation in the disposed of produce was the key performance indicator (KPI) related to food waste considered in this study; during the simulation campaign, it was registered to observe whether, and to what extent, the introduction of the penalty decreased the occurrence of food wastage under optimal operating conditions. This evaluation was carried out considering both an age-sensitive demand and a case without age-sensitivity, to evaluate the impact of this important modelling assumption.

Results and discussion

The first results that can be observed summarize the trend in the operating leverages as the disposal cost increases due to penalties for the case with age-sensitivity of the demand (Figure 5.18a) and without (Figure 5.18b).

Overall, $OUTL$ levels in the second case appear higher, and both operating leverages appear more insensitive to the disposal cost compared to the case with age-sensitive demand, with the ratio $OUTL/DT$ being fairly constant.

This is related to the fact that, in the first case, i.e., with the age-sensitive demand, the customers tend to buy fresher products and leave the older ones unsold with the risk of them being disposed of. In the second case, on the other hand, the customers are assumed to not make distinctions between products of different ages, and buy the product they came for regardless of their residual SL.

In the case of food products, especially those highly perishable like fresh meat, this is a very strong and unrealistic assumption: the results, indeed, highlight the importance of including the sensitivity of the demand to the product age in the simulation models.

As the disposal cost increases, the ratio of $OUTL$ to DT decreases, exposing the retail store to stock-out risks in case of high demand variability. This highlights how it is essential to accurately model the demand distribution in order to obtain reliable data and minimize the risk of shortages and wastages due to wrong estimates during the definition of the management policy.

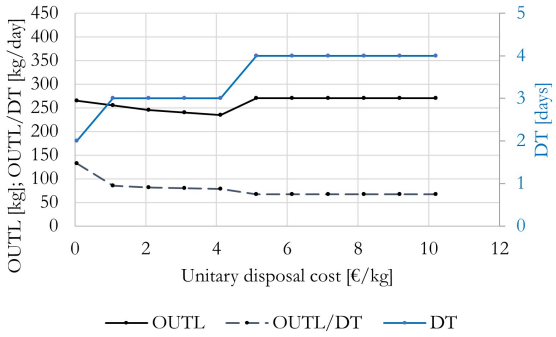

(a) Trend in the optimal operating leverages, and their ratio, at increasing disposal cost values; case with age-sensitive demand.

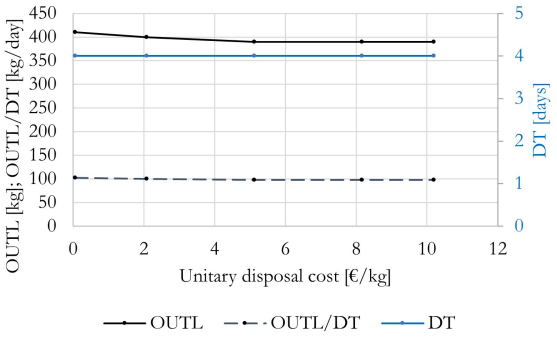

(b) Trend in the optimal operating leverages, and their ratio, at increasing disposal cost values; case without age-sensitivity of the demand.

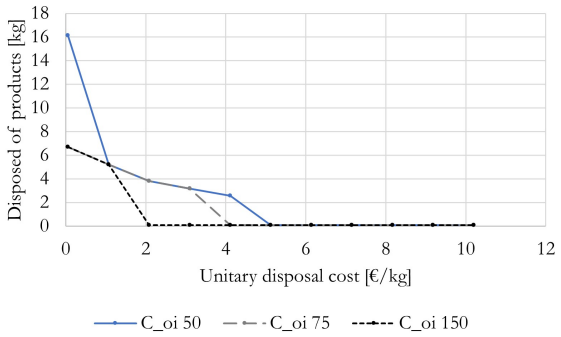

(c) Trend in the quantity of disposed of products as the unitary disposal cost increases (with age-sensitivity of the demand).

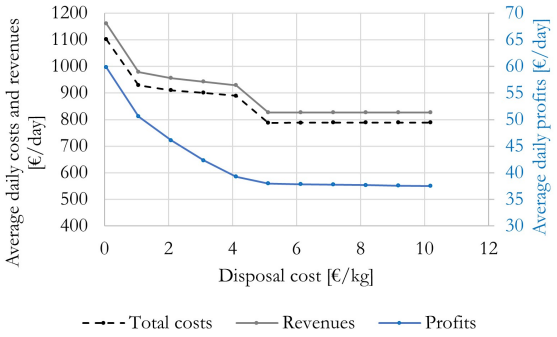

(d) Trend in the average daily costs, revenues, and resulting profits, as the disposal cost increases due to penalties (with age-sensitivity of the demand).

Figure 5.18: Impact of considering the age-sensitivity of demand on the simulation outcomes

To this end, it would be necessary to further develop the simulation model to include additional demand features, such as trends and seasonality. In Figure 5.18c, the trend in the monitored food waste *KPI*, i.e., the disposed of products, is presented as the unitary disposal cost increases due to penalties.

It can be seen that, as expected, for higher penalty values, the disposals decrease. It can be noted, however, that the trends tend to differ when varying other costs, such as order issuing.

While all three cases tend to stabilize over a zero-waste configuration at a certain point, when the overall cost levels are lower, the disposals tend to decrease more gradually with the penalty. On the other hand, with high operating costs, the system tends to reach the optimal situation more rapidly, to limit the occurrence of operating costs.

Also, the initial disposal level with the lowest disposal cost resulted in being higher than the cases with higher operating costs. Since the optimal operating leverages were determined based on the maximization of the profit, it is possible that other costs, e.g., stock-out cost, were more significant and more in need of minimization to achieve the

best operating conditions.

As the disposal cost increases, the optimization of the model tends to minimize the wastage of products to reduce the occurrence of economic penalties. This is achieved by reducing the quantity of products ordered, as observed also in Figure 5.18a, resulting in lower costs, but also lower revenues and profits for the retail store (Figure 5.18d).

Conclusions

In this study, a discrete-time simulation model of a retail store selling beef was generated. The model featured age-dependent inventory classification of the stored highly perishable products and *LEFO* fulfilment policy of an age-sensitive demand. The stock-on-hand was replenished according to a periodic review policy as it was deemed particularly efficient for highly perishable items that need to be re-ordered often.

The effect of the disposal cost and the introduction of economic sanctions on unsold products were investigated. It emerged that both the optimal operating leverages, intended as those that allow to maximize the profits in given operating conditions, and the disposed of products strongly depend on the disposal cost. This effect appears to be much more significant when the age sensitivity of the demand is included in the model, highlighting the importance of correctly defining the assumptions. Moreover, the impact of the increase in the disposal cost appears to depend on the levels of the other operating costs.

While economic penalties might be leveraged to reduce food waste, great attention and consideration are needed from the policy makers to accurately and clearly define the strategies and policies to apply. To this end, simulation can be a valuable tool, allowing them to test what-if scenarios on a digital and tunable tool.

Obviously, economic penalties are not the only possible tool to leverage to minimize food waste: it is also possible to implement incentives, discounting policies, regulations, and other sustainable strategies that could also be integrated to enhance their efficiency. The effect of these measures should be evaluated with appropriate KPIs, assessing both economic and sustainable aspects.

Future research activities will aim to investigate these topics, as well as to further develop the simulation model to account for its present limitations. To make the model more realistic, it would be particularly important to accurately assess and model the customer demand, which undoubtedly is one of the main aspects to take into account when defining the appropriate reorder policy for highly perishable products that are particularly prone to being wasted.

Other aspects worth including in the investigation are the introduction of discounting policies and the evaluation of the service levels in the case of highly perishable items. Moreover, with regard to the items, other perishable products, as well as multi-product

inventories, can be analyzed to derive further insights. Finally, in future research activities, the results of the generated model will be evaluated against other approaches available in the literature, to compare and validate the obtained outcomes.

Chapter 6

Future research activities

Future research activities originating from the presented projects will involve both the continuation of these analyses and the development of advanced and integrated digital systems for industrial monitoring and control.

In the next sections of these chapter, some possible implementations integrating different digital technologies are briefly introduced.

With regard to the presented projects, next investigation steps are outlined below.

- Application of UV-C radiation for the treatment of solid and liquid food products: the research will proceed with the next design stages of the industrial device for horticultural products. In particular, the hormetic effect holds great promise for investigation and deployment, as it would allow to extend the product shelf life while minimizing the necessary radiation dose. Additionally, the feasibility of treating different food product categories with UV-C radiation will be evaluated.

- Continuous ohmic treatment: the presented simulation model will be soon evaluated with experimental tests on both an industrial-scale device processing egg products, and on a pilot plant. This will make it possible to extensively validate the model and carry out experimental evaluations useful for relaxing simplifying assumptions and reproducing more accurately the process. Other possible investigations, including the development and use of vision-based controls, are described in the following pages.

- Sloshing in unsealed beverage cans: The results generated with the simulation model will be validated using a pilot-scale test bench. Once the baseline approach has been confirmed, the model will be extended to include other fluids, operating conditions, and system configurations. Additionally, the possibility of adopting different simulation models is currently under evaluation.

- Concentration of tomato products: The consistency of the obtained preliminary results with the real conditions has been already confirmed by plant operators. The obtained model, therefore, will be further developed and integrated with other sections of the evaporator. Experimental tests aimed at improving and validating the model are expected. Other possible evaluations are presented in one of the following sections of this chapter.

- Simulation of industrial filtering systems: the pilot plant located at the University of Parma will be further investigated with experimental tests, for instance addressing the impact of increasing clogging conditions on the vibrations in the system. Other possible developments include the installation of transparent panels and the use of appropriate expedients to trace and observe streamlines and the system operation.

  Furthermore, micro-scale simulation approaches for filtering applications are currently being investigated in collaboration with the COMEA group of Turku University of Applied Sciences.

- Heat exchanger for viscous fluids: experimental tests will be soon carried out to develop and test virtual sensors based on simulation results, and their ability to provide insights about the temperature distributions where physical sensors could not be implemented.

6.1 Proposal of frameworks for monitoring and control of food industry facilities

6.1.1 Ohmic treatment of heat-sensitive products

Ohmic heating is effectively applied to products that are highly sensitive to high temperatures and uneven temperature distributions.

Non-optimal processing conditions can irreversibly impact product quality, often resulting in visible alterations in food structure (e.g., in the case of egg products) or colour (e.g., basil pesto).

This sensitivity to colour change, in particular, can be explored to develop and fine-tune vision-based virtual sensors. By implementing borosilicate glass tubes similar to those used inside the reactor [78], vision systems can effectively track product characteristics and colour in the wall region, which, as presented in Section 3.3.2, has been identified as the most critical area.

Integrating data collected by the vision system with sensor readings and the simulation-based digital model will enable effective troubleshooting of significant colour deviations, allowing for rapid corrective actions if the issue stems from operating settings.

Indeed, this integration could help identify quality issues not related to processing conditions but instead linked to the characteristics or storage conditions of the raw materials.

This innovative approach to quality monitoring and control opens up exciting possibilities for future research and has the potential to set new standards in creating responsive, data-driven food processing systems.

6.1.2 Integrated control of tomato concentration plants

Tomato evaporation plants are designed to achieve specific product characteristics as outputs of the processing plant. These characteristics mainly include the Brix degree of the finished product, which measures the grams of solid content (generally sucrose) per 100 ml of solution, and the Bostwick degree, which indicates product consistency. Product colour is also assessed, as excessive thermal treatments can cause colour changes that are easily noticeable to consumers.

In the final product, these characteristics depend not only on the processing conditions—such as the operating points of the pumps—but also on the properties of the raw materials (i.e., the tomatoes) and their initial Brix degree. The integrated approach proposed, which will be explored in future research, is based on the following steps:

- a control system of the evaporation plant will be developed based on the simulation model [4].
- when a truckload of tomatoes arrives at the processing plant, acceptance quality controls are performed. One of these is the measurement of the Brix degree.
- through efficiently managed information integration, this data can be sent to the plant's control system to fine-tune operating conditions, if needed, according to the properties of the arriving materials. This helps avoid unnecessary energy use for excessive water removal.
- the control system of the plant would also integrated with real-time sensor data.
- all of the above could be integrated with virtual sensors based on machine vision systems, continuously evaluating the colour of the product and correlating it to exposure to excessive thermal treatment. Indeed, colour degradation of tomato paste in response to thermal treatment has been characterized in the literature and can be exploited to this end [337, 338].

This approach lays a foundation for more responsive and efficient processing in tomato evaporation plants, aiming to optimize product quality and resource optimization through advanced modelling, dedicated vision systems, and efficient data integration across the plant. potentially setting new standards in quality control and resource optimization for food processing.

6.1.3 Integrating CFD warehouse characterization with inventory management of perishables

The proposed application aims to enhance inventory management for perishable goods by integrating CFD-based warehouse characterization with real and virtual sensor data. This system would enable dynamic shelf-life updates and generate alerts in cases of thermal abuse, contributing to more accurate and efficient storage management.

The proposed approach involves the following steps:

- the warehouse would be reproduced with CFD simulation to create a detailed model of the environment. This model would provide insights into temperature and humidity distribution, identifying areas of potential risk for perishable storage.
- real sensors would provide live data on environmental conditions, while virtual sensors based on the the CFD model would simulate environmental conditions in areas where physical sensors are not available or impractical. Integrated, these data sources would offer a complete view of the storage conditions.
- by combining sensor data with product-specific storage requirements, the system could adjust shelf life in real time, based on the actual storage conditions. This approach would improve shelf life accuracy and potentially reduce waste based on the consequent inventory management measures implemented.
- the system would be designed to trigger alarms in cases of thermal abuse (e.g., exposure to temperatures outside safe limits), based on the specific characteristics of each product. This proactive measure would help prevent spoilage and maintain product integrity, once again contributing to reduce food waste, but also do improve food safety.
- by updating shelf life dynamically and identifying items at risk, the system would support smarter inventory management decisions. For example, it could prioritize items for sale based on real-time conditions and estimated product characteristics, thus minimizing spoilage and waste, while maximizing the efficiency and sustainability of the system.

The proposed integrated approach leverages CFD simulation and real-time data to enhance storage conditions, optimize inventory management, and enhance the sustainability of the system. Future research will investigate the development, validation and performance of the control system, as well as explore additional applications of similar approaches in food logistics and storage management.

Chapter 7

Conclusions

This doctoral thesis highlights the powerful role that digital technologies can play in advancing and optimizing the food industry.

Through various case studies, the thesis explored how tools like Computational Fluid Dynamics, Digital Twins, virtual sensors, machine vision, and simulation-based inventory management can address real challenges in food processing and handling.

Several projects were carried out in close collaboration with industrial partners, ensuring that the models and findings addressed practical needs while also contributing to advance academic research in the field.

Each application demonstrated the flexibility and effectiveness of the investigated digital techniques in improving plant and process performance, enhancing product quality, and making operations more sustainable.

A few key takeaways from this work:

- First, CFD and numerical simulations proved invaluable for understanding and optimizing complex food processes. These modeling approaches enabled in-depth characterization of both innovative and traditional treatments and technologies, including some previously under-explored in scientific literature, thereby strongly contributing to both academic and applied research.

- The thesis also examined the use of CFD simulation beyond its usual applications in the food sector.

  Specifically, the thesis explored the potential of simulation-based virtual sensors, developed through parametric simulation campaigns, to support monitoring and control of food industry plants. These virtual sensors could provide valuable insights in areas where physical sensors are unavailable, or impossible to install. The development and application of this promising application will be further investigated in future research.

- Furthermore, the implementation of CFD-based models in Digital Twin contexts was examined by proposing Digital Twin frameworks, based on experimentally validated digital models, for two pilot plants installed at the University of Parma. After ensuring real-time communication between physical and digital counterparts, the Digital Twins will be deployed to assess their effectiveness in dynamically adjusting the operating point to maintain quality standards and adapt to system conditions that evolve over time.

- This research also explored the potential for machine vision to extend beyond its typical quality control role, to support broader and more impactful monitoring and control functions within food processing plants. Integrating vision-based techniques into Digital Twins could allow to create adaptive environments aimed at achieving zero-defect manufacturing.

- Additionally, the work on inventory management for perishables proposes a modelling approach and investigates practical solutions for reducing food waste. By linking in future researh activities the simulation results with real-world consumer behaviour investigated through a dedicated survey, these studies will offer practical insights to improve both sustainability and profitability of food industry inventory systems.

To summarize, the main innovative contribution of this doctoral thesis is twofold:

1. Characterization of emerging food industry techniques through the use of computational methods, to provide valuable insights for their implementation, and generate digital models that could be further leveraged for extensive sensibility analyses and optimizations [78, 176, 177].

2. Proposal of an integrated approach, aimed at the development of innovative advanced control frameworks combining traditional and digital technologies.

   In this context, the use of simulation techniques would go beyond usual characterization and geometrical optimization purposes, serving as a basis for the development of tools for real-time plant monitoring, automation, and control [92]. In particular, these models would be integrated, through efficient real-time data sharing, with sensor data and machine vision systems, achieving significantly greater beneficial impacts than stand-alone implementations of these technologies. For instance, the integration of sensor measurements with the results of simulation campaigns aiming to characterize fault conditions would support the development of predictive maintenance approaches and reactive automated plant controls [97, 205].

This integrated approach results in the configuration of a niche research topic, dealing with multi-layer, multi-scale, and multi-technology Digital Twin frameworks, able to drastically increase quality and efficiency in the food industry through deep knowledge of plant operation.

In conclusion, this thesis makes a significant contribution to the pursuit of digitalization in the food industry. As the demand for food products rapidly grows, and quality standards rise, the importance of digital technologies will only continue to increase. This work provides practical insights to address current industry challenges and sets a foundation for future innovations that balance efficiency, sustainability, and continuous improvement in the food sector.

Bibliography

[1] David Ian Wilson and Yong Min John Chew. Fluid mechanics in food engineering. *Current Opinion in Food Science*, 51:101038, June 2023.

[2] René Haijema and Stefan Minner. Improved ordering of perishables: The value of stock-age information. *International Journal of Production Economics*, 209:316–324, March 2019.

[3] J.F. Steffe. *Rheological Methods in Food Process Engineering*. Freeman Press, 1996.

[4] F. Solari, N. Lysova, A. Dalla Fiora, A. Volpi, A. Rizzi, and R. Montanari. Mitigating design errors in standardized food processing plants: Insights from cfd simulation of a tomato concentration process. In *Proceedings of the 10th International Food Operations and Processing Simulation Workshop (FoodOPS 2024)*, 2024.

[5] Jorge Aliomar Trocoli Abdon Dantas and Jorge Andrey Wilhelms Gut. Modeling sterilization value and nutrient degradation in the thermal processing of liquid foods under diffusive laminar flow with associations of tubular heat exchangers. *Journal of Food Process Engineering*, 41(8), October 2018.

[6] Passakorn Kingwascharapong, Yuki Iida, Fumina Tanaka, and Fumihiko Tanaka. Simulation of a uv–c conveyor system using computational fluid dynamics techniques on the uniformity of the incident uv–c dose distribution to strawberry. *Journal of the Faculty of Agriculture, Kyushu University*, 65(2):371–378, September 2020.

[7] Narjes Malekjani and Seid Mahdi Jafari. Simulation of food drying processes by computational fluid dynamics (cfd); recent advances and approaches. *Trends in Food Science & Technology*, 78:206–223, August 2018.

[8] Natalya Lysova, Federico Solari, and Roberto Montanari. Investigating research trends in computer vision for food quality control: A bibliometric approach. In *Proceedings of the 6th International Conference on Industry 4.0 and Smart Manufacturing*, 2024.

[9] Konstantinos V. Kotsanopoulos and Ioannis S. Arvanitoyannis. The role of auditing, food safety, and food quality standards in the food industry: A review. *Comprehensive Reviews in Food Science and Food Safety*, 16(5):760–775, August 2017.

[10] Nidhi Rajesh Mavani, Jarinah Mohd Ali, Suhaili Othman, M. A. Hussain, Haslaniza Hashim, and Norliza Abd Rahman. Application of artificial intelligence in food industry—a guideline. *Food Engineering Reviews*, 14(1):134–175, August 2021.

[11] Rijwan Khan, Santosh Kumar, Niharika Dhingra, and Neha Bhati. The use of different image recognition techniques in food safety: A study. *Journal of Food Quality*, 2021:1–10, November 2021.

[12] Maninder Meenu, Chinmay Kurade, Bala Chakravarthy Neelapu, Sahil Kalra, Hosahalli S. Ramaswamy, and Yong Yu. A concise review on food quality assessment using digital image processing. *Trends in Food Science & Technology*, 118:106–124, December 2021.

[13] Tadhg Brosnan and Da-Wen Sun. Improving quality inspection of food products by computer vision—a review. *Journal of Food Engineering*, 61(1):3–16, January 2004.

[14] Sudau Eh Teet and Norhashila Hashim. Recent advances of application of optical imaging techniques for disease detection in fruits and vegetables: A review. *Food Control*, 152:109849, October 2023.

[15] Subir Kumar Chakraborty, Subeesh A., Kumkum Dubey, Dilip Jat, Narendra Singh Chandel, Rahul Potdar, N.R.N.V. Gowripathi Rao, and Deepak Kumar. Development of an optimally designed real-time automatic citrus fruit grading–sorting machine leveraging computer vision-based adaptive deep learning model. *Engineering Applications of Artificial Intelligence*, 120:105826, April 2023.

[16] Swathi Sirisha Nallan Chakravartula, Andrea Bandiera, Marco Nardella, Giacomo Bedini, Pietro Ibba, Riccardo Massantini, and Roberto Moscetti. Computer vision-based smart monitoring and control system for food drying: A study on carrot slices. *Computers and Electronics in Agriculture*, 206:107654, March 2023.

[17] Yujie Wang, Luqing Li, Ying Liu, Qingqing Cui, Jingming Ning, and Zhengzhu Zhang. Enhanced quality monitoring during black tea processing by the fusion of nirs and computer vision. *Journal of Food Engineering*, 304:110599, September 2021.

[18] Mohamed Benouis, Leandro D. Medus, Mohamed Saban, Grzegorz Łabiak, and Alfredo Rosado-Muñoz. Food tray sealing fault detection using hyperspectral imaging and pcanet. *IFAC-PapersOnLine*, 53(2):7845–7850, 2020.

[19] Michela Palumbo, Maria Cefola, Bernardo Pace, Giovanni Attolico, and Giancarlo Colelli. Computer vision system based on conventional imaging for non-destructively evaluating quality attributes in fresh and packaged fruit and vegetables. *Postharvest Biology and Technology*, 200:112332, June 2023.

[20] Julio Beltrán Ortega, Diego M Martínez Gila, Daniel Aguilera Puerto, Javier Gámez García, and Juan Gómez Ortega. Novel technologies for monitoring the in-line quality of virgin olive oil during manufacturing and storage. *Journal of the Science of Food and Agriculture*, 96(14):4644–4662, May 2016.

[21] Jasmina Lukinac, Kristina Mastanjević, Krešimir Mastanjević, Gjore Nakov, and Marko Jukić. Computer vision method in beer quality evaluation—a review. *Beverages*, 5(2):38, June 2019.

[22] Amin Taheri-Garavand, Soodabeh Fatahi, Mahmoud Omid, and Yoshio Makino. Meat quality evaluation based on computer vision technique: A review. *Meat Science*, 156:183–195, October 2019.

[23] M. Nerandi Madhubhashini, Chamara P. Liyanage, Amali U. Alahakoon, and Rumesh Prasanga Liyanage. Current applications and future trends of artificial senses in fish freshness determination: A review. *Journal of Food Science*, 89(1):33–50, December 2023.

[24] Dianyuan Wang, Min Zhang, Qiyong Jiang, and Arun S. Mujumdar. Intelligent system/equipment for quality deterioration detection of fresh food: Recent advances and application. *Foods*, 13(11):1662, May 2024.

[25] Anthony C. Iheonye, Vijaya Raghavan, Frank P. Ferrie, Valérie Orsat, and Yvan Gariepy. Monitoring visual properties of food in real time during food drying. *Food Engineering Reviews*, 15(2):242–260, February 2023.

[26] Dharmendrakumar Patel, Suresh Bhise, S. S. Kapdi, and Tanmay Bhatt. Non-destructive hyperspectral imaging technology to assess the quality and safety of food: a review. *Food Production, Processing and Nutrition*, 6(1), May 2024.

[27] Krishna Kumar Patel and Pankaj B. Pathare. Principle and applications of near-infrared imaging for fruit quality assessment—an overview. *International Journal of Food Science & Technology*, 59(5):3436–3450, December 2023.

[28] Benjamin Oluwamuyiwa Olorunfemi, Nnamdi I. Nwulu, Oluwafemi Ayodeji Adebo, and Kosmas A. Kavadias. Advancements in machine visions for fruit sorting and grading: A bibliometric analysis, systematic review, and future research directions. *Journal of Agriculture and Food Research*, 16:101154, June 2024.

[29] Rongrong Xia, Zhenshan Hou, Heran Xu, Yunting Li, Yong Sun, Yafei Wang, Jiayi Zhu, Zijian Wang, Song Pan, and Guang Xin. Emerging technologies for preservation and quality evaluation of postharvest edible mushrooms: A review. *Critical Reviews in Food Science and Nutrition*, 64(23):8445–8463, April 2023.

[30] Lihang Cui, Wenjie Tang, Xiaoshang Deng, and Bing Jiang. Farm animal welfare is a field of interest in china: A bibliometric analysis based on citespace. *Animals*, 13(19):3143, October 2023.

[31] Fotios K. Konstantinidis, Vasiliki Balaska, Symeon Symeonidis, Foivos Psarommatis, Athanasios Psomoulis, Georgios Giakos, Spyridon G. Mouroutsos, and Antonios Gasteratos. Achieving zero defected products in diary 4.0 using digital twin and machine vision. In *Proceedings of the 16th International Conference on PErvasive Technologies Related to Assistive Environments*, PETRA '23. ACM, July 2023.

[32] Adam Fadlalla and Farzaneh Amani. A keyword-based organizing framework for erp intellectual contributions. *Journal of Enterprise Information Management*, 28(5):637–657, September 2015.

[33] N. Sarkar and R. R. Wolfe. Computer vision based system for quality separation of fresh market tomatoes. *Transactions of the ASAE*, 28(5):1714–1718, 1985.

[34] Ansys, Inc. *ANSYS Fluent Theory Guide, Release 18.0*, 2017. (a).

[35] Federico Solari, Natalya Lysova, Francesco Martelli, Andrea Volpi, Benedetta Bottari, and Roberto Montanari. Performance assessment, through numerical simulation and experimental evaluation, of a thin-film ultraviolet reactor for the processing of fruit juices. *International Journal of Food Engineering*, March 2024.

[36] Roberto Montanari, Andrea Volpi, Federico Solari, and Natalya Lysova. Performance assessment, through cfd simulation, of an ultraviolet reactor for the processing of fruit juices. In *Proceedings of the 8th International Food Operations and Processing Simulation Workshop (FoodOPS 2022)*, FoodOPS 2021. CAL-TEK srl, 2022.

[37] Beatriz de Cássia Martins Salomão. *Pathogens and Spoilage Microorganisms in Fruit Juice*, page 291–308. Elsevier, 2018.

[38] Ayşe H. Baysal. *Short-Wave Ultraviolet Light Inactivation of Pathogens in Fruit Juices*, page 463–510. Elsevier, 2018.

[39] Centers for Disease Control and Prevention (CDC). Surveillance for foodborne disease outbreaks — united states, 2007. MMWR Morb Mortal Wkly Rep, 59, 973–979, 2010.

[40] A. Quintero-Ramos, J.J. Churey, P. Hartman, J. Barnard, and R.W. Worobo. Modeling of escherichia coli inactivation by uv irradiation at different ph values in apple cider. *Journal of Food Protection*, 67(6):1153–1156, June 2004.

[41] Michelle D. Danyluk, Renée M. Goodrich-Schneider, Keith R. Schneider, Linda J. Harris, and Randy W. Worobo. Outbreaks of foodborne disease associated with fruit and vegetable juices, 1922–2010: Fshn12-04/fs188, rev. 1/2012. *EDIS*, 2012(3), March 2012.

[42] Food and Drug Administration, Department of Health and Human Services. Hazard analysis and critical control point (haccp); procedures for the safe and sanitary processing and importing of juice. Federal Register, 2001.

[43] Roger K. Abrahamsen and Judith A. Narvhus. Can ultrasound treatment replace conventional high temperature short time pasteurization of milk? a critical review. *International Dairy Journal*, 131:105375, August 2022.

[44] Somnath Basak and Snehasis Chakraborty. The potential of nonthermal techniques to achieve enzyme inactivation in fruit products. *Trends in Food Science & Technology*, 123:114–129, May 2022.

[45] Somnath Basak, Sagar Mahale, and Snehasis Chakraborty. Changes in quality attributes of pulsed light and thermally treated mixed fruit beverages during refrigerated storage (4 °c) condition. *Innovative Food Science & Emerging Technologies*, 78:103025, June 2022.

[46] Muhammad Umair, Sidra Jabeen, Zekai Ke, Saqib Jabbar, Faiqa Javed, Muhammad Abid, Kashif-ur Rehman Khan, Yu Ji, Sameh A. Korma, Mohamed T. El-Saadony, Liqing Zhao, Ilaria Cacciotti, Clara Mariana Gonçalves Lima, and Carlos Adam Conte-Junior. Thermal treatment alternatives for enzymes inactivation in fruit juices: Recent breakthroughs and advancements. *Ultrasonics Sonochemistry*, 86:105999, May 2022.

[47] Kewen Wang and Zhenzhen Xu. Comparison of freshly squeezed, non-thermally and thermally processed orange juice based on traditional quality characters, untargeted metabolomics, and volatile overview. *Food Chemistry*, 373:131430, March 2022.

[48] Eva Kontopodi, Bernd Stahl, Johannes B. van Goudoever, Sjef Boeren, Rian A. H. Timmermans, Heidy M. W. den Besten, Ruurd M. Van Elburg, and Kasper Hettinga. Effects of high-pressure processing, uv-c irradiation and thermoultrasonication on donor human milk safety and quality. *Frontiers in Pediatrics*, 10, March 2022.

[49] Hafiz Muhammad Shahbaz, Jeong Un Kim, Sun-Hyoung Kim, and Jiyong Park. *The Inactivation of Pathogens in Fruit Juice*, page 341–361. Elsevier, 2018.

[50] Giuseppe Vignali, Mario Gozzi, Massimiliano Pelacci, and Roberta Stefanini. Non-conventional stabilization for fruit and vegetable juices: Overview, technological constraints, and energy cost comparison. *Food and Bioprocess Technology*, 15(8):1729–1747, March 2022.

[51] US Food and Drug Administration. Irradiation in the production, processing and handling of food. final rule. Federal Register, 77, 71316–71320, 2012.

[52] Institute of Food Technologists for the Food and Drug Administration of the U.S. Department of Health and Human Services. Kinetics of microbial inactivation for alternative food processing technologies. *Journal of Food Science*, 65, 2008.

[53] Tatiana Koutchma. Advances in ultraviolet light technology for non-thermal processing of liquid foods. *Food and Bioprocess Technology*, 2(2):138–155, January 2009.

[54] Atikah Mansor, Rosnah Shamsudin, Noranizan Mohd Adzahan, and Mohd Nizar Hamidon. Efficacy of ultraviolet radiation as non-thermal treatment for the inactivation of salmonella typhimurium tistr 292 in pineapple fruit juice. *Agriculture and Agricultural Science Procedia*, 2:173–180, 2014.

[55] Alexandra Müller, Mario R. Stahl, Volker Graef, Charles M.A.P. Franz, and Melanie Huch. Uv-c treatment of juices to inactivate microorganisms using dean vortex technology. *Journal of Food Engineering*, 107(2):268–275, December 2011.

[56] Rosnah Shamsudin, Noranizan Mohd Adzahan, Yap Pui Yee, and Atikah Mansor. Effect of repetitive ultraviolet irradiation on the physico-chemical properties and microbial stability of pineapple juice. *Innovative Food Science & Emerging Technologies*, 23:114–120, June 2014.

[57] Maricel Keyser, Ilze A. Műller, Frans P. Cilliers, Wihann Nel, and Pieter A. Gouws. Ultraviolet radiation as a non-thermal treatment for the inactivation of microorganisms in fruit juice. *Innovative Food Science & Emerging Technologies*, 9(3):348–354, July 2008.

[58] Mai Thu Thi Tran and Mohammed Farid. Ultraviolet treatment of orange juice. *Innovative Food Science & Emerging Technologies*, 5(4):495–502, December 2004.

[59] Elisa Gayán, Santiago Condón, and Ignacio Álvarez. Continuous-flow uv liquid food pasteurization: Engineering aspects. *Food and Bioprocess Technology*, 7(10):2813–2827, January 2014.

[60] Çiğdem Uysal Pala and Ayşegül Kırca Toklucu. Microbial, physicochemical and sensory properties of uv-c processed orange juice and its microbial stability during refrigerated storage. *LWT - Food Science and Technology*, 50(2):426–431, March 2013.

[61] Nor Nadiah Abdul Karim Shah, Rosnah Shamsuddin, Russly Abdul Rahman, and Noranizan Mohd Adzahan. Effects of physicochemical characteristics of pummelo fruit juice towards uv inactivation of salmonella typhimurium. *Agriculture and Agricultural Science Procedia*, 2:43–52, 2014.

[62] Mahesh V. Bule, Kiran M. Desai, Brian Parisi, Satish J. Parulekar, Peter Slade, Rekha S. Singhal, and Alfredo Rodriguez. Furan formation during uv-treatment of fruit juices. *Food Chemistry*, 122(4):937–942, October 2010.

[63] F. Solari, G. Girolimetti, R. Montanari, and G. Vignali. A new method for the validation of ultraviolet reactors by means of photochromic materials. *Food and Bioprocess Technology*, 8(11):2192–2211, August 2015.

[64] Chen Xu, X.S. Zhao, and G.P. Rangaiah. Performance analysis of ultraviolet water disinfection reactors using computational fluid dynamics simulation. *Chemical Engineering Journal*, 221:398–406, April 2013.

[65] Patrick C. Young and Yuri A. Lawryshyn. A computational fluid dynamics analysis of placing uv reactors in series. *Water Quality Research Journal*, 52(2):79–89, May 2015.

[66] S.Kucuk Unluturk, H. Arastoopour, and T. Koutchma. Modeling of uv dose distribution in a thin-film uv reactor for processing of apple cider. *Journal of Food Engineering*, 65(1):125–136, November 2004.

[67] Sofie Buhler, Federico Solari, Alessandra Gasparini, Roberto Montanari, Stefano Sforza, and Tullia Tedeschi. Uv irradiation as a comparable method to thermal treatment for producing high quality stabilized milk whey. *LWT*, 105:127–134, May 2019.

[68] T. Sultan, Z. Ahmad, K. Hayat, and I. A. Chaudhry. Computational analysis of three lamp close conduit water disinfection uv reactor. *International Journal of Environmental Science and Technology*, 19(5):4393–4406, May 2021.

[69] Tatiana Koutchma, Brian Parisi, and Eduardo Patazca. Validation of uv coiled tube reactor for fresh juices. *Journal of Environmental Engineering and Science*, 6(3):319–328, May 2007.

[70] Ansys, Inc. *ANSYS SpaceClaim User's Guide*. Ansys, Inc., Canonsburg, PA, USA, 2016.

[71] Ansys, Inc. *ANSYS Fluent User's Guide, Release 18.0*. Ansys, Inc., Canonsburg, PA, USA, 2017.

[72] ANSYS. *Discrete Ordinates (DO) Radiation Model Theory*, 2022. Fluent Theory Guide.

[73] Regina Sommer, Miranda Lhotsky, Thomas Haider, and Alexander Cabaj. Uv inactivation, liquid-holding recovery, and photoreactivation of escherichia coli o157 and other pathogenic escherichia coli strains in water. *Journal of Food Protection*, 63(8):1015–1020, August 2000.

[74] Tatiana Koutchma, Brian Parisi, and S. Kucuk Unluturk. Evaluation of uv dose in flow-through reactors for fresh apple juice and cider. *Chemical Engineering Communications*, 193(6):715–728, June 2006.

[75] T.K. Gachovska, S. Kumar, H. Thippareddi, J. Subbiah, and F. Williams. Ultraviolet and pulsed electric field treatments have additive effect on inactivation of e. coli in apple juice. *Journal of Food Science*, 73(9), November 2008.

[76] N. Basaran, A. Quintero-Ramos, M. M. Moake, J. J. Churey, and R. W. Worobo. Influence of apple cultivars on inactivation of different strains of escherichia coli o157:h7 in apple cider by uv irradiation. *Applied and Environmental Microbiology*, 70(10):6061–6065, October 2004.

[77] Wladyslaw Kowalski. *Ultraviolet Radiometry*, page 313–335. Springer Berlin Heidelberg, 2009.

[78] N. Lysova, F. Solari, G. Aprili, and R. Montanari. Advancing ohmic treatment of egg products: Insights from numerical simulation. In *Proceedings of the 6th International Conference on Industry 4.0 and Smart Manufacturing (ISM 2024)*, 2024.

[79] Yan Zhang, Lu Dong, Jinhui Zhang, Jiaqi Shi, Yaya Wang, and Shuo Wang. Adverse effects of thermal food processing on the structural, nutritional, and biological properties of proteins. *Annual Review of Food Science and Technology*, 12(1):259–286, March 2021.

[80] Iesel Van der Plancken, Ann Van Loey, and Marc E. Hendrickx. Effect of heat-treatment on the physico-chemical properties of egg white proteins: A kinetic study. *Journal of Food Engineering*, 75(3):316–326, August 2006.

[81] M. Le Denmat, M. Anton, and G. Gandemer. Protein denaturation and emulsifying properties of plasma and granules of egg yolk as related to heat treatment. *Journal of Food Science*, 64(2):194–197, March 1999.

[82] C. Alamprese. The effects of novel pasteurization technologies on egg product functionalities. In *European Symposium on the Quality of Eggs and Egg Products*, Nantes, France, 2015. Presented at the European Symposium on the Quality of Eggs and Egg Products.

[83] Daniela Bermudez-Aguirre and Brendan A. Niemira. A review on egg pasteurization and disinfection: Traditional and novel processing technologies. *Comprehensive Reviews in Food Science and Food Safety*, 22(2):756–784, December 2022.

[84] Filiz Icier. *Ohmic Heating of Fluid Foods*, page 305–367. Elsevier, 2012.

[85] Mukul Sain, P. S. Minz, Hima John, and Ajay Singh. Effect of ohmic heating on food products: An in-depth review approach associated with quality attributes. *Journal of Food Processing and Preservation*, 2024:1–17, January 2024.

[86] Ramon Silva, Ramon S. Rocha, Jonas T. Guimarães, Celso F. Balthazar, Gustavo Luís P.A. Ramos, Hugo Scudino, Tatiana C. Pimentel, Erica M. Azevedo, Marcia C. Silva, Rodrigo N. Cavalcanti, Verônica O. Alvarenga, Maria Carmela K.H. Duarte, Erick. A. Esmerino, Mônica Q. Freitas, and Adriano G. Cruz. Ohmic heating technology in dulce de leche: Physical and thermal profile, microstructure, and modeling of crystal size growth. *Food and Bioproducts Processing*, 124:278–286, November 2020.

[87] Ramon Silva, Ramon S. Rocha, Jonas T. Guimarães, Celso F. Balthazar, Hugo Scudino, Gustavo Luís P.A. Ramos, Tatiana C. Pimentel, Marcia C. Silva, Paulo Henrique F. Silva, Maria Carmela K.H. Duarte, Mônica Q. Freitas, Adriano G. Cruz, and Erick. A. Esmerino. Dulce de leche submitted to ohmic heating treatment: Consumer sensory profile using preferred attribute elicitation (pae) and temporal check-all-that-apply (tcata). *Food Research International*, 134:109217, August 2020.

[88] Yvan Llave, Satoshi Fukuda, Mika Fukuoka, Naomi Shibata-Ishiwatari, and Noboru Sakai. Analysis of color changes in chicken egg yolks and whites based on degree of thermal protein denaturation during ohmic heating and water bath treatment. *Journal of Food Engineering*, 222:151–161, April 2018.

[89] Filiz Icier and Hayriye Bozkurt. Ohmic heating of liquid whole egg: Rheological behaviour and fluid dynamics. *Food and Bioprocess Technology*, 4(7):1253–1263, July 2009.

[90] Cristina Alamprese, Massimo Cigarini, and Andrea Brutti. Effects of ohmic heating on technological properties of whole egg. *Innovative Food Science & Emerging Technologies*, 58:102244, December 2019.

[91] Debora Almeida Rosa, Jonas de Toledo Guimarães, Louise A. Cabral, Marcia Cristina Silva, Renata S.L. Raices, Gustavo Luis Paiva Anciens Ramos, Tatiana Colombo Pimentel, Erick Almeida Esmerino, Adriano Gomes da Cruz, and Mônica Queiroz de Freitas. Effect of ohmic heating temperature and voltage on liquid whole egg processing. *Innovative Food Science & Emerging Technologies*, 89:103490, October 2023.

[92] Natalya Lysova, Federico Solari, and Giuseppe Vignali. Optimization of an indirect heating process for food fluids through the combined use of cfd and response surface methodology. *Food and Bioproducts Processing*, 131:60–76, January 2022.

[93] Chunsen Wang, Yvan Llave, Noboru Sakai, and Mika Fukuoka. Analysis of thermal processing of liquid eggs using a high frequency ohmic heating: Experimental and computer simulation approaches. *Innovative Food Science & Emerging Technologies*, 73:102792, October 2021.

[94] Mario Calderon-Ramirez, Jesus A. Gomez-Nafate, Ramiro Rico-Martinez, Ramon Rodriguez-Castro, Micael G. Bravo-Sanchez, and Luis A. Alcaraz-Caracheo. Improvement of ohmic pasteurization in mango pulp through cfd and rsm. *IEEE Access*, 10:81380–81389, 2022.

[95] Chunsen Wang, Yvan Llave, and Mika Fukuoka. Agitation of liquid eggs during ohmic heating pasteurization—experimental and computer simulation study. *Journal of Food Process Engineering*, 47(1), January 2024.

[96] Jane S.R. Coimbra, Ana L. Gabas, Luis A. Minim, Edwin E. Garcia Rojas, Vânia R.N. Telis, and Javier Telis-Romero. Density, heat capacity and thermal conductivity of liquid egg products. *Journal of Food Engineering*, 74(2):186–190, May 2006.

[97] Federico Solari, Natalya Lysova, and Roberto Montanari. Digital twin based on historical data and simulation results: Fault detection and estimation of the remaining useful life of a cyclone bag filter. *Applied Sciences*, 13(14):8297, July 2023.

[98] European Union. Industrial emissions directive. Official Journal of the European Union, L334, 17–119, 2010.

[99] Trevor Sparks and George Chase. Section 3 - air and gas filtration. In Trevor Sparks and George Chase, editors, *Filters and Filtration Handbook (Sixth Edition)*, pages 117–198. Butterworth-Heinemann, Oxford, sixth edition edition, 2016.

[100] Akira Ogawa. Mechanical separation process and flow patterns of cyclone dust collectors. *Applied Mechanics Reviews*, 50(3):97–130, March 1997.

[101] Friedrich Löffler. *Fundamental Principles of Particle Separation in Fabric Filters*, page 1–54. Vieweg+Teubner Verlag, 1988.

[102] Biao Xie, Shihang Li, Hao Jin, Shuda Hu, Fei Wang, and Fubao Zhou. Analysis of the performance of a novel dust collector combining cyclone separator and cartridge filter. *Powder Technology*, 339:695–701, November 2018.

[103] E.H. Tanabe, P.M. Barros, K.B. Rodrigues, and M.L. Aguiar. Experimental investigation of deposition and removal of particles during gas filtration with various fabric filters. *Separation and Purification Technology*, 80(2):187–195, July 2011.

[104] G. Krammer, A. Kavouras, and A. Anzel. Optimization of pulse cleaning frequency during bag filter operation. *Chemical Engineering & Technology*, 26(9):951–955, September 2003.

[105] B.O. Andersen, N.F. Nielsen, and J.H. Walther. Numerical and experimental study of pulse-jet cleaning in fabric filters. *Powder Technology*, 291:284–298, April 2016.

[106] Samirys Sara Rodrigues Cirqueira, Eduardo Hiromitsu Tanabe, and Mônica Lopes Aguiar. Experimental investigation of particle deposition in filter media during filtration cycles with regeneration by pulse jet cleaning. *Process Safety and Environmental Protection*, 127:288–298, July 2019.

[107] Ercan Oztemel and Samet Gursev. Literature review of industry 4.0 and related technologies. *Journal of Intelligent Manufacturing*, 31(1):127–182, July 2018.

[108] Victor Bittencourt, Felipe Saldanha, Anabela Carvalho Alves, and Celina Pinto Leão. *Contributions of Lean Thinking Principles to Foster Industry 4.0 and Sustainable Development Goals*, page 129–159. Springer International Publishing, 2019.

[109] Judit Oláh, Nemer Aburumman, József Popp, Muhammad Asif Khan, Hossam Haddad, and Nicodemus Kitukutha. Impact of industry 4.0 on environmental sustainability. *Sustainability*, 12(11):4674, June 2020.

[110] Michael Grieves. Digital twin: manufacturing excellence through virtual factory replication. *White paper*, 1(2014):1–7, 2014.

[111] Aidan Fuller, Zhong Fan, Charles Day, and Chris Barlow. Digital twin: Enabling technologies, challenges and open research. *IEEE Access*, 8:108952–108971, 2020.

[112] Mohaiad Elbasheer, Francesco Longo, Giovanni Mirabelli, Letizia Nicoletti, Antonio Padovano, and Vittorio Solina. Shaping the role of the digital twins for human-robot dyad: Connotations, scenarios, and future perspectives. *IET Collaborative Intelligent Manufacturing*, 5(1), October 2022.

[113] Mohd Javaid, Abid Haleem, and Rajiv Suman. Digital twin applications toward industry 4.0: A review. *Cognitive Robotics*, 3:71–92, 2023.

[114] He Liu, Min Xia, Darren Williams, Jianzhong Sun, and Hongsheng Yan. Digital twin-driven machine condition monitoring: A literature review. *Journal of Sensors*, 2022:1–13, July 2022.

[115] Raymon van Dinter, Bedir Tekinerdogan, and Cagatay Catal. Predictive maintenance using digital twins: A systematic literature review. *Information and Software Technology*, 151:107008, November 2022.

[116] Yingchao You, Chong Chen, Fu Hu, Ying Liu, and Ze Ji. Advances of digital twins for predictive maintenance. *Procedia Computer Science*, 200:1471–1480, 2022.

[117] Dong Zhong, Zhelei Xia, Yian Zhu, and Junhua Duan. Overview of predictive maintenance based on digital twin technology. *Heliyon*, 9(4):e14534, April 2023.

[118] Itxaro Errandonea, Sergio Beltrán, and Saioa Arrizabalaga. Digital twin for maintenance: A literature review. *Computers in Industry*, 123:103316, December 2020.

[119] Mengnan Liu, Shuiliang Fang, Huiyue Dong, and Cunzhi Xu. Review of digital twin about concepts, technologies, and industrial applications. *Journal of Manufacturing Systems*, 58:346–361, January 2021.

[120] Stefan Boschert and Roland Rosen. *Digital Twin—The Simulation Aspect*, page 59–74. Springer International Publishing, 2016.

[121] Bahar Biller, Xi Jiang, Jinxin Yi, Paul Venditti, and Stephan Biller. Simulation: the critical technology in digital twin development. In *2022 Winter Simulation Conference (WSC)*, page 1340–1355. IEEE, December 2022.

[122] Rakesh Kumar Phanden, Priavrat Sharma, and Anubhav Dubey. A review on simulation in digital twin for aerospace, manufacturing and robotics. *Materials Today: Proceedings*, 38:174–178, 2021.

[123] Roberto Molinaro, Joel-Steven Singh, Sotiris Catsoulis, Chidambaram Narayanan, and Djamel Lakehal. Embedding data analytics and cfd into the digital twin concept. *Computers & Fluids*, 214:104759, January 2021.

[124] Sean Reed, Magnus Löfstrand, and John Andrews. Modelling cycle for simulation digital twins. *Manufacturing Letters*, 28:54–58, April 2021.

[125] Zixin Dou, Yanming Sun, Zhidong Wu, Tao Wang, Shiqi Fan, and Yuxuan Zhang. The architecture of mass customization-social internet of things system: Current research profile. *ISPRS International Journal of Geo-Information*, 10(10):653, September 2021.

[126] Cesar H. Guzmán, José L. Carrera, Héctor A. Durán, Javier Berumen, Arturo A. Ortiz, Omar A. Guirette, Angélica Arroyo, Jorge A. Brizuela, Fabio Gómez, Andrés Blanco, Héctor R. Azcaray, and Marlen Hernández. Implementation of virtual sensors for monitoring temperature in greenhouses using cfd and control. *Sensors*, 19(1):60, December 2018.

[127] Cristina Bengoechea-Cuadrado, Maria Garcia-Camprubi, Valentina Zambrano, Francois Mazuel, and Salvador Izquierdo. Virtual sensor development based on reduced order models of cfd data. In *2019 IEEE 17th International Conference on Industrial Informatics (INDIN)*, page 1644–1648. IEEE, July 2019.

[128] Nirupaplava Metta, Marianthi Ierapetritou, and Rohit Ramachandran. A multiscale dem-pbm approach for a continuous comilling process using a mechanistically developed breakage kernel. *Chemical Engineering Science*, 178:211–221, March 2018.

[129] Ruiqing Shen, Zeren Jiao, Trent Parker, Yue Sun, and Qingsheng Wang. Recent application of computational fluid dynamics (cfd) in process safety and loss prevention: A review. *Journal of Loss Prevention in the Process Industries*, 67:104252, September 2020.

[130] L. Raynal, F. Augier, F. Bazer-Bachi, Y. Haroun, and C. Pereira da Fonte. Cfd applied to process development in the oil and gas industry – a review. *Oil & Gas Science and Technology – Revue d'IFP Energies nouvelles*, 71(3):42, August 2015.

[131] Hyeon Woo Park and Won Byong Yoon. Computational fluid dynamics (cfd) modelling and application for sterilization of foods: A review. *Processes*, 6(6):62, May 2018.

[132] Timilehin Oyinloye and Won Yoon. Application of computational fluid dynamics (cfd) simulation for the effective design of food 3d printing (a review). *Processes*, 9(11):1867, October 2021.

[133] Ashim Datta, Bart Nicolaï, Olivier Vitrac, Pieter Verboven, Ferruh Erdogdu, Francesco Marra, Fabrizio Sarghini, and Chris Koh. Computer-aided food engineering. *Nature Food*, 3(11):894–904, November 2022.

[134] Dzmitry Misiulia, Sergiy Antonyuk, Anders Gustav Andersson, and Tord Staffan Lundström. High-efficiency industrial cyclone separator: A cfd study. *Powder Technology*, 364:943–953, March 2020.

[135] Lakhbir Singh Brar. Application of response surface methodology to optimize the performance of cyclone separator using mathematical models and cfd simulations. *Materials Today: Proceedings*, 5(9):20426–20436, 2018.

[136] H. Safikhani, A. Hajiloo, and M.A. Ranjbar. Modeling and multi-objective optimization of cyclone separators using cfd and genetic algorithms. *Computers & Chemical Engineering*, 35(6):1064–1071, June 2011.

[137] Khairy Elsayed and Chris Lacor. Optimization of the cyclone separator geometry for minimum pressure drop using mathematical models and cfd simulations. *Chemical Engineering Science*, 65(22):6048–6058, November 2010.

[138] Thomas Wilis Cândido Pereira, Felipe Bezerra Marques, Fábio de Assis Ressel Pereira, Daniel da Cunha Ribeiro, and Sandra Mara Santana Rocha. The influence of the fabric filter layout of in a flow mass filtrate. *Journal of Cleaner Production*, 111:117–124, January 2016.

[139] Zihui Zhang, Sijie Dong, Kejun Dong, Li'an Hou, Wenzheng Wang, Yi Wei, and Bo Wang. Experimental and numerical study of a gas cyclone with a central filter. *Particuology*, 63:47–59, April 2022.

[140] Federico Solari, Giorgia Tagliavini, Roberto Montanari, Eleonora Bottani, N. Malagoli, and Mattia Armenzoni. Cfd model validation of a bag filter for air filtration in a milling plant. 2017.

[141] Ansys, Inc. *ANSYS Meshing User's Guide, Release 18.0*. Ansys, Inc., Canonsburg, PA, USA, 2017.

[142] Haofu Chen, Xiaoqing Zhou, Zhuangbo Feng, and Shi-Jie Cao. Application of polyhedral meshing strategy in indoor environment simulation: Model accuracy and computing time. *Indoor and Built Environment*, 31(3):719–731, July 2021.

[143] Marcin Sosnowski, Jaroslaw Krzywanski, Karolina Grabowska, and Renata Gnatowska. Polyhedral meshing in numerical analysis of conjugate heat transfer. *EPJ Web of Conferences*, 180:02096, 2018.

[144] F. R. Menter. Two-equation eddy-viscosity turbulence models for engineering applications. *AIAA Journal*, 32(8):1598–1605, August 1994.

[145] Alan S. Morris and Reza Langari. *Data Acquisition with LabVIEW*, page 347–374. Elsevier, 2016.

[146] Lindsay P. Owens and Martin A. Hubbe. Performance factors for filtration of air using cellulosic fiber-based media: A review. *BioResources*, 18(1), January 2023.

[147] Wenjun Qin, Manuel Dekermenjian, and Richard J. Martin. Prediction of particulate loading in exhaust from fabric filter baghouses with one or more failed bags. *Journal of the Air & Waste Management Association*, 56(8):1177–1183, August 2006.

[148] F. Solari, N. Lysova, R. Montanari, F. Scano, E. Bedogni, and G. Copelli. Computational fluid dynamics simulation of sloshing inside beverage cans on a rotary filling machine. In Daniel Grzonka, Natalia Rylko, Grazyna Suchacka, and Vladimir Mityushev, editors, *ECMS 2024 Proceedings*, pages 394–400, 2024.

[149] R. Elahi, M. Passandideh-Fard, and A. Javanshir. Simulation of liquid sloshing in 2d containers using the volume of fluid method. *Ocean Engineering*, 96:226–244, March 2015.

[150] Miao-Zi Zheng, Ying Gou, Bin Teng, and Hyojae Jo. A practical prescreening method for sloshing severity evaluation. *Petroleum Science*, 17(4):1119–1134, May 2020.

[151] Lian Cheng Guo, Shuai Zhang, Koji Morita, and Kenji Fukuda. Fundamental validation of the finite volume particle method for 3d sloshing dynamics. *International Journal for Numerical Methods in Fluids*, 68(1):1–17, November 2010.

[152] Arkadiusz Szpicer, Weronika Bińkowska, Iwona Wojtasik-Kalinowska, Salih Mustafa Salih, and Andrzej Półtorak. Application of computational fluid dynamics simulations in food industry. *European Food Research and Technology*, 249(6):1411–1430, March 2023.

[153] Dongming Liu and Pengzhi Lin. A numerical study of three-dimensional liquid sloshing in tanks. *Journal of Computational Physics*, 227(8):3921–3939, April 2008.

[154] Francesco Saltari, Alessandro Traini, Francesco Gambioli, and Franco Mastroddi. A linearized reduced-order model approach for sloshing to be used for aerospace design. *Aerospace Science and Technology*, 108:106369, January 2021.

[155] Yong Tang, Baozeng Yue, and Yulong Yan. Improved method for implementing contact angle condition in simulation of liquid sloshing under microgravity. *International Journal for Numerical Methods in Fluids*, 89(4–5):123–142, October 2018.

[156] Liting Yu, Mi-An Xue, and Aimeng Zhu. Numerical investigation of sloshing in rectangular tank with permeable baffle. *Journal of Marine Science and Engineering*, 8(9):671, September 2020.

[157] Enhui Zhang. Numerical research on sloshing of free oil liquid surface based on different baffle shapes in rectangular fuel tank. *Proceedings of the Institution of Mechanical Engineers, Part D: Journal of Automobile Engineering*, 234(2–3):363–377, June 2019.

[158] Luca Guagliumi, Alessandro Berti, Eros Monti, and Marco Carricato. A simple model-based method for sloshing estimation in liquid transfer in automatic machines. *IEEE Access*, 9:129347–129357, 2021.

[159] Luca Guagliumi, Alessandro Berti, Eros Monti, and Marco Carricato. Antisloshing trajectories for high-acceleration motions in automatic machines. *Journal of Dynamic Systems, Measurement, and Control*, 144(7), April 2022.

[160] C.W Hirt and B.D Nichols. Volume of fluid (vof) method for the dynamics of free boundaries. *Journal of Computational Physics*, 39(1):201–225, January 1981.

[161] P.G. Smith. *Evaporation and Drying*, page 299–334. Springer US, December 2010.

[162] William L. Kerr. *Food Drying and Evaporation Processing Operations*, page 353–387. Elsevier, 2019.

[163] Rukiye Gundogan, Gizem Sevval Tomar, Asli Can Karaca, and Vural Gökmen. *Evaporation in the tomato paste industry*, page 247–265. Elsevier, 2024.

[164] Jianfei Pei, Shanshan Gao, Sarper Sarp, Haihua Wang, Xiaonan Chen, Jin Yu, Tianli Yue, Wirote Youravong, and Zhenyu Li. Emerging forward osmosis and membrane distillation for liquid food concentration: A review. *Comprehensive Reviews in Food Science and Food Safety*, 20(2):1910–1936, January 2021.

[165] Catherine Charcosset. Classical and recent applications of membrane processes in the food industry. *Food Engineering Reviews*, 13(2):322–343, November 2020.

[166] Amanda Alves Prestes, Cristiane Vieira Helm, Erick Almeida Esmerino, Ramon Silva, Adriano Gomes da Cruz, and Elane Schwinden Prudencio. Freeze concentration techniques as alternative methods to thermal processing in dairy manufacturing: A review. *Journal of Food Science*, 87(2):488–502, January 2022.

[167] Osato Miyawaki and Takahiro Inakuma. Development of progressive freeze concentration and its application: a review. *Food and Bioprocess Technology*, 14(1):39–51, August 2020.

[168] Food products evaporation. In Theodoros Varzakas and Constantina Tzia, editors, *Food Engineering Handbook: Food Engineering Fundamentals*, page 58. CRC Press, 1st edition edition, 2014.

[169] Christian O. Díaz-Ovalle and Seid Mahdi Jafari. Multiple-effect evaporators in the food industry: Fundamentals, design, simulation, control, and applications. *Food Engineering Reviews*, 15(4):691–717, June 2023.

[170] Dong Han, Junjie Chen, Tianhao Zhou, and Zetian Si. Experimental investigation of a batched mechanical vapor recompression evaporation system. *Applied Thermal Engineering*, 192:116940, June 2021.

[171] Yurim Kim, Jonghun Lim, Hyungtae Cho, and Junghwan Kim. Novel mechanical vapor recompression-assisted evaporation process for improving energy efficiency in pulp and paper industry. *International Journal of Energy Research*, 46(3):3409–3427, October 2021.

[172] Deming Yang, Bingqin Leng, Tao Li, and Ming Li. Energy saving research on multi-effect evaporation crystallization process of bittern based on mvr and tvr heat pump technology. *American Journal of Chemical Engineering*, 8(3):54, 2020.

[173] Fakhreddin Salehi. Rheological and physicochemical properties of vegetable juices and concentrates: A review. *Journal of Food Processing and Preservation*, 45(4), February 2021.

[174] Marco Ferrari, Gianluca Boccardo, Antonio Buffo, Marco Vanni, and Daniele L. Marchisio. Cfd simulation of a high-shear mixer for food emulsion production. *Journal of Food Engineering*, 358:111655, December 2023.

[175] Natalya Lysova, Federico Solari, Michele Bocelli, Antonio Rizzi, and Roberto Montanari. Exploring the impact of the process parameters on the thermal treatment of viscous food fluids in a tube-in-tube heat exchanger. *Procedia Computer Science*, 232:2347–2357, 2024.

[176] Federico Solari, Natalya Lysova, Francesco Martelli, Andrea Volpi, Benedetta Bottari, and Roberto Montanari. Performance assessment, through numerical simulation and experimental evaluation, of a thin-film ultraviolet reactor for the processing of fruit juices. *International Journal of Food Engineering*, March 2024.

[177] Natalya Lysova, Federico Solari, Michele Bocelli, Andrea Volpi, and Roberto Montanari. Industrial device for the continuous uv-c treatment of fruit and vegetables: simulation-aided design and model validation. *International Journal of Food Engineering*, April 2024.

[178] Andrea Volpi, Federico Solari, Natalya Lysova, and Michele Bocelli. Design and optimization through simulation of an industrial system for the continuous uv-c treatment of fruits and vegetables. In *Proceedings of the 8th International Food Operations and Processing Simulation Workshop (FoodOPS 2022)*, FoodOPS 2021. CAL-TEK srl, 2022.

[179] FAO. *The State of Food and Agriculture. Moving Forward on Food Loss and Waste Reduction*. Rome, 2019. License: CC BY-NC-SA 3.0 IGO.

[180] United States Food and Drug Administration. Ultraviolet radiation for the processing and treatment of food. Code of Federal Regulations (21 CFR 179 Section 179.39), Federal Register 65: 230, 2000.

[181] Giulia Andreani, Giovanni Sogari, Alessandra Marti, Federico Froldi, Hans Dagevos, and Daniela Martini. Plant-based meat alternatives: Technological, nutritional, environmental, market, and social challenges and opportunities. *Nutrients*, 15(2):452, January 2023.

[182] JR Gadelha, A Allende, F López-Gálvez, P Fernández, MI Gil, and JA Egea. Chemical risks associated with ready-to-eat vegetables: quantitative analysis to estimate formation and/or accumulation of disinfection byproducts during washing. *EFSA Journal*, 17, September 2019.

[183] Andreza B. Silva, Nelson M. Lima Filho, Maria A.P.F. Palha, and Sandra M. Sarmento. Kinetics of water disinfection using uv-c radiation. *Fuel*, 110:114–123, August 2013.

[184] Thi Tham Nguyen, Graham R. Johnson, Scott C. Bell, and Luke D. Knibbs. A systematic literature review of indoor air disinfection techniques for airborne bacterial respiratory pathogens. *International Journal of Environmental Research and Public Health*, 19(3):1197, January 2022.

[185] William A. Rutala, Maria F. Gergen, and David J. Weber. Room decontamination with uv radiation. *Infection Control & Hospital Epidemiology*, 31(10):1025–1029, October 2010.

[186] Timothy D. Cutler and Jeffrey J. Zimmerman. Ultraviolet irradiation and the mechanisms underlying its inactivation of infectious agents. *Animal Health Research Reviews*, 12(1):15–23, June 2011.

[187] Tatiana Koutchma. *Ultraviolet Light in Food Technology*. CRC Press, May 2019.

[188] Xuetong Fan, Runze Huang, and Haiqiang Chen. Application of ultraviolet c technology for surface decontamination of fresh produce. *Trends in Food Science & Technology*, 70:9–19, December 2017.

[189] Julia Reichel, Corinna Kehrenberg, and Carsten Krischek. Inactivation of yersinia enterocolitica and brochothrix thermosphacta on pork by uv-c irradiation. *Meat Science*, 158:107909, December 2019.

[190] Maria Lúcia G. Monteiro, Denes K.A. Rosário, Anna Paula A. de Carvalho, and Carlos A. Conte-Junior. Application of uv-c light to improve safety and overall quality of fish: A systematic review and meta-analysis. *Trends in Food Science & Technology*, 116:279–289, October 2021.

[191] Valentina Lacivita, Amalia Conte, Lara Manzocco, Stella Plazzotta, Vittorio A. Zambrini, Matteo A. Del Nobile, and Maria Cristina Nicoli. Surface uv-c light treatments to prolong the shelf-life of fiordilatte cheese. *Innovative Food Science & Emerging Technologies*, 36:150–155, August 2016.

[192] Mariana M. Delorme, Jonas T. Guimarães, Nathália M. Coutinho, Celso F. Balthazar, Ramon S. Rocha, Ramon Silva, Larissa P. Margalho, Tatiana C. Pimentel, Marcia C. Silva, Monica Q. Freitas, Daniel Granato, Anderson S. Sant'Ana, Maria Carmela K.H. Duart, and Adriano G. Cruz. Ultraviolet radiation: An interesting technology to preserve quality and safety of milk and dairy foods. *Trends in Food Science & Technology*, 102:146–154, August 2020.

[193] Sıla Barut Gök. Uv-c treatment of apple and grape juices by modified uv-c reactor based on dean vortex technology: Microbial, physicochemical and sensorial parameters evaluation. *Food and Bioprocess Technology*, 14(6):1055–1066, March 2021.

[194] Vanessa R. Souza and Tatiana Koutchma. *Ultraviolet Light Microbial Inactivation in Liquid Foods*, page 146–170. Elsevier, 2021.

[195] Salvatore Zaffina, Vincenzo Camisa, Marco Lembo, Maria Rosaria Vinci, Mario Graziano Tucci, Massimo Borra, Antonio Napolitano, and Vittorio Cannatà. Accidental exposure to uv radiation produced by germicidal lamp: Case report and risk assessment. *Photochemistry and Photobiology*, 88(4):1001–1004, April 2012.

[196] Magalí Darré, Ariel Roberto Vicente, Luis Cisneros-Zevallos, and Francisco Artés-Hernández. Postharvest ultraviolet radiation in fruit and vegetables: Applications and factors modulating its efficacy on bioactive compounds and microbial growth. *Foods*, 11(5):653, February 2022.

[197] Shruti Sethi, Alka Joshi, and Bindvi Arora. *UV Treatment of Fresh Fruits and Vegetables*, page 137–157. Elsevier, 2018.

[198] Harpreet Singh, Sanjeev K. Bhardwaj, Madhu Khatri, Ki-Hyun Kim, and Neha Bhardwaj. Uvc radiation for food safety: An emerging technology for the microbial disinfection of food products. *Chemical Engineering Journal*, 417:128084, August 2021.

[199] *Stewart Postharvest Review*, 3(3):1–8, 2007.

[200] Laurent Urban, Florence Charles, Maria Raquel Alcântara de Miranda, and Jawad Aarrouf. Understanding the physiological effects of uv-c light and exploiting its agronomic potential before and after harvest. *Plant Physiology and Biochemistry*, 105:1–11, August 2016.

[201] Gilbert Shama. Process challenges in applying low doses of ultraviolet light to fresh produce for eliciting beneficial hormetic responses. *Postharvest Biology and Technology*, 44(1):1–8, April 2007.

[202] Health Canada. Ultraviolet light treatment of apple juice/cider using the cidersure 3500, 2003.

[203] European Commission. Commission implementing regulation (eu) 2017/2470 of 20 december 2017 establishing the union list of novel foods in accordance with regulation (eu) 2015/2283 of the european parliament and of the council on novel foods. Official Journal of the European Union, 351, 72–2001, December 2017.

[204] Fumihiko Tanaka, Kohei Nashiro, Vipavee Trivittayasil, and Toshitaka Uchino. Simulation of uv-c dose distribution and inactivation of mold spore on strawberries in a conveyor system. *Food Science and Technology Research*, 22(4):461–466, 2016.

[205] Federico Solari, Natalya Lysova, and Roberto Montanari. Monitoring and control of air filtration systems: Digital twin based on 1d computational fluid dynamics simulation and experimental data. *Computers & Industrial Engineering*, 197:110607, November 2024.

[206] Trevor Sparks and George Chase. *Filtration – Introduction, Physical Principles and Ratings*, page 1–54. Elsevier, 2016.

[207] W. J. Souza, K. M. C. Santos, A. A. Cruz, E. Franceschi, C. Dariva, A. F. Santos, and C. C. Santana. Effect of water content, temperature and average droplet size on the settling velocity of water-in-oil emulsions. *Brazilian Journal of Chemical Engineering*, 32(2):455–464, June 2015.

[208] Chun-Hsing Wu and Jia-Ming Chern. Experiment and simulation of sludge batch settling curves: A wave approach. *Industrial & Engineering Chemistry Research*, 45(6):2026–2031, February 2006.

[209] Jiacheng Yu, Changqian Cao, and Yongxin Pan. Advances of adsorption and filtration techniques in separating highly viscous crude oil/water mixtures. *Advanced Materials Interfaces*, 8(16), July 2021.

[210] Hajime Tamon, Takashi Saito, Masaaki Kishimura, Morio Okazaki, and Ryozo Toei. Solvent regeneration of spent activated carbon in wastewater treatment. *JOURNAL OF CHEMICAL ENGINEERING OF JAPAN*, 23(4):426–432, 1990.

[211] Henryk Grajek. Regeneration of adsorbents by the use of liquid, subcritical and supercritical carbon dioxide. *Adsorption Science & Technology*, 18(4):347–371, May 2000.

[212] B. Ledesma, S. Román, A. Álvarez Murillo, E. Sabio, and J.F. González. Cyclic adsorption/thermal regeneration of activated carbons. *Journal of Analytical and Applied Pyrolysis*, 106:112–117, March 2014.

[213] Seo-Hyun Pak and Yong-Woo Jeon. Effect of vacuum regeneration of activated carbon on volatile organic compound adsorption. *Environmental Engineering Research*, 22(2):169–174, November 2016.

[214] Giacomo Viccione, Stefania Evangelista, Andrea Armenante, and Vincenzo Ricciardi. Clogging process and related pressure drops in wire-wound filters: laboratory evidence. *Environmental Science and Pollution Research*, 27(19):23464–23476, July 2019.

[215] Changqi Liu, Qiu Bao, and Wen Nie. The influence of ventilation parameters on dust pollution in a tunnel's environment using the cfd method. *Journal of Wind Engineering and Industrial Aerodynamics*, 230:105173, November 2022.

[216] G. Dwars and C. Mehring. Reduced-order model for predicting the performance of small-scale unidirectional cyclone aerosol separators. *Advanced Powder Technology*, 35(1):104273, January 2024.

[217] Xin Zhang and Junjie Liu. Simplified model for the calculation of the particle capture process in air filter media. *Chemical Engineering Science*, 249:117358, February 2022.

[218] Y. K. Liu, S. K. Ong, and A. Y. C. Nee. State-of-the-art survey on digital twin implementations. *Advances in Manufacturing*, 10(1):1–23, January 2022.

[219] Yoo Ho Son, Goo-Young Kim, Hyeon Chan Kim, Chanmo Jun, and Sang Do Noh. Past, present, and future research of digital twin for smart manufacturing. *Journal of Computational Design and Engineering*, 9(1):1–23, December 2021.

[220] Luca Preite, Federico Solari, and Giuseppe Vignali. Technologies to optimize the water consumption in agriculture: A systematic review. *Sustainability*, 15(7):5975, March 2023.

[221] R.P. Chhabra and J.F. Richardson. *Heat transfer characteristics of non-Newtonian fluids in pipes*, page 260–288. Elsevier, 1999.

[222] R. Paul Singh and Dennis R. Heldman. *Heat Transfer in Food Processing*, page 265–419. Elsevier, 2014.

[223] Norman Maloney and Michael Harrison. *Advanced Heating Technologies for Food Processing*, page 203–256. Elsevier, 2016.

[224] Chirag Maradiya, Jeetendra Vadher, and Ramesh Agarwal. The heat transfer enhancement techniques and their thermal performance factor. *Beni-Suef University Journal of Basic and Applied Sciences*, 7(1):1–21, March 2018.

[225] L. D'Addio, F. Di Natale, A. Budelli, and R. Nigro. Cfd simulation for the pasteurization of fruit puree with pieces. *Chemical Engineering Transactions*, 39:1699–1704, 2014.

[226] Juan Ignacio Córcoles, Ernesto Marín-Alarcón, and Jose Antonio Almendros-Ibáñez. Heat transfer performance of fruit juice in a heat exchanger tube using numerical simulations. *Applied Sciences*, 10(2):648, January 2020.

[227] Claudio Perone, Roberto Romaniello, Alessandro Leone, Pasquale Catalano, and Antonia Tamborrino. Cfd analysis of a tubular heat exchanger for the conditioning of olive paste. *Applied Sciences*, 11(4):1858, February 2021.

[228] G. Tagliavini, T. Defraeye, and J. Carmeliet. Multiphysics modeling of convective cooling of non-spherical, multi-material fruit to unveil its quality evolution throughout the cold chain. *Food and Bioproducts Processing*, 117:310–320, September 2019.

[229] Pieter Verboven, Thijs Defraeye, Ashim K Datta, and Bart Nicolai. Digital twins of food process operations: the next step for food process models? *Current Opinion in Food Science*, 35:79–87, October 2020.

[230] Prakash Mishra and Farhad Ein-Mozaffari. Intensification of suspension of solid particles in non-newtonian fluids with coaxial mixers. *Chemical Engineering and Processing-Process Intensification*, 168:108553, 2021.

[231] Mahmoud Yolmeh and Seid Mahdi Jafari. Applications of response surface methodology in the food industry processes. *Food and Bioprocess Technology*, 10(3):413–433, January 2017.

[232] Mehdi Khodashenas and Mohammad Jouki. Optimization of stabilized probiotic doogh formulation by edible gums and response surface methodology: assessment of stability, viability and organoleptic attributes. *Journal of Food Science and Technology*, 57(9):3201–3210, April 2020.

[233] Mohammad Jouki, Seyed Ali Mortazavi, Farideh Tabatabaei Yazdi, and Arash Koocheki. Optimization of extraction, antioxidant activity and functional properties of quince seed mucilage by rsm. *International Journal of Biological Macromolecules*, 66:113–124, May 2014.

[234] S.N. Jha and Suresh Prasad. Determination of processing conditions for gorgon nut (euryale ferox). *Journal of Agricultural Engineering Research*, 63(2):103–111, February 1996.

[235] Chulin Yu, Jian Chen, Min Zeng, and Bingjun Gao. Numerical study on turbulent heat transfer performance of a new parallel-flow shell and tube heat exchanger with sinusoidal wavy tapes using rsm analysis. *Applied Thermal Engineering*, 150:875–887, March 2019.

[236] Poornodaya Venkata Krishna Varma Kola, Srinivas Kishore Pisipaty, Siva Subrahmanyam Mendu, and Rajesh Ghosh. Optimization of performance parameters of a double pipe heat exchanger with cut twisted tapes using cfd and rsm. *Chemical Engineering and Processing - Process Intensification*, 163:108362, June 2021.

[237] Hamed Arjmandi, Pezhman Amiri, and Mohsen Saffari Pour. Geometric optimization of a double pipe heat exchanger with combined vortex generator and twisted tape: A cfd and response surface methodology (rsm) study. *Thermal Science and Engineering Progress*, 18:100514, August 2020.

[238] Shaobei Liu, Weixing Huang, Zewei Bao, Tao Zeng, Min Qiao, and Jiancheng Meng. Analysis, prediction and multi-objective optimization of helically coiled tube-in-tube heat exchanger with double cooling source using rsm. *International Journal of Thermal Sciences*, 159:106568, January 2021.

[239] Eleonora Bottani, Giuseppe Vignali, and Giovanni Paolo Carlo Tancredi. A digital twin model of a pasteurization system for food beverages: tools and architecture. In *2020 IEEE International Conference on Engineering, Technology and Innovation (ICE/ITMC)*, volume 11, page 1–8. IEEE, June 2020.

[240] Arsenio M. Fialho, Leonilde M. Moreira, Ana Teresa Granja, Alma O. Popescu, Karen Hoffmann, and Isabel Sá-Correia. Occurrence, production, and applications of gellan: current state and perspectives. *Applied Microbiology and Biotechnology*, 79(6), July 2008.

[241] Massimiliano Rinaldi, Matteo Cordioli, Marcello Alinovi, Matteo Malavasi, Davide Barbanti, and Germano Mucchetti. Development and validation of cfd models of thermal treatment on milk whey proteins dispersion in batch and continuous process condition. *International Journal of Food Engineering*, 14(9–10), September 2018.

[242] A. B. Metzner and J. C. Reed. Flow of non-newtonian fluids—correlation of the laminar, transition, and turbulent-flow regions. *AIChE Journal*, 1(4):434–440, December 1955.

[243] Paul J. LaNasa and E. Loy Upp. *Basic Flow Measurement Laws*, page 19–29. Elsevier, 2014.

[244] Aroon Shenoy. *Heat Transfer to Non-Newtonian Fluids: Fundamentals and Analytical Expressions*. Wiley, December 2017.

[245] D. C. Montgomery. *Design and Analysis of Experiments*. John Wiley and Sons, New York, 5th edition, 2001. Response Surface Methods and Other Approaches to Process Optimization.

[246] G. E. P. Box and K. B. Wilson. On the experimental attainment of optimum conditions. *Journal of the Royal Statistical Society Series B: Statistical Methodology*, 13(1):1–38, January 1951.

[247] M. J. Hernández, J. Dolz, Jesús Delegido, C. Cabeza, and M. Dolz. Thixotropic behavior of salad dressings stabilized with modified starch, pectin, and gellan gum. influence of temperature. *Journal of Dispersion Science and Technology*, 29(2):213–219, January 2008.

[248] M.C. García, M.C. Alfaro, and J. Muñoz. Yield stress and onset of nonlinear time-dependent rheological behaviour of gellan fluid gels. *Journal of Food Engineering*, 159:42–47, August 2015.

[249] Aprajeeta Jha, J.A. Moses, and C. Anandharamakrishnan. *Optimizing Beverage Pasteurization Using Computational Fluid Dynamics*, page 237–271. Elsevier, 2019.

[250] Nantawan Therdthai. *Modeling and optimization of food processes*, page 419–441. Elsevier, 2021.

[251] Giovanni Tancredi, Eleonora Bottani, and Giuseppe Vignali. *Digital Twin Application for the Temperature and Steam Flow Monitoring of a Food Pasteurization Pilot Plant*, page 612–619. Springer International Publishing, 2021.

[252] Renato Alexandre Ferreira Cabral, Carlos Eduardo Orrego-Alzate, Ana Lúcia Gabas, and Javier Telis-Romero. Rheological and thermophysical properties of blackberry juice. *Ciência e Tecnologia de Alimentos*, 27(3):589–595, September 2007.

[253] P. Amorim, H. Meyr, C. Almeder, and B. Almada-Lobo. Managing perishability in production-distribution planning: a discussion and review. *Flexible Services and Manufacturing Journal*, 25(3):389–413, November 2011.

[254] K. van Donselaar, T. van Woensel, R. Broekmeulen, and J. Fransoo. Inventory control of perishables in supermarkets. *International Journal of Production Economics*, 104(2):462–472, December 2006.

[255] M.E. Buisman, R. Haijema, and J.M. Bloemhof-Ruwaard. Discounting and dynamic shelf life to reduce fresh food waste at retailers. *International Journal of Production Economics*, 209:274–284, March 2019.

[256] Han-Wen Tuan, Kuo-Chen Hung, and Gino K. Yang. Inventory model with fixed shelf life under generalized non-increasing demand. *Mathematics*, 9(21):2735, October 2021.

[257] Shikha Yadav and Aditi Khanna. Sustainable inventory model for perishable products with expiration date and price reliant demand under carbon tax policy. *Process Integration and Optimization for Sustainability*, 5(3):475–486, March 2021.

[258] Emre Berk and Ülkü Gürler. Analysis of the (q, r) inventory model for perishables with positive lead times and lost sales. *Operations Research*, 56(5):1238–1246, October 2008.

[259] Alejandro Gutierrez-Alcoba, Roberto Rossi, Belen Martin-Barragan, and Eligius M.T. Hendrix. A simple heuristic for perishable item inventory control under non-stationary stochastic demand. *International Journal of Production Research*, 55(7):1885–1897, June 2016.

[260] Eleonora Bottani and Roberto Montanari. Supply chain design and cost analysis through simulation. *International Journal of Production Research*, 48(10):2859–2886, June 2009.

[261] R. Montanari, E. Bottani, A. Volpi, F. Solari, and G. Scozzesi. An economic order interval-based simulation model for perishable products. In *Proceedings of the 7th International Food Operations and Processing Simulation Workshop (FoodOPS 2021)*, pages 8–14, 2021.

[262] René Haijema, Jan van der Wal, and Nico M. van Dijk. Blood platelet production: Optimization by dynamic programming and simulation. *Computers & Operations Research*, 34(3):760–779, March 2007.

[263] René Haijema and Stefan Minner. Stock-level dependent ordering of perishables: A comparison of hybrid base-stock and constant order policies. *International Journal of Production Economics*, 181:215–225, November 2016.

[264] Harshal Lowalekar, Rahul Nilakantan, and N Ravichandran. Analysis of an order-up-to-level policy for perishables with random issuing. *Journal of the Operational Research Society*, 67(3):483–505, March 2016.

[265] Chaaben Kouki, Zied Jemai, Evren Sahin, and Yves Dallery. Analysis of a periodic review inventory control system with perishables having random lifetime. *International Journal of Production Research*, 52(1):283–298, October 2013.

[266] R. Montanari, E. Bottani, A. Volpi, F. Solari, N. Lysova, and M. Bocelli. Eoq: A simulation approach for perishable products. In *Proceedings of the XXVII Summer School Francesco Turco*, 2022. Paper presented at the XXVII Summer School Francesco Turco.

[267] Chun-Chin Wei and Liang-Tu Chen. Supply chain replenishment decision for newsvendor products with multiple periods and a short life cycle. *Sustainability*, 13(22):12777, November 2021.

[268] Elena Piva, Letizia Tebaldi, Giuseppe Vignali, and Eleonora Bottani. Simulation of different reordering policies for optimizing the inventory of perishable food: an italian case study. *International Journal of Food Engineering*, 18(3):201–238, September 2021.

[269] Stefan Minner and Sandra Transchel. Periodic review inventory-control for perishable products under service-level constraints. *OR Spectrum*, 32(4):979–996, February 2010.

[270] Brian A. Kapalka, Kaan Katircioglu, and Martin L. Puterman. Retail inventory control with lost sales, service constraints, and fractional lead times. *Production and Operations Management*, 8(4):393–408, December 1999.

[271] M. Mahdi Tajbakhsh. On the distribution free continuous-review inventory model with a service level constraint. *Computers & Industrial Engineering*, 59(4):1022–1024, November 2010.

[272] Marco Bijvank. Periodic review inventory systems with a service level criterion. *Journal of the Operational Research Society*, 65(12):1853–1863, December 2014.

[273] Karin G.J. Pauls-Worm, Eligius M.T. Hendrix, René Haijema, and Jack G.A.J. van der Vorst. An milp approximation for ordering perishable products with non-stationary demand and service level constraints. *International Journal of Production Economics*, 157:133–146, November 2014.

[274] Elia Balugani, Francesco Lolli, Rita Gamberini, Bianca Rimini, and M. Z. Babai. A periodic inventory system of intermittent demand items with fixed lifetimes. *International Journal of Production Research*, 57(22):6993–7005, January 2019.

[275] Mohamed Zied Babai, Aris Syntetos, and Ruud Teunter. Intermittent demand forecasting: An empirical study on accuracy and the risk of obsolescence. *International Journal of Production Economics*, 157:212–219, November 2014.

[276] R. Patriarca, G. Di Gravio, F. Costantino, and M. Tronci. Eoq inventory model for perishable products under uncertainty. *Production Engineering*, 14(5–6):601–612, October 2020.

[277] Lina Tang, Yizhong Ma, Jianjun Wang, Linhan Ouyang, and Jai-Hyun Byun. Robust parameter design of supply chain inventory policy considering the uncertainty of demand and lead time. *Scientia Iranica*, 0(0):0–0, May 2018.

[278] Chia-Nan Wang, Thanh-Tuan Dang, and Ngoc-Ai-Thy Nguyen. A computational model for determining levels of factors in inventory management using response surface methodology. *Mathematics*, 8(8):1210, July 2020.

[279] Kenneth W. Bauer, Gregory S. Parnell, and David A. Meyers. Response surface methodology as a sensitivity analysis tool in decision analysis. *Journal of Multi-Criteria Decision Analysis*, 8(3):162–180, May 1999.

[280] Elena Katok, Douglas Thomas, and Andrew Davis. Inventory service-level agreements as coordination mechanisms: The effect of review periods. *Manufacturing & Service Operations Management*, 10(4):609–624, October 2008.

[281] Angel A. Juan, Scott E. Grasman, Jose Caceres-Cruz, and Tolga Bektaş. A simheuristic algorithm for the single-period stochastic inventory-routing problem with stock-outs. *Simulation Modelling Practice and Theory*, 46:40–52, August 2014.

[282] Bhakti Stephan Onggo, Javier Panadero, Canan G. Corlu, and Angel A. Juan. Agri-food supply chains with stochastic demands: A multi-period inventory routing problem with perishable products. *Simulation Modelling Practice and Theory*, 97:101970, December 2019.

[283] Johan Bjerre Bach Clausen and Hongyan Li. Big data driven order-up-to level model: Application of machine learning. *Computers & Operations Research*, 139:105641, March 2022.

[284] Dimitris Bertsimas and Nathan Kallus. From predictive to prescriptive analytics. *Management Science*, 66(3):1025–1044, March 2020.

[285] R. Manzini, R. Accorsi, E. Ferrari, M. Gamberi, V. Giovannini, H. Pham, et al. Weibull vs. normal distribution of demand to determine the safety stock level when using the continuous-review (s, s) model without backlogs. *International Journal of Logistics Systems and Management*, 24(3):298–332, 2016.

[286] T. Vijayan and M. Kumaran. Inventory models with a mixture of backorders and lost sales under fuzzy cost. *European Journal of Operational Research*, 189(1):105–119, August 2008.

[287] Emin Ozyoruk, Nesim Kohen Erkip, and Çağın Ararat. End-of-life inventory management problem: Results and insights. *International Journal of Production Economics*, 243:108313, January 2022.

[288] Wenhong Luo. An integrated inventory system for perishable goods with backordering. *Computers & Industrial Engineering*, 34(3):685–693, July 1998.

[289] Cinzia Muriana. An eoq model for perishable products with fixed shelf life under stochastic demand conditions. *European Journal of Operational Research*, 255(2):388–396, December 2016.

[290] S.K. Ghosh, S. Khanra, and K.S. Chaudhuri. Optimal price and lot size determination for a perishable product under conditions of finite production, partial backordering and lost sale. *Applied Mathematics and Computation*, 217(13):6047–6053, March 2011.

[291] Abdullah Ali H. Ahmadini, Umar Muhammad Modibbo, Ali Akbar Shaikh, and Irfan Ali. Multi-objective optimization modelling of sustainable green supply chain in inventory and production management. *Alexandria Engineering Journal*, 60(6):5129–5146, December 2021.

[292] Gino K. Yang, Shuo-Yan Chou, Chih-Young Hung, Jennifer Shu-Jen Lin, and Peter Chu. Research note on the criteria for the optimal solution of the inventory model with a mixture of partial backordering and lost sales. *Applied Mathematical Modelling*, 32(9):1758–1768, September 2008.

[293] Gour Chandra Mahata. An epq-based inventory model for exponentially deteriorating items under retailer partial trade credit policy in supply chain. *Expert Systems with Applications*, 39(3):3537–3550, February 2012.

[294] Bappa Mondal, Arindam Garai, Arindum Mukhopadhyay, and Sanat Kumar Majumder. Inventory policies for seasonal items with logistic-growth demand rate under fully permissible delay in payment: a neutrosophic optimization approach. *Soft Computing*, 25(5):3725–3750, November 2020.

[295] Ali Khaleel Dhaiban. Two models of inventory system with stochastic demand and deteriorating items: case study of a local cheese factory. *OPSEARCH*, 59(1):78–101, April 2021.

[296] Federico Solari, Natalya Lysova, Michele Bocelli, Andrea Volpi, and Roberto Montanari. Perishable product inventory management in the case of discount policies and price-sensitive demand: Discrete time simulation and sensitivity analysis. *Procedia Computer Science*, 232:1233–1241, 2024.

[297] N. Lysova, F. Solari, E. Bottani, and R. Montanari. Impact of the discount policies on the purchasing behaviour of perishable items. *IFAC-PapersOnLine*, 58(19):433–438, 2024.

[298] FAO. Global food losses and food waste - extent, causes and prevention. SAVE FOOD: An initiative on food loss and waste reduction, 9, 2011, 2011.

[299] UNEP. Food waste index report 2021, 2021.

[300] Xiaojun Wang and Dong Li. A dynamic product quality evaluation based pricing model for perishable food supply chains. *Omega*, 40(6):906–917, December 2012.

[301] Shukai Li, Jianxiong Zhang, and Wansheng Tang. Joint dynamic pricing and inventory control policy for a stochastic inventory system with perishable products. *International Journal of Production Research*, 53(10):2937–2950, September 2014.

[302] Md. Al-Amin Khan, Shifat Ahmed, Md. Shohel Babu, and Nahid Sultana. Optimal lot-size decision for deteriorating items with price-sensitive demand, linearly time-dependent holding cost under all-units discount environment. *International Journal of Systems Science: Operations & Logistics*, 9(1):61–74, September 2020.

[303] S. Panda, S. Saha, and M. Basu. Optimal pricing and lot-sizing for perishable inventory with price and time dependent ramp-type demand. *International Journal of Systems Science*, 44(1):127–138, January 2013.

[304] Borga Deniz, Itir Karaesmen, and Alan Scheller-Wolf. A comparison of inventory policies for perishable goods. *Operations Research Letters*, 48(6):805–810, November 2020.

[305] Michael Tsiros and Carrie M. Heilman. The effect of expiration dates and perceived risk on purchasing behavior in grocery store perishable categories. *Journal of Marketing*, 69(2):114–129, April 2005.

[306] Wedad Elmaghraby and Pınar Keskinocak. Dynamic pricing in the presence of inventory considerations: Research overview, current practices, and future directions. *Management Science*, 49(10):1287–1309, October 2003.

[307] Monique Bakker, Jan Riezebos, and Ruud H. Teunter. Review of inventory systems with deterioration since 2001. *European Journal of Operational Research*, 221(2):275–284, September 2012.

[308] J. Gustavsson, C. Cederberg, and U. Sonesson. *Global Food Losses and Food Waste*. Swedish Institute for Food and Biotechnology (SIK), Gothenburg, Sweden, 2011.

[309] Food and Agriculture Organization of the United Nations. Food loss and waste database. `https://www.fao.org/platform-food-loss-waste/flw-data/en`, 2024.

[310] S. Lebersorger and F. Schneider. Food loss rates at the food retail, influencing factors and reasons as a basis for waste prevention measures. *Waste Management*, 34(11):1911–1919, November 2014.

[311] Jessica Aschemann-Witzel, Ilona De Hooge, Pegah Amani, Tino Bech-Larsen, and Marije Oostindjer. Consumer-related food waste: Causes and potential for action. *Sustainability*, 7(6):6457–6477, May 2015.

[312] George Tsalis, Birger Boutrup Jensen, and Jessica Aschemann-Witzel. The relationship between retail price promotions and household-level food waste: Busting the myth with behavioural data? *Waste Management*, 173:29–39, January 2024.

[313] Jaekwon Chung. Effective pricing of perishables for a more sustainable retail food market. *Sustainability*, 11(17):4762, August 2019.

[314] Pierre Chandon, J. Wesley Hutchinson, Eric T. Bradlow, and Scott H. Young. Does in-store marketing work? effects of the number and position of shelf facings on brand attention and evaluation at the point of purchase. *Journal of Marketing*, 73(6):1–17, November 2009.

[315] Urszula Samotyja and Maria Sielicka-Różyńska. How date type, freshness labelling and food category influence consumer rejection. *International Journal of Consumer Studies*, 45(3):441–455, December 2020.

[316] Marilisa Alongi, Sandro Sillani, Corrado Lagazio, and Lara Manzocco. Effect of expiry date communication on acceptability and waste of fresh-cut lettuce during storage at different temperatures. *Food Research International*, 116:1121–1125, February 2019.

[317] Alba J. Collart and Matthew G. Interis. Consumer imperfect information in the market for expired and nearly expired foods and implications for reducing food waste. *Sustainability*, 10(11):3835, October 2018.

[318] Norbert L. W. Wilson, Ruiqing Miao, and Carter Weis. Seeing is not believing: Perceptions of date labels over food and attributes. *Journal of Food Products Marketing*, 24(5):611–631, June 2018.

[319] Oliver Koll and Andreas Plank. Do shoppers choose the same brand on the next trip when facing the same context? an empirical investigation in fmcg retailing. *Journal of Retailing*, 98(4):576–592, December 2022.

[320] Anne-Katrin Kleih and Kai Sparke. Visual marketing: The importance and consumer recognition of fruit brands in supermarket fruit displays. *Food Quality and Preference*, 93:104263, October 2021.

[321] Sofia B. Villas-Boas, Kristin Kiesel, Joshua P. Berning, Hayley H. Chouinard, and Jill J. McCluskey. Consumer and strategic firm response to nutrition shelf labels. *American Journal of Agricultural Economics*, 102(2):458–479, January 2020.

[322] Anh Dang and Bridget Satinover Nichols. Consumer response to positive nutrients on the facts up front (fuf) label: A comparison between healthy and unhealthy foods and the role of nutrition motivation. *Journal of Marketing Theory and Practice*, 31(2):223–242, February 2022.

[323] Julia Lamberz, Thorsten Litfin, Özlem Teckert, and Gunther Meeh-Bunse. Is there a link between sustainability, perception and buying decision at the point of sale? *Business Systems Research Journal*, 11(3):1–13, November 2020.

[324] Tom Gordon-Hecker, Andrea Pittarello, Shaul Shalvi, and Marieke Roskes. Buy-one-get-one-free deals attract more attention than percentage deals. *Journal of Business Research*, 111:128–134, April 2020.

[325] Wee Kheng Tan. When do price discounts become attractive? a study comparing discount strategies on consumer perceptions. *Asia Pacific Journal of Marketing and Logistics*, 35(6):1404–1424, August 2022.

[326] Natalya Lysova, Federico Solari, Claudio Suppini, Letizia Tebaldi, Andrea Volpi, and Roberto Montanari. Leveraging economic sanctions to reduce food waste in retail: Insights from a discrete-time simulation approach. In *Proceedings of the XXIX Summer School "Francesco Turco" – Industrial Systems Engineering*, 2024. Presented at XXIX Summer School "Francesco Turco".

[327] Agatha Herman. Enchanting resilience: Relations of care and people–place connections in agriculture. *Journal of Rural Studies*, 42:102–111, December 2015.

[328] Lucius P. Brown. Food wastes—some causes and remedies. *Journal of the Franklin Institute*, 185(5):585–610, May 1918.

[329] EUROSTAT. Food waste and food waste prevention - estimates. `https://ec.europa.eu/eurostat/statistics-Explained/index.php?title=Food_waste_and_food_waste_prevention_estimates#Amounts_of_food_waste_at_EU_level`, 2021. Available at: `https://ec.europa.eu/eurostat/statistics-Explained/index.php?title=Food_waste_and_food_waste_prevention_estimates#Amounts_of_food_waste_at_EU_level`.

[330] Sahar Ahmadzadeh, Tahmina Ajmal, Ramakrishnan Ramanathan, and Yanqing Duan. A comprehensive review on food waste reduction based on iot and big data technologies. *Sustainability*, 15(4):3482, February 2023.

[331] Lusine Aramyan, Matthew Grainger, Katja Logatcheva, Simone Piras, Marco Setti, Gavin Stewart, and Matteo Vittuari. Food waste reduction in supply chains through innovations: a review. *Measuring Business Excellence*, 25(4):475–492, December 2020.

[332] Seth-Oscar Tromp, René Haijema, Hajo Rijgersberg, and Jack G.A.J. van der Vorst. A systematic approach to preventing chilled-food waste at the retail outlet. *International Journal of Production Economics*, 182:508–518, December 2016.

[333] Chule Qalase and Kevin G. Harding. Eco-efficiency assessment of pork production through life-cycle assessment and product system value in south africa. *E3S Web of Conferences*, 349:13002, 2022.

[334] Andreas Geß, Anna Tolsdorf, and Nathanael Ko. A life cycle perspective of lamb meat production systems from turkey and the eu. *Small Ruminant Research*, 208:106637, March 2022.

[335] ISMEA. Catena del valore della filiera carne bovina biologica, 2022. Coordinated by Antonella Giuliano. Contributions by Riccardo Meo, Alessandro Trotta, Giuseppe Fornaciari, Gianluigi Sagarriga Visconti, and Franco Torelli.

[336] ISMEA. Tendenze bovino da carne - dicembre 2023, 2023. Coordinated by Michele Di Domenico. Edited by Paola Parmigiani.

[337] J.A. Barreiro, M. Milano, and A.J. Sandoval. Kinetics of colour change of double concentrated tomato paste during thermal treatment. *Journal of Food Engineering*, 33(3–4):359–371, August 1997.

[338] Mohammad Ganje, Seid Mahdi Jafari, Vahid Farzaneh, and Narges Malekjani. Kinetics modelling of color deterioration during thermal processing of tomato paste with the use of response surface methodology. *Heat and Mass Transfer*, 54(12):3663–3671, June 2018.

Appendix A: List of Figures

Appendix B: List of Tables

Appendix C: List of Publications

Journal papers

1. Solari, F., Lysova, N., & Montanari, R. (2024). Monitoring and control of air filtration systems: Digital twin based on 1D computational fluid dynamics simulation and experimental data. Computers & Industrial Engineering, 197, 110607. https://doi.org/10.1016/j.cie.2024.110607

2. Solari, F., Suppini, C., Bocelli, M., Lysova, N., & Volpi, A. (2024). Abatement of volatile organic compounds in industrial bakery plants, a state-of-the-art analysis and technical-economic evaluation for a plant in northern Italy. International Journal of Food Engineering. https://doi.org/10.1515/ijfe-2023-0040

3. Solari, F., Lysova, N., Romagnoli, G., Montanari, R., & Bottani, E. (2024). Insights from 20 Years (2004–2023) of Supply Chain Disruption Research: Trends and Future Directions Based on a Bibliometric Analysis. Sustainability, 16(17), 7530. https://doi.org/10.3390/su16177530

4. Suppini, C., Lysova, N., Bocelli, M., Solari, F., Tebaldi, L., Volpi, A., & Montanari, R. (2024). From Single Orders to Batches: A Sensitivity Analysis of Warehouse Picking Efficiency. Sustainability, 16(18), 8231. https://doi.org/10.3390/su16188231

5. Solari, F., Lysova, N., Martelli, F., Volpi, A., Bottari, B., & Montanari, R. (2024). Performance assessment, through numerical simulation and experimental evaluation, of a thin-film ultraviolet reactor for the processing of fruit juices. International Journal of Food Engineering, 0(0). https://doi.org/10.1515/ijfe-2023-0033

6. Lysova, N., Solari, F., Bocelli, M., Volpi, A., & Montanari, R. (2024). Industrial device for the continuous UV-C treatment of fruit and vegetables: simulation-aided design and model validation. International Journal of Food Engineering, 0(0). https://doi.org/10.1515/ijfe-2023-0065

7. Bocelli, M., Bottani, E., Volpi, A., Solari, F., Lysova, N., & Montanari, R. (2024). Exploring the relationship between routing policies and market demand heterogeneity: A simulation analysis with different hardware and software configurations in traditional warehouses. Journal of Industrial Information Integration, 40, 100634. https://doi.org/10.1016/j.jii.2024.100634

8. Solari, F., Lysova, N., & Montanari, R. (2023). Digital Twin Based on Historical Data and Simulation Results: Fault Detection and Estimation of the Remaining Useful Life of a Cyclone Bag Filter. Applied Sciences, 13(14), 8297. https://doi.org/10.3390/app13148297

9. Lysova, N., Solari, F., & Vignali, G. (2022). Optimization of an indirect heating process for food fluids through the combined use of CFD and Response Surface Methodology. Food and Bioproducts Processing, 131, 60–76. https://doi.org/10.1016/j.fbp.2021.10.010

Conference proceedings

1. Lysova, N., Solari, F., and Montanari, R. (2024). Investigating Research Trends in Computer Vision for Food Quality Control: A Bibliometric Approach. Proceedings of the 6th International Conference on Industry 4.0 and Smart Manufacturing (ISM 2024).

2. Lysova N., Solari F., Aprili G. and Montanari R. Advancing Ohmic Treatment of Egg Products: Insights from Numerical Simulation. Proceedings of the 6th International Conference on Industry 4.0 and Smart Manufacturing (ISM 2024).

3. Suppini C., Volpi A., Solari F., Tebaldi L., Lysova N., Montanari R. (2024). Innovative teaching methodologies: Keyword-based analysis to monitor the trends of the last decade. Proceedings of the 6th International Conference on Industry 4.0 and Smart Manufacturing (ISM 2024).

4. Lysova N., Solari F., Bottani E., Montanari R. (2024). Impact of the Discount Policies on the Purchasing Behaviour of Perishable Items. Proceedings of the 18th IFAC Symposium on Information Control Problems in Manufacturing (INCOM 2024).

5. Lysova N., Solari F., Suppini C., Tebaldi L., Volpi A., Montanari R. (2024). Leveraging economic sanctions to reduce food waste in retail: Insights from a discrete-time simulation approach. Proceedings of the 29th Summer School Francesco Turco.

6. Solari F., Lysova N., Dalla Fiora A., Volpi A., Rizzi A., Montanari R. (2024). Mitigating Design Errors in Standardized Food Processing Plants: Insights from CFD Simulation of a Tomato Concentration Process. Proceedings of the 10th International Food Operations & Processing Simulation Workshop.

7. Suppini C., Lysova N., Solari F., Tebaldi L., Carloni A., Montanari R. (2024). Random vs Class-based Allocation Policies: Impact of the Warehouse Parameters on the Distance Traveled by Pickers. Proceedings of the 26th International Conference on Harbor, Maritime and Multimodal Logistic Modeling & Simulation (HMS 2024)

8. Tebaldi L., Volpi A., Suppini C., Lysova N., Montanari R., Bottani E. (2024). Radio Frequency Identification in the Food Industry: Preliminary results from a bibliometric analysis on case studies. Proceedings of the 10th International Food Operations & Processing Simulation Workshop.

9. Solari, F., Lysova, N., Montanari, R., Scano, F., Bedogni, E., & Copelli, G. (2024). Computational fluid dynamics simulation of sloshing inside beverage cans on a rotary filling machine. ECMS 2024 Proceedings Edited by Daniel Grzonka, Natalia Rylko, Grazyna Suchacka, Vladimir Mityushev. https://doi.org/10.7148/2024-0394

10. Montanari, R., Abdel-Malek, L., Ferretti, G., Bernazzoli, A., Bottani, E., Volpi, A., Solari, F., Tebaldi, L., Casella, G., Lysova, N., Bocelli, M., Suppini, C., Orlandini, L., Bertoli, M., & Pintus, A. (2023). The MEM project: 5 years of experiences, challenges, and outcomes of an international double master-level degree. 9th International Conference on Higher Education Advances (HEAd'23). https://doi.org/10.4995/head23.2023.16132

11. Lysova, N., Solari, F., Caccamo, D., Suppini, C., & Montanari, R. (2023). Periodic Review Inventory Management With Budget Constraints: Discrete-Event Simulation And Sensitivity Analysis. ECMS 2023 Proceedings Edited by Enrico Vicario, Romeo Bandinelli, Virginia Fani, Michele Mastroianni. https://doi.org/10.7148/2023-0291

12. Solari F., Lysova N., Iasoni F., Tancredi G.P., Montanari R., Volpi A. (2023). Simulation analysis of flow patterns inside a cyclone bag separator at increasing clogging levels. Proceedings of the 11th EUROSIM Congress.

13. Solari F., Lysova N., Bottani E., Romagnoli G., Volpi A., Montanari R. (2023). Supply chain resilience and Industry 4.0 in the last decade (2013-2022): a keyword-based analysis. Proceedings of the 28th Summer School "Francesco Turco"

14. Bottani E., Monferdini L., Lysova N., Bocelli M. (2023). Change Management in Public Sector: A Preliminary Analysis. Proceedings of the 28th Summer School "Francesco Turco"

15. Lysova N., Solari F., Suppini C., Bocelli M., Volpi A., Montanari R. (2023). Mixing of non-Newtonian fluids: from CFD simulations to predictive performance metrics. Proceedings of the 9th International Food Operations and Processing Simulation Workshop (FOODOPS). https://doi.org/10.46354/i3m.2023.foodops.003

16. Solari, F., Lysova, N., Bocelli, M., Volpi, A., & Montanari, R. (2024). Perishable Product Inventory Management In The Case Of Discount Policies And Price-Sensitive Demand: Discrete Time Simulation And Sensitivity Analysis. Procedia Computer Science, 232, 1233–1241. https://doi.org/10.1016/j.procs.2024.01.121

17. Lysova, N., Solari, F., Bocelli, M., Rizzi, A., & Montanari, R. (2024). Exploring the impact of the process parameters on the thermal treatment of viscous food fluids in a tube-in-tube heat exchanger. Procedia Computer Science, 232, 2347–2357. https://doi.org/10.1016/j.procs.2024.02.053

18. Montanari R., Bottani E., Volpi A., Solari F., Lysova N., Bocelli M. (2023). EOQ: a simulation approach for perishable products. Proceedings of the XXVII Summer School "Francesco Turco" - "Unconventional Plants: Technologies, tools and Methodologies for emerging domains", 7-9 Settembre 2022

19. Montanari R., Bottani E., Volpi A., Solari F., Lysova N., Bocelli M. (2022). Warehouse Design and Management: a simulative approach to minimize the distance travelled by pickers. Proceedings of the International Conference on Harbor, Maritime and Multimodal Logistic Modeling & Simulation, HMS. https://doi.org/10.46354/i3m.2022.hms.005

20. Solari, F., Lysova, N., Ferretti, G., Volpi, A., Bocelli, M., & Montanari, R. (2022). Abatement of volatile organic compounds from the exhaust gases of an industrial bakery oven: comparative analysis of different technological solutions. Proceedings of the 8th International Food Operations and Processing Simulation Workshop (FoodOPS 2022). https://doi.org/10.46354/i3m.2022.foodops.012

21. Montanari, R., Volpi, A., Solari, F., & Lysova, N. (2022). Performance assessment, through CFD simulation, of an ultraviolet reactor for the processing of fruit juices. Proceedings of the 8th International Food Operations and Processing Simulation Workshop (FoodOPS 2022). https://doi.org/10.46354/i3m.2022.foodops.010

22. Volpi A., Solari F., Lysova N., Bocelli M. (2022). Design and optimization through simulation of an industrial system for the continuous UV-C treatment of fruits and vegetables. Proceedings of the 8th International Food Operations and Processing Simulation Workshop (FoodOPS 2022). https://doi.org/10.46354/i3m.2022.foodops.011